# A NEW REVERSIBLE 1,3-DIPOLAR CYCLOADDITION AND ITS APPLICATION IN DYNAMIC COVALENT CHEMISTRY

David Van Brussel

A Thesis Submitted for the Degree of MPhil
at the
University of St Andrews

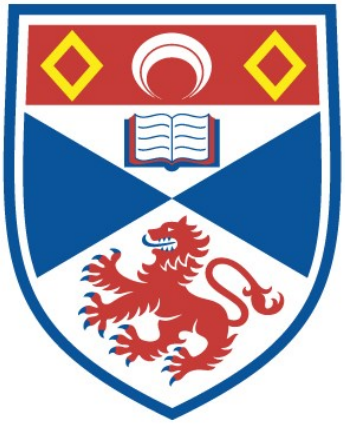

2016

# A New Reversible 1,3-Dipolar Cycloaddition and its Application in Dynamic Covalent Chemistry

David van Brussel

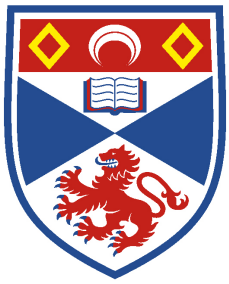

University of
St Andrews

This thesis is submitted in partial fulfilment for the degree of
Master of Philosophy
at the
University of St Andrews

September 2015

**1. Candidate's declarations:**

I, David van Brussel, hereby certify that this thesis, which is approximately 36000 words in length, has been written by me, and that it is the record of work carried out by me, or principally by myself in collaboration with others as acknowledged, and that it has not been submitted in any previous application for a higher degree.

I was admitted as a research student in September, 2013 and as a candidate for the degree of Master of Philosophy in September, 2013; the higher study for which this is a record was carried out in the University of St Andrews between 2013 and 2015.

Date ……. signature of candidate …….

**2. Supervisor's declaration:**

I hereby certify that the candidate has fulfilled the conditions of the Resolution and Regulations appropriate for the degree of Master of Philosophy in the University of St Andrews and that the candidate is qualified to submit this thesis in application for that degree.

Date ……. signature of supervisor …….

**3. Permission for publication:** (*to be signed by both candidate and supervisor*)

In submitting this thesis to the University of St Andrews I understand that I am giving permission for it to be made available for use in accordance with the regulations of the University Library for the time being in force, subject to any copyright vested in the work not being affected thereby. I also understand that the title and the abstract will be published, and that a copy of the work may be made and supplied to any bona fide library or research worker, that my thesis will be electronically accessible for personal or research use unless exempt by award of an embargo as requested below, and that the library has the right to migrate my thesis into new electronic forms as required to ensure continued access to the thesis. I have obtained any third-party copyright permissions that may be required in order to allow such access and migration, or have requested the appropriate embargo below.

The following is an agreed request by candidate and supervisor regarding the publication of this thesis:

PRINTED COPY

b) Embargo on all or part of print copy for a period of 1 year on the following ground(s):
   - Publication would preclude future publication

ELECTRONIC COPY

b) Embargo on all or part of electronic copy for a period of 1 year on the following ground(s):
   - Publication would preclude future publication

Date …… signature of candidate …… signature of supervisor …….

# Abstract

In the past decades, chemists have designed and investigated artificial self-replicating molecules. A self-replicating molecule is one that can assemble its building blocks through molecular recognition, the building blocks are brought in close proximity and can react to from another copy of the self-replicator. Self-replicators are important to consider in the context of the origin of life, as it is hypothesised that molecular self-replicating entities are at the basis of the emergence of life on earth. Previously, self-replicating molecules have been reported based on cycloaddition reactions, and in particular the Philp Laboratory worked on a self-replicating system based on the cycloaddition reaction between a maleimide and a nitrone. The thesis presented here, however, focuses on the implementation of another dipolarophile in a recognition-mediated reaction with a nitrone. 2-Arylidene-1,3-indandiones can react with nitrones in a 1,3-dipolar cycloaddition and these compounds can be functionalised with a recognition site.

Initially, the reactivity of the indandiones in a 1,3-dipolar cycloaddition with a nitrone is studied in the absence of recognition-mediated reaction pathways. The investigation is carried out experimentally and computationally with semi-emperical methods and Density Functional Theory. Secondly, we investigated the effect of molecular recognition on the rate and conversion of the cycloaddition reaction. Depending on the location of the recognition site relative to the reactive site on the nitrone, the rate can be accelerated up to almost seven times.

Synthetic chemists, traditionally, investigate chemical reactions in isolation and one product is purified after the chemical reaction. In biochemical systems, however, a mixture of many compounds is present. In the final part of this thesis, the recognition-mediated reaction is described between the indandione and a mixture of nitrones and any difference is behaviour between the reaction in isolation and the reaction in a mixture of starting materials is investigated.

# Acknowledgements

I've had a tremendously nice time the past two years I spend doing research for my MPhil in the Philp laboratory. First of all, I would like to thank my supervisor, Professor Douglas Philp for giving me the opportunity to do my MPhil project with him. I could not have wished for a better supervisor than Professor Philp who has always been easy-going and enthusiastic and I want to thank him very much for all his help throughout the past two years.

In the course of the last two years I have received a great deal of help from the other members of the Philp group. Josh, Leonardo, and Tamara made me feel welcome in the lab from the moment I arrived in September 2013. The same applies to all the members of the Kay group, Stefan, Will, Flavio and Nicolas. I look forward to becoming a PhD student in a few weeks and continue working with (most of) you!

There are also a few other people within the School of Chemistry that I would like to acknowledge. Melanja Smith and Dr. Thomas Lebl, who helped me a great deal with NMR spectroscopy, both for the characterisation of the cycloadducts and the kinetic studies. Catherine Botting for the Mass Spectrometry and Professor Alexandra Slawin for the single-crystal X-ray diffraction.

The past two years I've had great fun to help with organising events for the Postgraduate Society. In particular, I want to mention Scott Schorr, he has become a very good friend and fellow committee member and it was great to talk with him about science, politics and almost everything else.

Of course I also want to thank my sweet parents, Margot and Willem-Jan, and my brother, Coen. They have supported me a lot throughout the past two years during long skype calls and spoiling me when I came home in Monnickendam.

Last but not least, I want to thank Ilaria, my wonderful girlfriend. Ti amo Ilaria! Thank you for the support and the love and fun the past year and a half.

# Contents

# Abbreviations

| | |
|---|---|
| AC | Anti Michael-*cis* |
| AT | Anti Michael-*trans* |
| $CDCl_3$ | Deuterochloroform |
| COSY | Correlation Spectroscopy |
| DBU | 1,8-Diazabicyclo[5.4.0]undec-7-ene |
| DCC | Dynamic Covalent Chemistry |
| DCL | Dynamic Covalent Library |
| DCM | Dichloromethane |
| DEPTQ | Distortionless Enhancement by Polarisation Transfer with retention of Quaternaries |
| DMSO | Dimethylsulfoxide |
| DNA | Deoxyribonucleic acid |
| DFT | Density Functional Theory |
| $\varepsilon$ | Autocatalytic efficiency |
| EDCI | 1-Ethyl-3-(3-dimethylaminopropyl)carbodiimide |
| ES | Electrospray |
| EtOAc | Ethyl acetate |
| EtOH | Ethanol |
| HMBC | Heteronuclear Multiple-Bond Correlation Spectroscopy |
| HMTA | Hexamethylenetetramine |
| HRMS | High Resolution Mass Spectrometry |
| HSQC | Heteronuclear Single Quantum Coherence spectroscopy |
| $K_a$ | Association constant |
| $K_d$ | Dissociation constant |
| M11 | Minnesota 11 functional |
| m | Multiplet |
| MC | Michael-*cis* |
| MCMM | Multi-configuration molecular mechanics |
| Me | Methyl |
| MeCN | Acetonitrile |
| MeOH | Methanol |

| | |
|---|---|
| M.p. | Melting point |
| MT | Michael-*trans* |
| NBS | *N*-bromosuccinimide |
| NMR | Nuclear Magnetic Resonance |
| NOESY | Nuclear Overhauser Effect Spectroscopy |
| *p* | Autocatalytic reaction order |
| ppm | Parts per million |
| *p*TSA | *p*-Toluenelsulfonic acid |
| RM1 | Recife Model 1 |
| RNA | Ribonucleic acid |
| RT | Room Temperature |
| s | Singlet |
| t | Triplet |
| TFA | Trifuoroacetic acid |
| THF | Tetrahydrofuran |
| TLC | Thin Layer Chromatography |
| TSA | Transition State Analogue |

# 1

# Introduction

## 1.1 Complex systems

Complex systems are abundant in our daily lives. Examples of complex systems include[1] power grids, traffic flows, Internet and the economy. In nature, complexity is also a widely observed[2,3] phenomenon, for example in the weather, metabolism and ecological food webs (**Figure 1.1**). Scientific interest[4] into complex systems has grown considerably during the past decade. It is difficult to give a single definition[1] of complexity, however, there are several aspects of complex systems and complexity in general, which are common to many complex systems. A complex system is one in which[5] "multiple elements adapting or reacting to the pattern these elements create".

One common feature of complex systems is that they show emergent properties.[6] These are properties that cannot be deduced despite the understanding of the individual components of the system, but only become apparent when all components act together as a system. An example of such a phenomenon is the Internet, which essentially entails nothing more than connecting computers in the World Wide Web. However, the appearance of the Internet has revolutionised communication methods and the supply of news.[1]

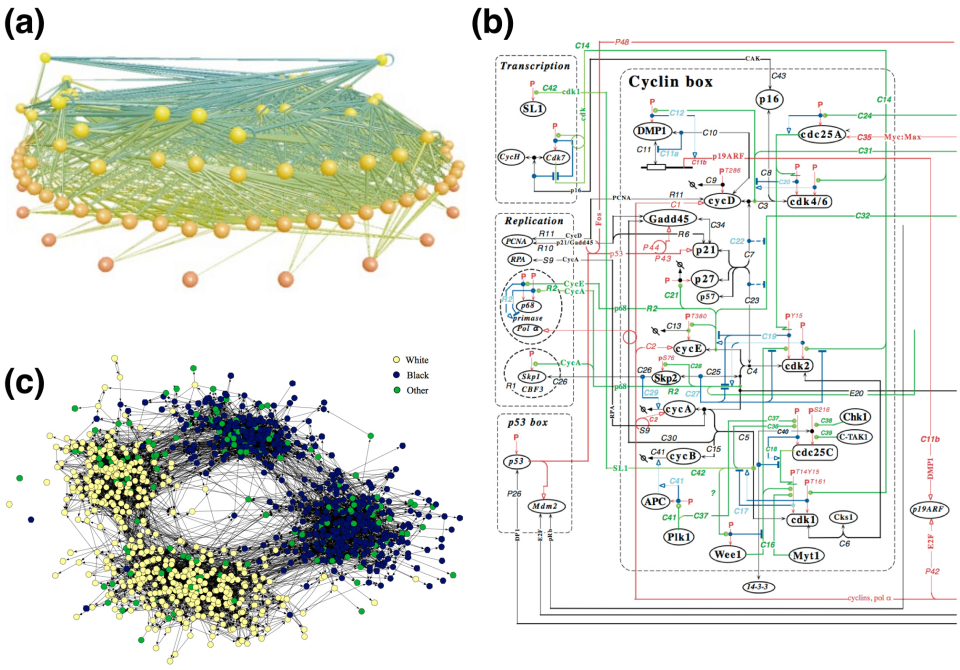


**Figure 1.1:** Examples of complex networks include (a) a mammalian food network, taken from reference 2, (b) a friend network of high school students, taken from reference 2 and (c) the mammalian cell regulatory network, taken from reference 7.

Another common feature of complex system is the interconnectedness of the individual components of the system, which means that the entire system can respond to a change that only directly affects one part of the system. In economics, these phenomena are of great importance.[5] In chemistry, it is also possible to design a system in which part of the system is directly affected by a stimulus but the entire system is changed as a result of the interconnectedness of the system. A hypothetical reaction network (**Figure 1.2**) consists of four compounds, **A**, **B**, **C** and **D**, which can react to form four products, **AB**, **AC**, **BD** and **CD**, depicted as the coloured bars.

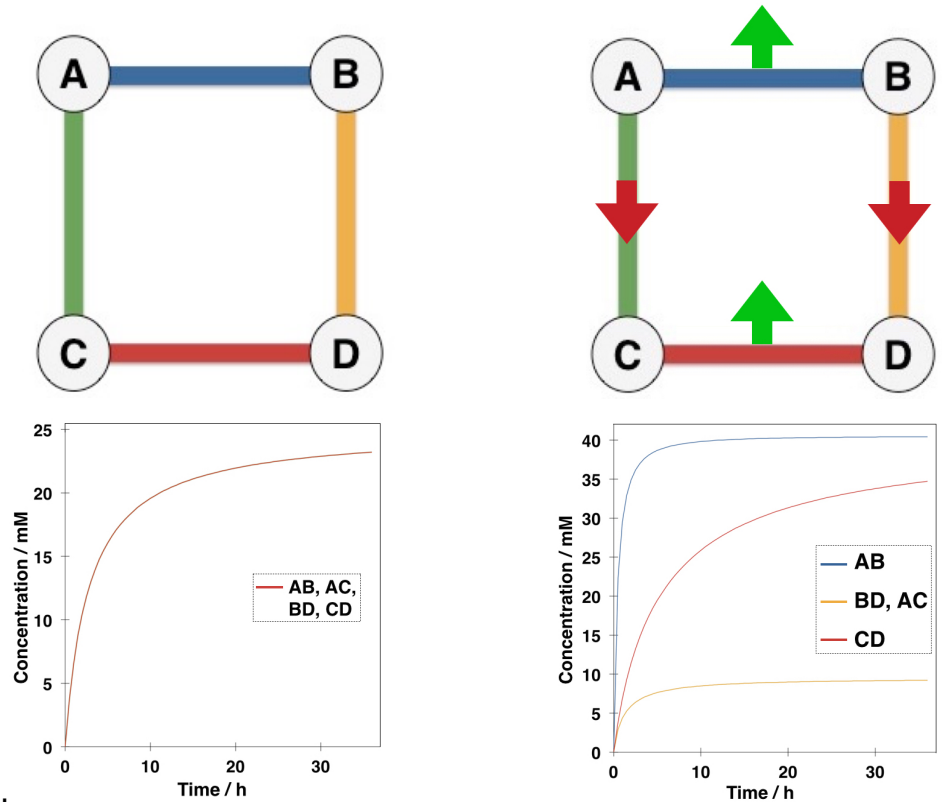


**Figure 1.2:** Left: A reaction network is modelled with Copasi software[8]. All rate constants are equal, $k = 1 \times 10^{-3}\,M^{-1}s^{-1}$. Right: Only the rate constant for the reaction between **A** and **B** is increased 10-fold to $k_{AB} = 1 \times 10^{-2}\,M^{-1}s^{-1}$, the other rate constants are set to $k = 1 \times 10^{-3}\,M^{-1}s^{-1}$.

The rate constants for the formation of the four products are $k_{AB}$, $k_{AC}$, $k_{BD}$, $k_{CD}$. When these rate constants for the four reactions are identical, the final composition of the reaction network will show equal distribution of the four products and equal depletion of the four reagents. However, when one rate constant, for example $k_{AB}$, is increased selectively relative to the other rate constants, the formation of one product, in this case of **AB**, is increased. The logical consequence of the enhancement of **AB** is the decrease in formation of **AC** and **BD** because two of the building blocks for these compounds are used to produce more **AB**. Another consequence of the increase of $k_{AB}$ is the enhancement of product **CD**, which is not a direct result of the increase of $k_{AB}$ but rather a system level property of the interconnected reaction network. Even though $k_{CD}$ is not affected by the changes to the system and the constituents **C** and **D** are not directly affected by the change the behaviour of this part of the system is altered, therefore this can be viewed as an emergent property.

A chemical example of a complex network was reported[9] by Ghadiri and co-workers in 2004. **Figure 1.3** shows that even a relatively small network with only nine nodes can result in a complex network architecture in which autocatalytic and cross catalytic pathways operate and a change in one part of the network can result in changes in different parts of the network despite the lack of a direct connection between them.

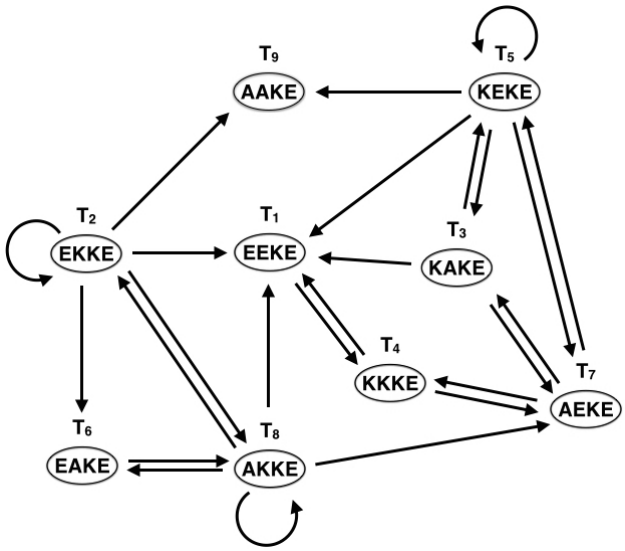


**Figure 1.3:** Ghadiri and co-workers created a network of peptides with different amino acid sequences. The nodes represent self-replicating peptide templates $\mathbf{T_1}$ – $\mathbf{T_9}$, and the straight arrows represent cross catalytic pathways. The curved arrows represent autocatalysis by the peptide templates. Adapted from reference 9.

The network, designed within the Ghadiri Laboratory consisted of nine different peptides that were formed from a common nucleophilic peptide building block and nine different electrophilic building blocks, resulting in the formation of nine different peptide templates, $\mathbf{T}_{1\text{-}9}$. These peptides were investigated for their ability to catalyse the ligation towards the formation of any of the other peptides (cross catalysis) and their ability to catalyse the ligation towards their own formation (autocatalysis). Additionally, the authors reported emergent properties in this system of peptides as they observed that the rate of formation of various templates in isolation is significantly different from those in the context of the network.

Complex systems also exhibit a degree of feedback from certain components of the system to others, this can either be negative feedback or positive. This means that one component of the system is able to report back to another component of the system and influence the behaviour in that part of the system. An example of this phenomenon can be found in ecology when looking at population dynamics. The Lotka-Volterra model [10] describes predator-prey interactions in ecology and consists of three steps.[11] **G** is the amount of grass for the rabbits, **R**, (prey) to consume and is assumed to be constant or in large excess. **L** represents the living lynxes (predators) and **D** the dead lynxes.

$$G + R \rightarrow 2R \qquad \textbf{Equation 1.1}$$

$$R + L \rightarrow 2L \qquad \textbf{Equation 1.2}$$

$$L \rightarrow D \qquad \textbf{Equation 1.3}$$

The irreversible steps in **Equations 1.1**, **1.2** and **1.3** can be written as a set of two differential equations that describe the behaviour of the populations of prey and predator.

$$\frac{dr}{dt} = k_r gr - k_l rl \qquad \textbf{Equation 1.4}$$

$$\frac{dl}{dt} = k_l rl - k_d l \qquad \textbf{Equation 1.5}$$

In these equations, $k_r$ represents the rate of growth of the rabbits, *r,* and $k_l$ is the rate of growth of the lynxes and $k_d$ is their mortality rate. In **Figure 1.4** the numerical solutions to **Equations 1.4** and **1.5** are shown for different initial values of rabbit and lynx, the rate of growth of the rabbits and lynxes as well as the mortality rate of the lynxes is kept constant in both simulations.

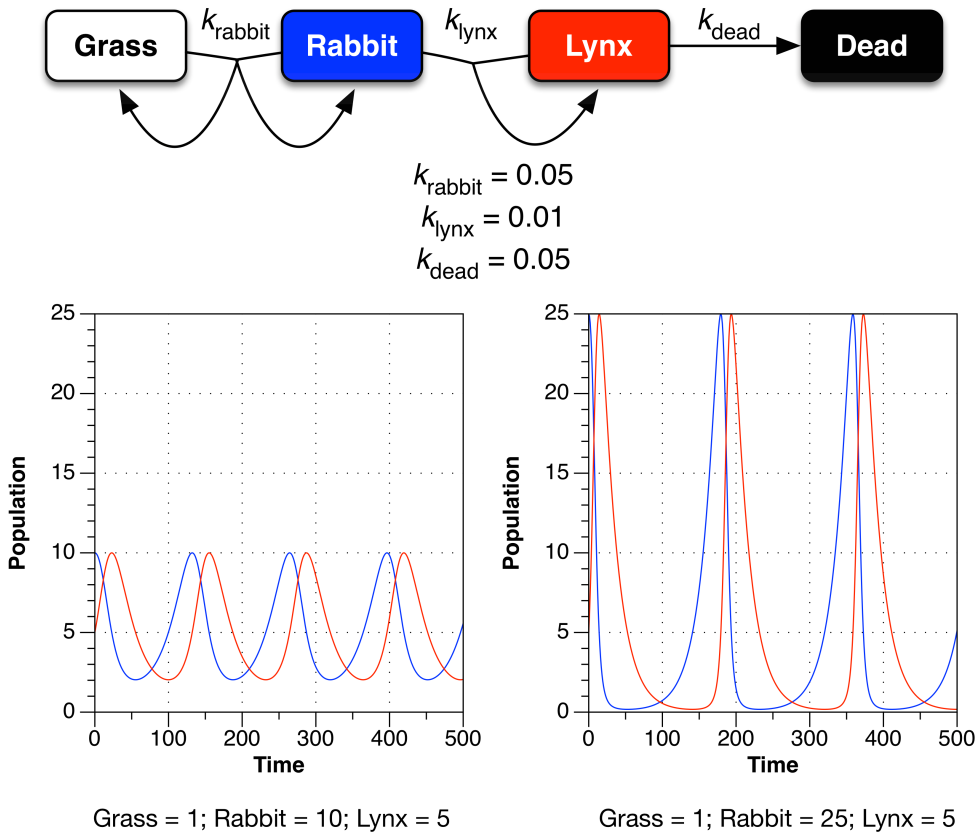


**Figure 1.4:** Numerical solutions to **Equations 1.4** and **1.5** describing rabbit and lynx population over time. The populations oscillate as a result of the feedback mechanism present in this ecological system.

The numerical solutions to **Equations 1.4** and **1.5** (**Figure 1.4**) show that there is a strong negative feedback relationship between the two processes described by this system (rabbit population growth and decline and lynx population growth and decline). An increase in rabbit population leads to an increase in lynx population, which in turn leads to a decrease in rabbit population, which in turn leads to a decrease in lynx population and this cycle will continue. The amplitude and the period of the cycles depend on the initial size of the rabbit population.

In 2013, Fujii and Rondelez reported[12] a molecular system in which predator-prey cycles were observed (**Figure 1.5**). Prey strand **N** can associate on template **G** and DNA polymerase (**Pol.**) will catalyse the polymerisation reaction to form the double stranded DNA. In the presence of a nicking enzyme (**Nick.**) the newly synthesised strand will be cleaved to form two copies of **N**. Predation

occurs when prey **N** associates on predator **P**, polymerase catalyses the elongation of **N** to form the [**P·P**] duplex, which can dissociate to afford two predator molecules. Finally, an exonuclease (**ExoN.**) can cleave both prey and predator to form smaller DNA fragments, which are inactive in the system. When this system is monitored using a green fluorescent dye that gives a stronger signal when intercalating with the predator DNA, an oscillating reaction pattern is observed (**Figure 1.5,** bottom).

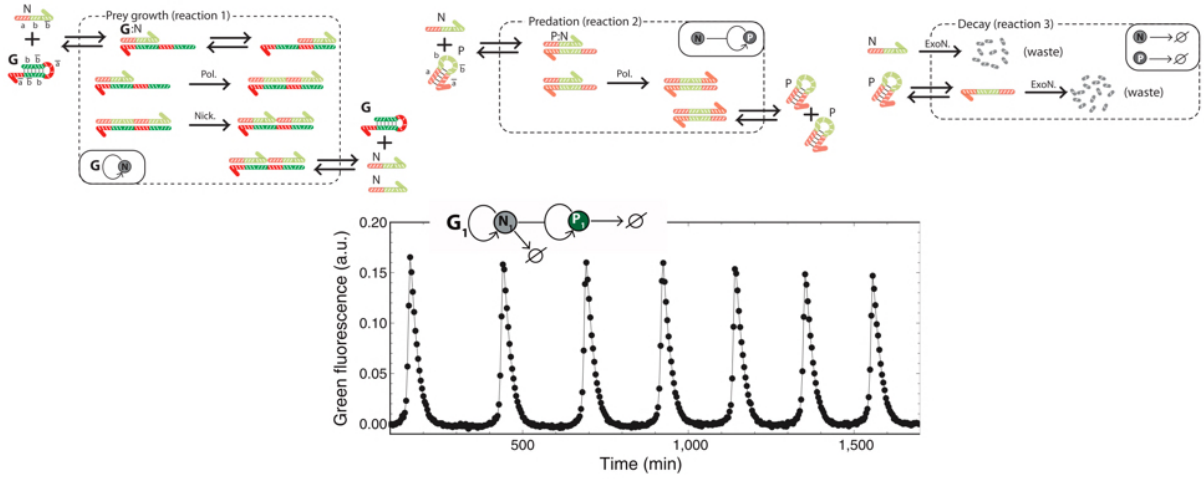


**Figure 1.5:** A molecular system in which predator-prey cycles were observed. Top: Strand **N** can associate on a template strand **G** and is consequently elongated and nicked affording two copies of **N**, the formation of **N** is autocatalytic. When **N** associates on predator strand **P** it is elongated affording two copies of **P**. Both strands **P** and **N** are decayed by an exonuclease. Bottom: following the formation of **P** gives an oscillating pattern. Taken from reference 12.

## 1.2 Networks in Chemistry: Replication

### 1.2.1 Replication in Biological Systems

Living organisms display a great level of complexity at both the ecological[13] level and the molecular level[4]. Organisms have evolved from relatively simple single-cellular organisms to multi-cellular and much more complex organisms such as mammals. Although the biological evolution of living organisms was first described[15] in the 19th century by Charles Darwin, there is no scientific consensus on how the first organism emerged on earth, or even whether it emerged on earth or whether it is extra-terrestial.[15] The general theory of how

life came about focuses on the emergence of molecular systems that could have evolved to organisms.[16-19]

Two characteristic properties of life on earth are metabolism and reproduction, hence the question arises of which of these properties emerged first.[18] It is not possible for a metabolic system to exist without a molecule to bear the genetic information encoding for the enzymes involved in the metabolism. DNA, the molecule that carries genetic information in nature, however, cannot be synthesised without enzymatic machinery available to catalyse the synthesis. RNA, the single-stranded brother of DNA, has the unique property to be both a bearer of genetic information and a catalyst for chemical reactions.[20] This observation led to the formulation of the "RNA World".[19] In this scenario, it is envisaged that RNA emerged as the first molecule to bear genetic information and is capable of non-enzymatic replication and managed to evolve further which led to the emergence of the first organism (**Figure 1.6**).

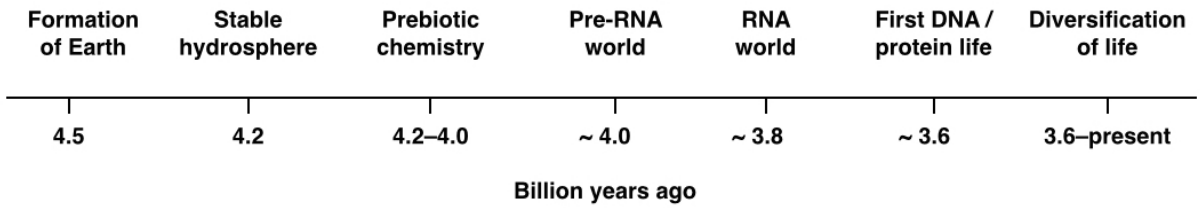


**Figure 1.6:** Timeline showing the events leading up to the emergence and evolution of life on earth. Approximate dates in billions of years before present. Adapted from reference 19.

Considering the hypothesis that life has emerged with the emergence of self-replicating RNA units, it is not surprising that synthetic chemists have focussed on the formation of RNA molecules under pre-biotic conditions. In 2009, the group of Sutherland reported[21] a synthesis towards ribonucleotide **8** under conditions that could have existed on the pre-biotic earth (**Scheme 1.1**). Their synthesis makes use of cyanamide **1**, cyanoacetylene **6**, glycoaldehyde **2**, glyceraldehyde **4** and inorganic phosphate, which are all compounds that were around on the early earth.[22] Inorganic phosphate functions in the system not only as reagent but also as catalyst for various reaction steps and as pH buffer, illustrating the importance of a systems level approach to the problem of the

origin of life, which has also been successful in the synthesis of amino acid precursors.[23]

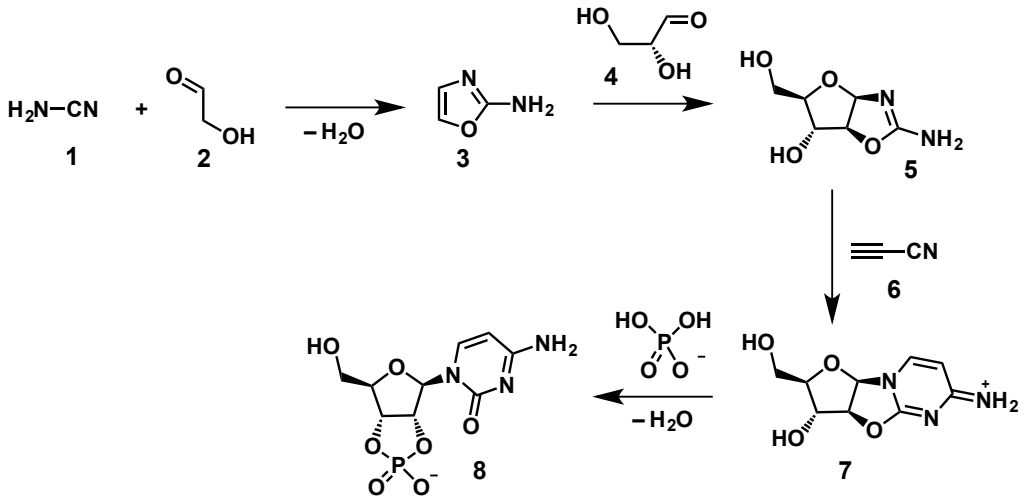

**Scheme 1.1:** Synthesis under pre-biotic plausible conditions leading to the formation of an RNA building block. Taken from reference 21.

Even though these attempts seem successful it is difficult to determine the pre-biotic conditions exactly and it is almost impossible to confirm whether life has indeed emerged *via* the pathways identified. Therefore, another attractive approach is to study self-replication in artificial systems, away from biologically relevant molecules.

### 1.2.2 The minimal model of self-replication

In order to study molecular replication, synthetic chemists have taken up the effort to design and create artificial molecular replicators.[24-29] If a molecule is a catalyst for its own formation from simpler building blocks it is called a minimal or self-replicator.[26,28,29] Reinhoudt *et al*. define self-replication as "autocatalysis by a reaction product which is able to recognise at least two individual reactants with a high degree of selectivity"[30]. A minimal replicator serves as a template for its own formation by preorganising the building blocks required for its own formation, in a way that facilitates a reaction between the building blocks in order to form another copy of the template. When the preorganisation event by the template accelerates the formation of the template, it is autocatalytic.[31] The minimal model of self-replication involves three distinct reaction channels (**Figure 1.7**). Firstly, building blocks **A** and **B** can react in a bimolecular

reaction, without involvement of the template, to form the template **T**. Secondly, since **A** and **B** both bear complementary recognition sites, they can associate to form complex [**A·B**] and react to form the closed template **T´**. Note that in this second reaction channel, rate acceleration is achieved through the recognition sites in the building blocks. However, the recognition lives on in the product affording a template that cannot associate new building blocks and is therefore catalytically inactive.

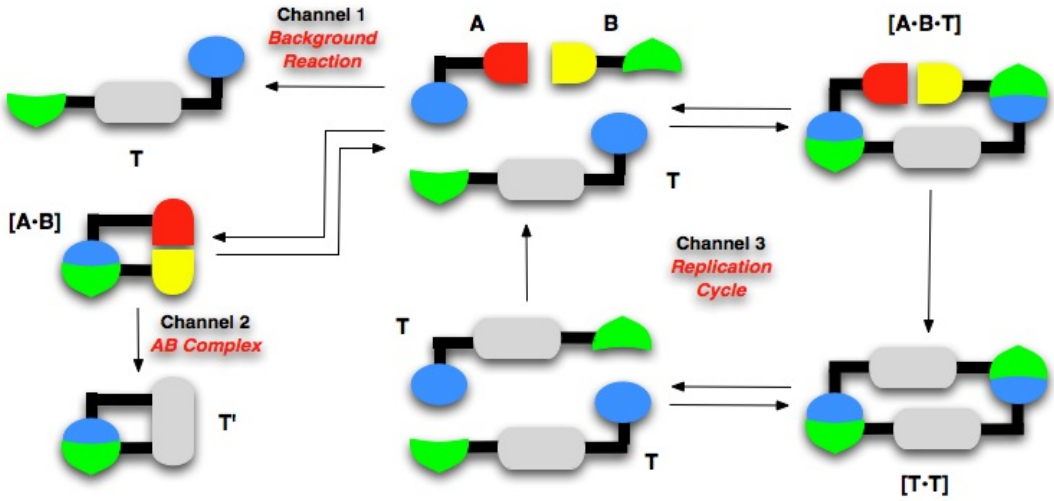


**Figure 1.7:** The minimal model of self-replication involves three reaction pathways. Channel 1 is the bimolecular pathway between **A** and **B** to form template **T**. In channel 2, reactants **A** and **B** associate to complex [**A·B**] and react to form the inactive template **T´**. Channel 3 involves the replication cycle in which **A** and **B** associate on the template and react for form complex [**T·T**], which can dissociate to give to template molecules. Taken from reference 32.

The [**A·B**] pathway can be used by itself to achieve rate acceleration in reactions that are disfavoured. In 1999, the Philp Laboratory reported[33] a Diels-Alder reaction between furan **9** and maleimide **10**. Furan **9** in **Scheme 1.2** is equipped with an amidopyridine recognition site and maleimide **10** with a carboxylic acid recognition site. These recognition sites can associate prior to the reaction in binary complex [**9·10**], then the reaction takes place in a pseudo-intramolecular fashion and the hydrogen bonding lives on in product **11**. Intramolecular reactions or pseudo-intramolecular reactions are kinetically favoured compared to their bimolecular counterparts[34] because the entropic

penalty associated with a bimolecular reaction is paid during the non-covalent association rather than during the chemical reaction.

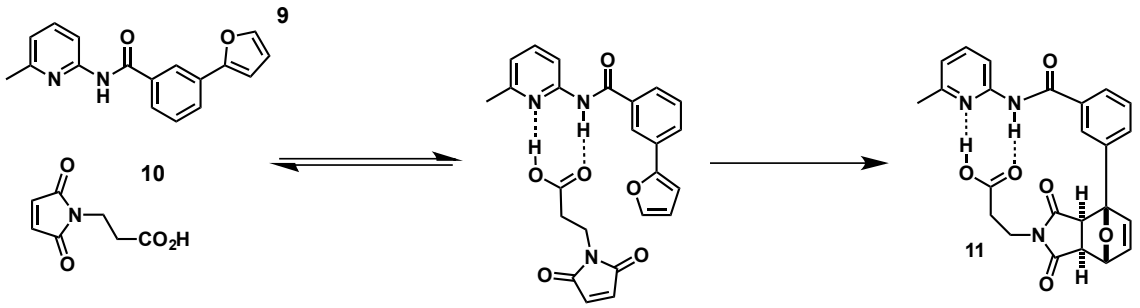


**Scheme 1.2:** Furan **9** and maleimide **10** can associate to from a hydrogen-bonded complex **[9·10]**. The reaction can consequently proceed in a pseudo intra-molecular fashion thus accelerating the reaction. Taken from reference 33.

The third reaction channel in the minimal model of self-replicating (**Figure 1.7**) involves the association of building blocks **A** and **B** on the template to form complex [**A·B·T**]. The association of the building blocks brings **A** and **B** in close proximity and they can react to form the template duplex [**T·T**]. Dissociation of the [**T·T**] duplex gives two template molecules. When these three reaction channels are taken into account, a few design elements of self-replicators become clear. First of all, reaction flow through the binary complex channel should be minimised. Secondly, product inhibition should be considered, template duplex [**T·T**] should be relatively unstable in order to minimise the formation of inhibited catalyst.

### 1.2.3 Kinetic Investigation of Self-replicating Systems

The rate profile, concentration *vs*. time, of an autocatalytic reaction typically has a sigmoidal shape (**Figure 1.8**). Unlike bimolecular reactions, the maximum rate of an autocatalytic cycle does not occur at $t = 0$. At the start of the reaction, when the template is not present at high concentrations, the reaction takes place predominantly through the bimolecular reaction channel resulting in a low reaction rate and an initial lag period in the concentration *vs*. time profile. Once a sufficient amount of the template is formed and the concentration of the template rises above the $K_d$ of the [**A·B·T**] complex, the building blocks will associate on the template and the autocatalytic cycle starts to work. When the

reactants are depleted from the reaction mixture, the rate decreases resulting in a decrease in reaction rate.

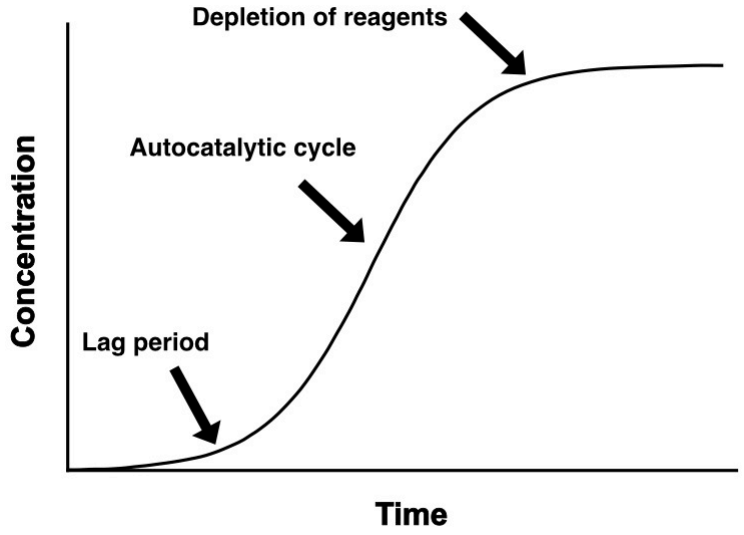


**Figure 1.8:** The concentration *vs*. time profile for an autocatalytic reaction shows a sigmoidal shape. In the first instances the template concentration is not high enough to catalyse the reaction. Once enough template is formed, the autocatalytic reaction starts to work. When the starting materials have been depleted the rate decreases.

There are a number of parameters that require optimisation to achieve efficient formation of the template through the autocatalytic reaction channel.[25,26] First of all, it is important to minimise reaction flow through the [**A**·**B**] pathway since it renders the inactive template. Secondly, the autocatalytic cycle itself requires optimisation in order to increase reaction rate through this pathway as compared to the uncatalysed bimolecular reaction. Finally, the autocatalytic cycle produces the template duplex [**T**·**T**], which should dissociate readily in order to put two template molecules back in solution. If the product duplex is too stable, there is no turnover of the catalyst as it is inactive in the template duplex. Thus, it is important to maximise template dissociation in order to achieve maximum rate enhancement through self-replication. Ideally, association of the reactants on the template is efficient and the covalent bond formation between the reactants results in conformational strain in the template duplex, resulting in dissociation.

There are two variables that can be changed easily in order to optimise the self-replication process; concentration of the reagents and temperature. If the concentration is decreased, the flow through the bimolecular reaction is decreased and flow through the autocatalytic cycle is increased. However, if the concentration used is below the $K_d$ of the ternary [**A·B·T**] complex, the ternary complex does not form at high enough concentrations for the replication process to take place. A decrease in temperature will increase the strength of the intra-molecular interactions that assemble the ternary complex and therefore an increase in rate of the autocatalytic cycle relative to the bimolecular reaction rate is expected. However, it will also, increase the strength of binding of the template duplex which inhibits the autocatalytic cycle.

In order to establish the autocatalytic and self-replicating potential of a system, a number of experiments must be carried out. First of all, in order to assess whether the reaction is autocatalytic, an amount of template can be added to the reaction at $t = 0$. An increase of the initial rate of the reaction and disappearance of the initial lag period should be observed as a consequence. Secondly, the importance of the recognition sites can be evaluated by disabling a recognition site, for example by methylation of one of these recognition sites. This modification should result in a decrease in reaction rate if the reaction is recognition mediated. Finally, an experiment must be carried out in which a competitive inhibitor is added to the reaction. This inhibitor should compete for one or both of the recognition sites on the template. If the reaction is recognition-mediated, a decrease in reaction rate should be observed.

von Kiedrowski introduced[35] several kinetic models to describe autocatalytic reactions. The simplest model assumes a purely autocatalytic reaction with an autocatalytic reaction order, *p*, for the product (**Equation 1.6**). The autocatalytic reaction order can lie between 0.5 and 1. If *p* tends towards 0.5, the system obeys the 'square root law' and shows parabolic growth of the concentration as a function of time (**Figure 1.9a**). The rate-limiting step of such a system is the dissociation of the template duplex [**T·T**]. When *p* tends towards 1, [**T·T**]

dissociation is no longer the overall rate-limiting step and as expected the system shows exponential growth of the template molecule as function of time (**Figure 1.9b**).

$$\mathrm{A} + \mathrm{B} + p\mathrm{T} \rightarrow (1+p)\mathrm{T} \qquad \textbf{Equation 1.6}$$

$$\mathrm{A} + \mathrm{B} \rightarrow \mathrm{T} \qquad \textbf{Equation 1.7}$$

$$\varepsilon = \frac{k_{cat}}{k_{uncat}} \qquad \textbf{Equation 1.8}$$

Despite the analysis presented above, a sigmoidal rate profile of an autocatalytic reaction is not necessarily observed. When the reaction rate through the bimolecular reaction channel (**Equation 1.7**) is comparable with the rate of the autocatalytic channel, the concentration *vs*. time profile will be obscured and a sigmoidal shape cannot be observed. The ratio of the reaction rate constant through the autocatalytic reaction channel, $k_{cat}$, and the bimolecular reaction, $k_{uncat}$, is the autocatalytic efficiency, $\varepsilon$ (**Equation 1.8**). Only above a certain value of $\varepsilon$ a sigmoidal concentration *vs*. time profile becomes apparent as shown in (**Figures 1.9e** and **19f**). Since the lack of a sigmoidal concentration *vs*. time profile does not mean that there is an absence of an autocatalytic reaction, it is useful to derive the reaction order another way. When a series of experiments is carried out in which the building blocks are seeded with increasing amounts of template **T**, the initial rate of formation of **T** scales as 1:√2:√4 in case of parabolic growth and as 1:2:4 in case of exponential growth.

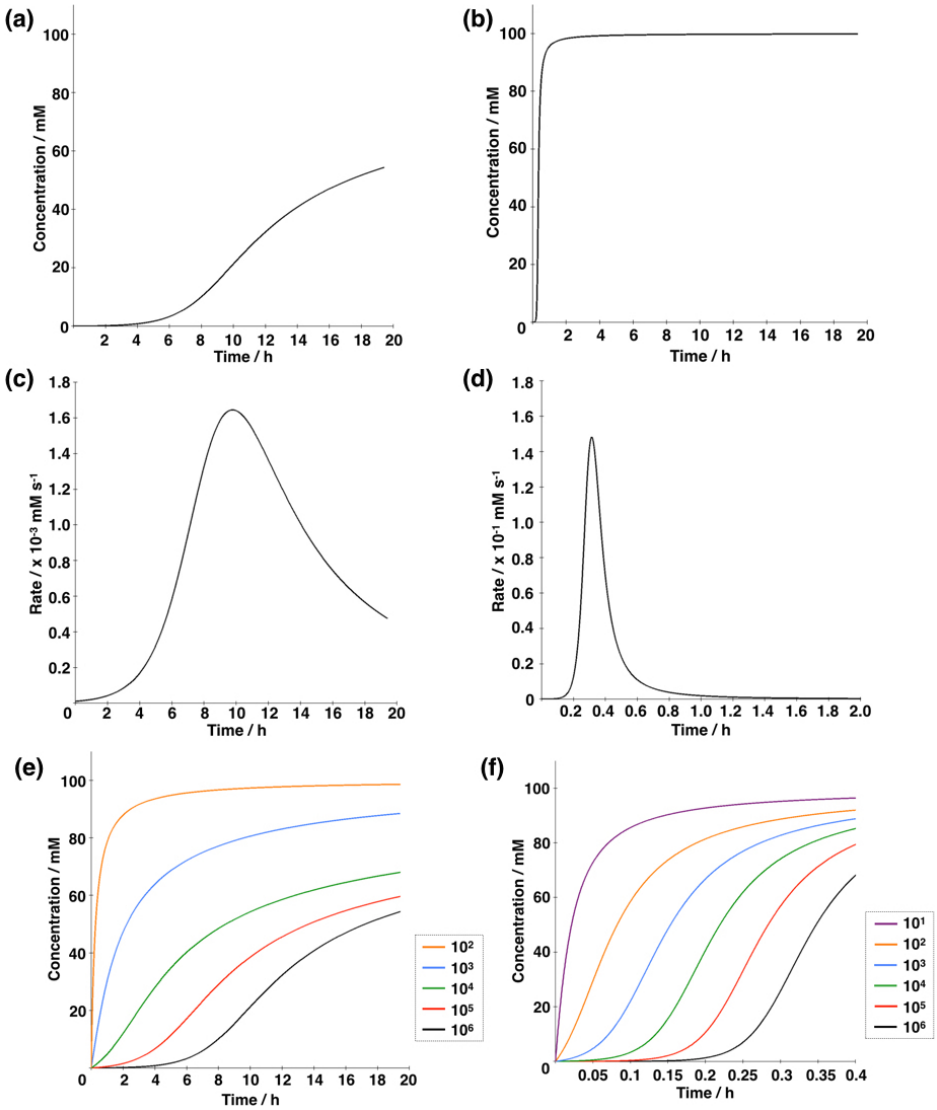


**Figure 1.9:** Simulation results of **Equations 1.6** and **1.7** with Copasi software[8]. Concentration *vs.* time profiles for $p = 0.5$ (a) and $p = 1$ (b). Rate *vs.* time profiles for $p = 0.5$ (c) and $p = 1$ (d). The influence of the autocatalytic efficiency $\varepsilon$ is shown in (e) for $p = 0.5$ and in (f) for $p = 1$. The rate constant is set to $k = 1 \times 10^{-6}$ M $s^{-1}$ for the bimolecular reaction and $k = 1$ M $\times$ $s^{-1}$ for the autocatalytic reaction for the simulation for (a), (b), (c) and (d). For (e) and (f) the reaction rate for the bimolecular reaction was varied, while the rate for the autocatalytic reaction was kept constant. Adapted from reference 26.

### 1.2.4 Examples of Artificial Self-replication

In 1986, von Kiedrowski published[36] the first example of a non-enzymatic self-replicating system. This system involves a self-complementary palindromic hexadeoxyribonucleotide template **14**, which is protected on the 5´ and 3´ ends. Two trideoxyribonucleotides, one protected on the 5´ end, the other on the 3´ end, can associate on the template, to form the ternary complex [**12**·**13**·**14**]

(**Scheme 1.3**). The condensation reaction between the unprotected hydroxyl on **13** with the unprotected phosphate on **12** forms the product duplex [**14·14**]. After dissociation of the product duplex, two template molecules are returned to the solution. Von Kiedrowski studied the autocatalytic properties of this template and concluded that it clearly exhibits autocatalytic behaviour, $p = 0.48$, and this system obeys the square root law.

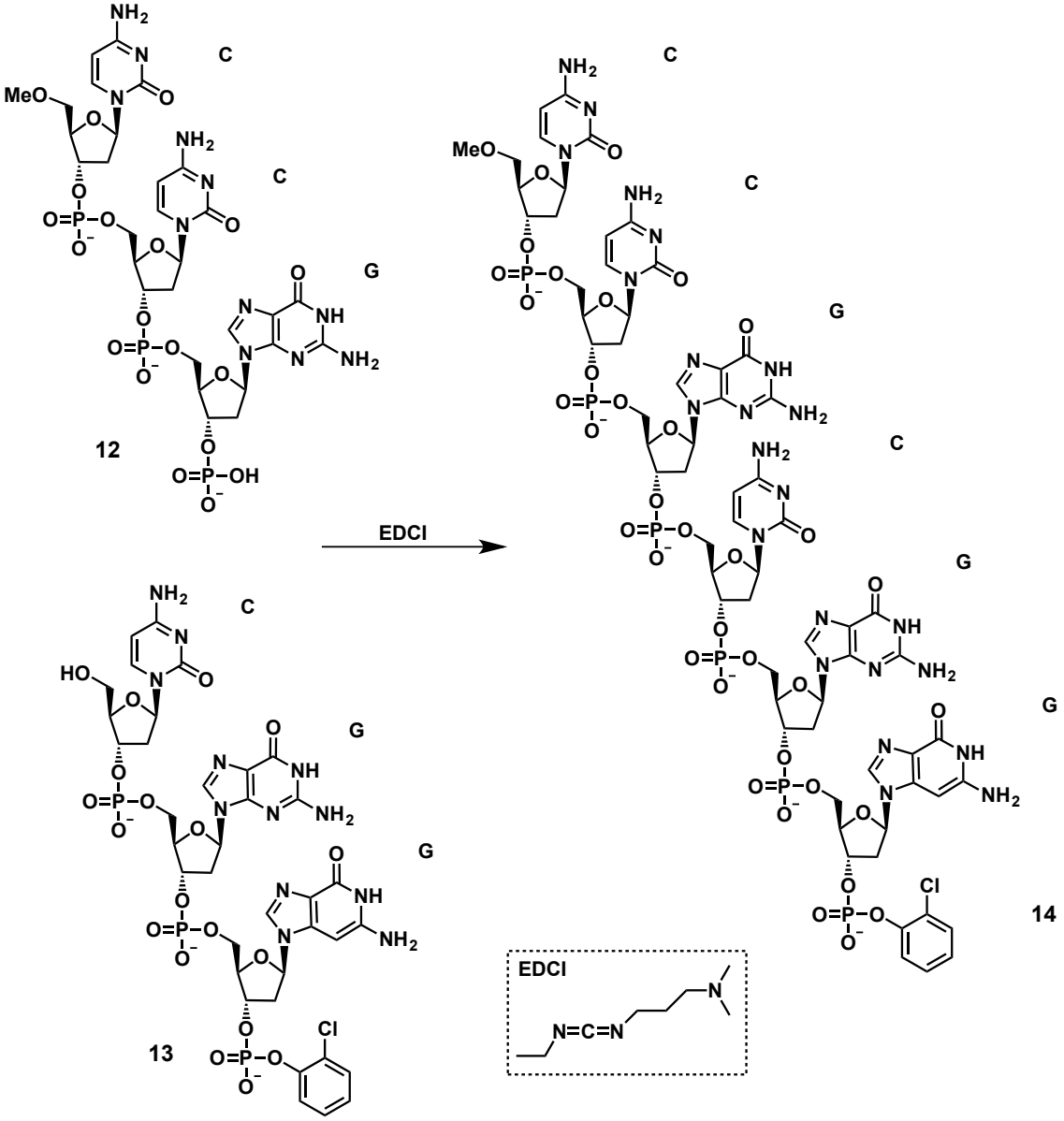


**Scheme 1.3:** The palindromic hexadeoxyribonucleotide **14** can function as a template for its own formation from building blocks **12** and **13**. Taken from reference 36.

The first example of a self-replicating system that was not based on biomolecules, was published[37] by Rebek and co-workers in 1990. The Rebek group developed a system based on the amide coupling reaction between an

amino adenosine, **15**, and a Kemp's triacid derivative, **16**, (**Scheme 1.4**). The starting materials contain complementary recognition sites in which the recognition event is based on hydrogen bonding between the two molecules. The importance of the recognition site was demonstrated by the fact that the reaction proceeds 10 times slower when the imide is *N*-methylated, which blocks the recognition site. The system reported by Rebek and co-workers involves three reaction channels, which is characteristic for self-replication. According to Rebek *et al.* the [**A·B**] channel forms *cis* amide **18**, which is catalytically inactive. However, the *cis* amide can undergo isomerisation to form the *trans* product **17**, which is catalytically active as a self-replicator. Autocatalysis in this system is confirmed by the fact that the reaction proceeds >40% faster when pre-formed template **17** is added.

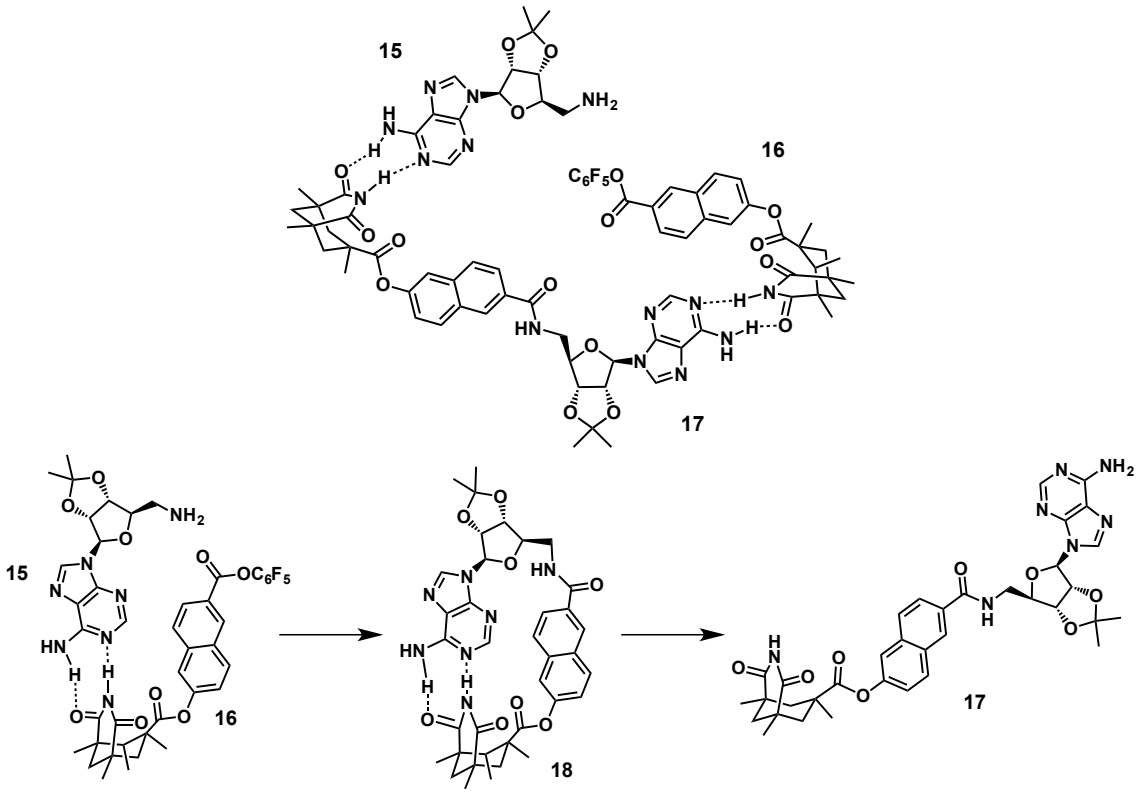


**Scheme 1.4:** Top: The self-replicating system of Rebek *et al.* features an amide coupling reaction. The recognition takes place between an amino adenosine **15** and Kemp's triacid derivative **16**. Bottom: Most of the reaction reported by Rebek proceeds through the [**A·B**] channel forming *cis*-amide **18**, which can undergo an intramolecular isomerisation to afford the open *trans*-template **17**. Taken from reference 37.

Initially, the Rebek group focussed on a similar system using a phenyl spacer separating the triacid with the ester rather than a naphthalene spacer.[38] This

system was found to be recognition-mediated as *N*-methylation of the triacid reduces the reaction rate six times. However, rate acceleration in this system was not achieved as a result of self-replication but the reaction proceeded through the [**A**·**B**] channel and resulted in the inactive compound, which is folded up on itself, which is the reason the Rebek laboratory explored the system with a naphthalene spacer rather than the shorter phenyl spacer.

In 1994, the Rebek system received criticism[39] from Menger *et al*. who suspected that the amide coupling reaction in the Rebek system was not accelerated through complex formation but rather relies on simple amide catalysis by the product. The capability of amides to stabilise the tetrahedral intermediate transition state, and thereby catalysing amide formation is well documented[40]. In an experiment in which a shorter alternative template was used, one that could not bind both starting materials at the same time, it was found that this template accelerated the formation of template as well. Other amides were also shown to accelerate the reaction, thus suggesting Rebek's claims that their system was self-replicating were premature. However, the conditions of Menger's experiments did not resemble those of Rebek's and it is found that amide catalysis is only relevant at higher concentrations than those used in the Rebek system.[41] Menger and co-workers also illustrated that the amide coupling in Rebek's system is catalysed in a non-hydrogen bonding system, leading them to conclude that the system is autocatalytic but not self-replicating.[42] The Rebek group responded[43] by stating that the template's ability to catalyse other reactions, apart from the self-replicating reaction, does not mean that the original system is not self-replicating.

Based on the controversy around the Rebek system, in 1996, Reinhoudt *et al.* published[30] a kinetic analysis of the system. This analysis shows a more complex picture of the system than the one that was suggested in the original publication. Reinhoudt and co-workers suggest that there are five different reaction channels rather than three, as was suggested by Rebek. In addition to the bimolecular reaction, the reaction through the ternary complex and the [**A**·**B**]

pathway, the reaction can proceed through a pathway in which the amine is associated to the template but the ester is not and finally a pathway in which the ester is hydrogen bonded to the template but the amine is not. Reinhoudt and co-workers argued that the relative contributions of the pathways to the rate of product formation are concentration dependent. At high concentrations, the flux through the pathway in which the amine is associated and the ester is not, increases. This research illustrates that a system that looks relatively simple at first, can turn out to be rather complicated.

Already in 1991, Rebek redesigned[44] the system and replaced the naphthalene spacer with a biphenyl spacer in order to prevent flux through the [**A·B**] pathway as shown in **Figure 1.10**. The concentration *vs*. time profile for this reaction shows a characteristic sigmoidal curve and autocatalysis was proven by addition of the template to the initial reaction mixture, which accelerates the reaction two times. However, the authors conclude that the system suffers from significant product inhibition as at 25% completion, 97% of the formed template is present as template duplex [**T·T**].

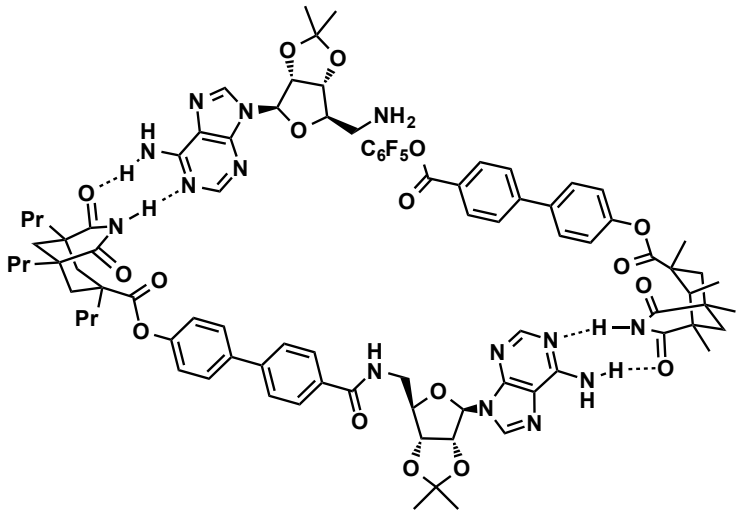

**Figure 1.10:** Rebek *et al.* redesigned their system in order to increase flux through the self-replicating pathway relative to the [**A·B**] channel. Taken from reference 44.

In 1992, von Kiedrowski also published[45] a self-replicating molecule that is not based on natural compounds. In this system, the reaction is based on imine

formation between an aniline derivative **19** and a benzaldehyde derivative **20** (**Scheme 1.5**). The recognition is provided by association of an amidinium group on the amine bearing molecule and a carboxylate on the benzaldehyde derivative that, upon association, form an amidinium-carboxylate salt bridge. Autocatalysis is present in this system in the formation of **21a** with an autocatalytic efficiency, $\varepsilon$, comparable to the Rebek system in **Scheme 1.4** and with the earlier von Kiedrowski system in **Scheme 1.3**. Additionally, there is also a cross catalytic reaction present in this system. The reaction of **19a** and **20a** affords template **21c**, which is able to catalyse the formation of **21b** from **19b** and **20b**. Interestingly, the reaction order, *p*, for the formation of the template was found to be first order. This example is the first that shows that exponential amplification is feasible in a self-replication system, even though the system is strictly speaking not self-replicating as there is cross catalysis rather than autocatalysis.

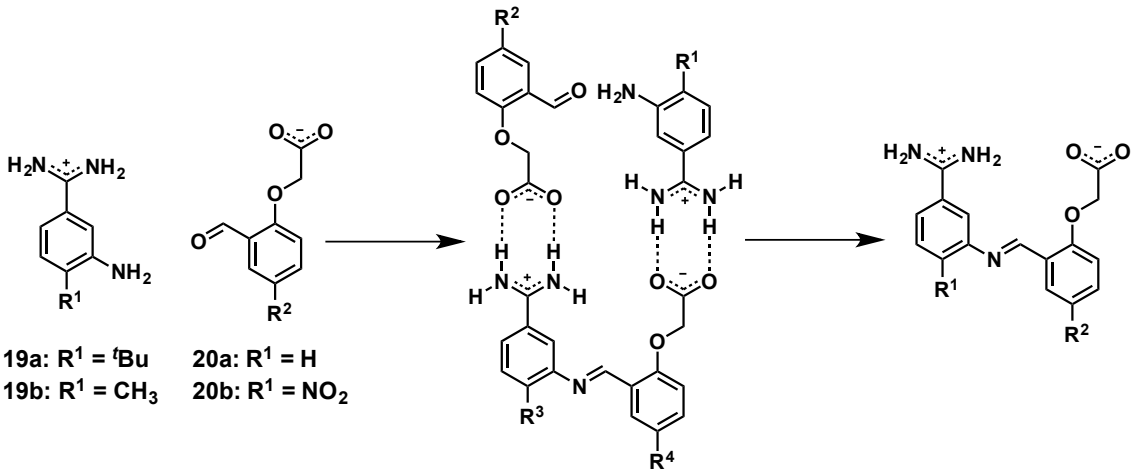

**19a:** $R^1 = {}^t\text{Bu}$ **20a:** $R^1 = H$
**19b:** $R^1 = CH_3$ **20b:** $R^1 = NO_2$

**21a:** $R^1 = {}^t\text{Bu}$, $R^2 = NO_2$
**21b:** $R^1 = CH_3$, $R^2 = NO_2$

**Scheme 1.5:** The system by von Kiedrowski *et al.* involves the formation of an imine. Recognition takes place in an amidinium-carboxylate salt bridge. Adapted from reference 45.

In 1997, Wang and Sutherland reported[46] a self-replicating system based on a Diels-Alder reaction between maleimide **22** and a cyclohexadiene **23**, which undergo a Diels-Alder reaction to form template **24**. Recognition takes place between an amidopyridone on the maleimide and an amidonaphthyridine on the

cyclohexadiene (**Figure 1.11**). Wang and Sutherland concluded that their system showed nearly exponential growth, $p = 0.8$.

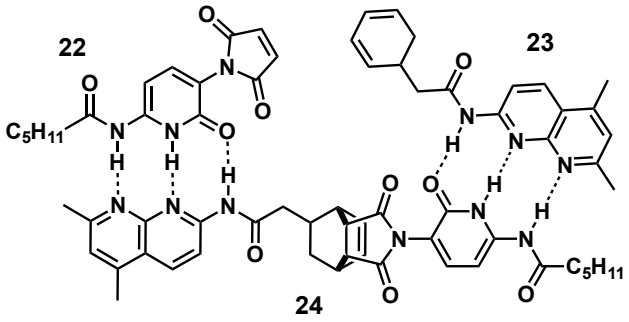


**Figure 1.11:** The system published[46] by Wang and Sutherland involves a Diels-Alder reaction. The recognition takes place by an amidopyridone and an amidonaphthyridine. Taken from reference 46.

The level of complexity of the system described by Wang and Sutherland is further increased by the fact that the cycloaddition can lead to the formation of four different cycloadducts. First of all, the Diels-Alder reaction between **22** and **23** produces an *exo*- and an *endo*-cycloadduct, the authors assume the products in their system have *endo*-stereochemistry. The chiral centre in the cyclohexadiene ring is still present in the products of the reaction and therefore there is the possibility for autocatalysis by one or both diastereoisomers or cross catalysis by one or both diastereoisomers. Unfortunately, Wang and Sutherland do not report the stereochemistry of the products. However, in 2005 the von Kiedrowski laboratory investigated[47] the stereochemical contributions to the Wang and Sutherland system. The authors adapted the system slightly (**Figure 1.12**) and proved there was no formation of the *exo*-cycloadduct. Furthermore, their kinetic model indicated that their system also showed exponential growth, $p = 0.89$ for the enantiomerically pure template and $p = 0.9$ for the racemic template. The authors also investigated the contribution of autocatalytic and cross catalytic pathways to the system. Addition of 10 mol% of (*R*)-template to the system illustrated that this template is autocatalytic and cross catalytic for the formation of the (*S*)-template. In addition they studied the system computationally in order to find out what causes the exponential behaviour in the system. Their conclusion is that it does not depend on the transition state leading to the product but rather the ground state of the product duplex that is unstable after covalent bond formation. This result confirms,

computationally, the conclusion in the paper by von Kiedrowksi on kinetics of self-replicating systems.[35]

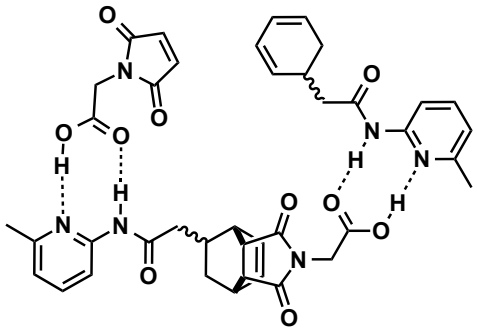

**Figure 1.12:** Von Kiedrowski *et al*. adapted[47] the system reported[46] by Wang and Sutherland and studied the contributions of different cross catalytic and autocatalytic pathways in the system. Taken from reference 47.

The Diels-Alder reaction, and cycloadditions in general, are attractive bond forming steps in self-replicating systems as the reaction is self-contained, all atoms in the starting materials are present in the products, and therefore no by-product is generated.[48] In the Philp laboratory, a Diels-Alder reaction between maleimide **27** and furans **25** and **26** has been studied as the bond-forming step in a self-replicating system.[49] The furan, which reacts as diene, is equipped with an amidopyridine recognition site, and maleimide **27**, reacting as dienophile, is equipped with a carboxylic acid recognition site (**Scheme 1.6**). The difference in the length of the alkyl spacer between the reactive site on each compound and the recognition site generates variation in this family of self-replicators. Additional variation is obtained by using a 2-functionalised furan **26** or a 3-functionalised furan **25**. The products of the Diels-Alder cycloaddition can have *endo* or *exo* stereochemistry. The Philp laboratory investigated the self-replicating potential of all these compounds and concluded that more conformational freedom in the molecules causes the compounds to react through the [**A**·**B**] pathway. Only when conformational freedom is limited and the template is forced in the open conformation, self-replication is observed. Furthermore, the position in which the furan was functionalised determined to a large extent the relative formation of *endo* and *exo* products.

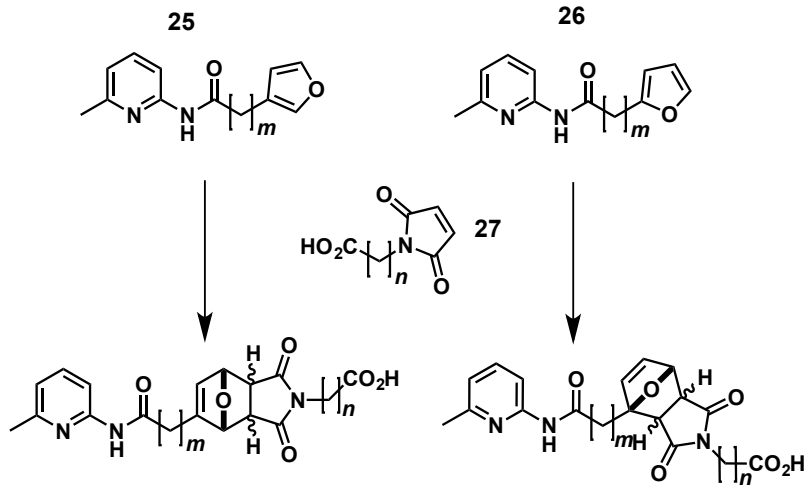


| | 3-functionalised furan | | 2-functionalised furan | |
|---|---|---|---|---|
| | $n = 1$ | $n = 2$ | $n = 1$ | $n = 2$ |
| $m = 1$ | *endo*: SR<br>*exo*: SR | *endo*: AB<br>*exo*: – | – | *endo*: SR<br>*exo*: AB |
| $m = 2$ | *endo*: AB<br>*exo*: – | *endo*: AB<br>*exo*: AB | *endo*: –<br>*exo*: AB | *endo*: –<br>*exo*: AB |

**Scheme 1.6:** The Philp laboratory investigated[49] a series of compounds to study their autocatalytic potential. Subtle structural changes can lead to remarkably different behaviour. AB = reaction proceeds predominantly through the AB complex pathway. SR = reaction proceeds predominantly through the self-replicating pathway. – = no recognition mediated reaction was observed. Adapted from reference 26.

The Philp laboratory proceeded by investigating the system with the recognition sites on the opposite reagent.[50] The amidopyridine recognition site was placed on maleimide **30** and furans **28** and **29** were appended with the carboxylic acid recognition site (**Scheme 1.7**). Interestingly, in this system only the template that is made up from 3-functionalised furan **28**, is able to perform as a self-replicator, and only when at least one of the spacers is the longer spacer. All the other compounds are either not reactive in a recognition-medatied fashion or the reaction proceeds predominantly through the [**A**·**B**] pathway. The work by the Philp group on these two families of replicators based on a Diels-Alder reaction shows that systematic investigation into structural changes in replicators can lead to the discovery of interesting structure-function relationships that are not predictable.

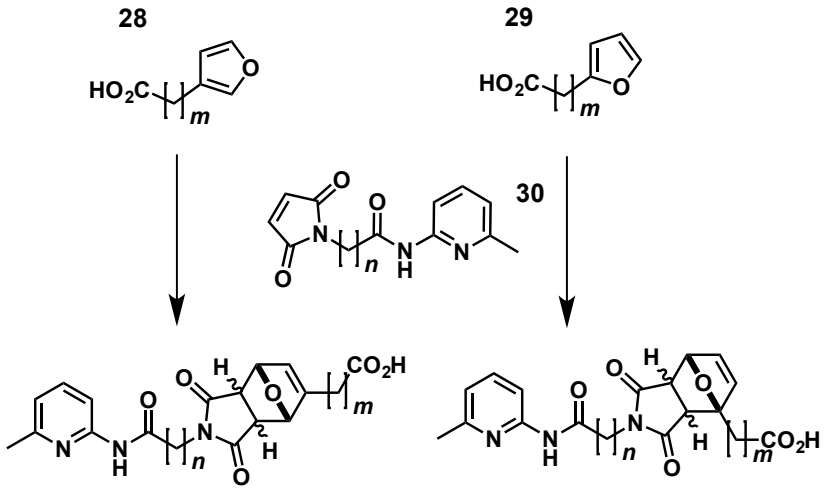


| | 3-functionalised furan | | 2-functionalised furan | |
|---|---|---|---|---|
| | *n* = 1 | *n* = 2 | *n* = 1 | *n* = 2 |
| *m* = 1 | – | *endo*: SR<br>*exo*: SR | – | – |
| *m* = 2 | *endo*: SR<br>*exo*: SR | *endo*: SR<br>*exo*: SR | *endo*: –<br>*exo*: AB | *endo*: –<br>*exo*: AB |

**Scheme 1.7:** The Philp laboratory investigated the compounds with recognition site on the opposite reagents relative to the system in **Scheme 1.6**. Subtle structural changes can lead to remarkably different behaviour. AB = reaction proceeds predominantly through the AB complex pathway. SR = reaction proceeds predominantly through the self-replicating pathway. – = no recognition mediated reaction was observed. Adapted from reference 26.

In similar research, members of the Philp laboratory were able to demonstrate[51] that another cycloaddition reaction can be employed in a self-replicating system. Azide **31** was equipped with an amidopyridine recognition site and maleimide **32** with a carboxylic acid recognition site. The compounds were allowed to react at 30 °C at a concentration of 25 mM in $CDCl_3$ (**Scheme 1.8**). The rate of formation of template **33** is significantly higher when maleimide **32** is equipped with the carboxylic acid as opposed to the methyl ester, thus providing evidence for a recognition-mediated reaction. Additionally, when the reaction was carried out in the presence of preformed template **33** the reaction rate increased. An autocatalytic cycle only works when the template duplex [**T**·**T**] dissociates after the reaction to return template molecules back to the solution. A stable duplex leads to product inhibition and prevents turnover of the catalyst. The Philp group investigated the template by kinetic simulation and fitting of the

kinetic data and obtained an autocatalytic reaction order, *p*, of 0.4 and an autocatalytic efficiency, *ε*, of 20. These results strongly suggest that the template forms a stable duplex, [**T·T**], and that dissociation of this duplex is rate limiting in this system. This made the authors conclude that the azide based system is self-replicating but not autocatalytic.

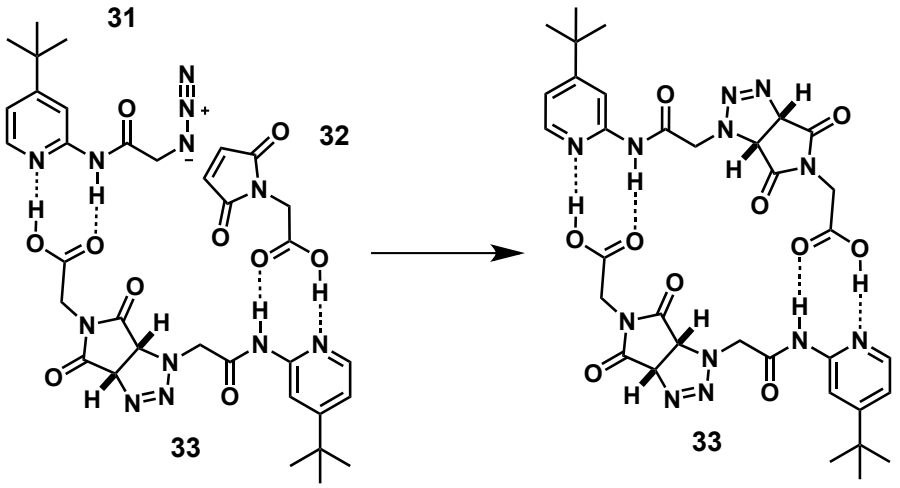


**Scheme 1.8:** The Philp group investigated a self-replicating system based on a 1,3-dipolar cycloaddition between an azide (**31**) bearing a amidopyridine recognition site and a maleimide (**32**) bearing a carboxylic acid recognition site. Taken from reference 51.

Another cycloaddition that was used in the Philp laboratory in a self-replicating system was the 1,3-dipolar cycloaddition between maleimide **32**, as dipolarophile, and nitrone **34** as 1,3-dipole (**Scheme 1.9**).[52,53] Similar to the Diels-Alder reaction, this reaction also forms two products, cycloadduct *cis*-**35** in which the hydrogens on the newly formed heterocycle are on the same face and cycloadduct *trans*-**35** in which the hydrogen atoms on the newly formed heterocycle are on opposite faces. Nitrone **34**, equipped with an amidopyridine recognition site and maleimide **32**, equipped with a carboxylic acid recognition site are allowed to react at 10 °C at a concentration of 25 mM in $CDCl_3$ (**Scheme 1.9**). The carboxylic acid and amidopyridine recognition sites of both compounds can associate through hydrogen bonding. The recognition-disabled reaction, in which the carboxylic acid is blocked as the methyl ester, reaches only 17% conversion after 16 hours with a *cis*:*trans* ratio of 1:4. In the recognition-mediated reaction, the rate of formation of *trans*-**35** increases in

comparison to the recognition-disabled reaction. Additionally, the rate profile exhibits a sigmoidal shape, characteristic of autocatalytic reactions. When an amount of pre-formed *trans*-**35** is added to the reaction mixture, acceleration of the reaction rate at $t = 0$ is observed in the formation of the same product, thus providing evidence for the autocatalytic nature of the reaction. Interestingly, addition of *cis*-**35** does not accelerate formation of the same (or other) products and this compound is therefore not autocatalytic nor cross catalytic. The authors conclude that the *trans* template is a "selfish autocatalyst" since it catalyses its own formation but not that of the diastereoisomer.

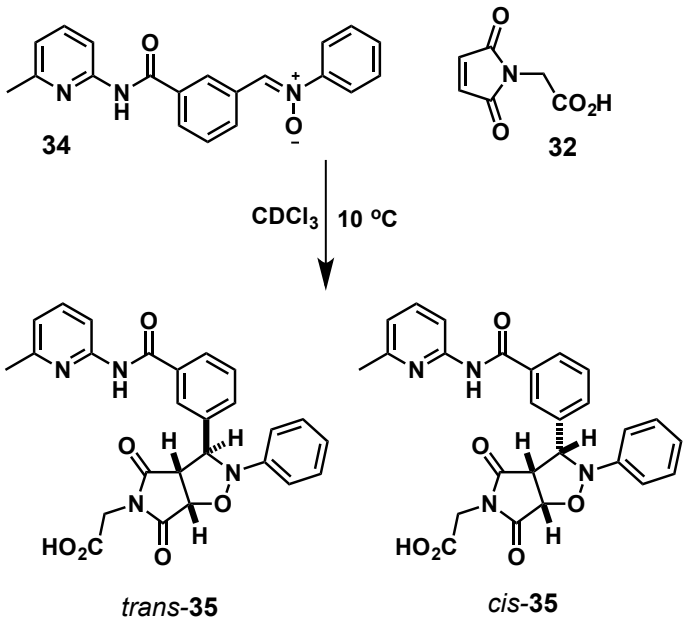


**Scheme 1.9:** The Philp group has explored a self-replicating system based on a 1,3-dipolar cylcoaddition between maleimide **32** and nitrone **34**. Recognition is facilitated by an amidopyridine and a carboxylic acid recognition site. Taken from reference 52.

### 1.2.5 Reciprocal Replication

A second class of replicating molecules are reciprocal replicators[26] (**Figure 1.13**); the most well known example of which is DNA. DNA is not a self-complementary molecule; it consists of two different strands, which are complementary, but not identical to each other. **Figure 1.13** shows a schematic representation of a reciprocal replication network in which building blocks **C** and **D** can react through the bimolecular pathway to form template $\mathbf{T_{CD}}$ and building

blocks **E** and **F** can react in a bimolecular way to form template $\mathbf{T_{EF}}$. In contrast to self-replication, the two templates are not able to assemble the building blocks needed for their own formation but they can associate the building blocks needed for the formation of the other template. In other words, template $\mathbf{T_{EF}}$ catalyses the formation of $\mathbf{T_{CD}}$ and *vice versa*. Note that in contrast with a self-replicator, a reciprocal replicator bears the same recognition site twice, rather than the two complementary recognition sites.

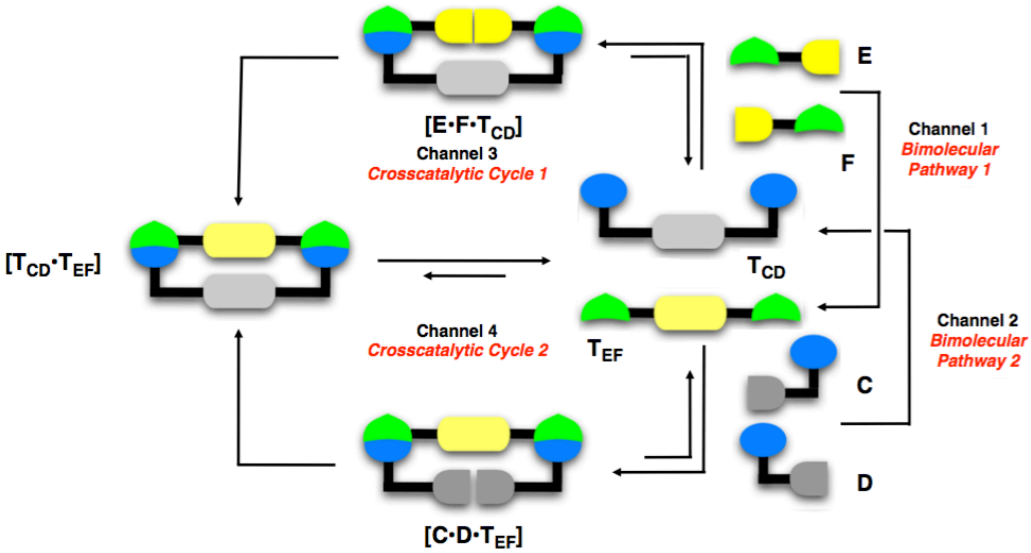


**Figure 1.13:** In reciprocal replication, **C** and **D** can react to form template $\mathbf{T_{CD}}$ and **E** and **F** can react to form $\mathbf{T_{EF}}$. These templates are cross catalytic since they bear complementary recognition sites. This means $\mathbf{T_{EF}}$ can catalyse the formation of $\mathbf{T_{CD}}$ by associating the relevant building blocks and *vice versa*.

Reciprocal replication is most well known in natural examples such as DNA and RNA replication.[54] Examples of artificial reciprocal replicators have been reported by Kelly[55] and Rebek[56]. The Philp laboratory has also worked on the development of reciprocal replicators by combining the nitrone-based self-replicator and the Diels–Alder based self-replicator (**Scheme 1.10**).[57] In this system it was found that addition of template *exo*-**43** to the 1,3-dipolar cycloaddition between maleimide **37** and nitrone **36** increases the rate of formation of *trans*-**42**. Similarly, addition of template *trans*-**42** to the Diels-Alder reaction between maleimide **38** and furan **39** increases the rate of formation of template *exo*-**43**. Additionally, nitrone **36** and maleimide **38** can react to form

the autocatalytic template *trans*-**40** and the reaction between furan **39** and maleimide **37** forms the autocatalytic template *exo*-**41**.

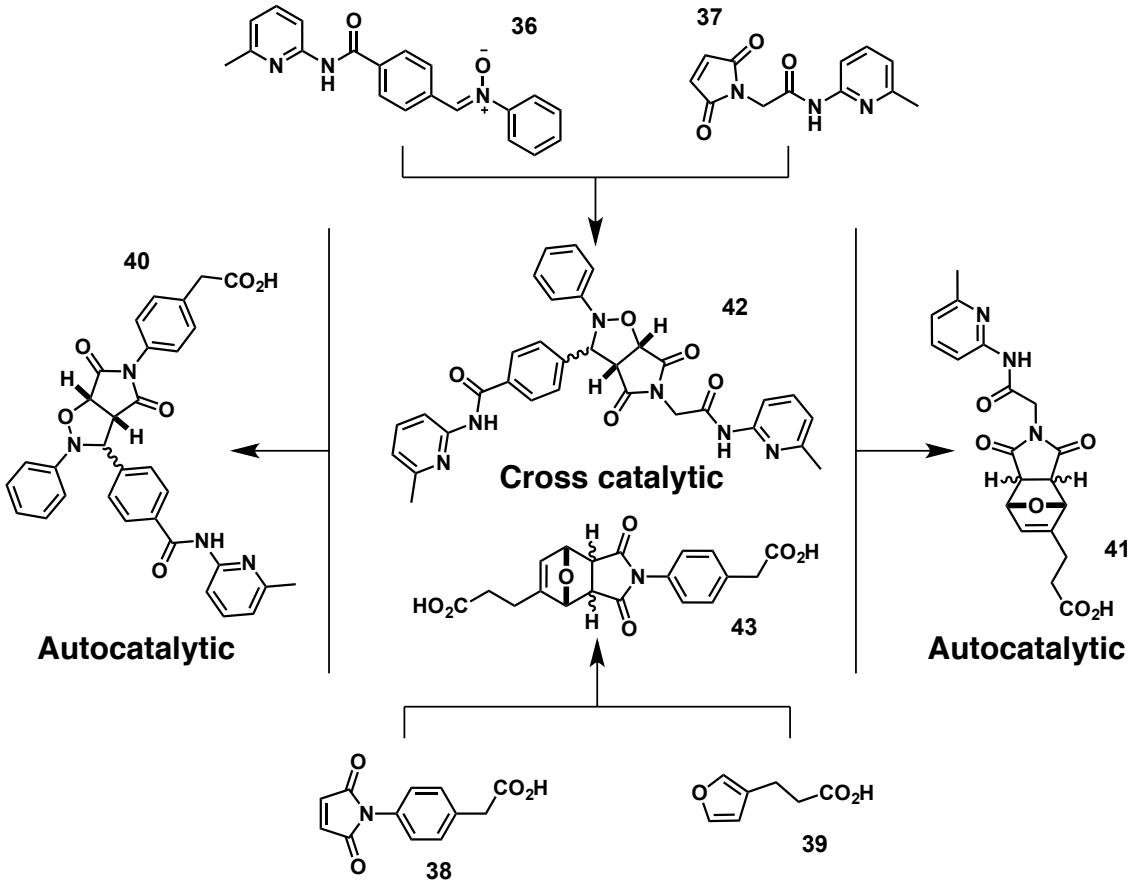


**Scheme 1.10:** The Philp group investigated the cross catalytic and autocatalytic potential of a number of replicators. Taken from reference 32.

## 1.3 Systems Chemistry: the Need for a Systems Level Approach

In biology, a systems level approach is being used in the field called systems biology. Systems biology is an inter-disciplinary science that aims to unravel the interplay of genomics, proteomics and metabolomics, which leads to the emergent properties observed in living organisms. In general, systems biology aims to explain how interactions between the molecular entities of the system are able to maintain a living organism.[58] A systems biologist tries to get insight in these properties of a system; structures (metabolic pathways, gene interactions), dynamics (how the system changes over time), control

mechanisms. A systems level approach has become increasingly popular in biology the past decade.[59] An organism is amazingly complex as there are many different levels that are interacting with each other. The genome is transcribed into RNA, which is translated into proteins, which bring us to the level of proteomics. The proteins are responsible for controlling the chemical reactions in the cell and receive feedback from the products and reactants of the reactions they catalyse. All these different levels, genes, proteins, metabolism, interact with each other and exhibit regulatory pathways to influence each other. In biology the study of complex systems has become possible due to technological advances such as high-throughput measurements and genome sequencing.

Traditionally, research in synthetic chemistry has focussed on observing chemical reactions in isolation. This was a requirement, mainly for the reason that mixtures are difficult to analyse. As analytical tools available to chemists develop, it has become more and more feasible to study mixtures of many molecules, which has led to the emergence of a new field known as systems chemistry.[60] Systems of molecules can give rise to new behaviour that will not be observed when studying single species of molecules in isolation. One can, for example, envisage a system in which different reactions take place at the same time, perhaps compete for starting material, and influence each other with positive or negative feedback loops. As in systems biology, systems chemistry takes a system level approach to study mixtures of molecules and derive properties of the system as a whole, which are brought about by the interactions of its parts. Examples of chemical systems include Dynamic Covalent Chemistry (DCC)[61], chemical waves[11,62], self-assembling systems[63], and self-replicators[25,26,28,47]. Although these systems are different, they share a number of important common features. First of all, apart from self-replicators, these systems tend to operate under thermodynamic control, although systems with an element of kinetic control have gained popularity. Secondly, non-covalent interactions are often employed to create molecular architectures.

### 1.3.1 Dynamic Covalent Chemistry

Mixtures of compounds are employed in chemical research in combinatorial libraries.[64] This type of research is widely used in the pharmaceutical industry for drug discovery. In this method a library of compounds is created and is added to an enzyme, for example. The compounds are, for example, studied for their ability to inhibit enzyme activity. One of the compounds in the library will bind the strongest to the enzyme and will be the strongest inhibitor for its activity. Further analysis will identify this one compound. Combinatorial chemistry is therefore an efficient way to test many compounds in a single experiment.

Supramolecular chemistry focuses[65] on the formation and breaking of non-covalent interactions. Non-covalent interactions operate under thermodynamic control and therefore their formation is reversible. This feature presents interesting opportunities such as error-correcting abilities. The drawback of supramolecular interactions is the fact that they are much weaker than covalent bonds. Inspired by combinatorial libraries, in which a large number of compounds can be accessed at the same time, and the reversible bond formation in supramolecular chemistry, chemists have started to study the formation of libraries through reversible covalent bonds. Dynamic Covalent Chemistry (DCC)[61] is the field that studies the opportunities that arise from using reversible covalent bonds.

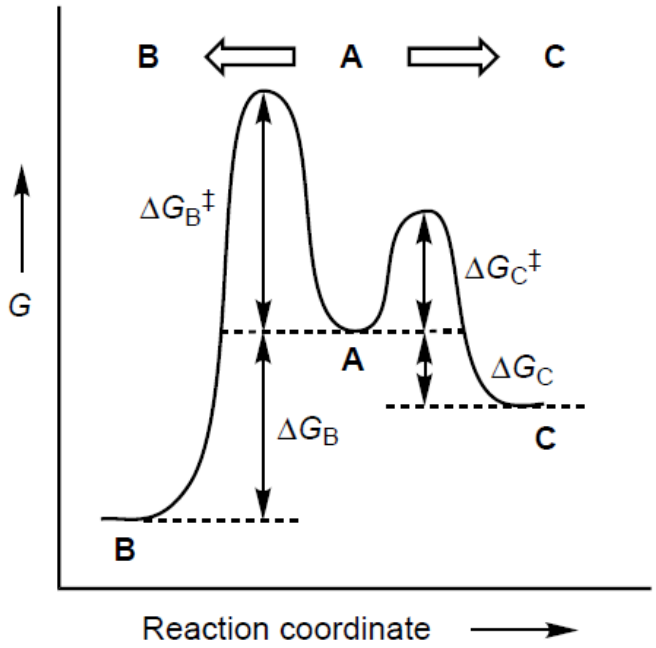


**Figure 1.14:** When a reaction takes place under kinetic control, product C is formed because $\Delta G^{\ddagger}$ is the most favourable. The thermodynamically controlled pathway leads to the product with the most favourable $\Delta G$, so product B is formed. Taken from reference 61c.

When a reaction is allowed to take place under thermodynamic control, the product distribution is determined by the relative stabilities of the possible products (**Figure 1.14**).[66,61c] If a mixture of compounds is allowed to equilibrate under thermodynamic control, it gives rise to a composition determined by thermodynamic factors. An example of DCC is the creation of circular helicates by Lehn and co-workers under thermodynamic control.[67] A chain with three bipyridine ligands connected by bismethylene linkers. The bipyridine ligands coordinate with the $Fe^{2+}$ metal centres. Under thermodynamic control a mixture of different sized cyclic helicates is constructed (**Figure 1.15**).

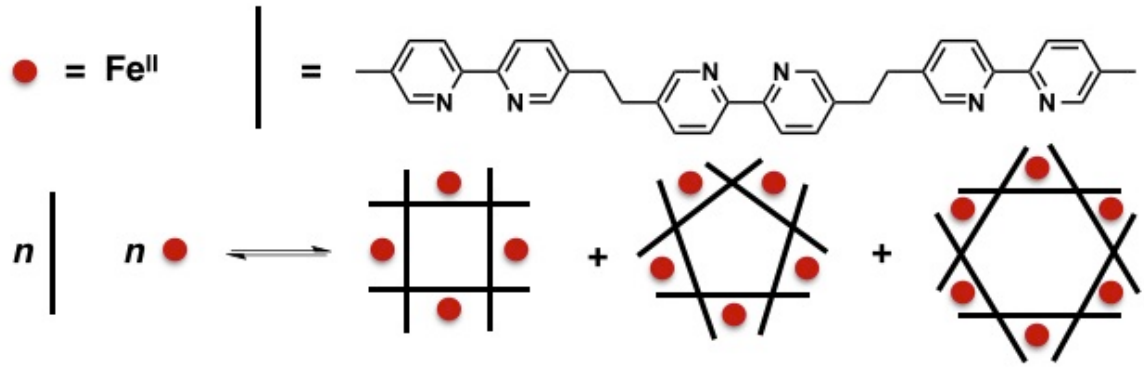


**Figure 1.15:** Lehn and co-workers reported the formation of a mixture of circular helicates formed by Iron ions and bipyridine ligands. Adapted from reference 67.

A mixture of compounds under thermodynamic control is called a Dynamic Combinatorial Library.[61f] The difference between a DCL and conventional combinatorial chemistry is that in a DCL, library members are in a dynamic equilibrium and can therefore interconvert. The library members in Combinatorial Chemistry experiments are synthesised using traditional synthetic steps under kinetic control. A library of compounds under thermodynamic control can respond to a change in conditions. The library depicted in **Figure 1.15**, consisting of circular helicates can respond to a change in conditions. An anion can function as a template to amplify one of the helicates relative to the other. Interestingly, when $Cl^-$ is added to the library, the pentamer library member is formed preferentially and when $SO_4^{2-}$ is added, the hexamer library member is formed preferentially.[67] The addition of a template as a tool for selection of a library member from a DCL is often used.[61f] Two ways of templating can be distinguished: casting and molding (**Figure 1.16**).[68,61b] In casting, the library members associate to a template in a similar way a substrate would to an enzyme, it would bind in the cavity. Molding is the type of binding in which library members form a structure around a template in a similar way as a crown ether is synthesised around a cation.

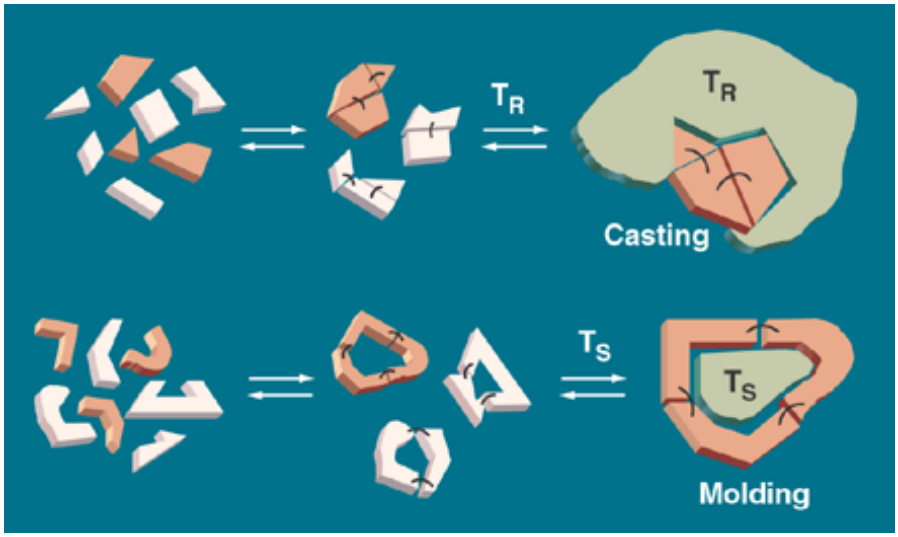


**Figure 1.16:** There are two forms of templating possible in a DCL. Casting involves the association of library members in a cavity on the template in a similar way a substrate would bind an enzyme. Molding involves the formation of a structure around the template. Taken from reference 61b.

As discussed previously, when a template is added to the DCL the equilibrium shifts. The shift of the equilibrium is a result of the fact that the library members have different affinities for the added template. The library will re-equilibrate to harvest binding energy from the favourable interaction between the template and the library member, and therefore the strongest binder should be produced at the expense of other library members. This principle could be used to find strong binders to a template from a large collection of compounds by looking for the compound that is mostly amplified. In reality, however, the strongest binder is not always the one that is amplified most strongly.[69-72]

Severin[70], along with others[69,71], has simulated different types of DCLs (**Figure 1.17**) in order to obtain information on the change in library composition upon addition of an external template. In all cases Severin found that not necessarily the best binder is amplified, it is even possible that the concentration of the best binder decreases. For example in a DCL where trimers, tetramers, pentamers etc. are formed from a single building block (**Figure 1.17, Type A**), library members consisting from a smaller number of building blocks are intrinsically favoured entropically. DCLs in which tetramers are formed from three different building blocks (**Figure 1.17, Type B**), the tetramer that consists of three different building blocks is inherently favoured, also for entropic reasons. A way

to overcome this problem in the latter type of DCL is to design library members that need a spacer to form (**Figure 1.17, Type B***). Severin found that when a low concentration of spacer is used, with respect to building blocks, the library member with highest affinity is amplified even if it is entropically disfavoured. These features of DCLs make it more difficult to identify the strongest binder to a template in a DCL, because the binder present in highest concentration might be there for other reasons than a high association constant to the template.

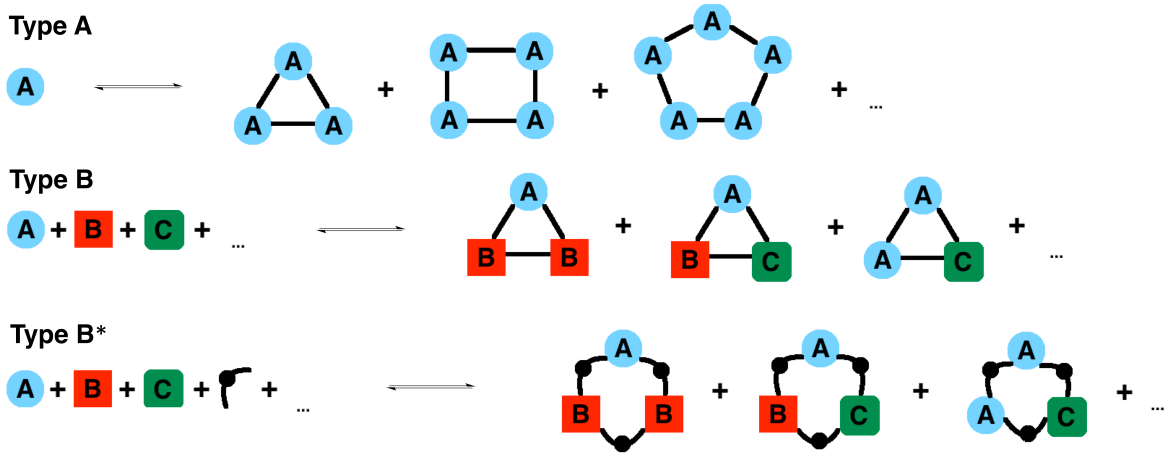


**Figure 1.17:** Severin modelled different types of DCLs. In type A, different sizes of macrocyles are formed from the same building block. In type B trimers are formed from three diferent building blocks. Type B* involves a DCL in which three building blocks associate with a spacer. Adapted from reference 70.

A general conclusion from these modelling studies is that a DCL will, upon addition of an external template, change the composition of the library in order to minimize the free energy of the system. This means that when a DCL is able to harvest a lot of moderately favourable binding energy rather than a small amount of highly favourable binding energy it is possible the first option will happen. Therefore, the best binder to the template is not necessarily amplified from the library mixture.

The theoretical observation that the strongest binder is not necessarily the one that is amplified, was illustrated experimentally for the first time by Corbett *et al.*[72] The authors reported the formation of a DCL based on disulfide formation between dithiol building blocks **44** and **45**. The major constituents of this DCL are heterotrimer **47** and homotrimer **48**. Separate binding studies indicated that

homotrimer **48** was the best binder for the ammonium template **46** (**Scheme 1.11**).

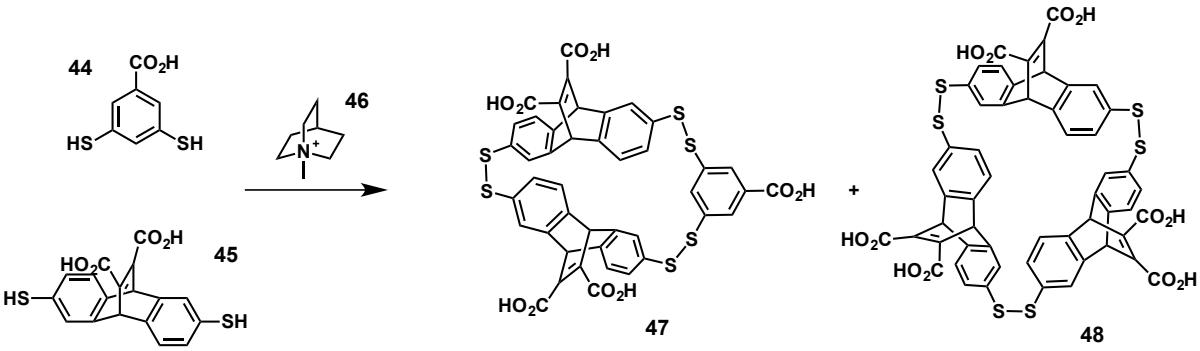


**Scheme 1.11:** A Dynamic Covalent Library is created from two building blocks. The major constituents are two macrocycles **47** and **48**. After addition of ammonium template **46** the heterotrimer is ampflified while the homotrimer is the best binder. Adapted from reference 72.

Upon addition of high concentration of ammonium template **46**, however, the heterotrimer **47** was amplified. The reason for the DCL to amplify the library member with lower affinity for the template originates from the fact that heterotrimers are intrinsically favoured over homotrimers because with a certain amount of building blocks more heterotrimers can be made and therefore more complexes to harvest the binding energy between the library member and the template. When low concentration of the ammonium template was added, however, this advantage is avoided and the homotrimer, the strongest binder, was amplified. The theoretical and experimental observation that the best binder in DCLs is amplified at low concentration is general.[72] In order to identify the strongest binder in a DCL two experiments should be carried out: one at stoichiometric template concentrations, if an effect is observed, template concentrations can be decreased and the strongest binder might be amplified in the latter experiment.

A final thing to note about DCLs is that amplification is a relative concept, the tightest binder of the template may be amplified most strongly but it may still be present only at low concentrations, depending on the concentrations prior to template addition.

Otto and co-workers also used a DCL in the search for a catalyst for a Diels-Alder reaction.[73] In this study, the product of the Diels-Alder reaction between **49** and **50**, **51**, is used as Transition State Analogue (TSA). Diels-Alder reactions have late transition states, which means that the transition state geometry resembles the product rather than the reactants.[66] A DCL was constructed using disulfide building blocks **44**, **45** and **52** in water (**Scheme 1.12**). Addition of TSA **51** changed the library composition so that macrocycles **47** and **48** were amplified. These compounds were assessed for catalytic activity and it turned out that one of the macrocycles was catalytically active and modestly accelerated the Diels-Alder reaction.

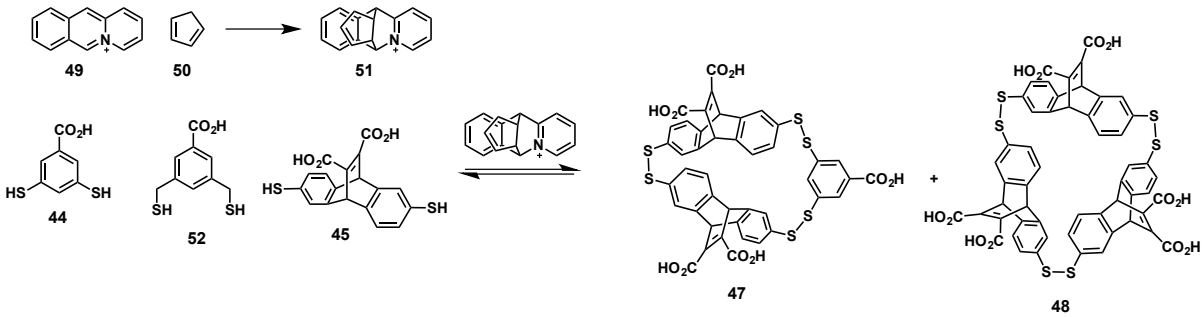


**Scheme 1.12:** Otto and co-workers used a dynamic library of macrocycles to identify a catalyst for a Diels-Alder reaction. It was found that the macrocycle that is amplified the strongest accelerates the Diels-Alder reaction. Adapted from reference 73.

### 1.3.2 Phase separation as a selection tool in DCLs

The Otto group also developed[74] a dynamic covalent system in which disulfide building block **53**, equipped with a peptide chain, was allowed to react to form cyclic disulfides **54** to **58** (**Figure 1.18**). It was observed that hexamer **57** and heptamer **58** were produced after stirring for 15 days. However, when shaking was used as mode of agitation, trimer **54** and hexamer **57** were produced. When no mode of agitation was used, trimer **54** and tetramer **55** were observed. The authors explain these observations by β-sheet formation between the library members, which leads to the formation of fibres. As soon as a cyclic disulfide is incorporated into a fibre, it is pulled away from the equilibrium and more is produced. Additionally, as the fibres grow they get more fragile and they can break, leading to more open ends in the solution, which in turn leads to

increasing fibre growth rate. In this system, the mode of agitation is also important. In an experiment in which a solution of disulfide building block is seeded with hexamer or heptamer, heptamer amplification is observed when the solution is not agitated or when stirring is used as mode of agitation. When the solution is shaken, equal formation of both cyclic disulfides is observed. Interestingly, in this system a combination of kinetic and thermodynamic controlled processes lead to the observed behaviour. The formation of macrocyles takes place under thermodynamic control but the incorporation of the library members into fibres is a kinetic trap, thereby irreversibly removing macrocyles from the interchanging DCL.

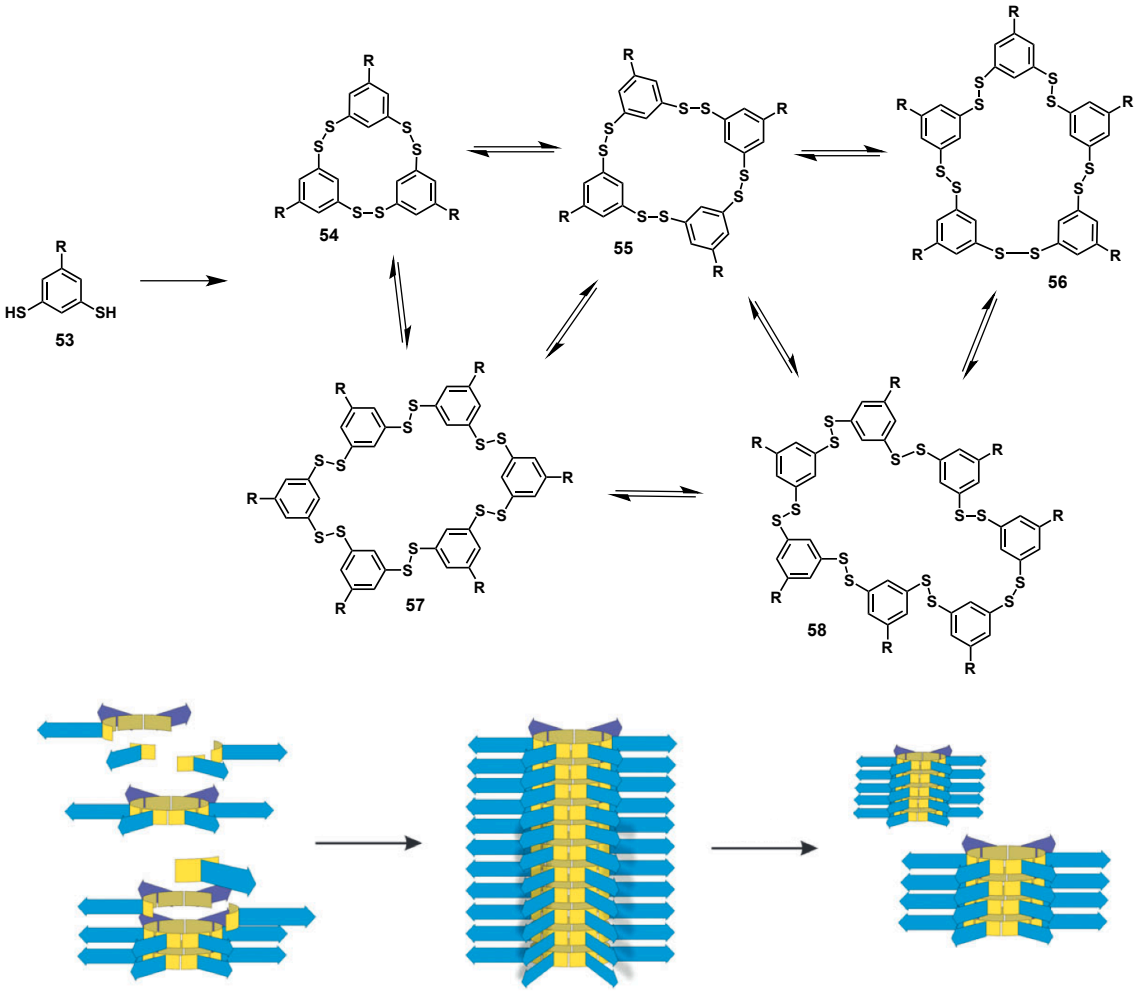


**Figure 1.18:** Otto *et al.* described a system in which building block **53** forms macrocycles of different sizes. Macrocycles **57** and **58** can form fibres through β-sheet formation of the amino acid side chains **R**. These fibres can break due to agitation and the more open ends there are in solution, the faster a fibre grows leading to selection of one of the macrocycles. Taken from reference 74.

Blackmond and co-workers reported[75] another example of phase separation coupled to a dynamic system. The dynamic system consisted of a chiral imine, in varying initial *ee*, which was equilibrated to form a solid-solution equilibrium (**Figure 1.19**). Subsequently, DBU was added to the solution, which causes the compounds in solution to racemise. When a crystal with single chirality is formed, this crystal can grow and use the compounds in solution to grow, which causes the solution equilibrium to shift. It was found that a small initial *ee* (2-3%) was required to achieve homochirality in the solid state. It was found that when the mixture was seeded with up to 10 mol% initial chiral compound, homochirality could be achieved more rapidly.

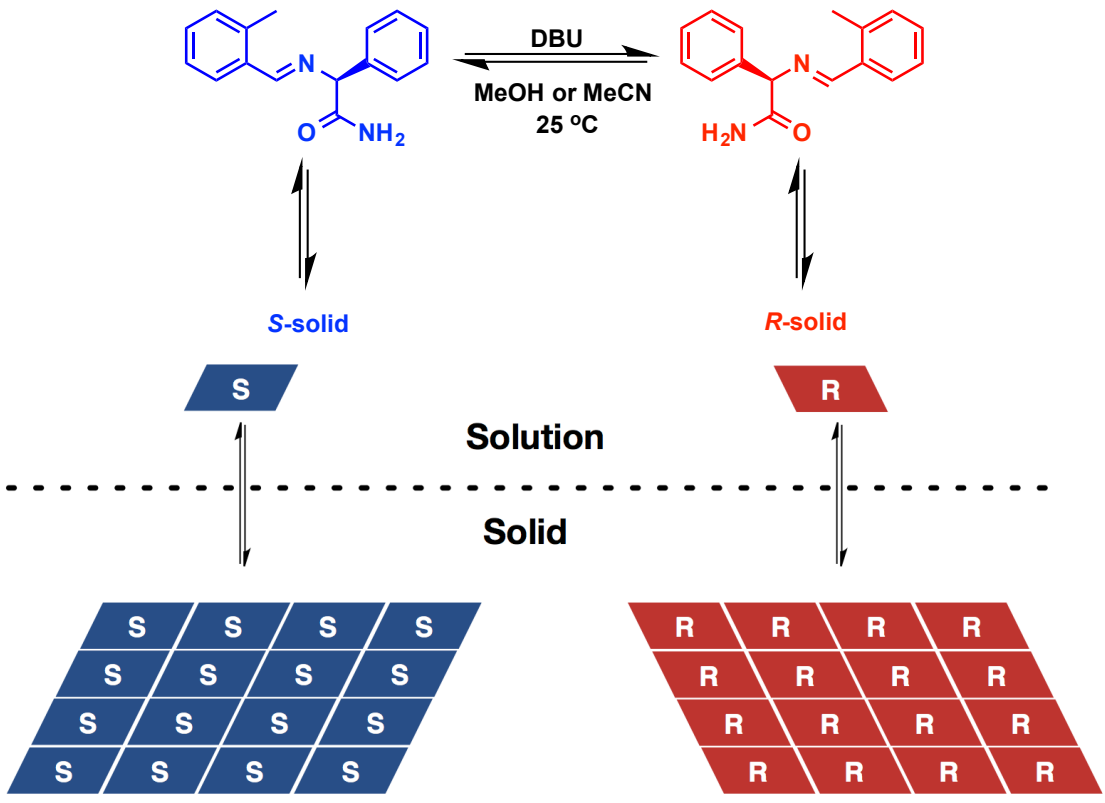


**Figure 1.19:** A small difference in initial *ee* can cause a complete shift to the formation of a single enantiomeric crystal. Adapted from reference 75.

### 1.3.3 Kinetic Selection in Dynamic Covalent Libraries

Selection strategies based on template association of library members are inherently limited by two factors.[76] First of all the concentration of template

added determines the proportion of the library members that is amplified and secondly the difference in association constant of the library members determines the level of amplification and selectivity that can be achieved. In order to overcome these limitations that are imposed by thermodynamic control it is attractive to use a kinetically controlled reaction step. Ramström and co-workers have introduced the term Dynamic Systemic Resolution to describe the process of achieving selectivity by coupling a dynamic library to a kinetic controlled reaction step.[77,78] In 2007, these workers reported[78] a system in which a dynamic covalent library is created from a reversible nitroaldol reaction between five aldehydes and 2-nitropropane to yield a number of different nitroaldol products with *R* and *S* enantiomers (**Scheme 1.13**). In order to select compounds from this library, an enzyme, lipase PS-C-I, was added to the library. The lipase catalyses the transesterification reaction between the nitroaldol products and uses *p*-chlorophenyl acetate as the acyl donor. The compounds that were the best substrates for the enzymes were selected from the library and 50% of the product pool was made up of one major product, moreover almost complete asymmetric discrimination was achieved. Interestingly, the corresponding nitroaldol product was among the compounds with the lowest concentrations in the original dynamic library indicating that kinetic control is a powerful tool to achieve dynamic resolution.

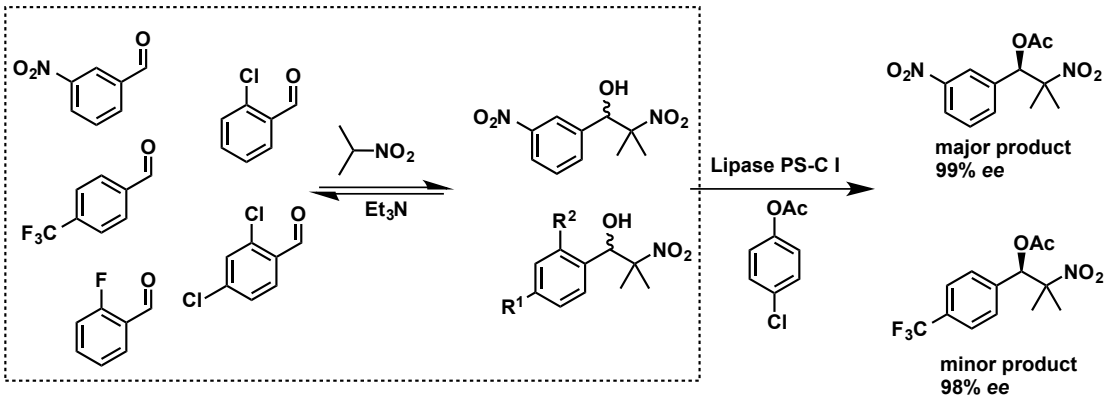


**Scheme 1.13:** Ramström and co-workers reported a library based on the nitroaldol reaction. Selection was based on the irreversible transesterification reaction catalysed by Lipase PS-C I. It was found that the major product after selection by the enzymatic step had a corresponding library member that was one of the minor constituents of the initial library. Adapted from reference 78.

More recently Hu and Ramström published[79] a dynamic system based on imine exchange and kinetic resolution based on a $Ag^+$ catalysed cycloaddition (**Scheme 1.15**). The imine of benzaldehyde and 2-aminoacetonitrile was equilibrated with twelve different aldehydes and $Sc(OTf)_3$ as a transamination catalyst to afford a DCL with thirteen different imines. The library constituents can parcipitate in a Ag(I)–Taniaphos catalysed 1,3-dipolar cycloaddition between the imines and dimethylfumarate as a kinetically controlled reaction step. The imine from furan-2-carbaldehyde and 2-aminoacetonitrile is the best substrate for the $Ag^+$ catalyst and therefore the cycloadducts formed between this imine and dimethylfumarate is the cycloadduct formed in highest yield. Moreover the diastereometric ratio obtained after the reaction is 89:11.

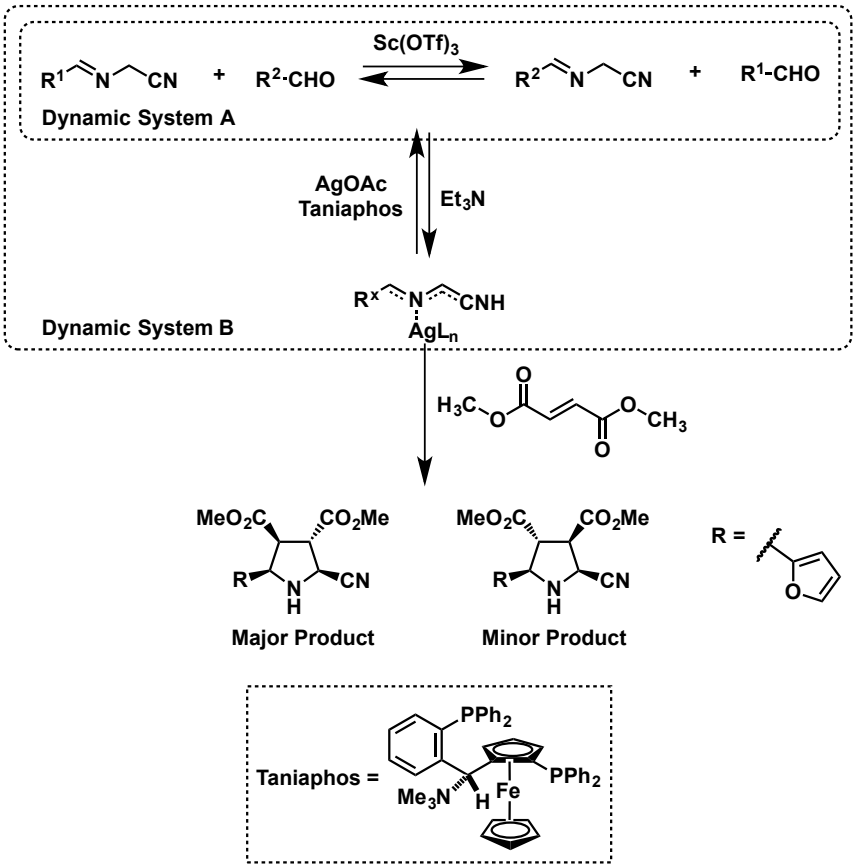


**Scheme 1.15:** Hu and Ramström constructed[79] a dynamic system based on transamination catalysed by $Sc(OTf)_3$. A $Ag^+$ complex catalyses the 1,3-dipolar cycloaddition between the imines and dimethylfumarate. Dynamic systemic resolution is observed as a result of the selectivity of the catalyst. Adapted from reference 79.

### 1.3.4 Self-replication in Dynamic Covalent Libraries

In the previous examples on Dynamic Systemic Resolution, selectivity is achieved by virtue of the one of the library members is a better substrate for the enzyme or catalyst and therefore the reaction of this compound proceeds faster than that of the other library members, causing the library to re-equilibrate. However, other ways of increasing reaction rates relatively to others can be envisaged. Earlier in this chapter, self-replication was introduced as a way of achieving rate acceleration through an autocatalytic reaction. If a DCL could be coupled to a reversible autocatalytic reaction step and the products could be stabilised by duplex formation, selectivity could be obtained (**Figure 1.20**), and a dynamic combinatorial self-replicating system can be created.[80]

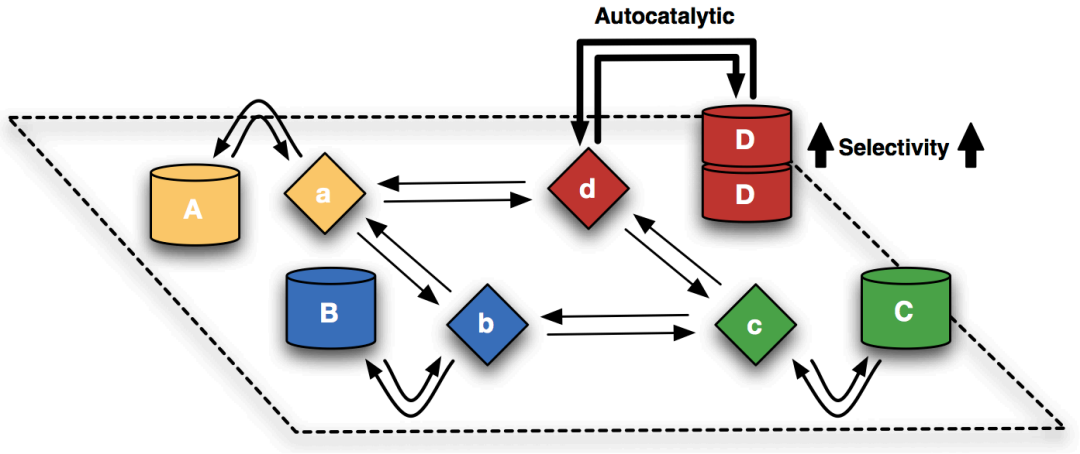


**Figure 1.20:** Schematic representation of a library containing four members (**a**-**d**). When the library is coupled to a reversible reaction step forming products (**A**-**D**). One of the products (**D**) is able to form a stabilising duplex. This causes selective amplification of this library member. Taken from reference 76.

An example of the schematic library outlined in **Figure 1.20** was reported[81] in 2008 by Xu and Giuseppone. They reported a DCL based on imine formation, the compounds used by the authors are reminiscent of those used by Rebek *et al*. but the covalent bond forming step is the formation of an imine rather than an amide. The compounds used consisted of three aldehydes $\mathbf{Al}_1$-$\mathbf{Al}_3$ and two amines $\mathbf{Am}_1$ and $\mathbf{Am}_2$. One aldehyde ($\mathbf{Al}_1$) bears the Kemp's triacid derivative capable of forming hydrogen bonds with the guanine derivative on amine $\mathbf{Am}_1$,

on $\mathbf{Am_2}$ the hydrogen bond formation is hindered by the *N*-benzyl protecting group (**Scheme 1.15**). In the dynamic library only one of the library members is stabilised by the formation of a duplex with another copy of itself. After equilibration this library member is the biggest constituent of the library. Also a kinetic study was carried out which confirmed that the formation of the duplex proceeded faster than the formation of the other library members, confirming that self-replication is responsible for the selectivity.

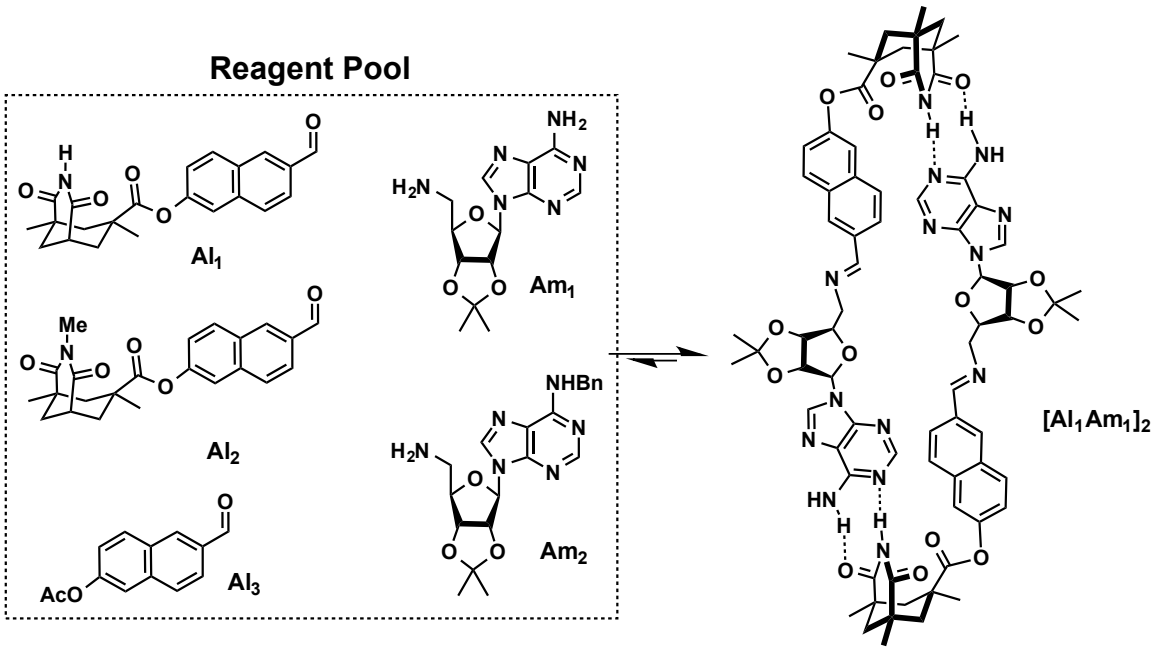


**Scheme 1.15:** A DCL was created using the reversible imine bond formation. One of the library members, $\mathbf{Al_1Am_1}$ is able to form a stable duplex $[\mathbf{Am_1Al_1}]_2$. The stabilising effect of the formation of a duplex causes selective amplification of this library member. Adapted from reference 76.

Another example of an imine replicator was reported[82] by the Philp laboratory. Aldehyde **60** with carboxylic acid recognition site was reacted with aniline derivative **59** with an amidopyridine recognition site (**Scheme 1.16**). These two compounds can react to form imine **61** with two recognition sites and this can function as a template for its own formation. In contrast with previous work from the Philp group, the reaction to form this template is reversible and therefore the products are formed under thermodynamic control. The reaction through the template-directed reaction pathway was accelerated compared to the bimolecular reaction because it takes place pseudo-intramolecularly. The

hydrolysis of the imine bond, however, is a bimolecular process both in the absence and presence of template and is therefore the same in both cases. As a result of the selective increase of the forward reaction, the equilibrium constant, which is made up of the forward and the backward rate of a chemical reaction, increases when a template-directed pathway is present and template formation is increased. It was found that the imine template was capable of self-replication through an autocatalytic cycle. However, the production of template is limited by its reversibility and in order to increase the amount of template that can be produced and therefore increase autocatalytic reaction rate, an irreversible step is added to the system. An established method to irreversibly trap imines is to reduce them *in situ* to amines.[83] Interestingly, amine template **62** was found to be a good cross-catalyst for the formation of the imine template, the maximum rate of formation in the cross-catalytic cycle was even higher than that in the autocatalytic cycle.

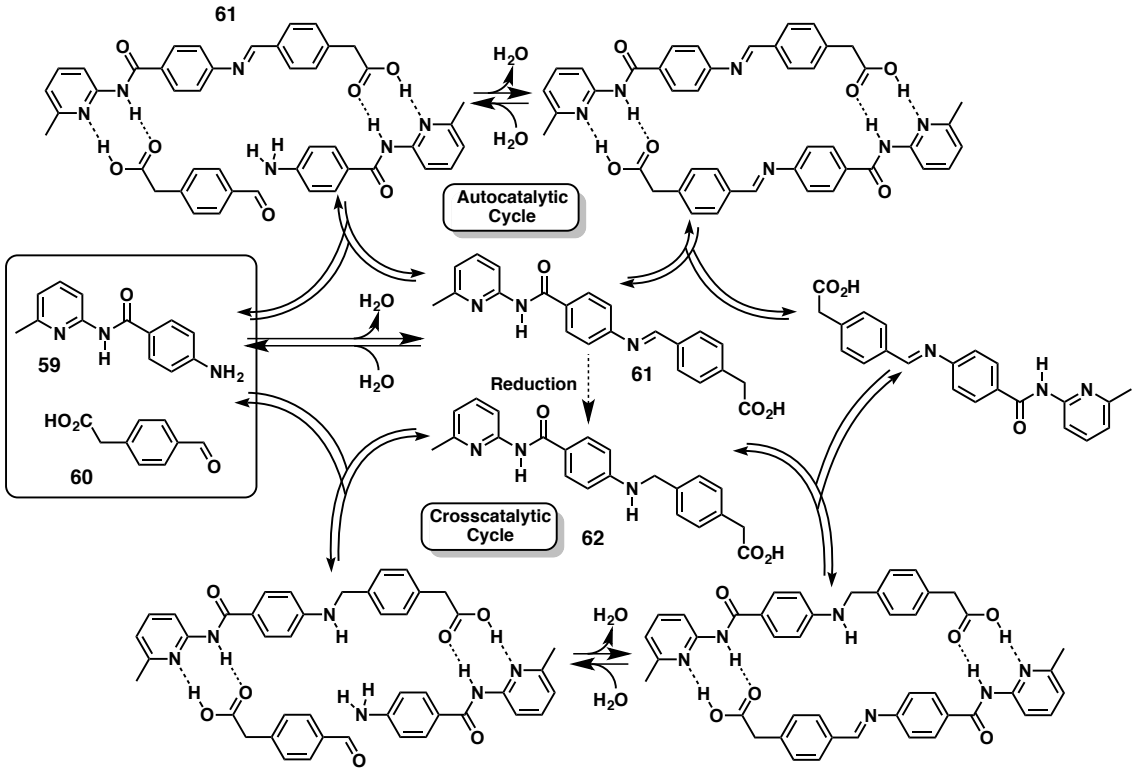


**Scheme 1.16:** A system in which imine formation leads to a template, which is autocatalytic. Additionally, this template can be reduced to the amine, which shows cross catalytic behaviour. Adapted from reference 82.

In the previous examples selectivity was obtained by the stabilising effects of the formation of a product duplex[80] or irreversible trapping of the product[77]. It would however, be much more efficient if a dynamic library could be coupled to an irreversible autocatalytic reaction (**Figure 1.21**). In **Figure 1.21** a DCL containing four library members, **a**-**d**, are coupled to an irreversible reaction, affording products **A**-**D**. Only compound **D** is a catalyst for its own formation and the rate for the formation of this product should increase during the reaction, causing selectivity for this product.

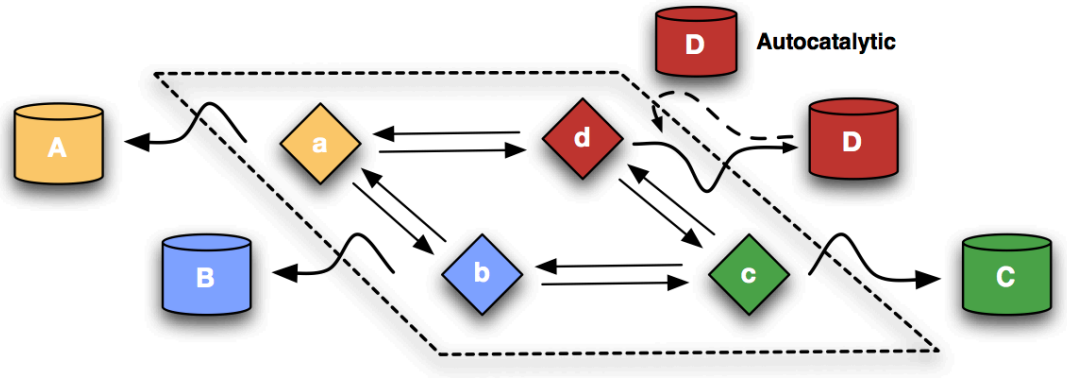


**Figure 1.21:** Library members **a**-**d** are coupled to an irreversible reaction affording products **A**-**D**. Only **D** is a catalyst for its own formation and the rate towards the formation of **D** should increase upon formation of **D**. This should cause the selectivity for the formation of **D** to increase as well. Taken from reference 76.

In 2008 members of the Philp group published[84] the first study on a dynamic nitrone library in chloroform. There were four different nitrone library members (**63**-**66**) that were in dynamic equilibrium (**Scheme 1.17**). When dicarboxylic acid **68** is added to the system the equilibrium shifts in favour of formation of nitrone **66** because it has two amidopyridine recognition sites and can associate to **68**. This shows that a dynamic nitrone library in an organic solvent and selective amplification of a library member based on molecular recognition is possible.

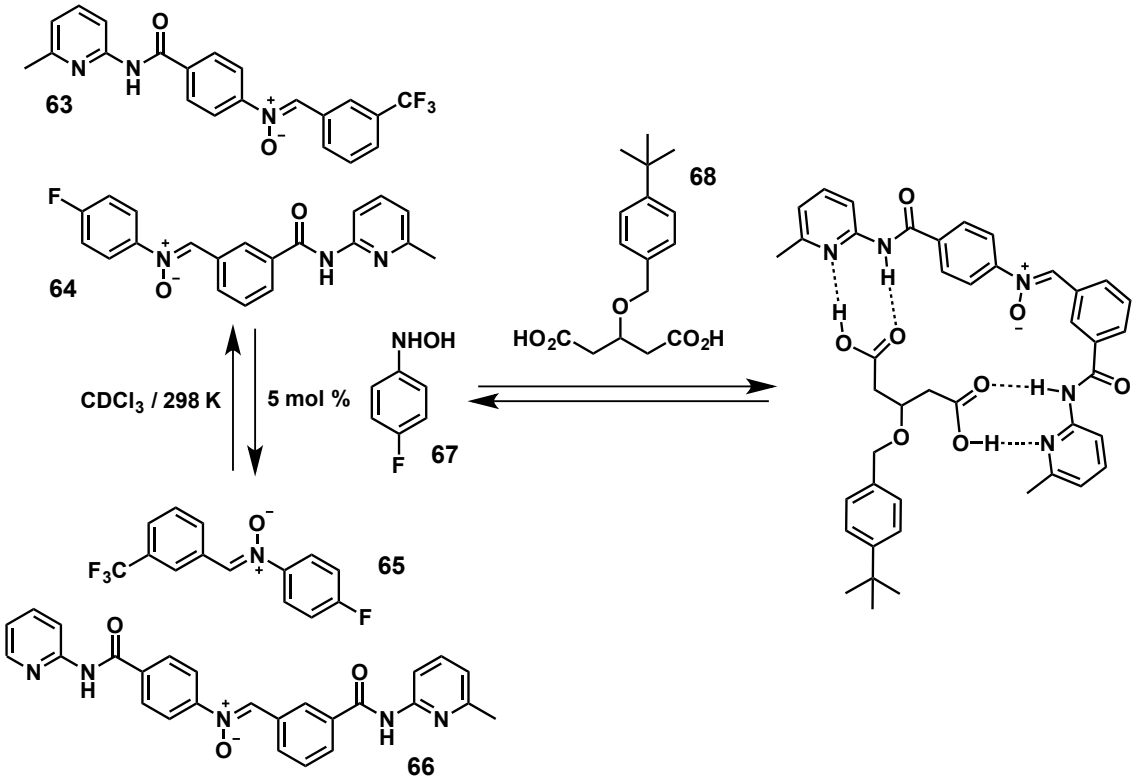


**Scheme 1.17:** The first interconverting, dynamic nitrone library in an organic solvent. Nitrones **63** - **66** can interconvert when 5 mol% hydroxylamine **67** is present. When diacid **68** is added, **66** is amplified. Adapted from reference 84.

The first example of replication-based selection of library members in DCC was published[85] by Sadownik and Philp in 2008. The DCL was constructed from four building blocks; two aldehydes **69** and **70**, of which **69** bears an amidopyridine recognition site, hydroxylamine **65** and amine **71** (**Scheme 1.18**). The building blocks can react and form nitrones **73** and **74** (condensation reaction between hydroxylamine and aldehyde) and imines **72** and **75** (condensation reaction between amine and aldehyde), which can exchange in a dynamic equilibrium. Upon addition of maleimide **38**, the nitrones can irreversibly react *via* a 1,3-dipolar cycloaddition to form *trans*- or *cis*-cycloadducts **76** and **77**. One nitrone in the dynamic library is equipped with an amidopyridine recognition site while the other is not. This difference in nitrone structure leads to the formation of cycloadducts with two recognition sites, **77**, and cycloadducts with only one recognition site, **76**. The products that bear both recognition sites are expected to be able to associate their building blocks and thus catalyse their own formation. The selective acceleration of one of the reaction channels relative to the other reaction channels should lead to selective formation of one of the

products, as depicted schematically in **Scheme 1.18**. It was found that only template *trans*-**77** is catalytically active as template *cis*-**77** has the recognition sites folded up upon itself and represents inactive template **T´**. In a control experiment in which the recognition site of the maleimide is methylated and thus is not available for hydrogen bonding to the amidopyridine on the nitrone, roughly equal formation of the four cycloadducts is observed.

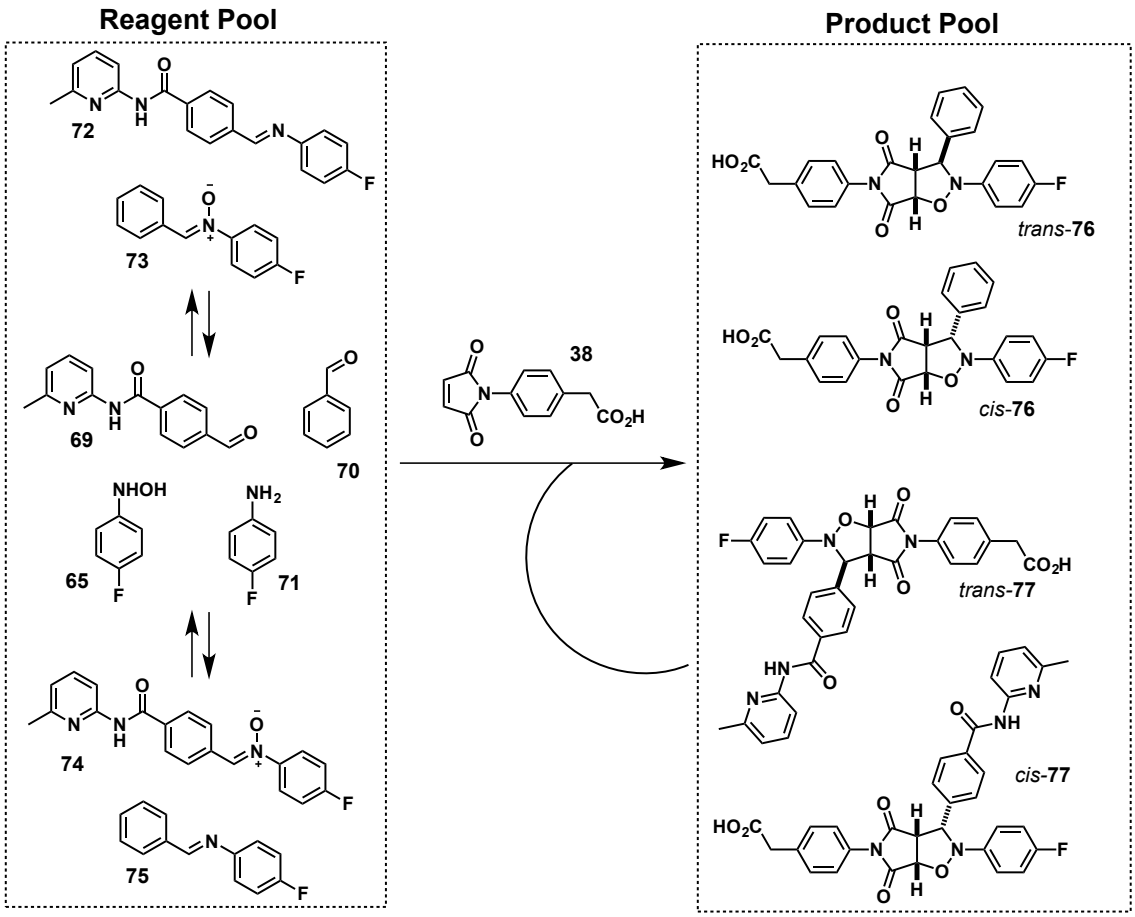


**Scheme 1.18:** Four library members (**72** - **75**) can interconvert. The two nitrones (**73**, **74**) can react with maleimide **38**, leading to the formation of four products (*trans*/*cis*-**76** and *trans/cis*-**77**). Product *trans*-**77** shows autocatalytic behaviour and is amplified from the dynamic reagent pool. Adapted from reference 85.

When the carboxylic acid on the maleimide is available for hydrogen bonding and the experiment is repeated, the concentration *vs*. time profile looks remarkably different (**Figure 1.22**). When recognition is enabled, the *trans*-**77** template is able to function as an autocatalyst and therefore increases rate for its own formation. The enhancement of the reaction rate causes more formation of the template *trans*-**77** and the equilibrium in the DCL shifts towards formation

of the nitrone **74**. With preformed template added to the reaction mixture the maximum rate increases and is reached sooner, also the conversion is higher after 16 hours.

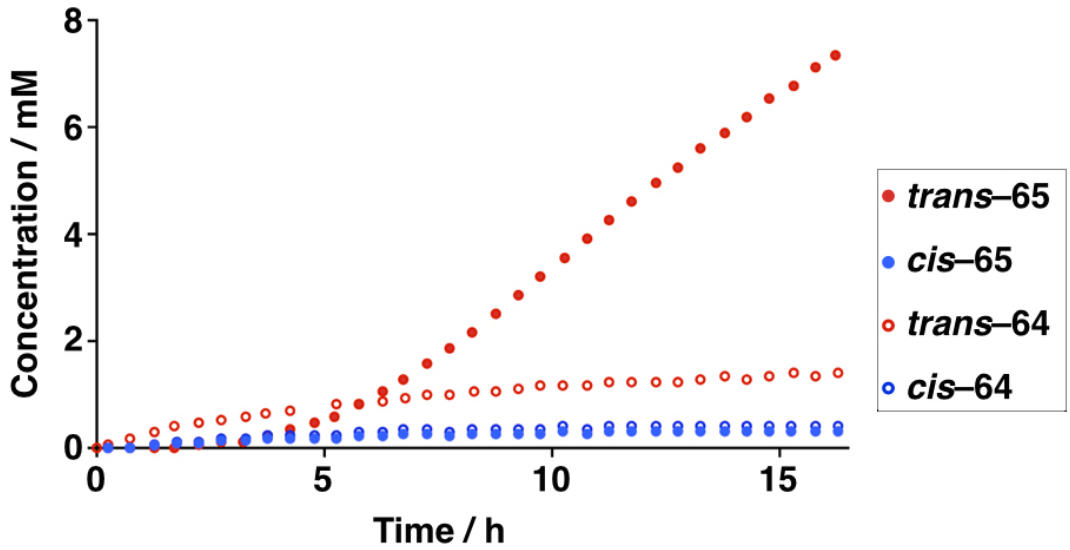


**Figure 1.22:** Concentration *vs*. time profile for the formation of the four cycloadducts in the recognition-mediated pathway. *Trans*-**77** is capable of catalysing its own formation and therefore production of this compound is enhanced relative to the other compounds. Taken from reference 86.

# 2

# System Design and Objectives

As outlined in **Chapter 1**, the Philp Laboratory has designed and investigated a number of different self-replicating systems. These systems exhibit a number of general features. First of all, the bond-forming step responsible for the formation of the template is based on a cycloaddition between a maleimide and a furan or a 1,3-dipole. Secondly, the recognition event in the self-replicating reaction is based on the association of a carboxylic acid with an amidopyridine. In this thesis, the development of a new self-replicating system is reported that is not based on the formation of a chemical bond with a maleimide. Instead another dipolarophile is equipped with a recognition site and tested for recognition-mediated or even self-replicating behaviour in the reaction with a nitrone.

## 2.1 The Recognition Sites

The Philp laboratory has developed self-replicating systems in which a template is capable of associating its two building blocks through molecular recognition based on hydrogen bonding. The recognition motif employed by the Philp laboratory consists of an amidopyridine unit, which can associate on a carboxylic acid unit (**Scheme 2.1**).

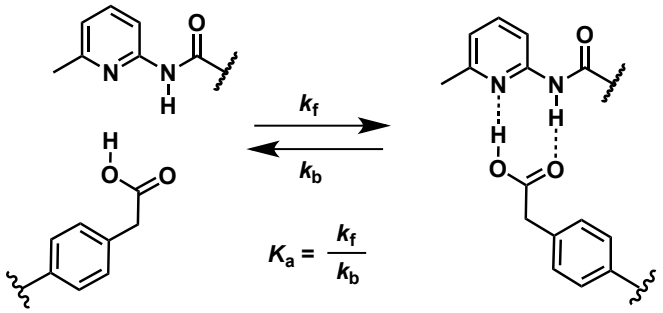


**Scheme 2.1:** The recognition motif used for the association of the building blocks on the template, in order to facilitate self-replication, is based on hydrogen bonding between an amidopyridine unit and a carboxylic acid unit.

The amidopyridine recognition motif has been first described[87] by Hamilton and co-workers. An important parameter that determines the association constant of a supramolecular complex, is the level of preorganization of the recognition sites prior to association. In case of the amidopyridine unit, cancelation of the dipoles of the amide and the pyridine, make sure the most favourable conformation of this functional group is the one shown in **scheme 2.1**, which is fully preorganised for association with a carboxylic acid. Unfortunately, the strength of a hydrogen bonding interaction is strongly dependent on the solvent. Polar and protic solvents can compete for the hydrogen bond acceptors and donors and as the solvent is present at much higher concentrations than the compounds of interest, the hydrogen bonding interactions between the compounds of interest will be diminished. Therefore, in this work, a solvent is chosen that does not compete with the hydrogen bonding interactions needed for the self-replicating system.

The strength of the hydrogen bonding acceptor properties of the pyridine nitrogen depends on the number of alkyl substituents on the pyridine ring (**Figure 2.1**), as these provide additional electron density to the pyridine nitrogen.

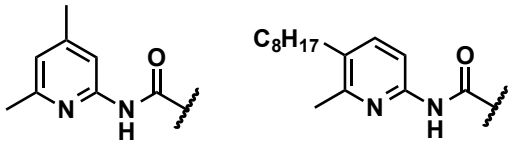

**Figure 2.1:** The two amidopyridine recognition motifs used in this work. The 4,6-dimethyl substituents provide extra electron density on the pyridine nitrogen and thereby enhance hydrogen bonding acceptor capability of this atom. The 5-octyl substituent is added to provide higher solubility in non-polar organic solvents.

## 2.2 The Chemical Reaction

The 1,3-dipolar cycloaddition between a nitrone and a maleimide has been used by the Philp Laboratory as the bond-forming step in a self-replicating system. The 1,3-dipolar cycloaddition, and cycloadditions in general, have the advantages that they do not require acidic or basic conditions and are applicable in a wide range of organic solvents.[88] Additionally, cycloaddition reactions are self-contained reactions, which means that all the atoms in the starting materials end up in the products.[48] The cycloaddition between a maleimide and a nitrone can be easily followed by $^1$H NMR spectroscopy by following the appearance of the proton signals that correspond to the protons on the newly formed heterocycle. This reaction can lead to the formation of two different isomers (**Scheme 2.2**).

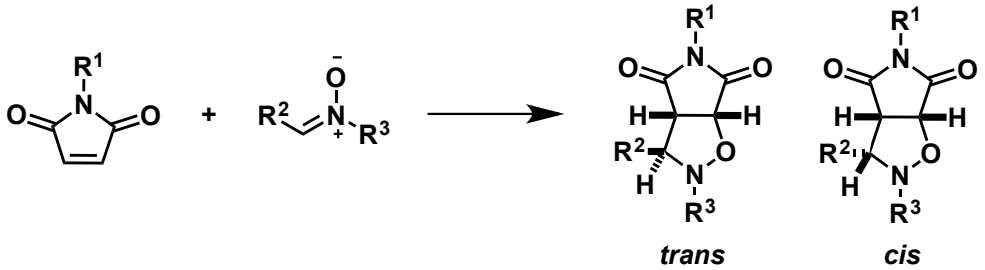


**Scheme 2.2:** The 1,3-dipolar cycloaddition between a maleimide and a nitrone can lead to the formation of two products. When the protons in the newly formed isoxazolidine ring are on the same face the *cis* isomer is formed. When the protons on the newly formed isoxazolidine ring are on opposite faces, the *trans* isomer is formed.

The *exo* transition state leads to the product in which the protons on the newly formed isoxazolidine ring are on the same face, this product is called the *cis*-product. The *endo* transition state leads to the formation of the product in which

the protons of the isoxazolidine ring end up on opposite faces, this product is called the *trans*-product. Previous research by the Philp laboratory has shown that when both reagents are equipped with complementary recognition sites, in the *exo* transition state the two recognition sites are hydrogen bonding and this lives on in the product. Thus the *exo* transition state resembles the [**A·B**] pathway and the *cis*-product resembles the inactive template **T´**. However, when the reaction proceeds through the *endo* transition state, the recognition sites are spatially separated and do not associate and thus the *trans*-product has an open conformation and resembles the template **T**, which can participate in the autocatalytic cycle.

In this work, however, the maleimde is not used a dipolarophile but the chemical reaction is based on the 1,3-dipolar cycloaddition between a nitrone and a 2-arylidene-1,3-indandione. 2-Functionalised 1,3-indandiones are often used in chemical research, one reason is that the 1,3-dione motif is found in many natural and biologically active products.[89] Spiro-1,3-indandione derivatives are under investigation as for example, anti-cancer drugs.[90] When a 1,3-indandione is reacted with a functionalised aldehyde under basic conditions in a Knoevenagel condensation the reaction in **Scheme 2.3** takes place.[91] The Knoevenagel condensation is a widely applied method for the formation of C–C double bonds.[92] Examples of the use of this reaction are found in combinatorial chemistry[92b], in the synthesis[93] of natural products. Condensation products have been used as diene in hetero Diels-Alder reactions[94].

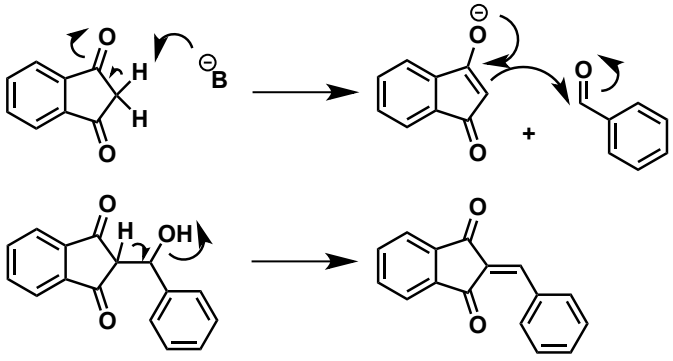


**Scheme 2.3:** 1,3-indandione can be functionalised on the 2-position by deprotonation and coupling to an aldehyde followed by ejection of the hydroxide group. This reaction is termed Knoevenagel condensation.

Common features of the indandiones and maleimides as dipolarophiles is the Electron Withdrawing Groups (EWGs) on either side of the double bond. In case of the indandione, the double bond might be more electron deficient due to the phenyl ring on one side of the double bond. In contrast to maleimides, nitrone addition affords regioisomers as well as diastereoisomers (**Scheme 2.4**).

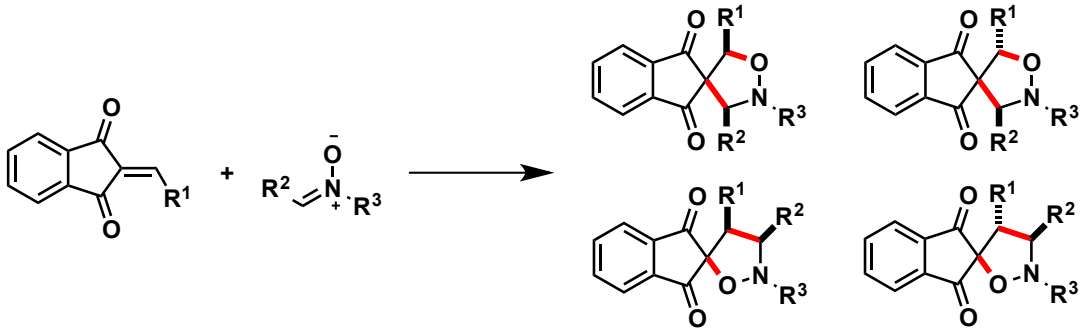

**Scheme 2.4:** The 1,3-dipolar cycloaddition between an indandione and a nitrone can give four products. The protons on the newly formed isoxazolidine ring can end up on the same face (*cis*) or on opposite faces (*trans*). Additionally, the oxygen can bond to either of the two carbons in the dipolarophile (Michael and Anti-Michael). For clarity, the newly formed bonds are highlighted in red.

A profound difference between the products in the reaction with the indandione with the maleimide reaction is that the bicyclic system in the latter is a fused system whereas the reaction between a nitrone and an indandione leads to the formation of a spiro ring system. A similarity between these two reactions is that in both cases the *endo* transition state leads to the formation of the *trans*-product and the *exo* transition state leads to the formation of the *cis*-product. There is however a remarkable difference between the two reactions that arises from the fact that the double bond in the indandione is not symmetrical, in contrast with the one in the maleimide. As a result of the asymmetrical double bond, the orientation of the nitrone relative to the double bond during the transition state gives rise to the possible formation of two regioisomers in addition to the two stereoisomers. When the oxygen on the nitrone forms a bond with the quaternary carbon on the indandione, the regioisomer that is formed is termed the Anti Michael regioisomer. When the oxygen on the nitrone forms a bond with the tertiary carbon on the indanione the Michael regioisomer is formed. This nomenclature is introduced here to describe the cycloadducts as

the reaction is reminiscent of a Michael addition on a 1,4-unsaturated carbonyl system.

### 2.2.1 The Reaction with Model Compounds

In order to study the reactivity of the 2-arylidene-1,3-indandione with a nitrone, we designed two model compounds and planned to study them in a 1,3-dipolar cycloaddition (**Figure 2.2**).

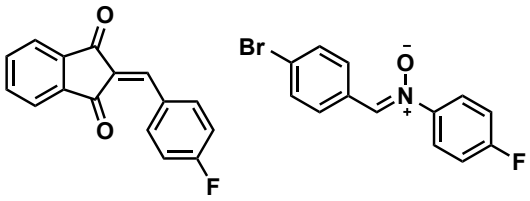


**Figure 2.2:** Model compounds were designed in order to study the reactivity of the 1,3-dipolar cycloaddition between a 2-functionalised 1,3-indandione and a nitrone. Both compounds are equipped with a fluorine tag that enables analysis with $^{19}F$ NMR spectroscopy.

These model compounds do not bear any recognition site and therefore can only react in a bimolecular reaction that is not enhanced, or influenced otherwise, by recognition. Additionally, as the model compounds do not bear any of the recognition sites, they are used as control compounds in order to compare the recognition-mediated reaction with the bimolecular reaction. The two model compounds are equipped with a fluorine tag that enables analysis with $^{19}F$ NMR spectroscopy.

### 2.2.2 Computational Studies

Computational chemistry is an attractive tool to assess the reactivity and the transition state geometry of the cycloaddition reaction. The Philp laboratory has previously used[95] computational studies to provide insight in the transition state of a reaction or the relative stabilities of a transition state or product. In this work, computational tools (RM1, DFT) calculations will be used to predict the stabilities of the products of the cycloaddition between an indandione and a nitrone.

### 2.2.3 Recognition-mediated Reaction

The aim of this work is to investigate the potential of using a 2-functionalised 1,3-indandione as a dipolarophile in a self-replicating system with a nitrone similar to the maleimide previously used by the Philp laboratory. In order to use the indandione reaction in a recognition-mediated reaction, 1,3-indandione must be functionalised with a recognition site. The Philp laboratory has reported self-replicating systems with the amidopyridine recognition site on the nitrone and the carboxylic acid recognition site on the dipolarophile and *vice versa*. Therefore, in this work, both options are explored (**Scheme 2.5**).

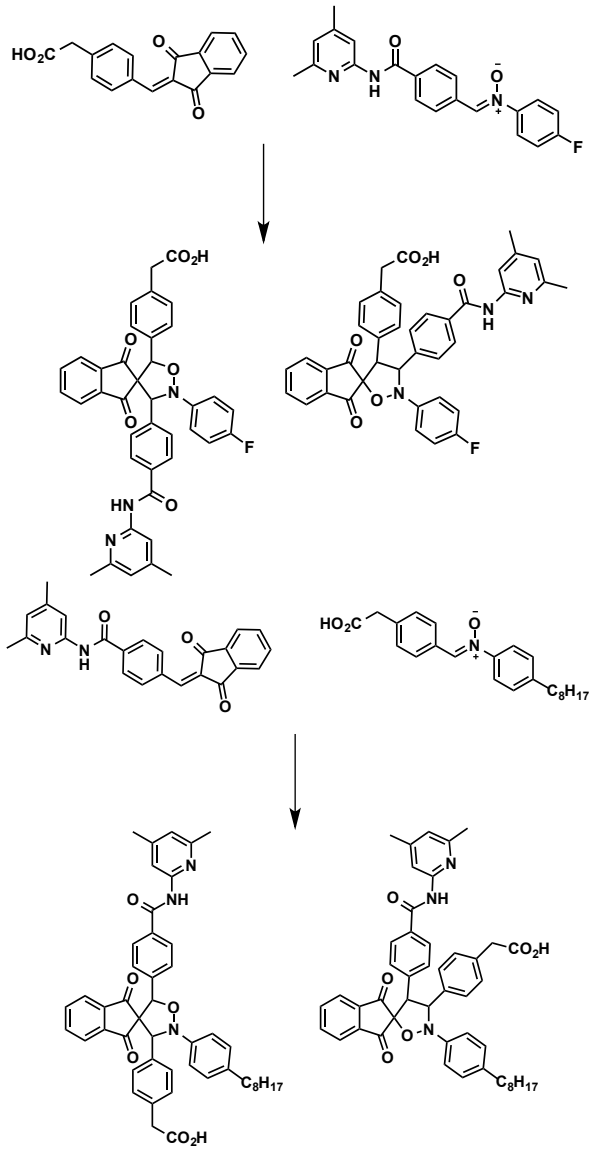

**Scheme 2.5:** The recognition sites can be placed on the indandione or on the nitrone. In this work both scenarios will be explored.

The reactivity of the indandione and the maleimide is orthogonal, therefore, a system could be designed in which the maleimide dipolarophile and the indandione dipolarophile are both used in the same experiment with a nitrone (**Scheme 2.6**). This system might show interesting behaviour since cycloadducts could be able to catalyse their own formation, but also the formation of their orthogonal counterpart.

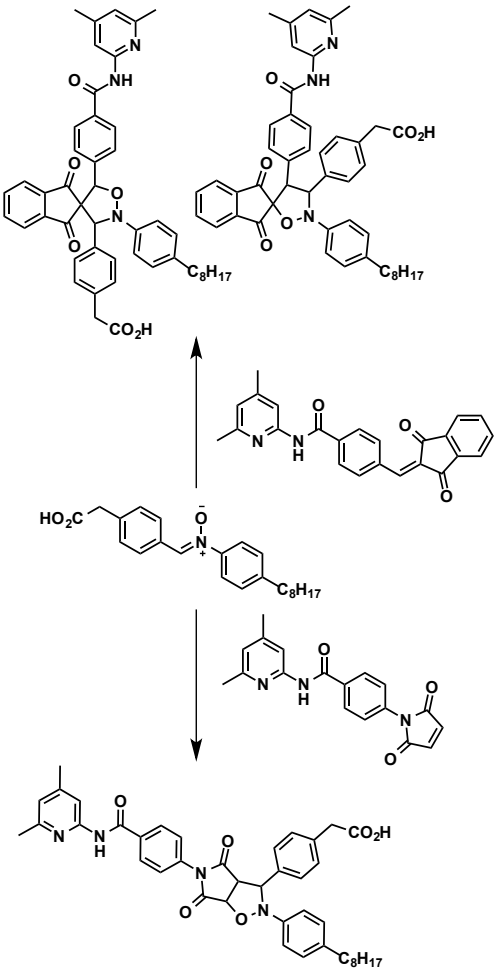

**Scheme 2.6:** The reactivity of the indandione and the maleimide is orthogonal. Therefore, these two compounds can be used to compete for a nitrone. The cycloadducts have the potential to catalyse their own formation and could have the potential to catalyse the formation of their orthogonal counterpart.

## 2.3 Dynamic Covalent Library

As outlined in **Chapter 1**, the Philp laboratory has been successful[85] in constructing a Dynamic Covalent Library (DCL) that consisted of imines and nitrones, which were generated from a mixture of aldehydes, anilines and hydroxylamines. When this DCL was coupled to a cycloaddition reaction, the recognition-mediated reaction outcompeted the other reaction channel in the system and thereby amplified one library member selectively. In previous work reported[85] by the Philp laboratory, a 2 x 2 matrix of aldehydes and nucleophiles was used to construct a DCL. In the work reported here a 3 × 3 DCL is constructed, using 3 aldehydes and 3 nucleophiles (**Figure 2.3**).

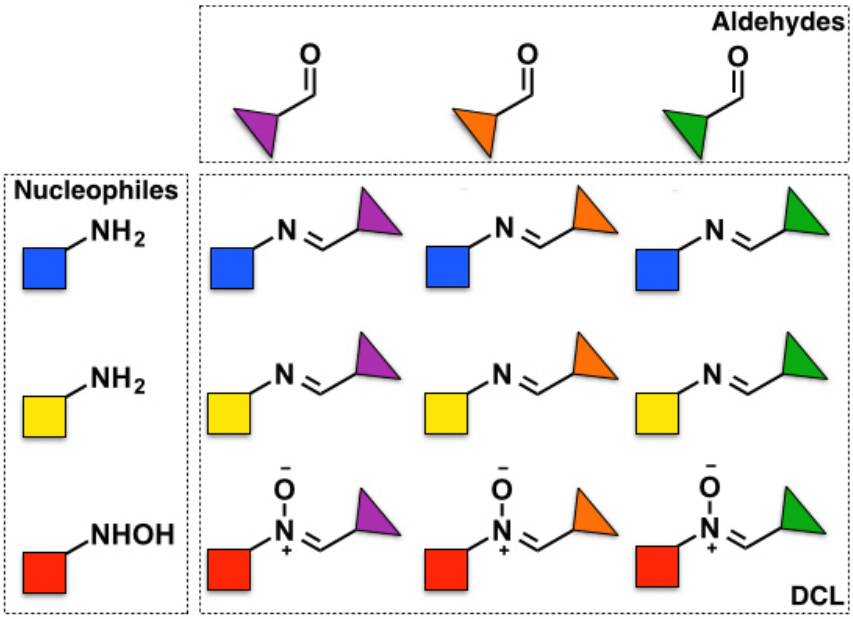


**Figure 2.3:** A Dynamic Covalent Library can be designed from two amines, one hydroxylamine and three aldehydes. Upon equilibration a mixture of three different nitrones and six imines is created. The nitrone constituents of the DCL can participate in a 1,3-dipolar cycloaddition with a dipolarophile, the imines are unreactive. Adapted from reference 96.

The DCL in **Figure 2.3** consists of 6 imines, which are unreactive towards the dipolarophile, and 3 nitrones, two of which are equipped with recognition sites. The two nitrones bearing recognition sites will be in competition for the dipolarophile to undergo the 1,3-dipolar cycloaddition reaction. In previous work, a maleimide was added to the library and the nitrones were able to react with it

to form the cycloadducts. The cycloadduct that is the most efficient autocatalyst, will be formed most rapidly and therefore the DCL will equilibrate to produce more of nitrone needed for the formation of the most efficient autocatalytic template. The objective in this work is to use the dipolarophile with a different design presented previously to amplify a member of a DCL.

## 2.4 Project Objectives

The work presented here focuses on the development of a self-replicating system using a 2-functionalised 1,3-indandione as dipolarophile in reaction with a nitrone. The research is based on the experience within the Philp laboratory on self-replicating systems that use a maleimde as dipolarophile in reaction with a nitrone. Additionally, a DCL will be constructed in which two nitrones equipped with recognition sites are present. This nitrones will compete for the indandione and the behaviour of this dynamic system will be studied.

The 1,3-dipolar cycloaddition will be studied in the absence of recognition-mediated reaction channels with model compounds. This model compound study will be carried out using experimental methods and computational chemistry.

The aims of this project are:

- The 1,3-dipolar cycloaddition between a 2-functionalised 1,3-indandione and a nitrone can lead to the formation of four products (**Scheme 2.4**). The first aim of this project is to study the reaction with model compounds, so in the absence of recognition-mediated reaction channels, in order to characterise the products of the cycloaddition.

- Explore synthetic routes towards the functionalisation of 1,3-indandione in the 2 position in order to generate the dipolarophile that bears a carboxylic acid or an amidopyridine recognition site (**Scheme 2.3**).

- Investigate the use of the indandione dipolarophile in a self-replicating system similar to the maleimide self-replicating systems reported previously by the Philp laboratory and described in **Chapter 1**. The recognition-mediated reactions will be investigated both experimentally and computationally.

- Construct a Dynamic Covalent Library with three nucleophiles and three aldehydes that equilibrate to generate a DCL containing three nitrones, two of which bear a recognition site. The behaviour of the dynamic system coupled to a self-replicating reaction with the indandione will be studied.

# 3

# Investigation of the Reactivity with Model Compounds

## 3.1 Design of Model Compounds

In order to investigate the reactivity of the 2-functionalised 1,3-indandione in a 1,3-dipolar cycladdition with a nitrone, two model compounds were designed that do not bear recognition sites. These model compounds allow the investigation of the bimolecular reaction only, as the reactivity is not affected by recognition-mediated reaction channels (**Scheme 3.1**).

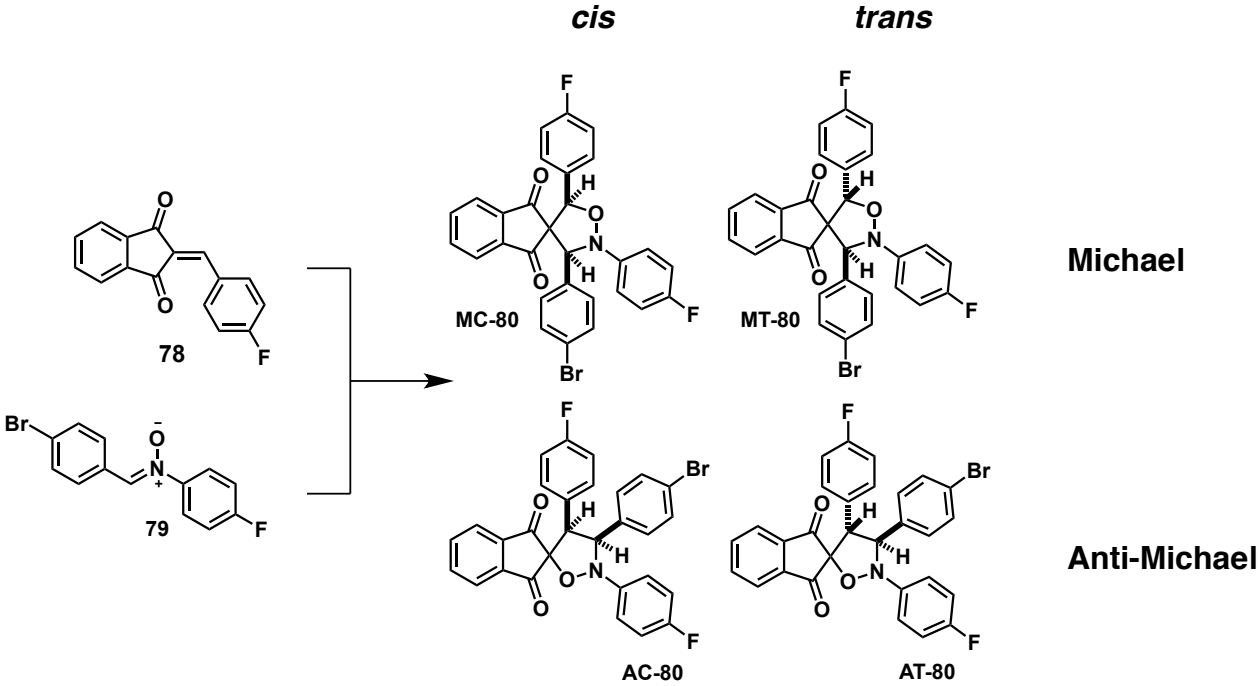


**Scheme 3.1:** The 1,3-dipolar cycloaddition between the two model compounds can lead to the formation of four products. The protons on the newly formed heterocycle can end up on the same face (*cis*) or on opposite faces (*trans*). Additionally, the nitrone oxygen can bond to the quaternary carbon atom on the indandione (Anti Michael) or to the tertiary carbon atom (Michael).

We decided to equip indandione model compound **78** with a fluorine-tag as this enables investigation with $^{19}F$ NMR spectroscopy, which affords a less complicated spectrum compared to the $^{1}H$ NMR spectrum. Nitrone model compound **79** is also equipped with a fluorine atom, which enables monitoring its reactivity by $^{19}F$ NMR spectroscopy.

## 3.2 Investigation of Cycloaddition using Computational Chemistry

### 3.2.1 Investigation with RM1 Calculations

In order to provide evidence for the reactivity observed in the experimental investigation of the model compounds, computational studies were carried out. The use of semi-emperical calculations to rapidly scan potential energy surfaces has been used successfully in the past in our laboratory. In particular, we have shown[95] that the RM1 method[97] is capable of providing transition state geometries almost identical to those located by much more computationally expensive DFT calculations (e.g. B3LYP/6-31+G(d,p)). Accordingly, the energy of the structures of the four products were minimised using molecular mechanics and these initial structures were used as the input for semi-empirical RM1 calculations. In order to locate the transition state leading to each diastereoisomeric product, the cycloadduct structure was used as a starting point and the bonds that are formed during the reaction extended in steps of 0.05 Å and the energy of the geometry at each step was optimised. This procedure affords a potential energy surface in which an approximate saddle point can be identified. This saddle point corresponds to the transition state. Subsequently, this approximate geometry is used as input for RM1 calculations in order to minimize the transition state geometry, which affords the internal energy of the transition state.

The transition states towards the formation of AC-**80** and MC-**80** have the highest and lowest transition state energy respectively. Both of these geometries and potential energy surfaces are shown in **Figure 3.1**.

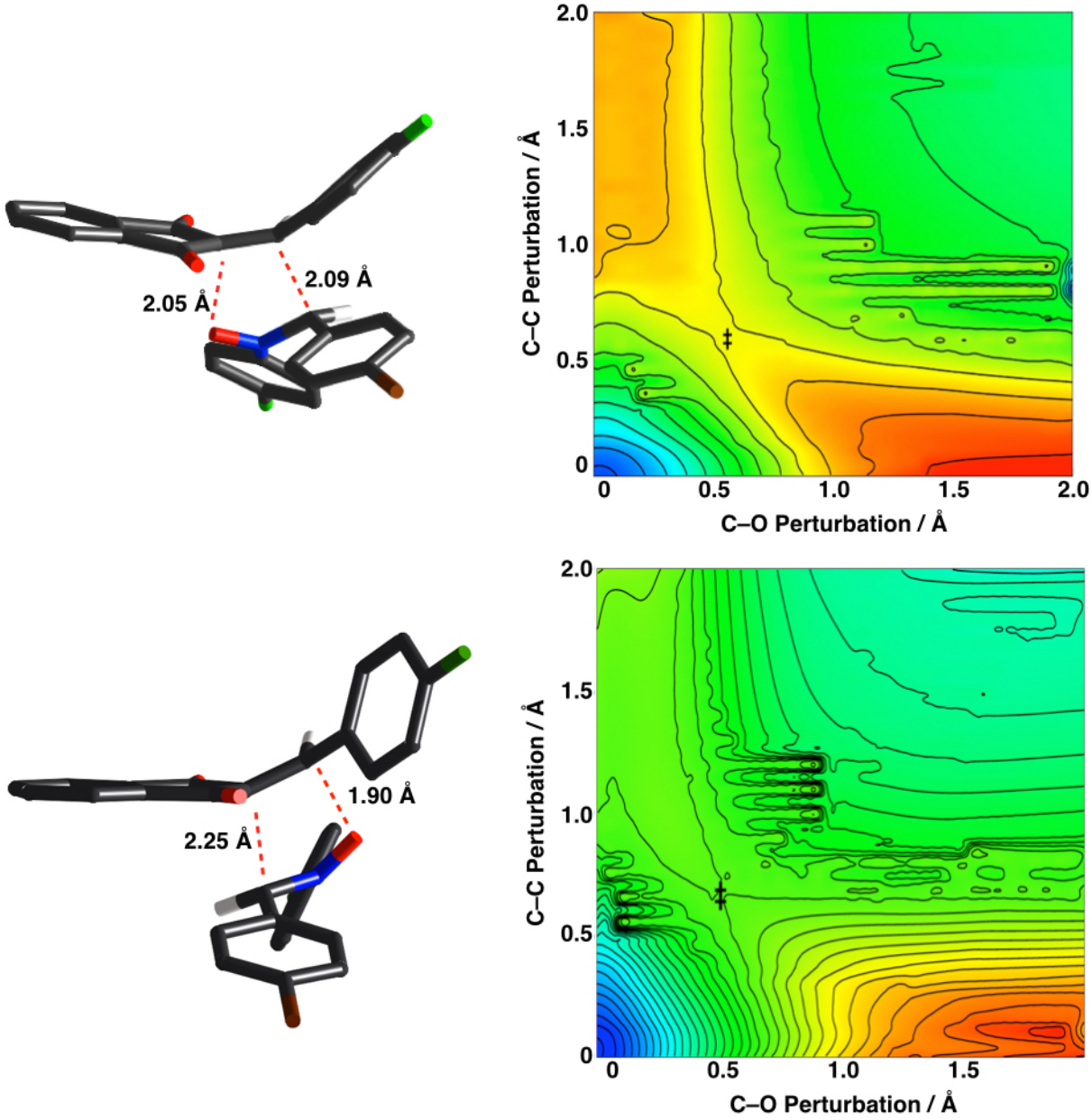


**Figure 3.1:** Top: Potential energy surface and transition state geometry for the reaction between nitrone **79** and indandione **78** towards the formation of AC-**80**. Bottom: Potential energy surface and transition state geometry for the reaction between nitrone **79** and indandione **78** towards the formation of MC-**80**. Carbon atoms are shown in grey, oxygen in red, nitrogen in blue, fluorine in green. For clarity, hydrogen atoms have been omitted. In the Potential Energy Surfaces, Blue/green represent low energy and red represents high-energy areas. The location of the transition state on the potential energy surface is marked with ‡.

In the transition state leading to the formation of MC-**80** (**Figure 3.1**), the C–O distance is 0.35 Å shorter than the C–C distance, indicating that the two bonds are not formed synchronously. However, in the transition state leading to the formation of AC-**80**, the C–O and C–C distances differ only by 0.05 Å, indicating that the two bonds are formed synchronously.

All products of the reaction of the model compounds, as shown in **Scheme 3.1**, were modelled in RM1 calculations. **Figure 3.2** shows the heat of formation of the ground state of the cycloadducts relative to the most stable product, the Michael-*cis* isomer, ($\Delta(\Delta H_f)$) and the heat of formation of the transition states relative to the lowest transition state energy, Michael-*cis*, ($\Delta(\Delta H_f^{\ddagger})$).

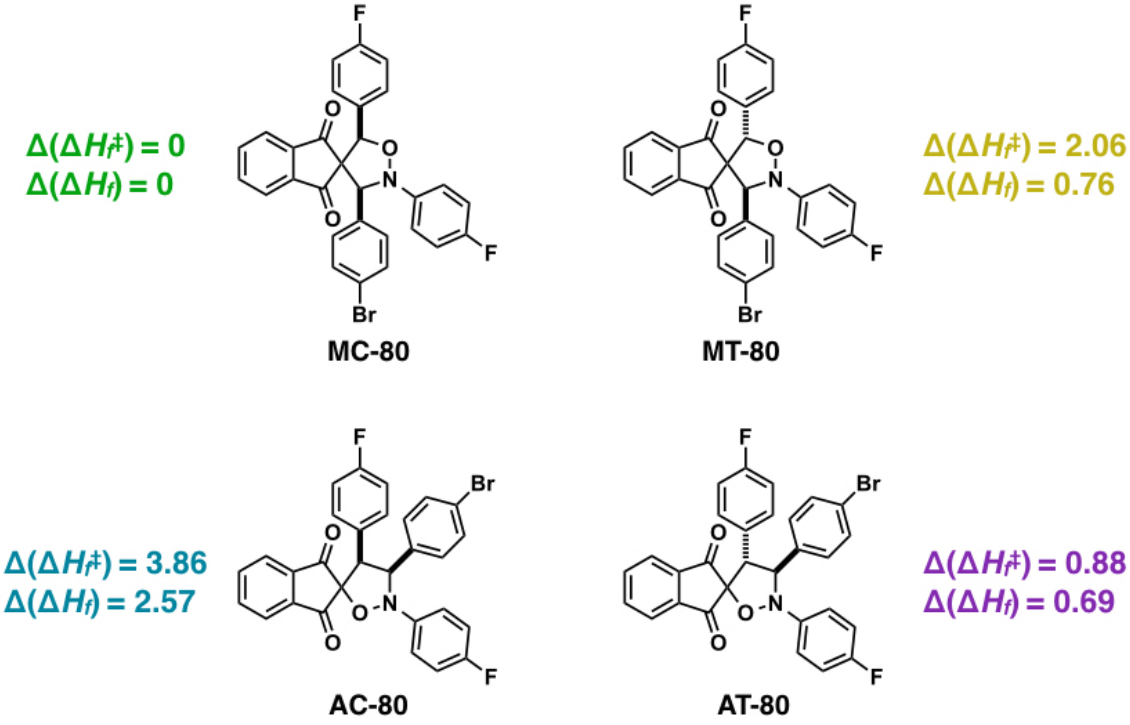


**Figure 3.2:** The activation barrier and the stabilization energy represent the differences between the ground state energy of the reactants and the transition state energy and the ground state energy of the products respectively. The values are presented in kcal $mol^{-1}$.

The difference in transition state energy of the four products can serve as an indication of the reactivity of the model compounds. The relative transition state energies suggest that MC-**80** would be formed preferentially, followed by AT-**80**. The transition state energy of AC-**80** and MT-**80** are the highest compared to the other products, which suggests that these product will not be observed. A

different trend is observed in the stabilization energies of the products. MC-**80** has the most favourable stabilization energy followed by MT-**80** and AT-**80**, which have similar stabilization energies. AC-**80** has the most unfavourable stabilisation energy compared to the other products and it is therefore expected that this compound is not observed. The structures of the ground states of the cycloadducts obtained from the RM1 calculations are shown in **Figure 3.3**.

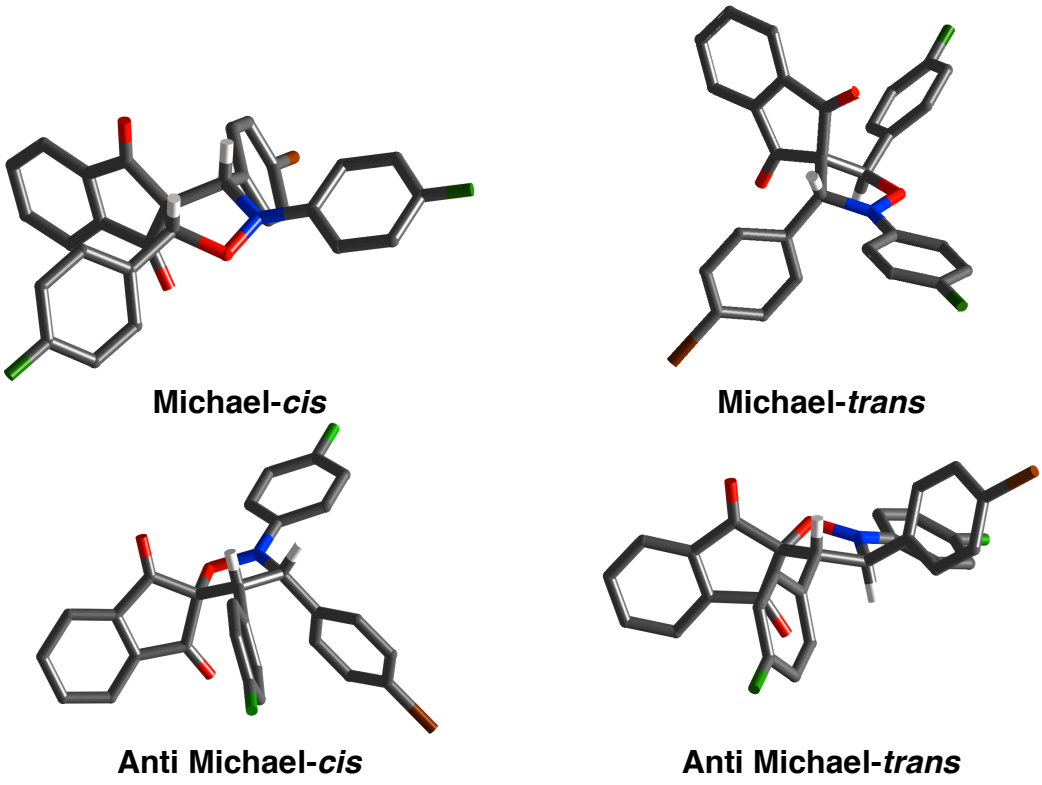


**Figure 3.3:** The calculated ground state structures of the four isomeric products of the cycloaddition between the two model compounds.

### 3.2.2 Estimating Diastereoisomer Stability using DFT Calculations

For comparison purposes, we undertook DFT calculations on the relative stabilities of the four diastereoisomeric cycloadduct products. For all four diastereoisomers, we employed the protocol employed in **Figure 3.4**. Initial models of each of the four diastereoisomers were constructed and optimised using the OPLS2005 forcefield. Each diastereoisomer was then subjected to a 20000 step multi-configuration molecular mechanics (MCMM) conformational search using the same forcefield. In each case, only one low energy

conformation was identified and was used as a basis for the DFT calculations. For each diastereoisomer, we optimised the ground state structure using three functionals, M06-2X, B3LYP and ωB97X-D and a double zeta basis set, 6-31G(d,p). This optimised structure was then used as the starting point for a frequency calculation that permitted the free energy of each diastereoisomer at 298 K to be computed. The results are summarised in **Figure 3.4** with the RM1 results presented for comparison. Strikingly, the AC diastereoisomer is predicted to be significantly less stable than all of the other three cycloadducts. All three functionals agree on the relative ordering of stability of the MC, MT and AT diastereoisomers, however, the relative energies are somewhat variable. Both B3LYP and ωB97X-D predict that MT and AT are somewhat close in energy and are both 1 to 2 kcal $mol^{-1}$ less stable than MC. These results are similar to those obtained using the semi-empirical RM1 method. By contrast, M06-2X predicts a clear hierarchy in stability, MC → MT→ AT→ AC, with significant steps in energy separating the diastereoisomers.

On the basis of these calculations, the consensus prediction would be that the experimental studies should show the formation of MC-**80** as the most stable product followed by MT-**80** and AT-**80**. These predictions are based on the two functionals that place both of the *trans* stereoisomers close in energy to each other and both higher in energy than the Michael-*cis* cycloadducts.

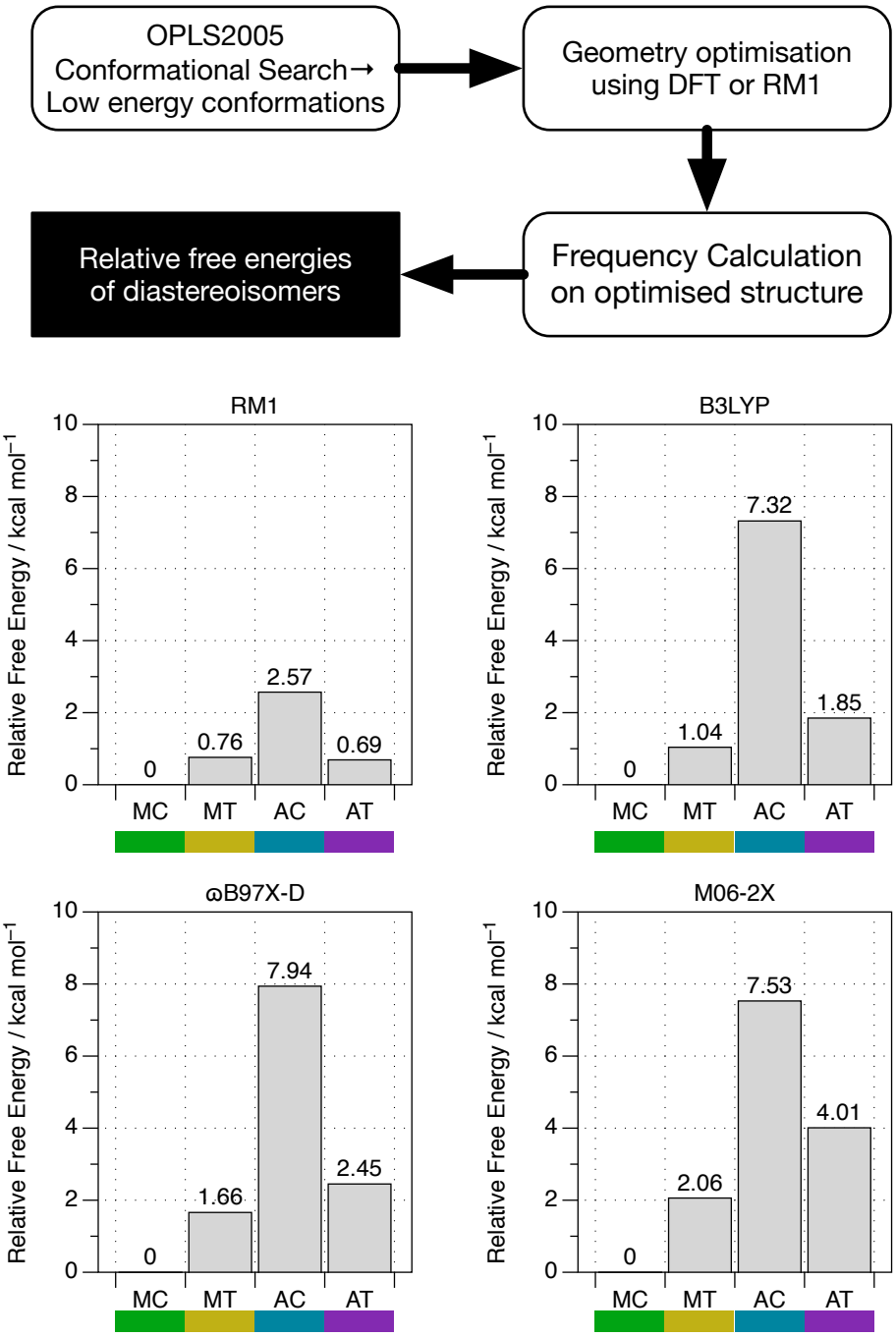


**Figure 3.4:** Top: Schematic of protocol used for calculation of relative free energies of each of the four possible diastereoisomers formed in the cycloaddition between indandione **78** and nitrone **79**. Bottom: Relative free energies at 298K of each diastereisomer calculated using either B3LYP, ωB97X-D or M06-2X and the 6-31G(d,p) basis set. The RM1 data is provided for comparison. Energies are in kcal $mol^{-1}$.

## 3.3 Experimental Investigation of Cycloaddition

### 3.3.1 Investigation to the Structure of the Cycloadducts

In the previous section, the reaction between the model compounds was described and investigated with RM1 and DFT. Based on the outcome of these calculations, we expect to observe one major product (Michael *cis*) and potentially two minor products (Michael *trans* and Anti-Michael *trans*) in the chemical reaction (**Scheme 3.2**).

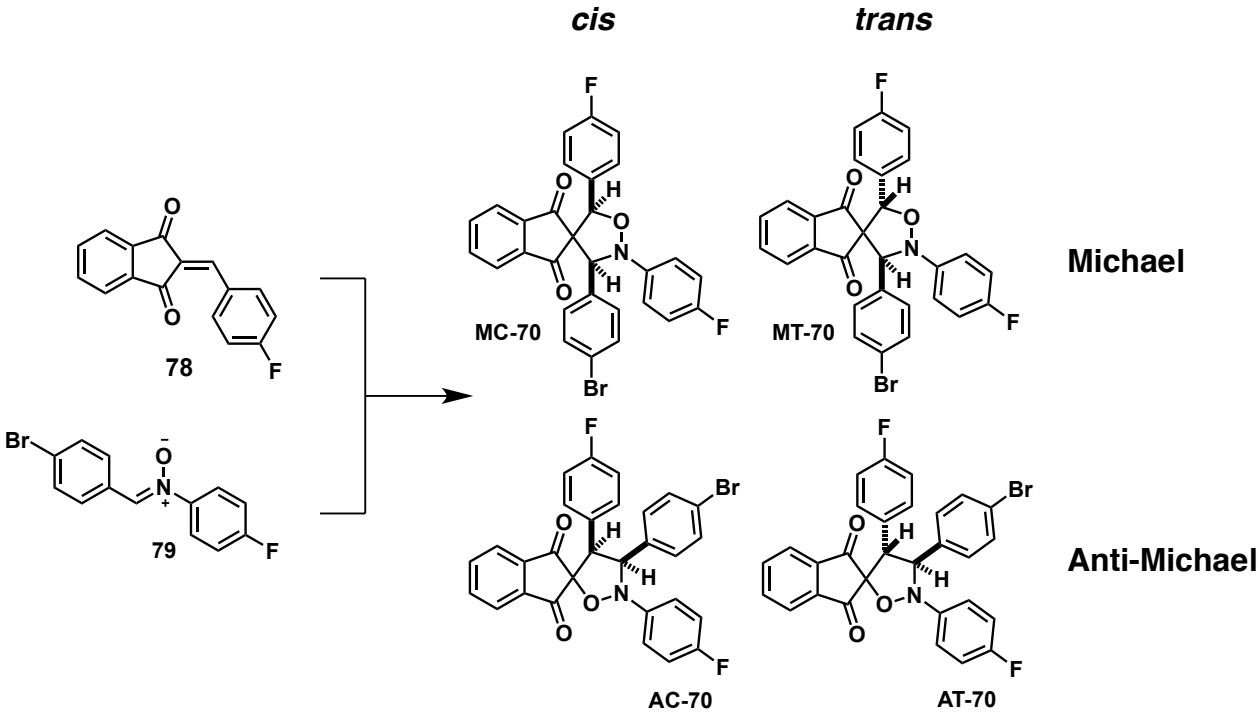


**Scheme 3.2:** The reaction with model compounds was studied experimentally at 25 °C in $CDCl_3$. The concentration of the starting materials was 100 mM and the reaction was monitored for 16 hours.

The reaction was carried out in $CDCl_3$ at 25 °C and followed by $^1H$ NMR and $^{19}F$ NMR spectroscopy. After 16 hours two products were observed in the $^1H$ NMR spectrum (**Figure 3.5**).

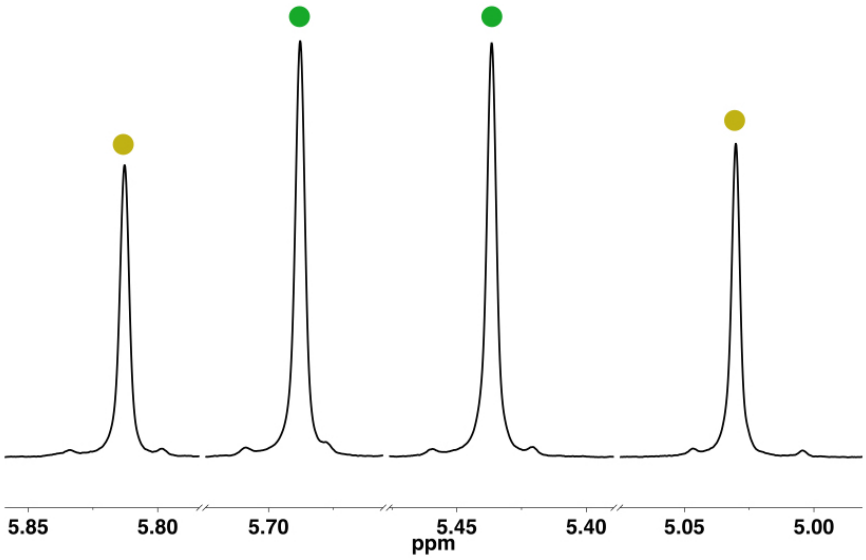


**Figure 3.5:** Partial 500.1 MHz $^{1}$H NMR spectrum of the reaction mixture with the model compounds at 100 mM after 16 hours at room temperature in $CDCl_3$. The region between 5.00 ppm and 5.80 ppm shows the resonances that correspond to the isoxazolidine ring protons of the products. The resonances are singlets, which suggests that the Michael regioisomers are formed. The colours indicate which resonances correspond to the same compound.

In order to characterize the two products, it is desirable to isolate the products and crystallise them in order to enable analysis with single-crystal X-ray diffraction. This method would unambiguously assign the relative stereochemistry and the regiochemistry of the products. However, because of the low conversion of the reaction between the model compounds, the products need to be isolated from the reaction mixture prior to crystallisation. An attempt was carried out to isolate the products with silica flash column chromatography, however only starting material was isolated, presumably because the reaction reverses when the starting material is removed from the reaction mixture.

Another approach to the isolation of the products of the model compound reaction is to trap the products in a way that preserves the stereochemistry and regiochemistry. The hydrogenation of isoxazolidine rings has been reported[98], either using $H_2$ in combination with Pd/C or using acetic acid in combination with Zn. The hydrogenation of isoxazolidine ring (**Scheme 3.3**) should lead to the ring opening to afford a secondary amine and a hydroxyl group. The hydrogenation should function as a kinetic trap in order to obtain the

hydrogenated product in high yield and sufficient purity to crystallise the product and analyse with single-crystal X-ray diffraction.

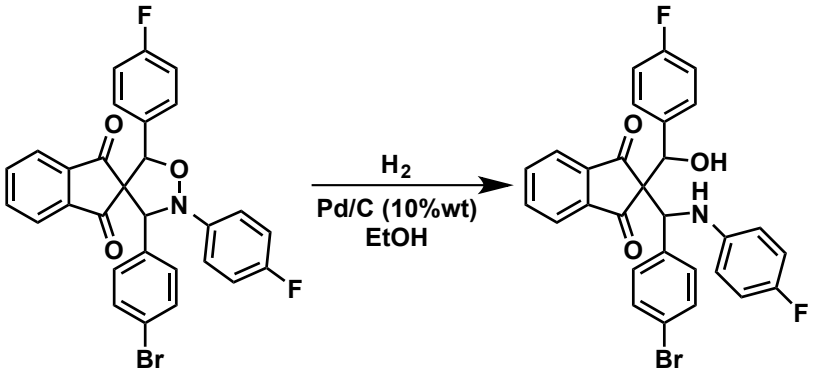


**Scheme 3.3:** Catalytic hydrogenation of isoxazolidine ring should trap the product irreversibly with conservation of the stereochemistry.

The catalytic hydrogenation was carried out by mixing the two model compounds in ethanol under 1 atmosphere of $H_2$ in the presence of Pd/C, 10 wt%, for 16 hours. The products of the catalytic hydrogenation were isolated using silica flash column chromatography (eluting with DCM), which did not afford the desired products. In the $^{19}F$ NMR spectra, acquired after purification of the products, only one $^{19}F$ signal was observed, which was attributed to over-hydrogenation of the compounds.

As a result of the difficulties of the isolation of the products of the reaction between the model compounds, attempts were made to characterise the products inside the reaction mixture using $^{1}H$ NMR spectroscopy. Therefore, the model compounds were mixed in $CDCl_3$ at 100 mM and the mixture was allowed to equilibrate for 16 hours at 25 °C. The $^{1}H$ NMR spectrum shows the resonances corresponding to the isoxazolidine ring protons in the region between 5.00 ppm and 5.85 ppm (**Figure 3.5**). Four resonances are observed in the $^{1}H$ NMR spectrum that correspond to the formation of two products, which is confirmed by the fact that the $^{19}F$ NMR spectrum also shows four product signals. **Scheme 3.2** shows the four possible products that can be formed in the reaction between the two model compounds.

The Anti Michael regioisomers have two vicinal protons on the isoxazolidine ring that are expected to show *J*-coupling in the $^{1}$H NMR spectrum (**Figure 3.6**).

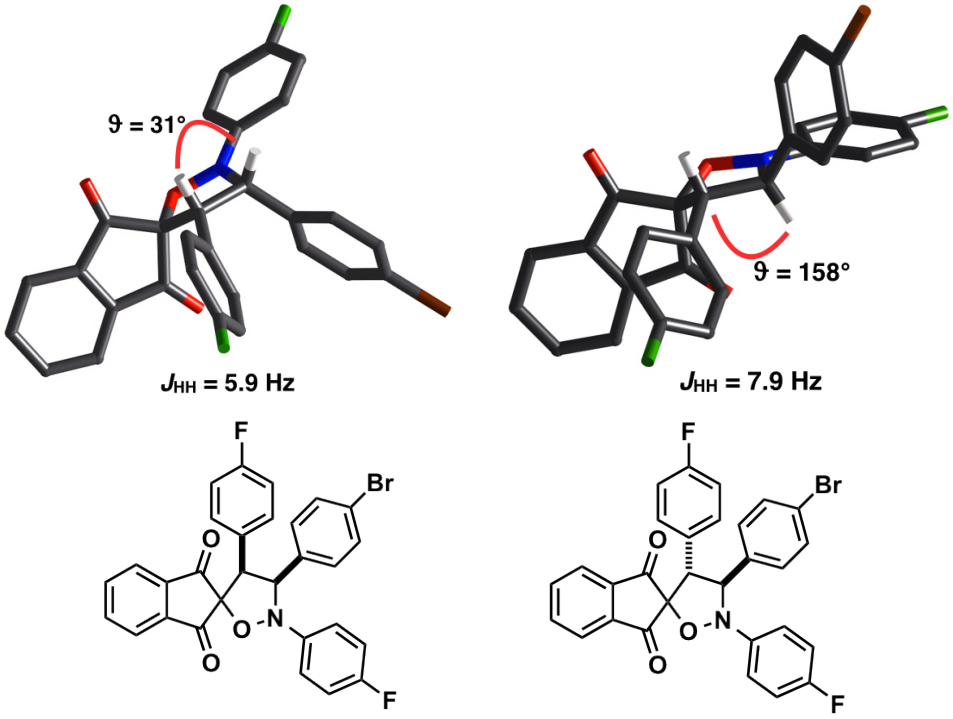


**Figure 3.6:** The vicinal protons on the Anti Michael-*cis* isomer (left) are expected to show *J*-coupling in $^{1}$H NMR spectroscopy. The vicinal protons in the Anti Michael-*trans* isomer (right) are also expected to show *J*-coupling in $^{1}$H NMR spectroscopy. The coupling constants were obtained using **Equations 3.1** and **3.2**. The structures on the top are the result of RM1 calculations. In the geometries, carbon atoms are shown in grey, oxygen in red, nitrogen in blue, fluorine in green and bromine in brown. For clarity, hydrogen atoms have been omitted.

However, it is possible for the Anti Michael regioisomers to not show *J*-coupling between the isoxazolidine protons despite the fact that they are vicinal protons. The Karplus equation describes[99,100] the relationship between the dihedral angle and the coupling constant between vicinal protons (**Equantion 3.1** and **3.2**).

For $0° \leq \vartheta \leq 90°$ $\quad J = 8.5cos^2(\vartheta) - 0.28$ **Equation 3.1**

For $90° \leq \vartheta \leq 180°$ $\quad J = 9.5cos^2(\vartheta) - 0.28$ **Equation 3.2**

The coupling constant of vicinal protons is smallest when the dihedral angle is 90° and largest when the dihedral angle is 180° or 0°. The computational

studies provide a model for the ground state conformation of the Anti Michael stereoisomer (**Figure 3.6**). These ground state models show that the dihedral angle in the Anti Michael-*cis* isomer is 31.28° and the dihedral angle in the Anti Michael-*trans* isomer is 158.10°. The corresponding coupling constants can be obtained by using **Equation 3.1** and **3.2** and are 5.9 Hz for AC-**80** and 7.9 Hz for AT-**80** (**Figure 3.6**).

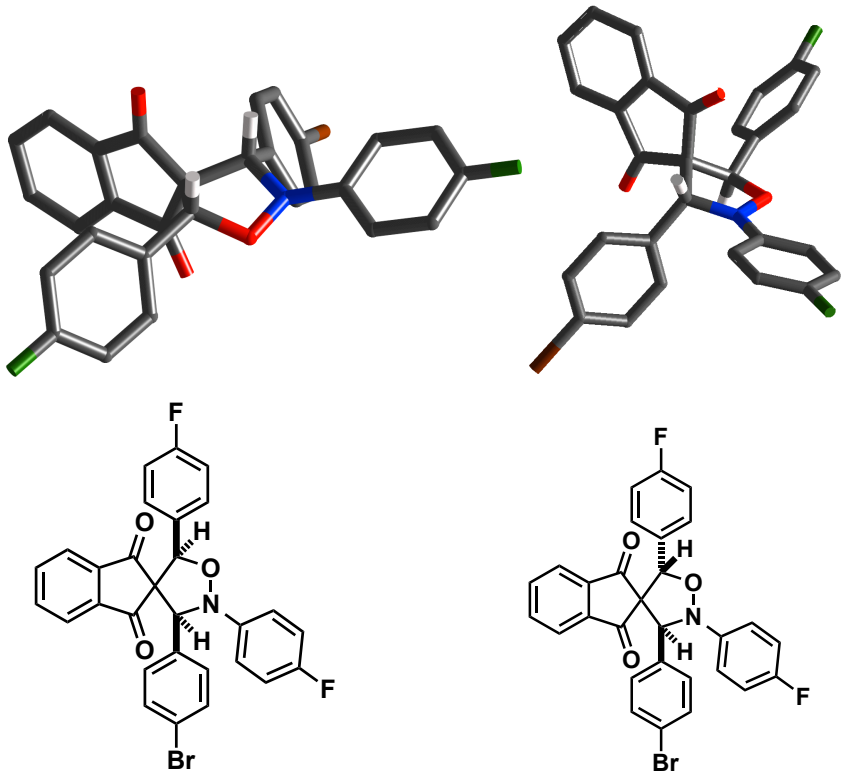


**Figure 3.7:** The Michael-*cis* isomer (left) is not expected to show *J*-coupling in $^{1}$H NMR spectroscopy but is expected to give a response in a 1D-NOESY experiment. The Michael-*trans* isomer (right) is also not expected to show *J*-coupling in $^{1}$H NMR spectroscopy and it is not expected to give a response in a 1D-NOESY experiment. The structures on the top are the result of RM1 calculations. In the geometries, carbon atoms are shown in grey, oxygen in red, nitrogen in blue, fluorine in green and bromine in brown. For clarity, hydrogen atoms have been omitted.

In contrast with the Anti Michael regioisomers, the protons in the isoxazolidine ring in the Michael regioisomers are not expected to show *J*-coupling in the $^{1}$H NMR spectrum as these protons are too far separated. The $^{1}$H NMR spectrum in **Figure 3.4** shows four singlets that correspond to the protons on the isoxazolidine ring. The appearance of singlets in the $^{1}$H NMR spectrum

suggests that the Michael regioisomers are formed in the reaction between the model compounds (**Figure 3.7**).

Further characterisation was carried out with 1D-NOESY experiments (**Figure 3.8**). The protons on the isoxazolidine ring in the Michael-*cis* isomer are expected to show a response upon irradiation in a 1D-NOESY experiment as they are on the same face of the isoxazolidine ring. A response in a 1D-NOESY experiment is not expected for the Michael-*trans* isomer as the protons are on different faces of the isoxazolidine ring.

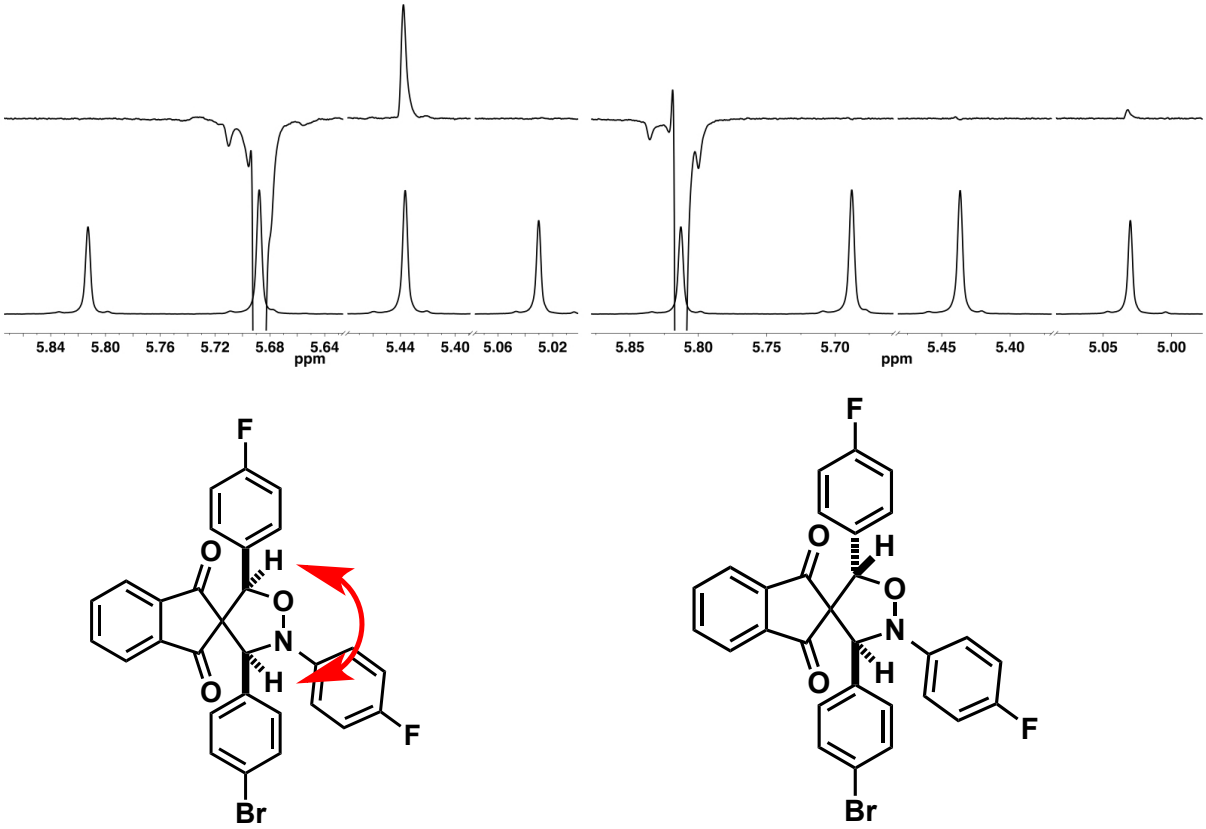


**Figure 3.8:** Irradiation of one proton on the isoxazolidine ring in the Michael-*cis* isomer (left) gives a strong response in the 1D-NOESY experiment (500 MHz, $CDCl_3$, RT). Irradiation of one proton on the isoxazolidine ring in the Michael-*trans* isomer does not give a response in a 1D-NOESY experiment.

In conclusion, using $^1$H NMR spectroscopy and 1D-NOESY experiments the products of the cycloaddition reaction between the model compounds have been identified. The cycloaddition could lead to the formation of four products (**Scheme 3.2**), however only two products are observed after 16 hours, in a 1:1 ratio. As the $^1$H NMR spectrum (**Figure 3.5**) of the products shows singlets, which correspond to the protons on the isoxazolidine ring, the products formed

are the Michael regioisomers. The relative stereochemistry can be assigned because there is a strong response when an isoxazolidine proton of MC-**80** is irradiated but no response when an isoxazolidine proton of MT-**80** is irradiated (**Figure 3.8**).

In order to confirm the absence of *J*-coupling between the isoxazolidine proton signals in the $^{1}$H NMR spectrum, a $^{1}$H-$^{1}$H COSY experiment was done on the sample (**Figure 3.9**).

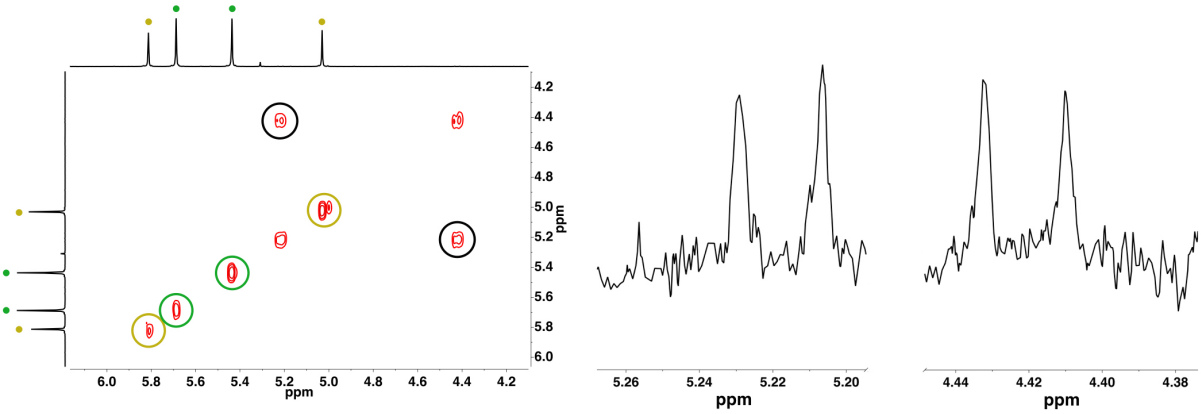


**Figure 3.9:** $^{1}$H-$^{1}$H COSY (500 MHz, $CDCl_3$, RT) experiment (left) of the reaction mixture of the model compounds shows cross coupling between two signals that were not observed before at 5.21 ppm and 4.42 ppm. These signals are visible as doublets in the partial $^{1}$H NMR spectrum (500 MHz, $CDCl_3$, RT) (right).

The $^{1}$H-$^{1}$H COSY spectrum confirmed the absence of cross coupling between the protons on the two major products, which supports the conclusion that these are MC-**80** and MT-**80**. Interestingly, in the $^{1}$H-$^{1}$H COSY spectrum cross coupling was observed between two signals that were not recognised in the analysis previously. The proton signals are present at 5.21 ppm and 4.42 ppm, which is in the spectral region of the newly formed heterocycle. When this region is amplified, two doublets are observed in the $^{1}$H NMR spectrum (**Figure 3.9**). The coupling constant of these doublets was determined to be $J = 11.5$ Hz. Although there is not enough evidence to support the conclusion that these two signals correspond to one of the Anti Michael regioisomers, the integrals of the two doublets match. The experimentally derived coupling constant is not in agreement with the theoretically obtained one with the Karplus equation. This

discrepancy can be caused by an error in the geometry obtained from RM1 studies. Deconvolution of the $^{1}$H NMR resonances afforded the area of the signals and these values can be compared to the areas of the resonances corresponding to the internal standard in order to obtain the concentration of the compound responsible for the signals. Deconvolution of the signals afforded a concentration of this compound of 0.13 mM compared to 16.7 mM for MC-**80** and 12.0 mM for MT-**80**.

We also decided to carry out crystallographic studies to the starting materials (**Figure 3.10**).

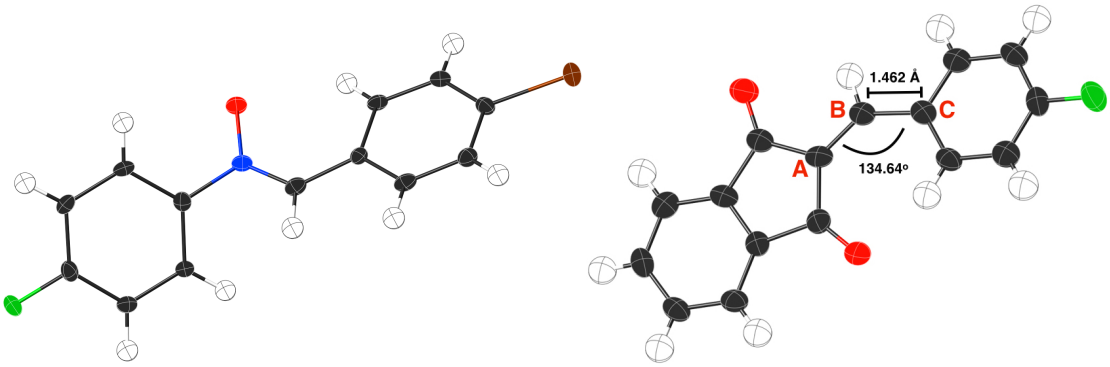


**Figure 3.10:** Crystal structures of the model nitrone compound (left) and the model indandione compound (right). The crystal structure of the indandione model compound shows an angle (indicated) of 134.64° for an $sp^2$ carbon. The bond length (indicated) for the B – C single bond is 1.462 Å, which is shorter than what would be expected for a C–C single bond.

An interesting feature of the crystal structure of indandione **78** is that the $C_A$–$C_B$–$C_C$ angle is 134.64°, which is larger than what would be expected for an $sp^2$ carbon. Moreover, the $C_B$–$C_C$ single bond is 1.46 Å, which is shorter than what would be expected for a C–C single bond. These geometric distortions presumably arise from the fact that the molecule in the solid state is almost flat, which brings the oxygen atom in proximity with one hydrogen atom on the fluorinated phenyl ring. However, it is unknown whether this geometry is only observed in the solid crystal phase or if the geometry is also adopted in solution. It is clear that the RM1 calculations predict a different ground state geometry of indandione **78**.

### 3.3.2 Kinetic Studies

In order to investigate the reactivity of the 1,3-dipolar cycloaddition, indandione **78** and nitrone **79** were reacted at 100 mM at 25 °C and the reaction was monitored for 16 hours by $^{1}$H NMR and $^{19}$F NMR spectroscopy. The products were observed in the $^{19}$F NMR spectrum (**Figure 3.11**) in the spectral region between –111 ppm and –122 ppm and were matched by integration of the resonances. The resonances corresponding to MC-**80** or MT-**80** were assigned by comparison with the $^{1}$H NMR spectrum described previously.

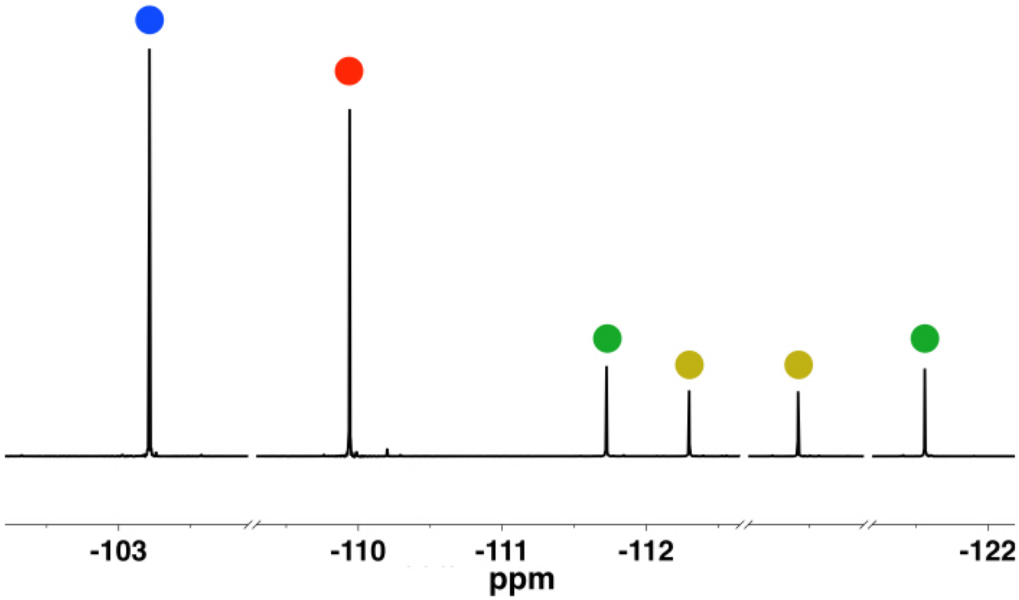


**Figure 3.11:** The 470.3 MHz $^{19}$F NMR spectrum ($CDCl_3$, 25 °C) of the reaction between model nitrone (●) and model indandione (●). Two products are observed after 24 hours, the product peaks are observed between –111 and –122 ppm. The two outer peaks (●) correspond to MC-**80** and the two inner peaks correspond to MT-**80** (●).

In the $^{1}$H NMR spectrum (**Figure 3.5**) the appearance of resonances corresponding to the isoxazolidine protons can be observed as the reaction progresses. Other signals that correspond to the cycloadducts overlap with that of the other aromatic protons of the starting materials. The product resonances are matched by integration.

The resonances in the $^{19}$F NMR spectra were deconvoluted and the data was fitted using the SimFit software package (**Figure 3.12**). A third product, not

shown in **Figure 3.9**, was observed in the $^{19}F$ NMR spectrum, which was also deconvoluted.

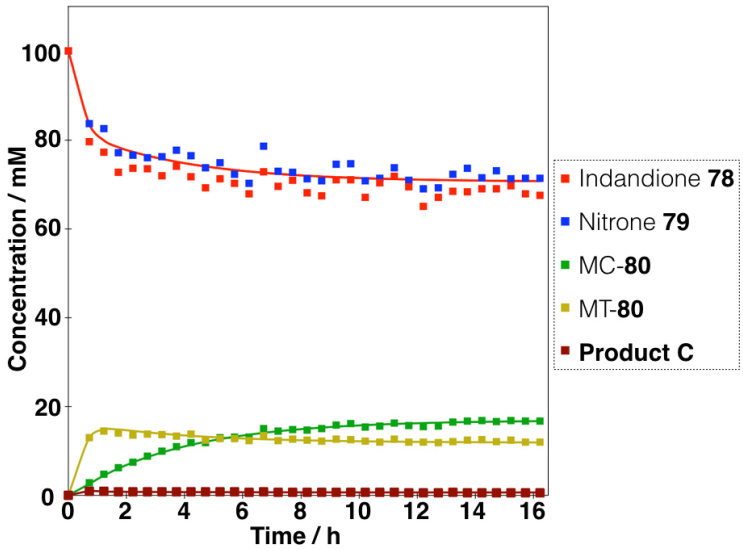


**Figure 3.12:** The concentration *vs.* time profile of the reaction between the model compounds. The experimental data is represented in data point and was obtained by deconvolution of the $^{19}F$ NMR spectroscopic data. The lines represent the result of the kinetic fit obtained by using the SimFit software package. The fit of **78** and **79** overlap.

The fitted data provides information about the kinetic and thermodynamic parameters of the chemical reaction. The output of the fitting provides the rate constant of the chemical reaction as well as the equilibrium constant for the forward and the back reaction (**Table 3.1**). Based on the results of the computational studies, which place AC-**80** significanlty higher in energy than AT-**80**, and considering the doublet that was observed in the $^{1}H$ NMR spectrum, we speculate that product C corresponds to AT-**80**.

**Table 3.1:** Fitting of the $^{19}F$ NMR spectroscopic data affords the rate constants of the forward and the backward reaction. The ratio of these rate constants is the equilibrium constant, K. The residual error is 3.4%.

| | ***K*** | $k_f$ / $10^{-4}$ L $mol^{-1}s^{-1}$ | $k_r$ / $10^{-4}$ L $mol^{-1}s^{-1}$ |
|---|---|---|---|
| MC-**80** | 3.38 | 1.87 | 0.55 |
| MT-**80** | 2.38 | 15.8 | 6.66 |
| Product C | 0.13 | 4.38 | 0.33 |

The free energy of the transition state was calculated using the Eyring equation (**Equation 3.3**). The free energy change of the reaction was calculated using **Equation 3.4**. The temperature used in the calculations of the free energies, was T = 298.15 K, the temperature of the experiment (**Figure 3.13**).

$$\Delta G^{\ddagger} = -RTln((\frac{h}{k_B \cdot T}) \cdot k) \qquad \textbf{Equation 3.3}$$

$$\Delta G = -RTlnK \qquad \textbf{Equation 3.4}$$

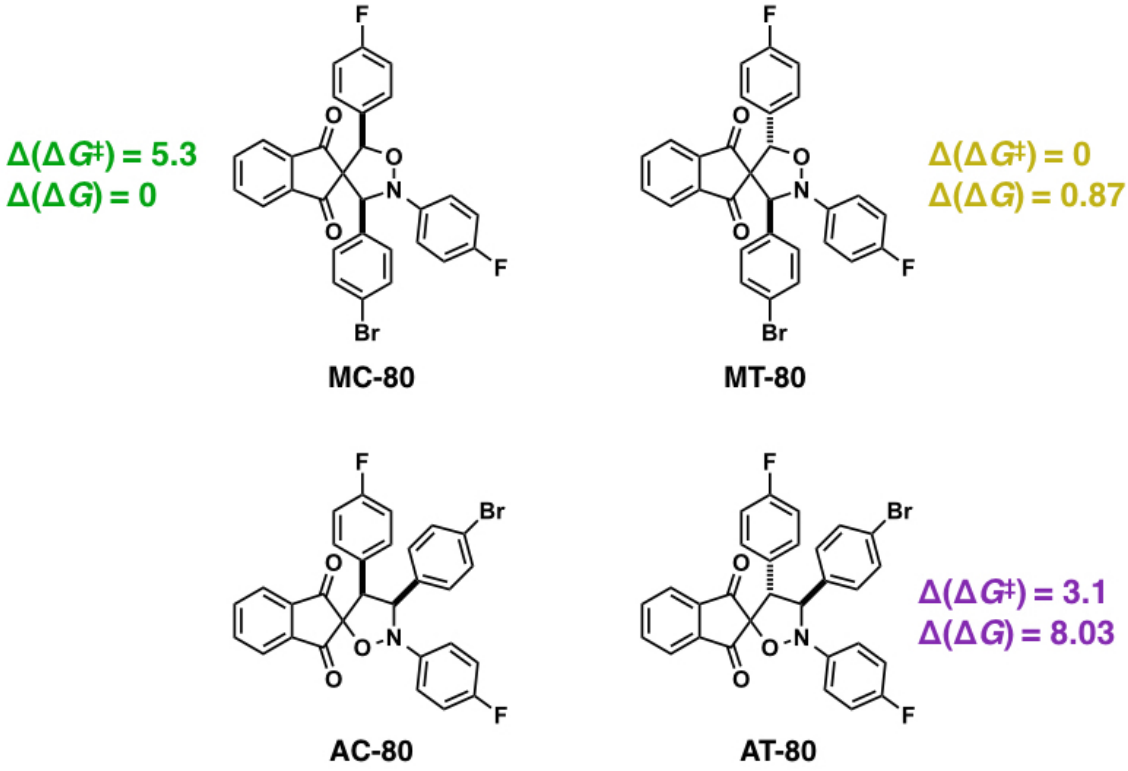


**Figure 3.13:** Fitting of the kinetic data affords the equilibrium constant and rate constant. Using **Equation 3.3** and **3.4**, the transition state free energy and the free energy of reaction can be calculated. The values are reported in kcal $mol^{-1}$.

In order to assess the response of the cycloaddition to increasing temperature, experiments at 60 °C, 80 °C and 120 °C were carried out at starting concentration of 10 mM. Decomposition of nitrone **79** was, however, observed after 4 hours at 80 °C and after 2 hours at 120 °C. Therefore, the results of these experiments are not considered. In **Figure 3.14** the results of the cycloaddition experiment at 60 °C are shown and compared to the results of a kinetic simulation for which data was used that were obtained at 25 °C.

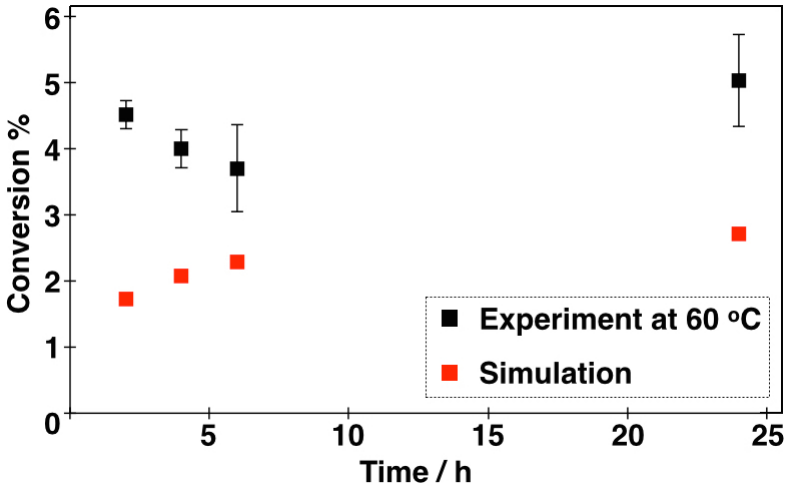


**Figure 3.14:** The conversion of the cycloaddition reaction between indandione **78** and nitrone **79** at 60 °C compared to simulated data at 25 °C. The experiments were carried out in duplicate and the value is averaged and the error bars that are shown are the standard deviation.

The experimental data obtained at 60 °C, compared to the simulation at 25 °C does not show a large increase in conversion when the reaction temperature is increased. In a recognition-mediated scenario the increase of temperature is undesirable because it weakens the strength of the hydrogen bonding interaction.

The low conversion of the cycloaddition between **78** and **79** as well as the small effect of temperature on the production of cycloadducts **80** raises questions about the nature of the chemical reaction and whether or not it might be an equilibrium process rather than a kinetically controlled reaction as the reaction with a maleimide. Therefore, an experiment was designed to test the reversibility of the cycloaddition towards **80** (**Scheme 3.4**).

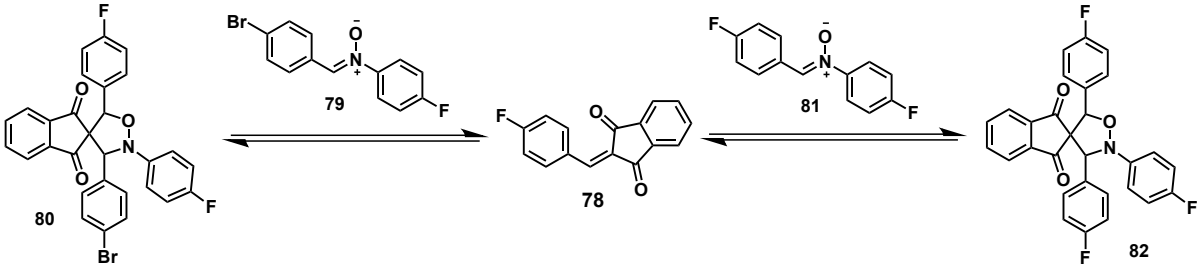


**Scheme 3.4:** If the cycloaddition between an indandione and a nitrone is reversible, addition of an excess of another nitrone should cause the reaction to re-equilibrate.

In this experiment, indandione **78** and nitrone **79** were dissolved at 10 mM in $CDCl_3$ and allowed to react at room temperature for 24 hours before the sample was analysed with $^{1}H$ and $^{19}F$ NMR spectroscopy. Subsequently, 100 mM of nitrone **81** was added to reaction and the mixture was allowed to react for 24 hours before the sample was analysed with $^{1}H$ NMR and $^{19}F$ NMR spectroscopy. If the cycloaddition is reversible, the concentration of both diastereoisomers of **80** should decrease as the formation of the diastereoisomers of **82** decreases the concentration of indandione **78**, which should cause the reaction to re-equilibrate (**Table 3.2**).

**Table 3.2:** The concentrations of the cycloadducts of the reaction between indandione **78** and either nitrone **79** or nitrone **81**. All concentrations are in mM.

| | MC-**80** | MT-**80** | MC-**82** | MT-**82** |
|---|---|---|---|---|
| Nitrone **79** | 0.29 | 0.23 | - | - |
| Nitrones **79, 81** | 0.20 | 0.15 | 1.30 | 0.89 |

Upon addition of an excess of nitrone **81** to the reaction mixture, the concentration of MC-**80** and MT-**80** in the mixture decreases. The ratio between MC-**82** and MT-**82** is 1.46 in favour of MC-**82**, which is similar to the final diastereometric ratio from the model compound reaction between **78** and **79**. As the cycloaddition reaction is reversible, it can be used to create a Dynamic Covelent Library under thermodynamic control.

### 3.3.3 Kinetic Simulations

In order to investigate the progress of the reaction at different initial concentrations, kinetic simulations with the Copasi software package were carried out using the parameters in **Table 3.1**. Initially, a model was created using the same conditions as in the experiment described previously, this afforded a model that gave the same output as the experimental data, which confirmed that this model can be used to simulate the progress of the reaction under different experimental conditions. The data used for the kinetic fitting was obtained in an experiment with starting concentration 100 mM. This

concentration is unrealistically high for a recognition-mediated reaction for two reasons. First of all, compounds that are equipped with recognition sites are generally not soluble at concentrations above 25 mM in $CDCl_3$. Second of all, at high concentrations the bimolecular reaction pathway is relatively fast compared to the recognition-mediated pathway and therefore experiments with recognition-enabled compounds are ideally carried out at lower concentrations. Initially the reaction progress was simulated with 10 mM initial concentration of the starting materials (**Figure 3.15**).

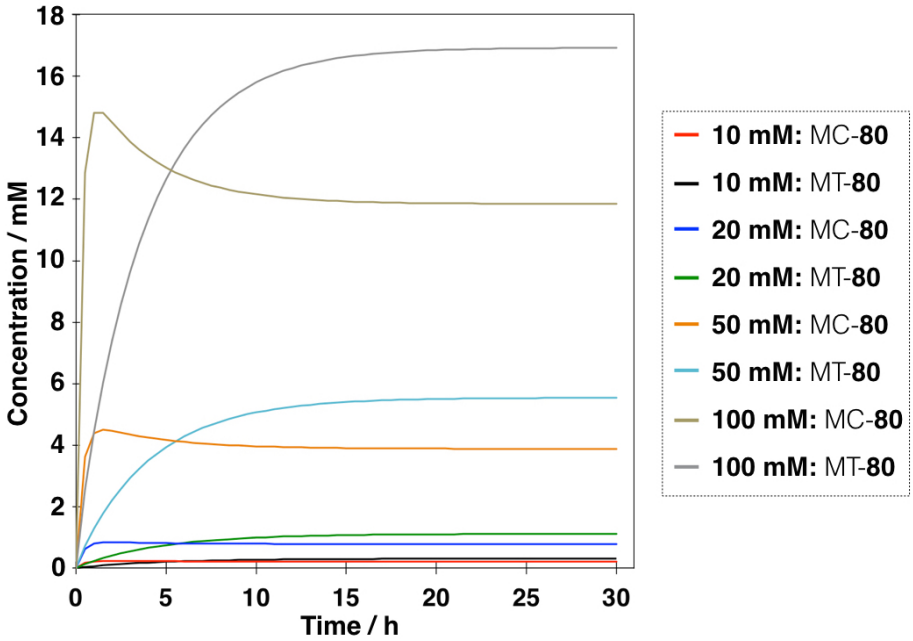


**Figure 3.15:** The progress of the reaction between indandione **78** and nitrone **79** was modelled at different initial concentrations using Copasi software[8]. The kinetic parameters from **Table 3.1** were used and the reaction progress was modelled for 30 hours.

The conversion of the starting materials is considerably lower when the starting concentration is lower. Subsequently, the reaction progress was simulated with Copasi with different starting concentrations ranging from 5 mM to 1 M (**Figure 3.16**).

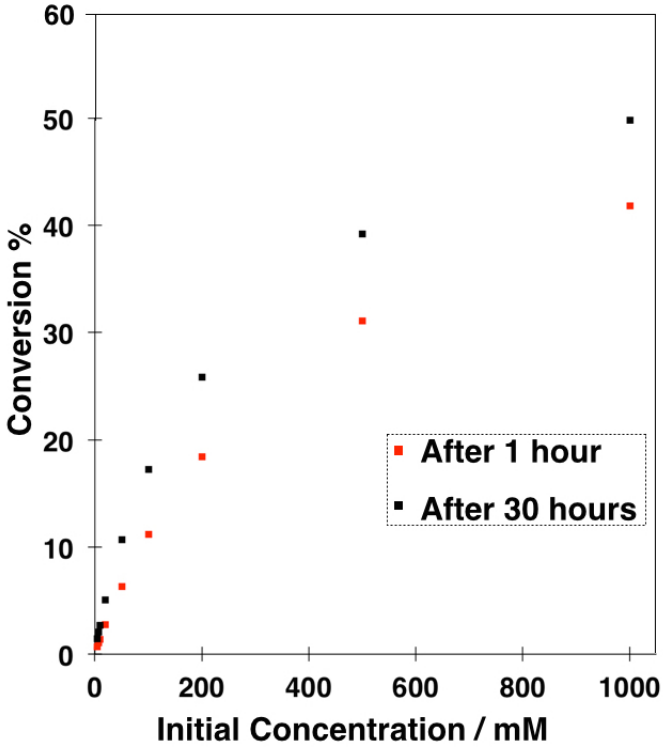


**Figure 3.16:** The conversion of the cycloaddition between indandione **78** and nitrone **79** was simulated using Copasi software[8] as a function of increasing concentration. The parameters from **Table 3.1** were used as input for the simulation. The conversion of the model reaction increases significantly when the starting concentration is increased.

The trend that conversion increases with increasing initial concentration is general. This trend indicates that, since the experiments with recognition-enabled compounds will be carried out at low concentration, the conversion of the bimolecular reaction is low at this concentration range. Therefore, the flux through the bimolecular reaction pathway will be low and the conversion can potentially be increased a lot with molecular recognition.

The two major products of the model compound reaction are MC-**80** and MT-**80**. From the simulations the ratio of the two isomers after 1 hour and 30 hours can be calculated (**Figure 3.17**).

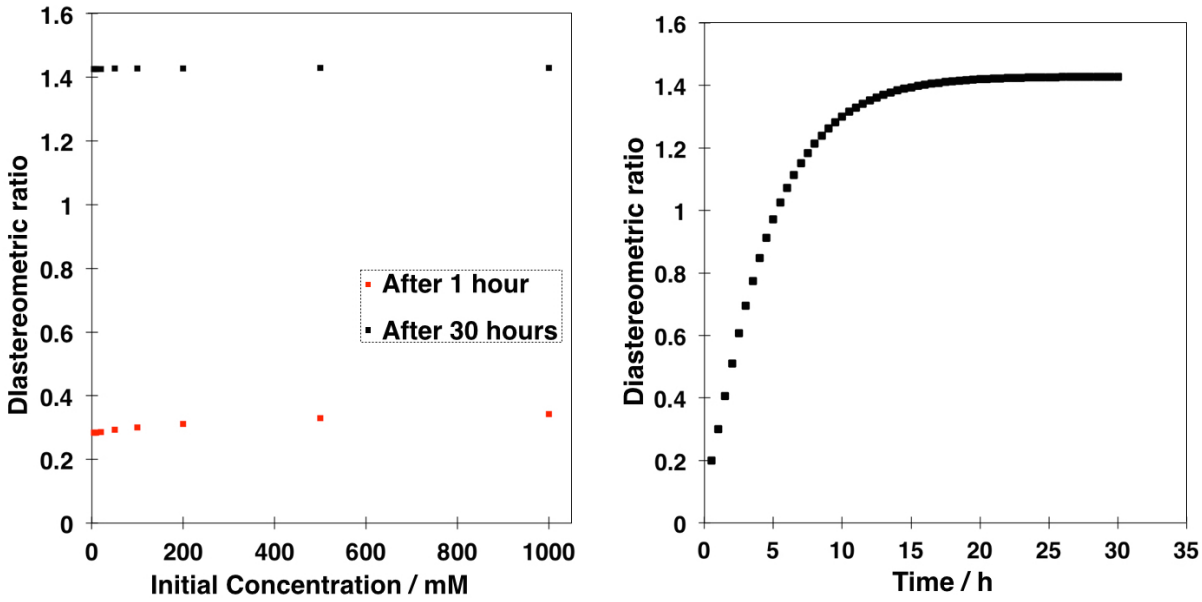


**Figure 3.17:** The diastereometric (Michael *cis* : Michael *trans*) ratio was simulated using the Copasi software[8]. The data from **Table 3.1** was used as input. Left: The diastereometric ratio at different concentration of starting material does not increase significantly with increasing the starting concentration of the starting materials. Right: The diastereometric ratio as a function of time during the reaction, 10 mM was used as initial concentration.

The *cis*:*trans* ratio of the products, both after 1 hour and 30 hours, does not change when the initial concentration of the starting materials is decreased or increased. The fact that low selectivity is obtained in the bimolecular reaction suggests that the selectivity cannot be improved by changing the initial concentration. Possibly, molecular recognition can improve the selectivity of the reaction.

## 3.5 Comparison between Experimental and Computational Results

In an ideal scenario, the trends obtained from the computational investigations should have predictive power and the same trends should be observed in the experimental investigation. The computational studies predict (**Figure 3.3**) that there is clearly one most stable product, always MC-**80**, two products with intermediate and equal relative stability and one product, AC-**80**, that is the least stable. These results predict that in the experiments one major product will be observed and two minor products will be observed and one isomer will not

be observed. However, when the reaction is followed for 16 hours, two products are observed (**Figure 3.12**) roughly in a 1:1 ratio. However, the order of stability of the cycloadducts is predicted correctly by DFT using the M06-2X functional. MC-**80** is the most stable, then MT-**80** and then AT-**80**, which is the doublet we observe in the $^{1}$H NMR spectrum. RM1 predicts MC-**80** to be the most stable cycloadduct and MT-**80** and AT-**80** to be similar in energy. The computationally derived stabilities are derived from calculations in the gas phase at 298 K whereas the experiments take place in solution. This difference in conditions is presumably the reason that the energy values are incorrect. Additionally, the RM1 calculations predict MC-**80** to have both the most favourable stabilisation energy and the most favourable transition state energy. However, the experimental investigation shows that MC-**80** is the most favourable product but it has a more unfavourable transition state energy associated with it than MT-**80**. Furthermore, even though the computational studies predict that MT-**80** and AT-**80** should have equal stabilisation and transition state energies and should therefore be observed in equal amounts. From the experimental data it is clear that MT-**80** is observed but certainly not in equal amounts as AT-**80**.

## 3.6 Conclusions

The computational studies on the cycloaddition reaction gave us a relative order of stabilities of the four diastereometric cycloadducts. Both RM1 calculations and DFT calculations predict that MC-**80** is the most stable product, then MT-**80** and AT-**80** and AC-**80** is the most unstable cycloadduct. Although the experimental results show a difference in terms of absolute energy values, the order of stability is correctly predicted by the computational studies both on DFT level and RM1 level.

Experimental studies of the 1,3-dipolar cycloaddition with model compounds has shown that two of the possible four isomers are formed preferentially in the reaction. Isolation of the cycloadducts is not possible as a result of the dynamic nature of the system. Therefore, the products were characterised in the reaction

mixture. Because of the fact that the resonances corresponding to the isoxazolidine ring protons in the $^{1}$H NMR spectrum are singlets and the Anti Michael regioisomers are expected to show doublets in the $^{1}$H NMR spectrum, it is concluded that the Michael regioisomers are formed. One compound is formed more rapidly but this compound is present the lowest concentration after the reaction, whereas the other product is formed more slowly and is present at highest concentration after the reaction is completed. As a result of the response in a 1D-NOESY experiment, it is concluded that the product that is formed relatively slowly is MC-**80**. The compound that is formed relatively quickly does not show a response in the 1D-NOESY experiment and therefore it is concluded that this is MT-**80**. A third product is formed, which is present at 0.13 mM, compared to 16.8 mM for MC-**80** and 12.0 mM for MT-**80**, and shows *J*-coupling, which suggests that this in one of the Anti Michael regioisomers.

The kinetic studies with the model compounds afforded kinetic and thermodynamic parameters. These parameters were used to create a kinetic model using Copasi to simulate the reaction with different starting concentrations. These kinetic simulations suggest that the product ratio does not change significantly when the starting concentration is increased. Experimental studies have also shown that the cycloaddition is reversible and can thus be used in Dynamic Covalent Chemistry.

# 4

# Development of a Recognition-Mediated Cycloaddition Reaction

The aim of this work is to develop a recognition-mediated system, similar to the ones reported previously by the Philp laboratory, but based on the reaction between an indandione and a nitrone rather than a maleimide. In this chapter, first of all, the challenges towards the synthesis of the indandiones that are equipped with a recognition site are discussed. Secondly, the computational investigation of the recognition-mediated reaction pathways as well as the experimental investigations and kinetic analyses are reported.

## 4.1 Design and Synthesis of Recognition-enabled Indandiones

The first step towards the new self-replicating system was the design and synthesis of indandione compounds that bear the amidopyridine or carboxylic acid recognition site. Since the recognition site can be located on either of the two components and the synthesis of the indandione with a carboxylic acid recognition site requires less synthetic steps, this route was explored first. **Scheme 4.1** shows the Knoevenagel condensation between 1,3-indandione and 4-carboxybenzaldehyde to afford indandione **83**, which is equipped with a benzoic acid recognition site.

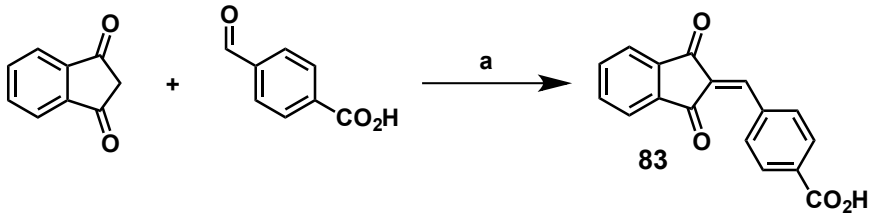


**Scheme 4.1:** Synthesis of indandione **83** with the carboxylic acid recognition site. a) $Et_3N$, MeCN, RT, 33%.

Indandione **83** was first tested for solubility in $CDCl_3$. Unfortunately, the compound was not sufficiently soluble in $CDCl_3$ to be tested in a recognition-mediated reaction. Based on previous research in the Philp group, an alternative compound, indandione **86**, was designed and synthesised according to the procedure in **Scheme 4.2**.

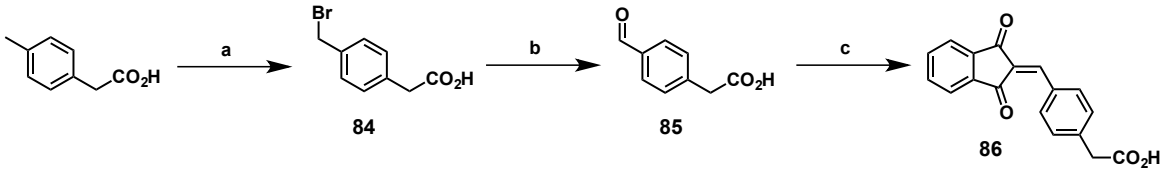


**Scheme 4.2:** Synthesis of indandione **86**, from 1,3-indandione and aldehyde **85**, with the carboxylic acid recognition site. a) $Br_2$, chlorobenzene, hv, RT, 54% b) HMTA, conc. HCl, EtOH/$H_2O$ (1:1), 100 °C, 60%. c) Pyridine, EtOH, RT, 64%.

Even though the maleimide **38**, the equivalent of indandione **86**, used in previous replicators, is soluble at 20 mM in $CDCl_3$, indandione **86** is not sufficiently soluble to test in a self-replicating system. In order to achieve better solubility with these compounds in $CDCl_3$, a solubilising octyl chain can be added on to the molecule. However, as the cycloaddition already leads to the formation of two regioisomers the symmetry of the indandione should not be reduced further as that would complicate the analysis of the products even further. The Philp laboratory has experience with functionalising compounds with alkyne or alkyl chains to increase the solubility of the compounds. Palladium catalysed cross-coupling is a widely used method to form C–C bonds in organic and organometallic chemistry,[101] and was used in the work described here to functionalise the compounds with an octyl chain that should provide improved solubility in $CDCl_3$. Therefore, based on previous research within the Philp laboratory, aldehyde **92** was synthesised and reacted with 1,3-indandione to form indandione **93**, which is equipped with a carboxylic

acid recognition site and an octyl chain that should provide improved solubility in $CDCl_3$.

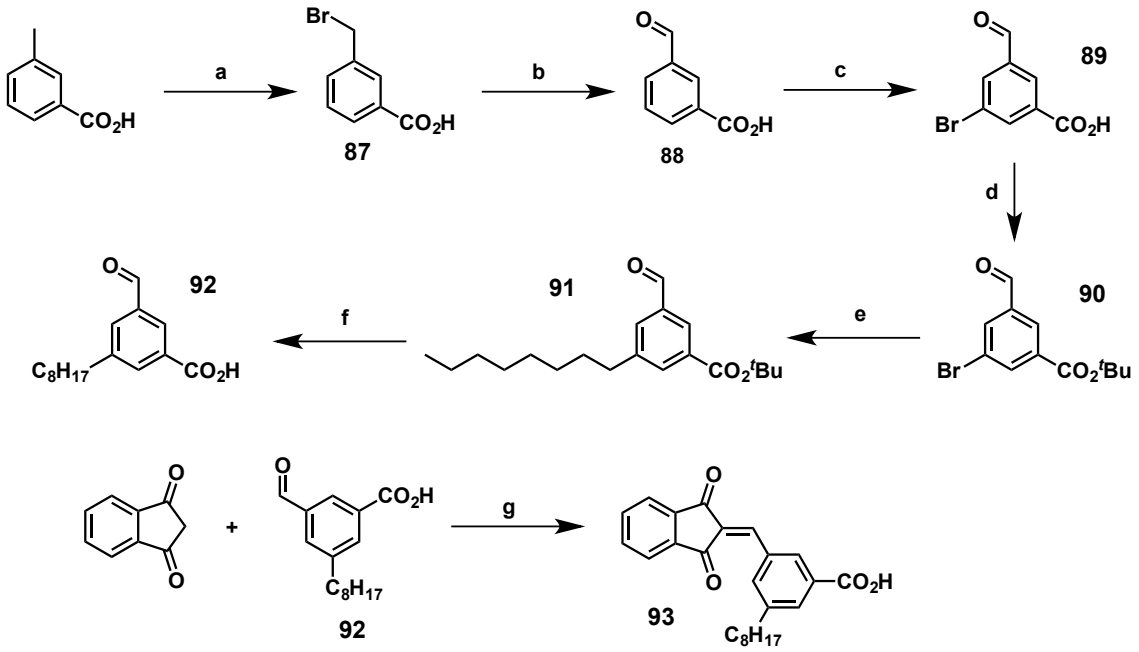


**Scheme 4.3:** Synthesis of indandione **93**, from aldehyde **92** and 1,3-indandione, with the carboxylic acid recognition site and octyl solubilising group. a) $Br_2$, chlorobenzene, hv, RT, 44%. b) HMTA, conc. HCl, EtOH/$H_2O$ (1:1), 100 $^oC$, 80%. c) NBS, conc. $H_2SO_4$, RT, 58%. d) 2-bromo-2-methyl propane, $NEt_3BnCl$, $K_2CO_3$, *N*,*N*-dimethylacetamide, 55 $^oC$, 77%. e) Octyl boronic acid, $K_2CO_3$, $Pd(PPh_3)_4$, toluene/$H_2O$ (3:1), 95 $^oC$, 66%. f) TFA, DCM, RT, 95%. g) pyridine, EtOH, RT, 40%.

Indandione **93** did not show the desired solubility properties in $CDCl_3$. The compound is soluble at 5 mM in $CDCl_3$. Even though the compound is soluble, concentrations above 5 mM are more ideal as the association of building blocks on a template is only quantitative when the concentration of the template rises above the $K_a$ for complex formation. In addition, the studies with model compounds described in **Chapter 3** have indicated that the bimolecular reaction affords low conversion and is slow at 5 mM.

The poor solubility of the indandiones equipped with a carboxylic acid recognition site is presumably the result of the carboxylic acid group. Therefore, the design strategy for the compounds was changed to put the amidopyridine recognition site on the indandione. In order to achieve this, aldehyde **95** was

synthesised from 4-carboxybenzaldehyde. The complete synthetic pathway of the amidopyridine-functionalised indandione **96** is shown in **Scheme 4.6**.

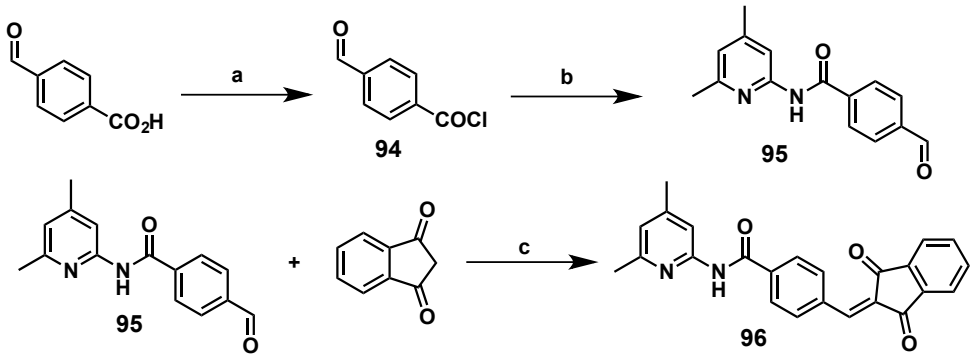


**Scheme 4.6:** Synthesis of indandione **96** with amidopyridine recognition site. a) $SOCl_2$, toluene, 150 °C, 91%. b) 4,6-methyl-2-amino pyridine, $Et_3N$, DCM, 0 °C → RT, 61%. c) pyridine, EtOH, RT, 43%.

Indandione **96** was found to be soluble in $CDCl_3$ at 10 mM. However, ideally a wider concentration range could be accessed to carry out experiments with the newly designed compounds. Therefore, similar to the design of aldehyde **92** and indandione **93**, the pyridine ring can be functionalised with an octyl chain. The synthesis of indandione **100** is shown in **Scheme 4.7**.

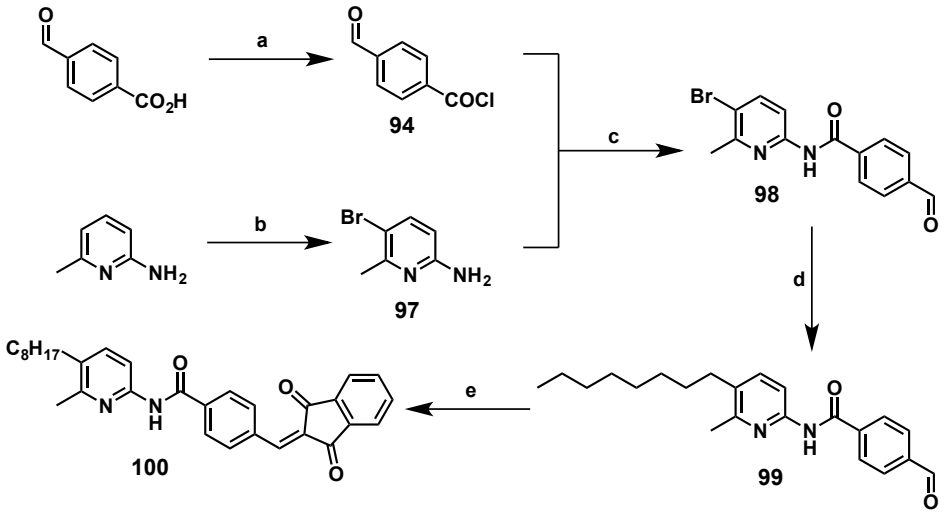


**Scheme 4.7:** Synthesis of indandione **100** with amidopyridine recognition site, equipped with a solubilising octyl chain: a) $SOCl_2$, toluene, 150 °C, 91%. b) NBS, MeCN, RT. c) DCM, 0 °C → RT, 50%. d) Octyl boronic acid, $K_2CO_3$, $Pd(PPh_3)_4$, toluene/$H_2O$ (3:1), 95 °C, 88%. e) 1,3-indandione, pyridine, EtOH, RT, 53%.

The octyl solubilising chain proved successful in increasing the solubility of indandione **100**, the compound is now soluble at 20 mM in $CDCl_3$.

## 4.2 Computational Investigation of Recognition-Mediated Reaction

Similar to the studies with model compounds described in **Chapter 3**, the recognition-mediated reaction was also studied computationally with RM1 calculations. Two nitrones, **101** and **102**, were selected for computational studies (**Figure 4.1**).

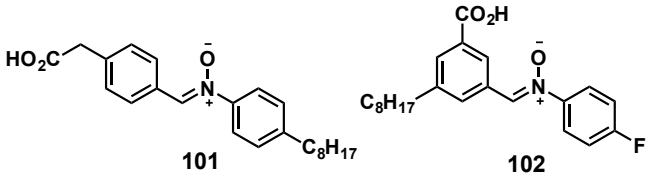


**Figure 4.1:** The two nitrones that are investigated in the 1,3-dipolar cycloaddition with the amidopyridine-equipped indandione and the subsequent desired recognition-mediated behaviour that the product may show.

The nitrones can react with the indandione, equipped with a recognition site, in three distinct reaction pathways. Two of these are modelled in the RM1 calculations; the bimolecular reaction pathway and the recognition-mediated autocatalytic cycle.

### 4.2.1 Computational Investigation of the Reaction between Indandione 96 and Nitrone 101

Nitrone **101** has a phenylacetic acid recognition site (**Scheme 4.8**) in which the distance between the recognition site and the reactive site on the nitrone is longer than in nitrone **102** and thus different behaviour is expected.

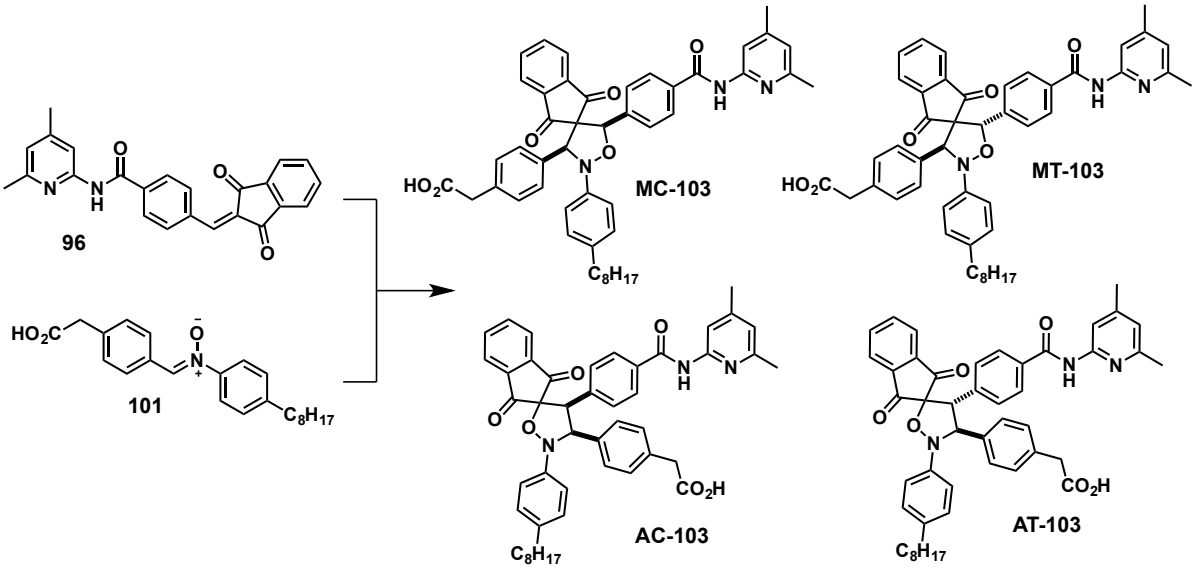


**Scheme 4.8:** The reaction between nitrone **101** and indandione **96** can form four isomers of **103**.

**Figures 4.2** shows the potential energy surfaces and the transition state geometries towards the formation of AC-**103** and MC-**103**.

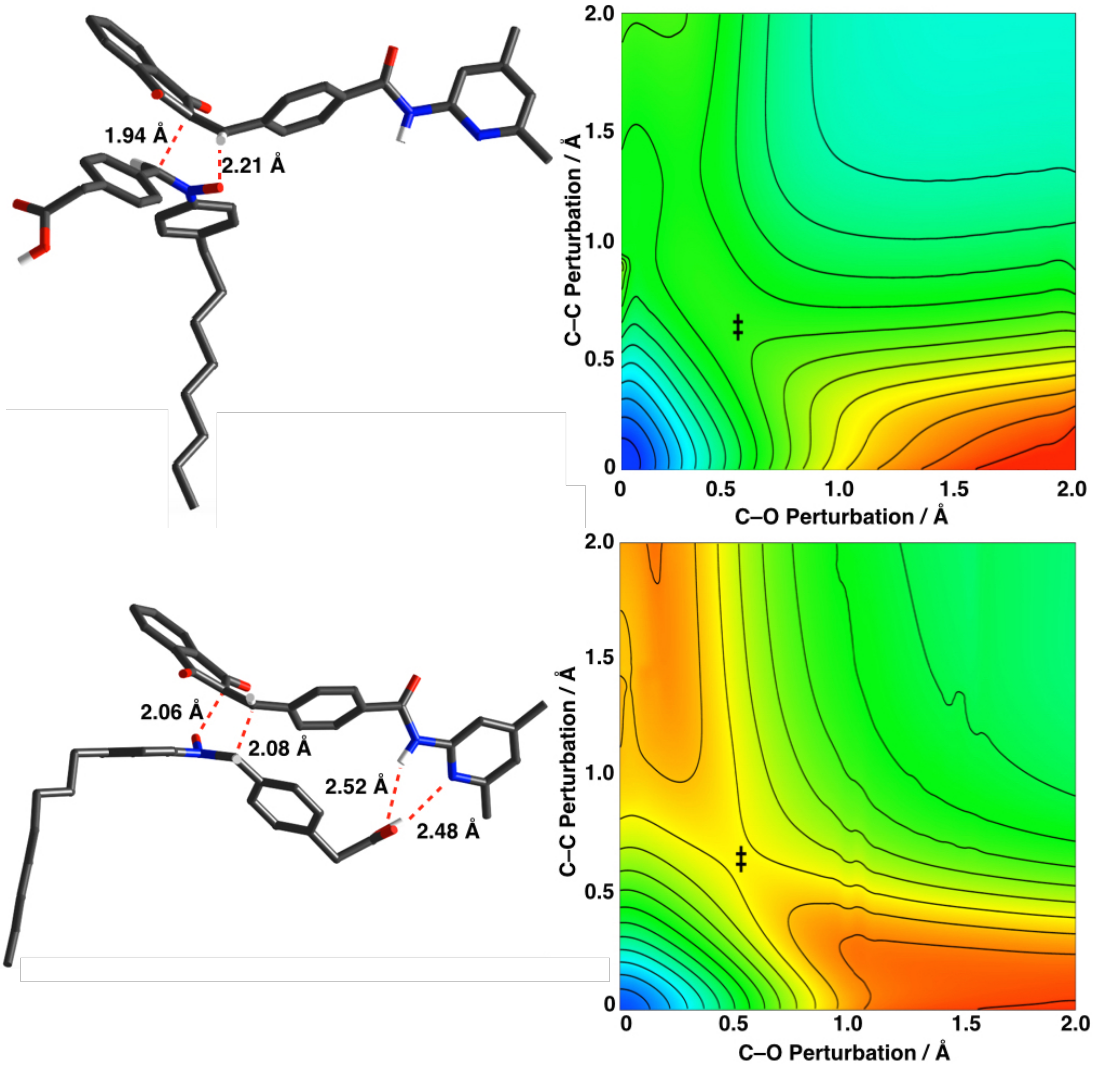


**Figure 4.2:** Top: Potential energy surface and transition state geometry for the bimolecular reaction between nitrone **101** and indandione **96** towards the formation of MC-**103**. Bottom: Potential energy surface and transition state geometry for the bimolecular reaction between nitrone **101** and indandione **96** towards the formation of AC-**103**. In the geometries, carbon atoms are shown in grey, oxygen in red, nitrogen in blue. For clarity, hydrogen atoms have been omitted. In the potential energy surfaces, blue/green represent low energy and red represents high-energy areas. The transition state location on the potential energy surface is marked with ‡.

Interestingly, in the transition state geometry of AC-**103**, hydrogen bonds are observed between the carboxylic acid on the nitrone and the amidopyridine on the indandione. This suggests that the formation of Anti-Michael *cis* preferentially takes place through the [**A•B**] complex pathway. The hydrogen bonds are also present in the product, thus forming the inactive template **T´** (**Figure 4.3**). The fact that the outcome of the RM1 calculations to the ground state of the Anti Michael *cis* isomeric product affords the inactive template

means that one of the lowest ground state conformations of AC-**103** shows hydrogen bonding in the product.

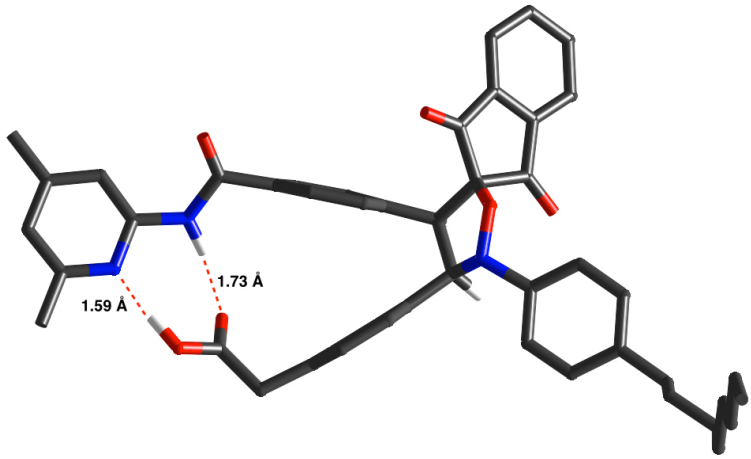


**Figure 4.3:** Hydrogen bonding is present in AC-**103**, thus forming the inactive template **T'**. Carbon atoms are shown in grey, oxygen in red, nitrogen in blue. For clarity, hydrogen atoms have been omitted.

The recognition-mediated reaction pathway is also modelled with RM1 calculations. **Figure 4.4** shows the potential energy surface for the recognition-mediated formation of AC-**103**, which is the most kinetically unfavourable.

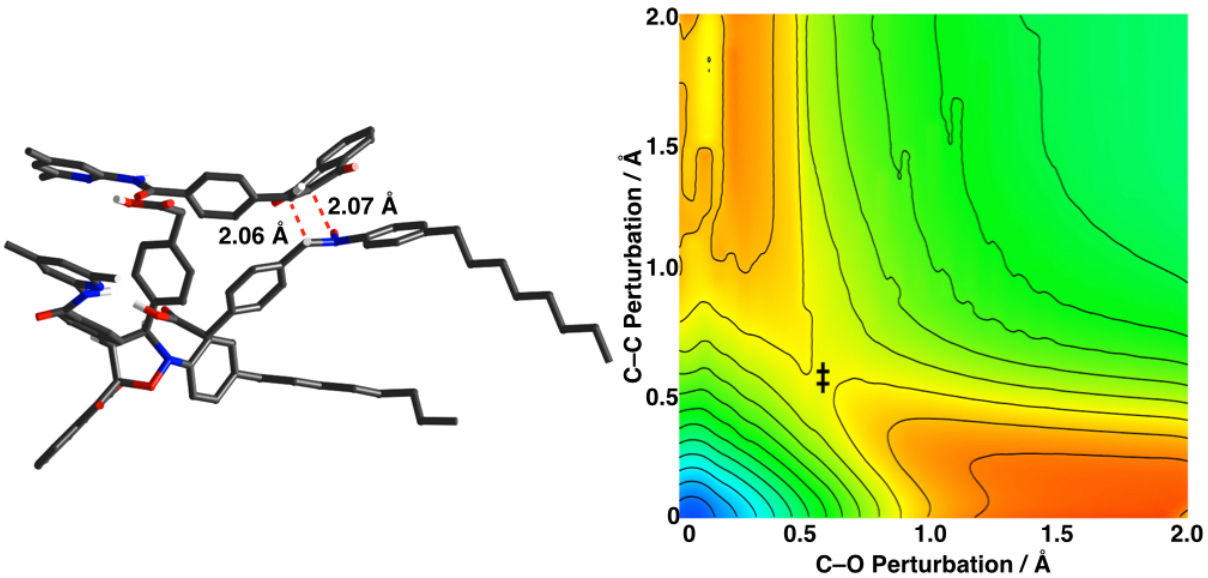


**Figure 4.4:** Potential energy surface and transition state geometry for the recognition-mediated reaction between nitrone **101** and indandione **96** towards the formation of the AC-**103**. In the geometries, carbon atoms are shown in grey, oxygen in red, nitrogen in blue. For clarity, hydrogen atoms have been omitted. In the potential energy surfaces, blue/green represent low energy and red represents high-energy areas. The transition state location on the potential energy surface is marked with ‡.

The RM1 calculations give the internal energy of the transition states and the products (**Table 4.1**).

**Table 4.1:** The relative heats of formations for the products of the cycloaddition between nitrone **101** and indandione **96** and their transition states. The values are reported in kcal $mol^{-1}$.

| | **Bimolecular reaction** | | **Autocatalytic** | |
|---|---|---|---|---|
| | **$\Delta(\Delta H_f^{\ddagger})$** | **$\Delta(\Delta H_f)$** | **$\Delta(\Delta H_f^{\ddagger})$** | **$\Delta(\Delta H_f)$** |
| MC-**103** | 1.4 | 5.1 | 6.7 | 0 |
| MT-**103** | 0 | 0 | 0 | 1.9 |
| AC-**103** | 7.0 | 3.2 | 12.5 | 6.8 |
| AT-**103** | 2.9 | 6.0 | 10.9 | 5.0 |

When the reaction takes place in the recognition-mediated pathway, the relative stabilities of the products changes. Whereas in the bimolecular reaction MT-**103** is the most stable product, in the recognition-mediated reaction its ground state energy is slightly higher than that of MC-**103**. Additionally, a change in relative transition state energies can be observed. In the bimolecular reaction, the transition state energies of AT-**103**, MC-**103**, MT-**103** are close together. In the recognition-mediated reaction, however, it is clear that MT-**103** is kinetically the most favourable product. Therefore, the expectation is that MT-**103** will be formed at a higher rate than the other template isomers. Since the templates are expected to have autocatalytic properties, the rate of formation of MT-**103** will increase even more dramatically with increasing template concentration. However, MT-**103** does not have the lowest ground state energy because MC-**103** is lower with 1.9 kcal/mol. Therefore, since the cycloaddition is reversible, it is expected that when the reaction takes place under thermodynamic control, MC-**103** will be the major product.

### 4.2.2 Computational Investigation of the Reaction between Indandione 96 and Nitrone 102

Nitrone **102** and indandione **96** can form four products, which are depicted in **Scheme 4.9**.

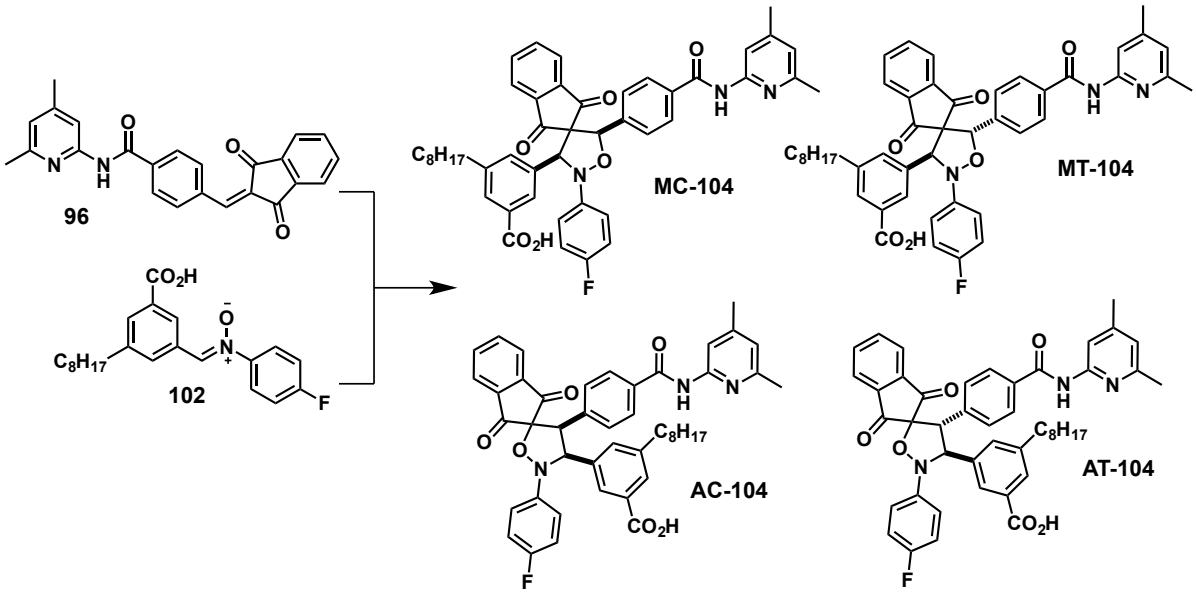


**Scheme 4.9:** The reaction between nitrone **102** and indandione **96** can form four isomers of **104**.

The RM1 calculations were used to create the potential energy plots of the isomeric products of the cycloaddition. The grid scans for the two isomeric products with the highest and the lowest transition state energy are shown in **Figure 4.5** together with the corresponding transition state geometries.

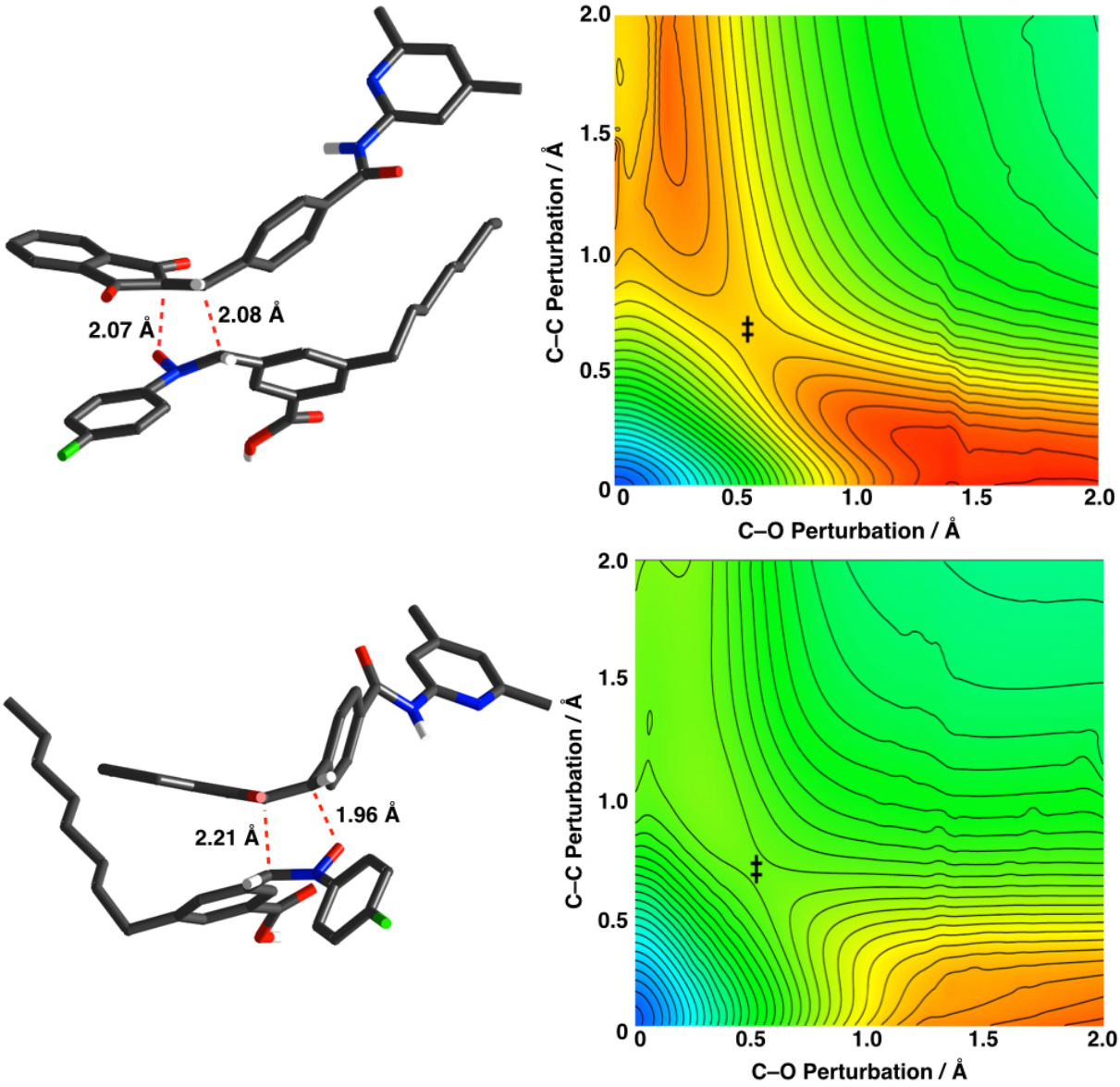


**Figure 4.5:** Top: Potential energy surface and transition state geometry for the bimolecular reaction between nitrone **102** and indandione **96** towards the formation of AC-**104**. Bottom: Potential energy surface and transition state geometry for the bimolecular reaction between nitrone **102** and indandione **96** towards the formation of MC-**104**. In the geometries, carbon atoms are shown in grey, oxygen in red, nitrogen in blue, fluorine in green. For clarity, hydrogen atoms have been omitted. In the potential energy surfaces, blue/green represent low energy and red represents high-energy areas. The transition state location on the potential energy surface is marked with ‡.

The transition state geometries of the reaction between nitrone **102** and indandione **96** towards the two different regioisomeric products show similar distances between the atoms involved in the bond forming step. In the transition state in the reaction towards the Michael regioisomers, the C–O bond appears to be formed prior to the C–C bond of the isoxazolidine ring, whereas in the Anti

Michael regioisomers the bonds appear to form synchronously. The same transition state geometry was observed with the model compounds described in **Chapter 3**. Apart from the bimolecular reaction, the recognition-mediated reaction is also modelled with RM1 calculations. The grid scans for the two Anti Michael regioisomers are shown in **Figure 4.6** together with the corresponding transition state geometries.

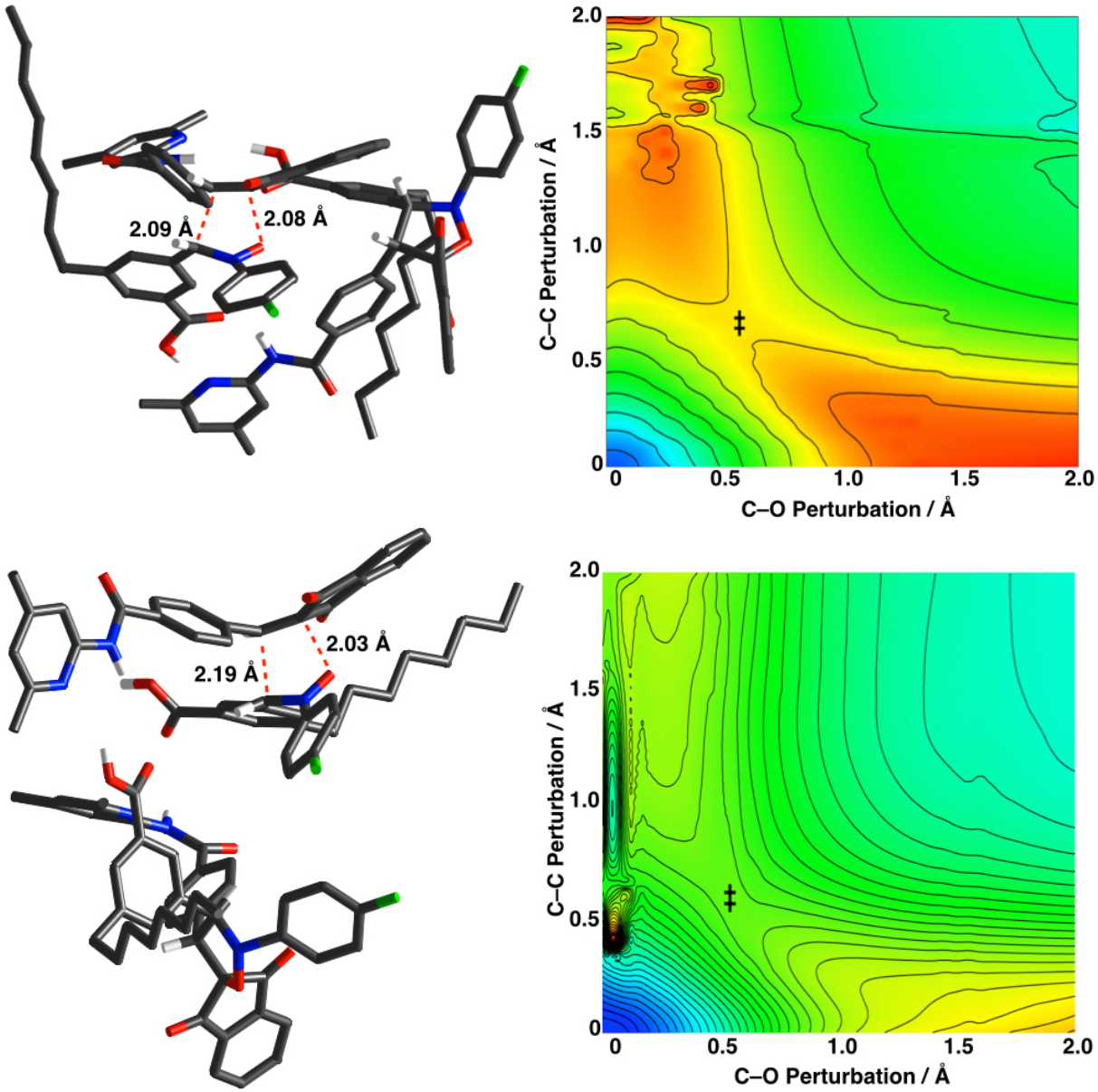


**Figure 4.6:** Top: Potential energy surface and transition state geometry for the recognition-mediated reaction between nitrone **102** and indandione **96** towards the formation of AC-**104**. Bottom: Potential energy surface and transition state geometry for the recognition-mediated reaction between nitrone **102** and indandione **96** towards the formation of AT-**104**. In the geometries, carbon atoms are shown in grey, oxygen in red, nitrogen in blue, fluorine in green. For clarity, hydrogen atoms have been omitted. In the potential energy surfaces, blue/green represent low energy and red represents high-energy areas. The transition state location on the potential energy surface is marked with ‡.

Interestingly, in the self-replicating reaction pathway, the transition state leading to the Anti Michael *cis* isomeric product shows similar transition state distances as previously observed for the Michael regioisomer, thus suggesting the recognition-mediated reaction can significantly alter the transition state geometry of the reaction.

The RM1 calculation gives the internal energies of the ground state of the products and the transition state towards the products (**Table 4.2**).

**Table 4.2:** The relative heats of formations for the products of the cycloaddition between nitrone **102** and indandione **96** and their transition states. The values are reported in kcal $mol^{-1}$.

| | **Bimolecular reaction** | | **Autocatalytic** | |
|---|---|---|---|---|
| | **$\Delta(\Delta H_f^{\ddagger})$** | **$\Delta(\Delta H_f)$** | **$\Delta(\Delta H_f^{\ddagger})$** | **$\Delta(\Delta H_f)$** |
| MC-**104** | 0.4 | 0 | 0 | 1.2 |
| MT-**104** | 3.6 | 0.7 | 8.4 | 19.0 |
| AC-**104** | 10.4 | 7.2 | 7.8 | 6.9 |
| AT-**104** | 0 | 0.6 | 1.9 | 0 |

Clearly, as observed for the model compounds, the AC-**104** isomer is the least favourable product in terms of transition state energy and ground state energy. The transition state energy of MC-**104** is again lower than MT-**104** and AT-**104**, which are close together.

In the recognition-mediated reaction, the MC-**104** and AT-**104** have the lowest ground state energies and transition state energies, which is similar to the bimolecular reaction. The MT-**104** product is favourable both kinetic and thermodynamic in the bimolecular reaction, but not in the recognition-mediated reaction. Hence, the MT-**104** product can form *via* the bimolecular pathway more efficiently than through the recognition-mediated reaction. The AC-**104** product is in both cases the most unfavourable product, both kinetically and thermodynamically. Hence, it is expected that this product would not be formed in an experiment.

## 4.3 Experimental Investigation of Recognition-Mediated Cycloaddition Reaction

### 4.3.1 Investigation of the Cycloaddition with Indandione 100 and Nitrone 79

In order to investigate whether indandione **100** is intrinsically more or less reactive compared to indandione model compound **79**, indandione **100** was reacted with model nitrone **79** at 10 °C (**Scheme 4.10**).

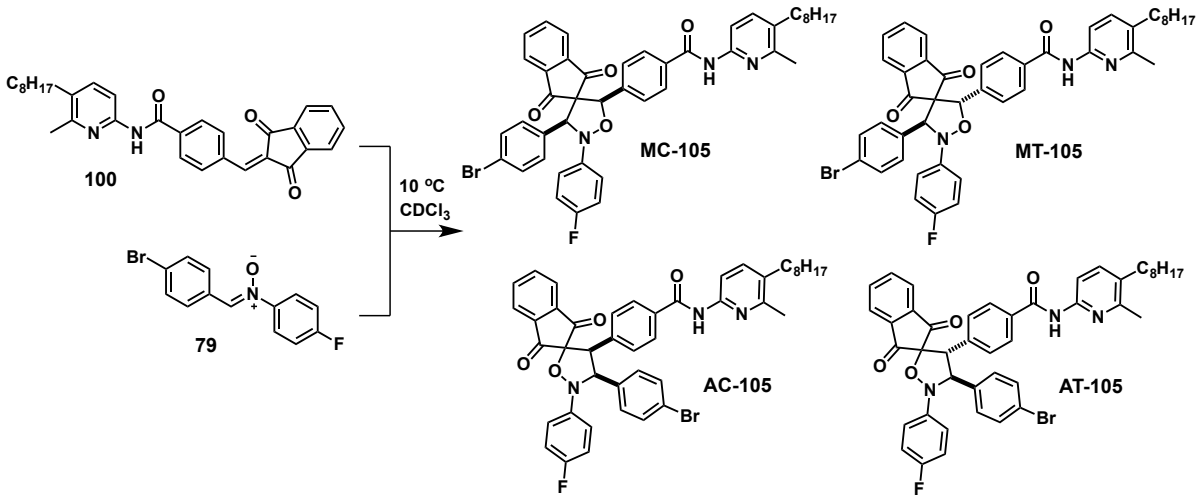


**Scheme 4.10:** The reaction between indandione **100** and nitrone **79** can lead to four isomeric products **105**. The reaction was carried out at 10 °C in $CDCl_3$ and was monitored for 36 hours by $^1H$ NMR and $^{19}F$ NMR spectroscopy.

The reaction between indandione **100** and nitrone **79** was monitored by $^1H$ NMR and $^{19}F$ NMR spectroscopy. The concentration of the species in the reaction was obtained by deconvolution of the relevant resonances and comparing the area to the area of the internal standard, 4-bromo-3-fluoro-nitrobenzene (**Figure 4.7**).

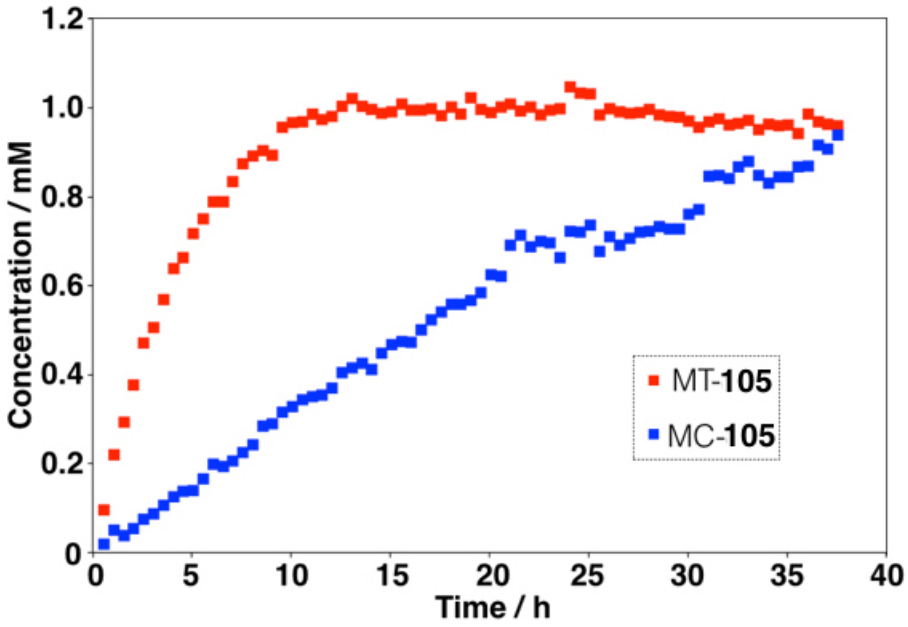


**Figure 4.7:** Concentration *vs.* time profile of the reaction between indandione **100** and nitrone **79**. The reaction was carried out at room temperature at 10 mM. The reaction was monitored by $^{1}H$ and $^{19}F$ NMR spectroscopy.

Presumably because of the low concentration of the starting materials and the low temperature this reaction was carried out at, the reaction took longer to reach completion that the 36 hours for which it was monitored. Therefore, up to 5 hours after the monitoring of the reaction was finished, the $^{1}H$ NMR and $^{19}F$ NMR spectra were recorded and these show that the final concentration of MC-**105** is 1.4 mM. The model compound reaction described in **Chapter 3** was carried out at 100 mM and in this reaction also two major products were observed, which were later confirmed to be MT-**80** and MC-**80**. A similar pattern of resonances corresponding to the isoxazolidine protons on the products is observed in the $^{1}H$ NMR spectrum (**Figure 4.8**) in the reaction between nitrone **79** and indandione **100** as in the model compound reaction discussed in **Chapter 3**. The chemical shift values, the shape of the peaks and the pattern is almost identical to the $^{1}H$ NMR spectrum in **Figure 3.5**. The experimental investigation to the model compound reaction was carried out at 100 mM but the kinetic simulations described in **Section 3.4.2** gives information on the conversion of this reaction at 10 mM. The concentration of the products after in the chemical reaction is similar to the results obtained from the kinetic

simulations. Therefore, we conclude that nitrone **79** is a suitable control compound for this reaction.

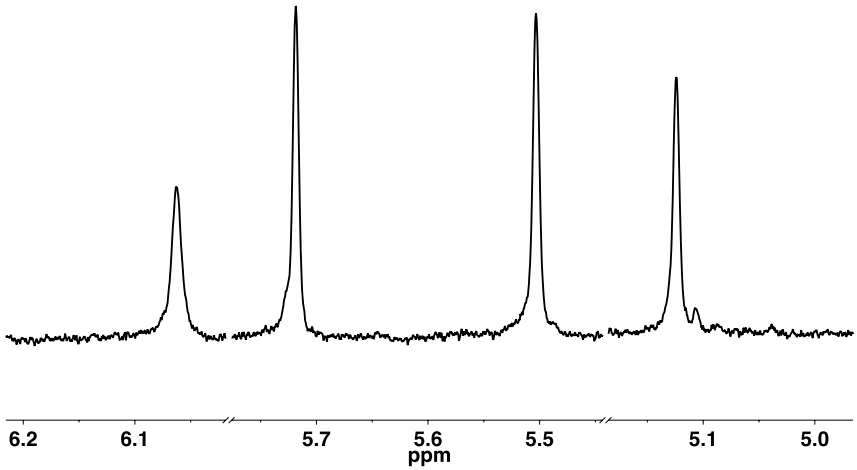


**Figure 4.8:** Partial 499.9 MHz $^{1}$H NMR spectrum ($CDCl_3$, 10 °C) showing the region with the resonances corresponding to the isoxazolidine protons on the products. The outside two signals correspond to MT-**105** and the inside two resonances correspond to MC-**105**.

### 4.3.2 Investigation of the Cycloaddition with Indandione 100 and Nitrone 101

In order to investigate the effect of a recognition-mediated reaction pathway, nitrone **101** was designed and synthesised (**Scheme 4.11**). The nitrone is equipped with a phenyl acetic acid recognition site. The phenyl acetic acid motif is used previously by the Philp laboratory in self-replicating systems.

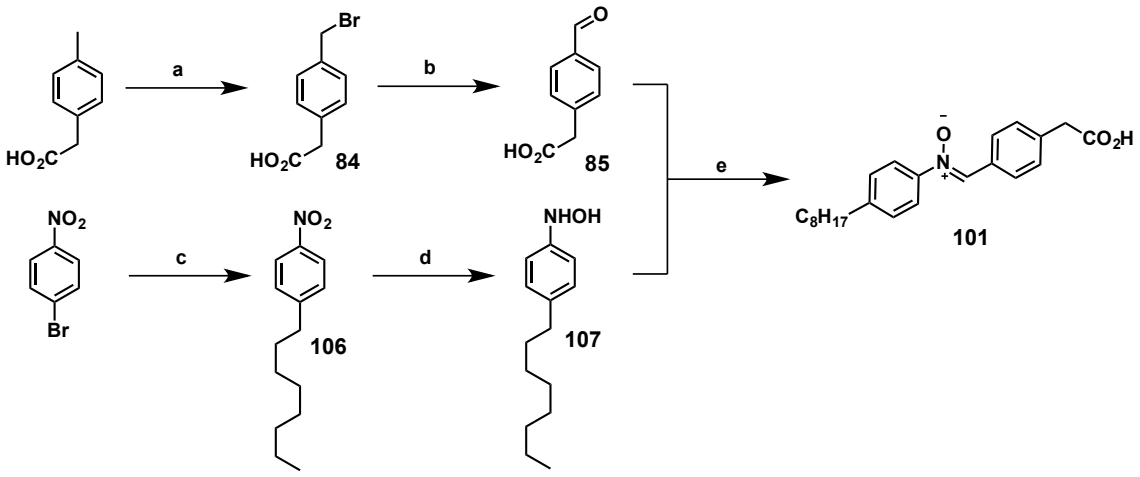


**Scheme 4.11:** Synthesis of nitrone **101** with carboxylic acid recognition site. a) $Br_2$, chlorobenzene, hv, RT, 54%. b) HMTA, conc. HCl, EtOH/$H_2O$ (1:1), 100 °C, 60%. c) Octyl boronic acid, $K_2CO_3$, $Pd(PPh_3)_4$, toluene/$H_2O$ (3:1), 95 °C, 17%, d) $N_2H_4 \bullet H_2O$, Rh/C, THF, RT, 37%. e) $CDCl_3$, –20 °C, 51%.

Previous work in the Philp laboratory established that nitrones with a carboxylic acid recognition site are not soluble in $CDCl_3$ without an alkyl chain. Ideally, a nitrone is equipped with a $^{19}F$-tag, which enables analysis by $^{19}F$ NMR spectroscopy. A similar nitrone to nitrone **101** has been previously synthesised in the Philp group in which a fluorine-tag was present in on the *meta* position of the hydroxylamine. However, it was found that this caused significant instability of the nitrone and decomposition was observed during the course of the cycloaddition reaction. The decreased stability is probably caused by the electron withdrawing effects of the fluorine, which makes the reactive site of the nitrone electron deficient and thus more sensitive to hydrolysis.

The investigation to the cycloaddition reaction between indandione **100** and nitrone **101** was carried out at 10 °C in $CDCl_3$ for 36 hours (**Scheme 4.12**).

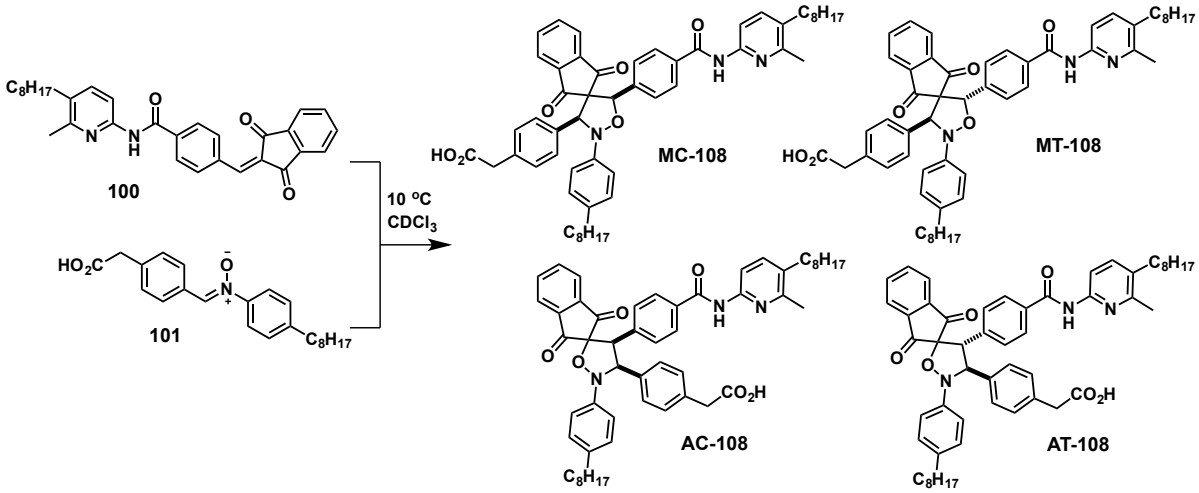


**Scheme 4.12:** The reaction between indandione **100** and nitrone **101** can lead to four isomeric products. The reaction was carried out at 10 °C in $CDCl_3$ and was monitored for 36 hours by $^1H$ NMR spectroscopy.

The $^1H$ NMR spectroscopic data was deconvoluted and the concentration was obtained by comparing the area of each resonance to that of the internal standard, 1-methyl-2,4-dinitrobenzene.

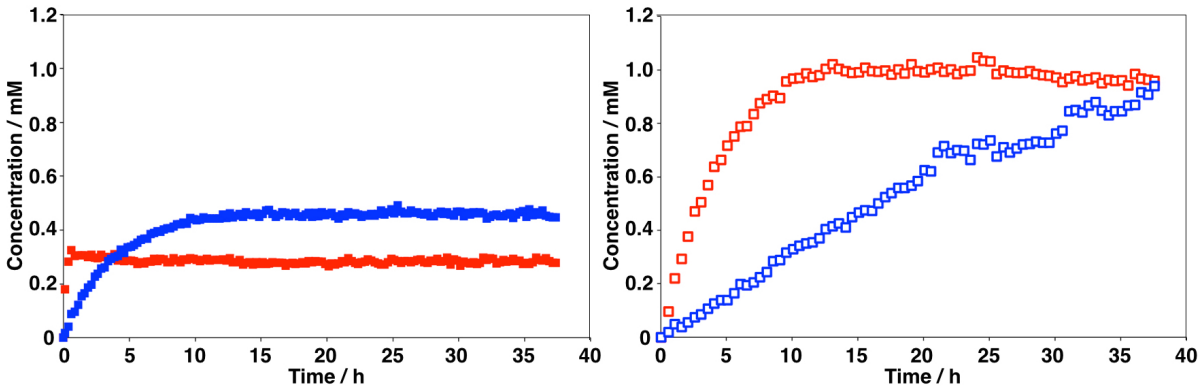


**Figure 4.9:** Left: The concentration *vs.* time profile showing the formation of the Michael-*cis* (■) and Michael-*trans* (■) diastereoisomers in the reaction between indandione **100** and nitrone **101**. Right: The concentration *vs.* time profile showing the formation of the Michael-*cis* (□) and Michael-*trans* (□) diastereoisomers in the control reaction between indandione **100** and nitrone **79**.

Compared to the control reaction, the recognition-mediated reaction with nitrone **101** does increase the initial rate of formation towards MC-**108**. This indicates that the presence of the complementary recognition sites on the compounds stabilizes the transition state and therefore the rate of the reaction is increased. The concentration *vs.* time profile does not show the characteristic sigmoidal

shape of a self-replicating reaction. Rather, the self-replicating potential of the reaction cannot be studied because the products of the reaction could not be isolated. In order to study the self-replicating potential an amount of pre-formed template should be added to the reaction mixture, which should lead to an increase in the initial rate. Since, the product could not be isolated, this experiment could not be carried out. The concentration *vs*. time profile instead is characteristic of the existence of an [**A•B**] complex pathway. In the [**A•B**] complex pathway, the recognition sites of the two starting materials associate upon each other prior to the reaction, and the association of the two recognition sites lives on in the product, which affords the inactive template **T´** (**Figure 4.10**).

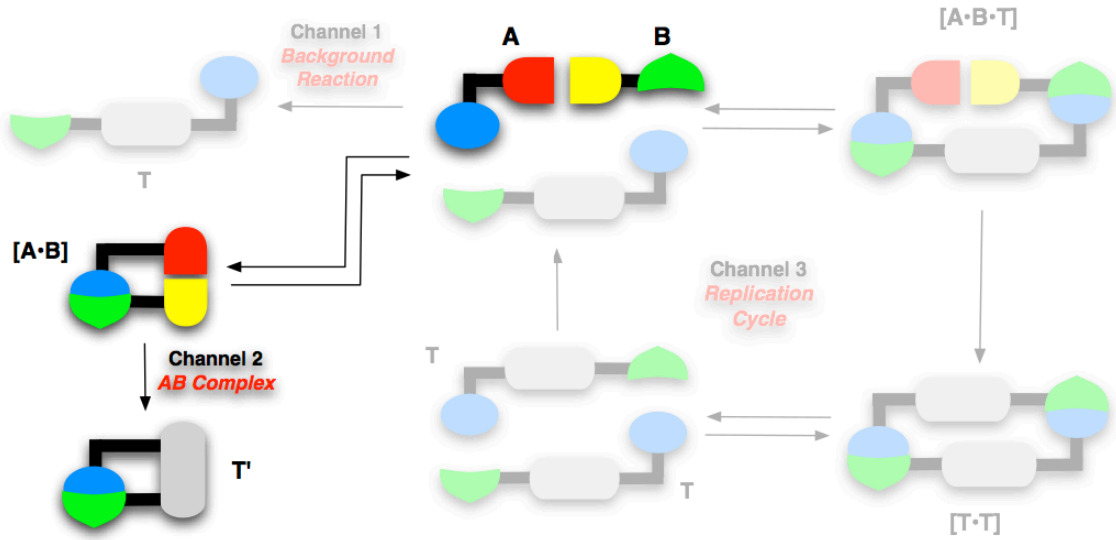


**Figure 4.10:** In the [**A•B**] complex pathway, the recognition sites on the starting materials will associate prior to the reaction and the association will live on in the product affording the inactive template T´. Taken from reference 96.

The kinetic data also shows that the conversion of the cycloaddition between nitrone **101** and indandione **100** is lower than that of the control reaction. These results indicate that, in contrast with the transition-state, the ground state of the products is not stabilised in the presence of recognition-sites. Therefore, either the association of the recognition sites in the product destabilise it or the cycloaddition with nitrone **101** is intrinsically unfavourable compared to the cycloaddition with nitrone **79**. We attempted to fit the data to the bimolecular rate law and the rate law corresponding to the reaction taking place in the [**A•B**] pathway. However, presumably because of the shape of the concentration *vs*.

time profile of MT-**108**, the SimFit software package did not afford a fit for the data obtained. In order to compare the kinetics of the recognition-mediated reaction to the non-recognition-mediated reaction, however, the initial rate can be obtained from the first few data points of **Figure 4.9** of **108** and thus the relative rate can be calculated (**Table 4.3**).

**Table 4.3:** The initial rates of formation of **105** and **108** can be calculated from the data in **Figure 4.9**. The rate accelaration can be calculated by dividing one over the other.

| | **Initial rate** / $10^{-4}$ mM $s^{-1}$ | **Relative rate** |
|---|---|---|
| MT-**105** | 0.6 | – |
| MT-**108** | 1.4 | 2.3 |
| MC-**105** | 0.1 | – |
| MC-**108** | 0.3 | 2.4 |

The EM is a measure of the effect of the recognition event prior to the chemical reaction on the reaction rate. Formally, the EM should be obtained by dividing the rate constants of the reactions rather than the initial rates. However, since we were unable to fit the kinetic data to a rate constant we decided to use the initial rates as this gives an indication of the effect of the recognition-mediated pseudo-intramolecular reaction. The value of the EM indicates that the formation of the Michael-*trans* product as well as the Michael-*cis* is more than two times faster with recognition than without.

In order to find an explanation for the low stability of the cycloadducts in the presence of a recognition-mediated reaction pathway, RM1 calculations were carried out in order to obtain the lowest energy conformation of the two Michael cycloadducts (**Figure 4.11**). From the ground state structures in **Figure 4.11** it is not clear why the cycloaddition reaction is unfavourable. The recognition-mediated reaction does stabilize the transition state as it accelerates the reaction. However, the recognition seems to destabilize the products. The structures do not seem to be unstable from the RM1 calculations, however, the reaction with nitrone **101** can be intrinsically unfavourable.

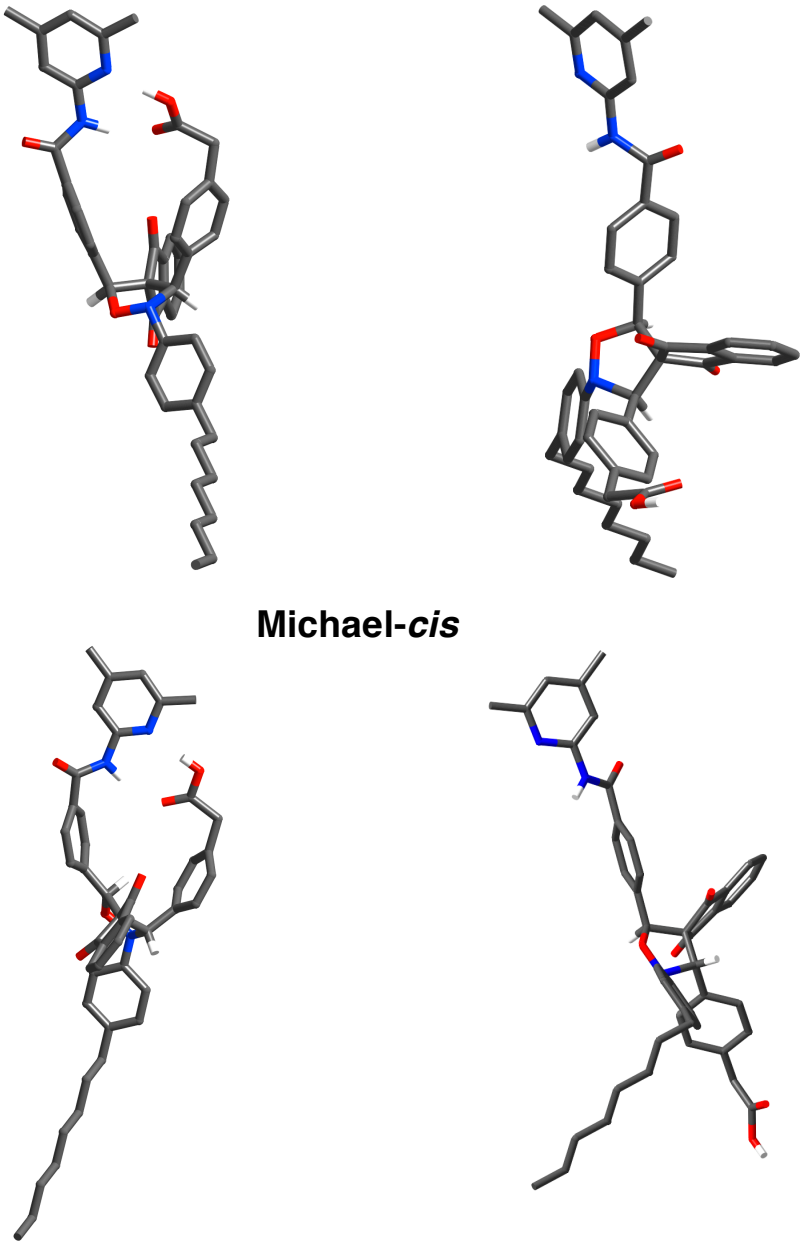


**Figure 4.11:** Top: The closed and open conformation of the Michael *cis* isomer of the reaction between nitrone **101** and indandione **100**. Bottom: The closed and open conformation of the Michael *trans* isomer of the reaction between nitrone **101** and indandione **100**. In the geometries, carbon atoms are shown in grey, oxygen in red, nitrogen in blue. For clarity, hydrogen atoms have been omitted.

### 4.3.3 Investigation of the Cycloaddition with Indandione 100 and Nitrone 102

As the recognition-mediated cycloaddition with indandione **100** and nitrone **102** does not afford the desired thermodynamic stabilization of the product, but

rather the contrary, nitrone **102** (**Scheme 4.13**) was used in the investigation of recognition effects in the cycloaddition reaction with indandione **100**.

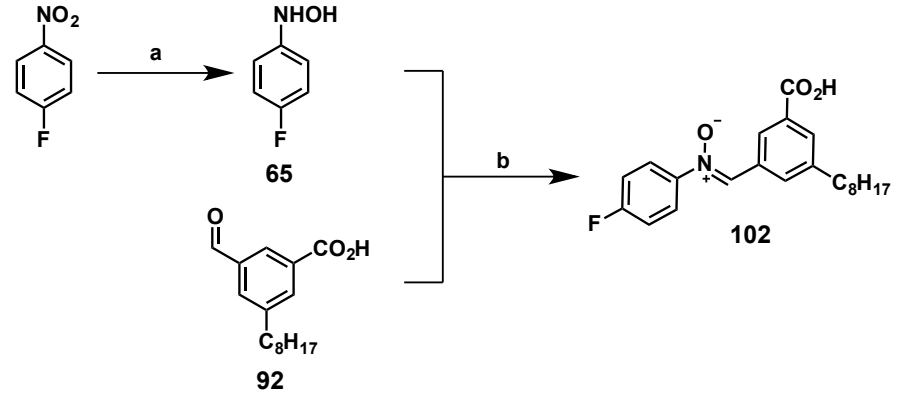


**Scheme 4.13:** Synthesis of nitrone **102** with carboxylic acid recognition site in *meta* position. a) $N_2H_4 \bullet H_2O$, Rh/C, THF, RT, 37%. b) $CDCl_3$, –20 °C, 51%.

The reaction was carried out at room temperature in $CDCl_3$ and the starting concentrations were 10 mM (**Scheme 4.14**).

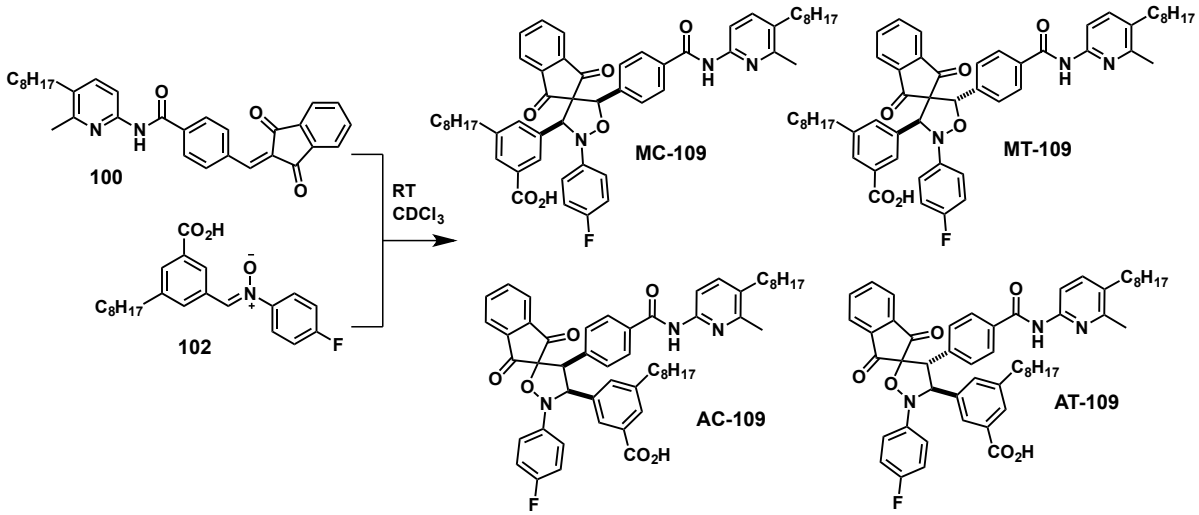


**Scheme 4.14:** The reaction between nitrone **102** and indandione **100** was carried out at room temperature in $CDCl_3$.

The reaction between indandione **100** and nitrone **102** was monitored by $^{1}H$ and $^{19}F$ NMR spectroscopy, and the resonances in the $^{19}F$ NMR spectrum were deconvoluted and the concentration was determined with the internal standard, 4-bromo-3-fluoro-1-nitrobenzene.

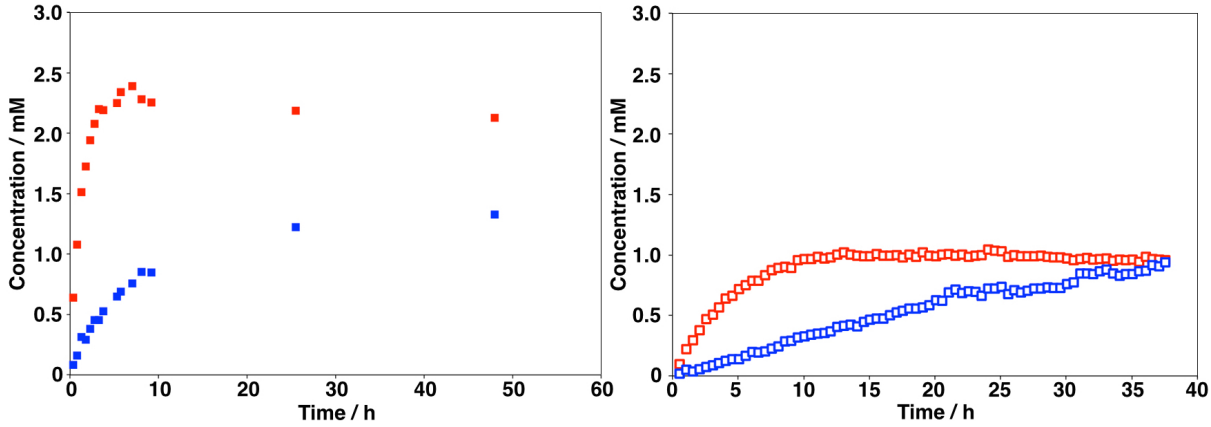


**Figure 4.12:** Left: The concentration *vs.* time profile showing the formation of the Michael-*cis* (■) and Michael-*trans* (■) diastereoisomers in the reaction between indandione **100** and nitrone **102**. Right: The concentration *vs.* time profile showing the formation of the Michael-*cis* (□) and Michael-*trans* (□) diastereoisomers in the control reaction between indandione **100** and nitrone **79**.

In contrast with the cycloaddition with nitrone **101**, the reaction with nitrone **102** does lead to both stabilisation of the transition state, causing the reaction to be faster, and stabilisation of the products, causing the conversion to increase. The formation of MT-**109** is accelerated to a greater extent than MC-**109**, which causes the selectivity to increase initially during the course of the reaction. However, after 25 hours the ratio between the two products is comparable to the control reaction with nitrone **79**. The kinetic profile of the reaction is characteristic of an [**A•B**] pathway as the initial rate increases rapidly at the start of the reaction and thus does not show the characteristic sigmoidal shape for a self-replicating reaction. Because the products could not be isolated, the autocatalytic potential of the product could not be investigated experimentally. In order to quantify the contribution of the recognition-mediated reaction pathway to the rate of formation of the products the initial rate are calculated from the data and compared to the control (**Table 4.4**).

**Table 4.4:** The initial rates of formation of **105** and **109** can be calculated from the data in **Figure 4.12**. The rate accelaration can be calculated by dividing one over the other.

| | **Initial rate** / $10^{-4}$ mM $s^{-1}$ | **Relative rate** |
|---|---|---|
| MT-**105** | 0.57 | – |
| MT-**109** | 3.9 | 6.8 |
| MC-**105** | 0.13 | – |
| MC-**109** | 0.58 | 4.5 |

The relative rates in **Table 4.4** show that the initial rate of the reaction is increased 4.5 times in case of the formation of the Michael-*cis* product and almost 7 times in case of the formation of the Michael-*trans* product. Even though the increase in reaction rate was high in the system based on nitrone **101**, putting the carboxylic acid recognition site in the *meta* position in the nitrone, as in nitrone **102**, has a significant effect in the reaction rate.

The resonances in the $^{19}$F NMR spectrum corresponding to the products of the reaction are broad singlets. The broadening of the $^{19}$F NMR signals could be caused by fast exchange between the inactive template **T'**, in which the product displays intramolecular hydrogen bonds, and the open conformation in which no hydrogen bonds are present. In order to test this hypothesis, 0.06 mL, which was 10% of the total volume, of DMSO-$d_6$ was added to the experiment and the reaction was left at 5 °C and after 12 hours the sample was analysed by $^{19}$F NMR spectroscopy (**Figure 4.13**). DMSO is able to form hydrogen bonds with the two recognition sites and therefore it is expected that if the broadening of the $^{19}$F NMR signals is caused by hydrogen bonding, the broadening will disappear upon addition of DMSO. **Figure 4.13** clearly shows the disappearance of the broadening of the resonances corresponding to the product in the presence of DMSO-$d_6$, which indicates that intramolecular hydrogen bonding was responsible for the broadening of the signal. Interestingly, the addition of DMSO-$d_6$ to the sample also led to re-equilibration of the reaction mixture because after 12 hours the ratio of the two products was reversed. The diastereometric ratio changed from 1.6 to 0.7 after the addition of

DMSO-$d_6$ and the nitrone concentration increased from 6.8 mM to 8.5 mM, which indicates that the retro cycloaddition takes place. These results clearly show the effect of the recognition sites on the two reagents as breaking up the hydrogen bonding with DMSO reverses the selectivity of this system.

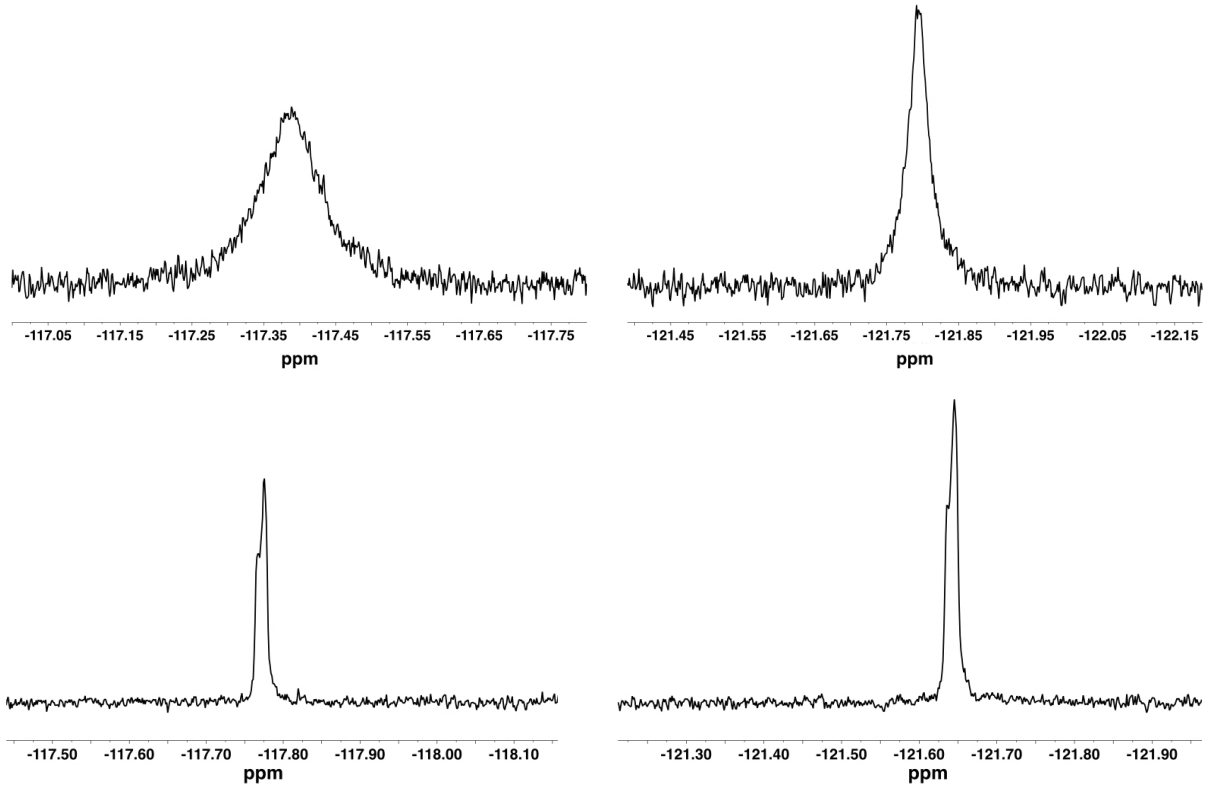


**Figure 4.13:** Top: Partial 376.6 MHz $^{19}$F NMR spectra ($CDCl_3$, RT) showing the resonances that correspond to MT-**109** (left) and MC-**109** (right). Bottom: Partial 376.6 MHz $^{19}$F NMR spectra (DMSO-$d_6$, RT) showing the resonances that correspond to MT-**109** (left) and MC-**109** (right) after addition of DMSO-$d_6$.

In order to find an explanation for the behaviour observed, it is instructive to look at the molecular structure prediction from RM1 calculations (**Figures 4.14**). Compared to the theoretical ground state structures of MC-**108** and MT-**108**, shown in **Figure 4.11**, the ground state structures of MC-**109** and MT-**109** look less stable and in that respect the structures do not explain the significant difference in reactivity between the two nitrones. Compared to the control reaction with nitrone **79**, the reaction with nitrone **102** shows significant rate acceleration and product stabilisation in the presence of a recognition-mediated reaction pathway. From the broad resonances in the $^{19}$F NMR spectrum we concluded that the recognition sites dissociate in the product. This conclusion is

supported by the calculated ground state structures as the ground state structures with recognition sites associated show non-planar phenyl rings, which is not a favourable ground state geometry.

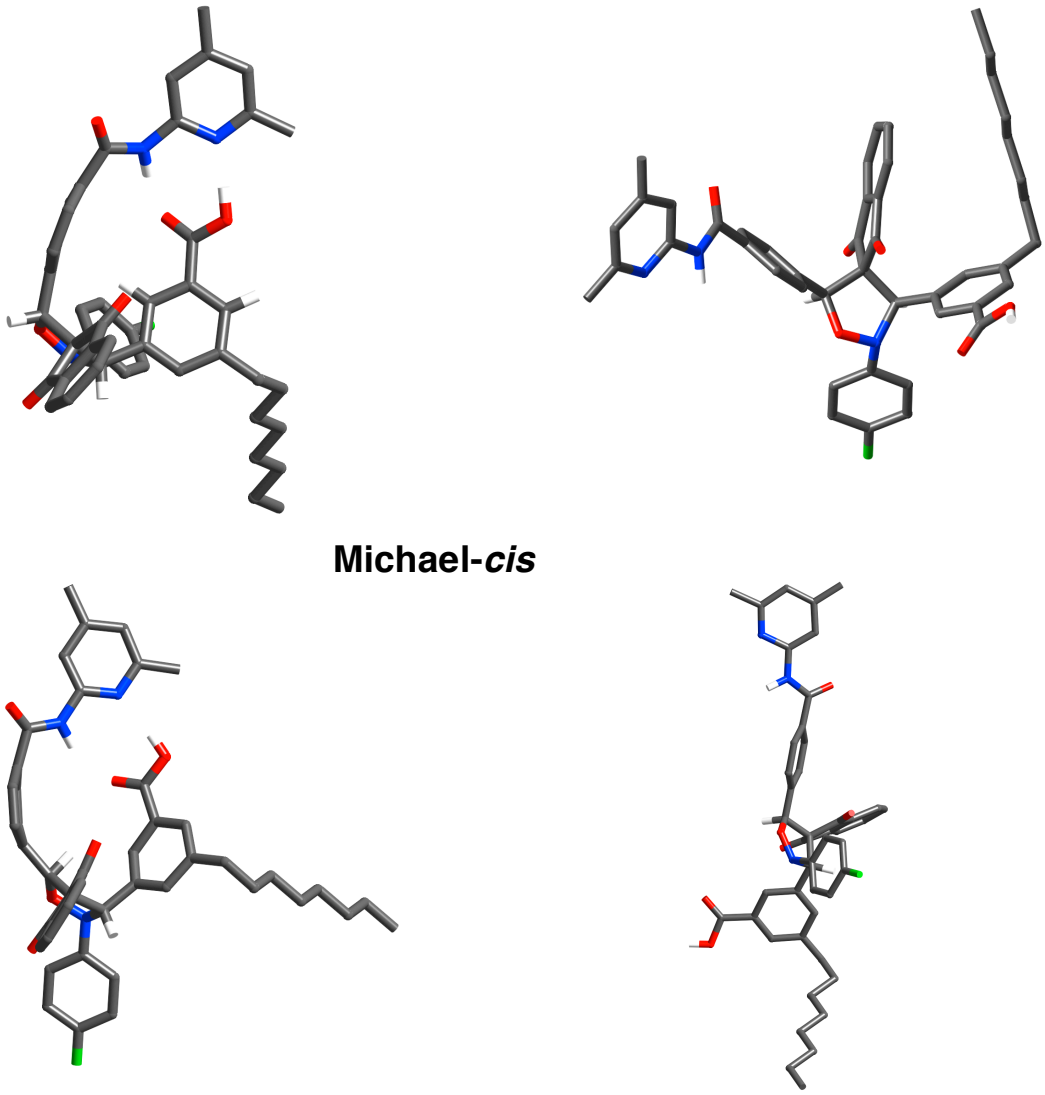


**Figure 4.14:** Top: The closed and open conformation MC-**109**. Bottom: The closed and open conformation of MT-**109**. In the geometries, carbon atoms are shown in grey, oxygen in red, nitrogen in blue, fluorine in green. For clarity, hydrogen atoms have been omitted.

The difference in reactivity between nitrone **101** and **102** might not be caused by the relative stability of the products of the cycloaddition but rather nitrone **101** might be inherently less reactive than nitrone **102**. The most important difference between the two nitrones that might affect the reactivity is the fluorine atom on the phenyl ring in the hydroxylamine, which presumably makes the

reactive site of nitrone **101** less electron rich than the reactivie site of nitrone **102**. However, it is not likely that this increased electron deficiency causes nitrone **102** to be more reactive as increased electron deficiency would make the nitrone more reactive towards nucleophiles and the indandione is relatively electron poor and does not act as a nucleophile. Therefore, the difference in reactivity is presumably due to the instability of **108**.

### 4.3.4 Investigation of the Cycloaddition with Indandione 93 and Nitrone 110

With the maleimide system the Philp laboratory worked on previously, recognition-mediated acceleration was observed when the carboxylic acid site was present on the nitrone or on the maleimide. Since we observed recognition-mediated behaviour with the amidopyridine recognition site on the indandione and the carboxylic acid recognition site on the nitrone, we investigated the reaction between an indandione and a nitrone where the positions of the recognition sites were reversed.

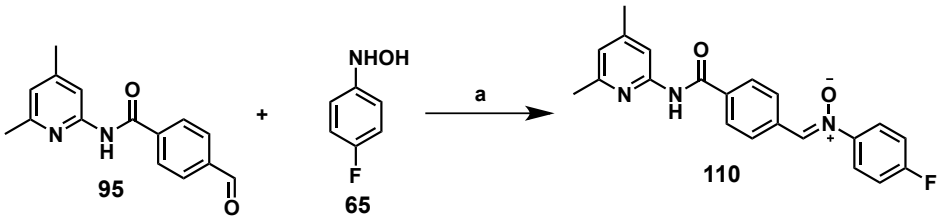


**Scheme 4.15:** Synthesis of nitrone **110**, which is equipped with the amidopyridine recognition site. a) $CDCl_3$, –10 °C, 58%.

Previously in this chapter, the synthesis of indandione **93** was described, which is soluble in $CDCl_3$ at 5 mM. The two compounds were dissolved in $CDCl_3$ and were left to react at room temperature and the reaction was followed by $^{1}H$ and $^{19}F$ NMR spectroscopy for 24 hours (**Scheme 4.16**).

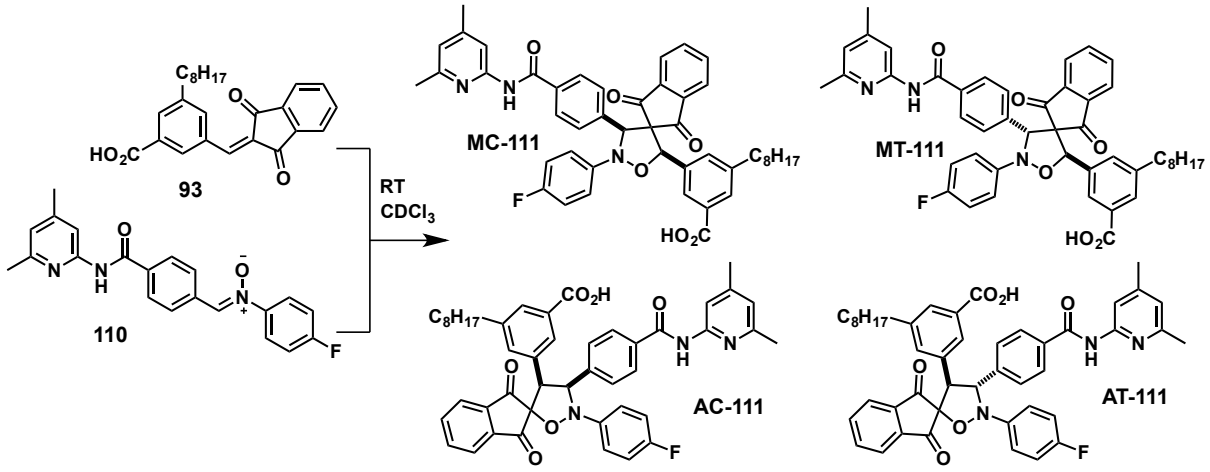


**Scheme 4.16:** Indandione **93** and nitrone **110** bear complementary recognition sites and can react *via* a recognition-mediated reaction channel to form products **111**.

The reaction between indandione **93** and nitrone **110** was followed by $^{1}$H NMR and $^{19}$F NMR spectroscopy, at room temperature. The nitrone and product $^{19}$F NMR resonances were deconvoluted in iNMR. In order to investigate the contribution of the recognition-mediated reaction pathway to the rate of the reaction and the conversion, the reaction between indandione **93** and nitrone **79** is used as a control. **Figure 4.15** shows the concentration *vs*. time profiles for the formation of the two diastereoisomeric products of the reaction of both the recognition-enabled cycloaddition and the control.

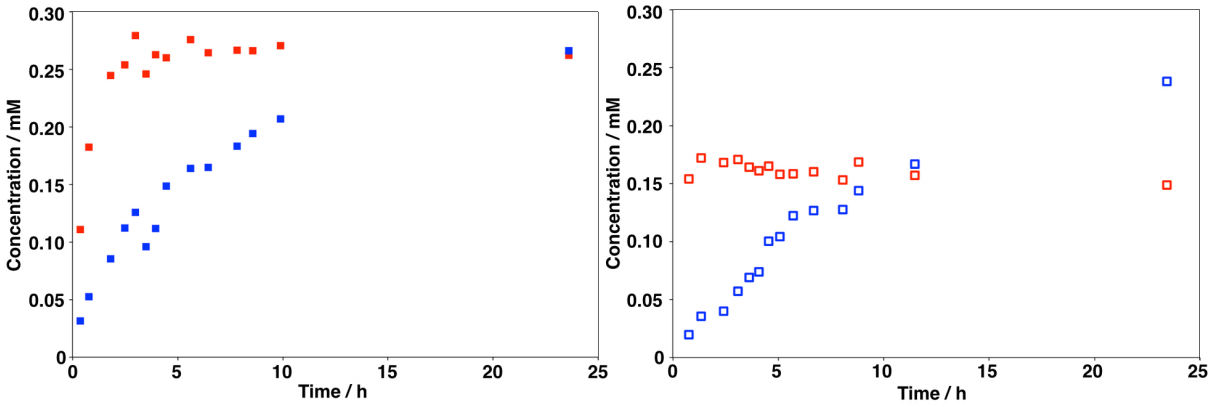


**Figure 4.15:** Left: The concentration *vs.* time profile showing the formation of the MC-**111** (■) and MT-**111** (■) diastereoisomers in the reaction between indandione **93** and nitrone **110**. Right: The concentration *vs*. time profile showing the formation of the Michael-*cis* (□) and Michael-*trans* (□) diastereoisomers in the control reaction between indandione **93** and nitrone **79**.

Interestingly, the recognition-mediated reaction based on indandione **93** and nitrone **110** showed increasing conversion compared to the control reaction with nitrone **79**. The rate of formation of MT-**111** does not seem to increase compared to the recognition-disabled control. Interestingly, in the control reaction with nitrone **79** the diastereometric ratio between the two products is 0.6 in favour of the Michael-*cis* diastereoisomer, but the diastereometric ratio in the recognition-mediated reaction is 1. The change is selectivity is mainly caused by the increased stability of MT-**111** in the recognition-mediated reaction, which causes the selectivity to disappear.

In order to quantify the effect of molecular recognition on the rate of the reaction, the relative rate was calculated as the ratio of the initial rate of formation of **111** relative to **105** (**Table 4.5**).

**Table 4.5:** The initial rates of formation of **105** and **111** can be calculated from the data in **Figure 4.15**. The rate accelaration can be calculated by dividing one over the other.

| | **Initial rate** / $10^{-5}$ mM $s^{-1}$ | **Relative rate** |
|---|---|---|
| MT-**105** | 3.6 | – |
| MT-**111** | 6.5 | 1.8 |
| MC-**105** | 0.74 | – |
| MC-**111** | 1.9 | 2.5 |

Even though the initial rate of formation of MT-**111** is highest, the rate of formation of MC-**111** is increased most as a result of the recognition-mediated reaction and the increase in rate is similar to that observed with indandione **100** and nitrone **101**. From these results it is clear that it does not matter which molecule bears the amidopyridine recognition site and which one bears the carboxylic acid recognition site, recognition-mediated behaviour is observed in both cases.

## 4.4 Conclusions

Indandiones **83**, **86** and **93**, equipped with the carboxylic acid recognition site were successfully synthesised. Unfortunately, **83** and **86** were not sufficiently soluble in $CDCl_3$ and **93** was only soluble at the low concentration of 5 mM. Therefore, indandiones **96** and **100** were synthesised, which were sufficiently soluble in order to test them in a recognition-mediated reaction with a nitrone. In order to compare the results of a recognition-mediated reaction to a simple bimolecular reaction, we used nitrone model compound **79**. The recognition-mediated reaction between indandione **100** and nitrone **101** shows a doubling of the initial rate of formation towards the formation of MT-**108** and MC-**108**. However, the total conversion of the reaction is lower than the control. Therefore, nitrone **102** was investigated for recognition-mediated behaviour with indandione **100**. The initial rate was increased even more in the reaction with **102** compared to **101**. Additionally, the conversion towards the products and the selectivity in favour of MT-**109** was also increased. Interestingly, the conversion and selectivity decreases upon addition of DMSO-$d_6$, which presumably breaks up the hydrogen bonds that stabilise the product. We have also shown that the position of the recognition sites can be reversed, the recognition sites can be on either of the two reagents. Indandione **93** and nitrone **110**, on which the recognition sites are reversed relative to the other systems investigated, also show doubling of the initial rate of formation towards the cycloadducts MT-**111** and MC-**111**, thus inidicating that the location of the recognition sites is not relevant for the extend of the recognition-mediated rate acceleration.

The RM1 calculations to the reaction in the presence of recognition sites give a similar trend as the results described in **Chapter 3** with the model compounds. The experimental results also show a similar trend as the results with the model compounds as only the MC and MT products are observed in the experimental investigations. However, it is possible to change the rate of formation and the ratio between MT and MC in the presence of recognition-mediated reaction channels.

# 5

# Construction of a Dynamic Covalent Library and Manipulation Using Molecular Recognition

## 5.1 Studying the Recognition-Mediated Reaction in a Mixture

Synthetic chemists traditionally study chemical processes in isolated conditions in which one reagent reacts with another reagent sometimes in the presence of a catalyst. However, chemical processes in living organisms take place in a mixture of lots of different compounds in the presence of lots of enzymes. Systems chemistry is the field that aims to create artificial chemical systems of mixtures of molecules that can show emergent properties. The Philp laboratory has previously studied[85,96] systems in which a recognition-mediated reaction step is coupled to a dynamic library of compounds. In such a dynamic system, more than one nitrone is available to react with the indandione, however only one nitrone bears the carboxylic acid recognition site. A dynamic system of nitrones and imines could show different behaviour than a nitrone on its own which react with a dipolarophile. **Chapter 4** describes the investigation to the reaction between nitrone **102** and indandione **100** in isolation. In this chapter the differences between the recognition-mediated reaction occurring in isolation and of that in a dynamic system are studied and described.

## 5.2 Design and Construction of a Static Library

In **Chapter 3**, we established that the 1,3-dipolar cycloaddition between a nitrone and an indandione is reversible and therefore it is suitable for the construction of a library of compounds under thermodynamic control (**Scheme 5.1**).

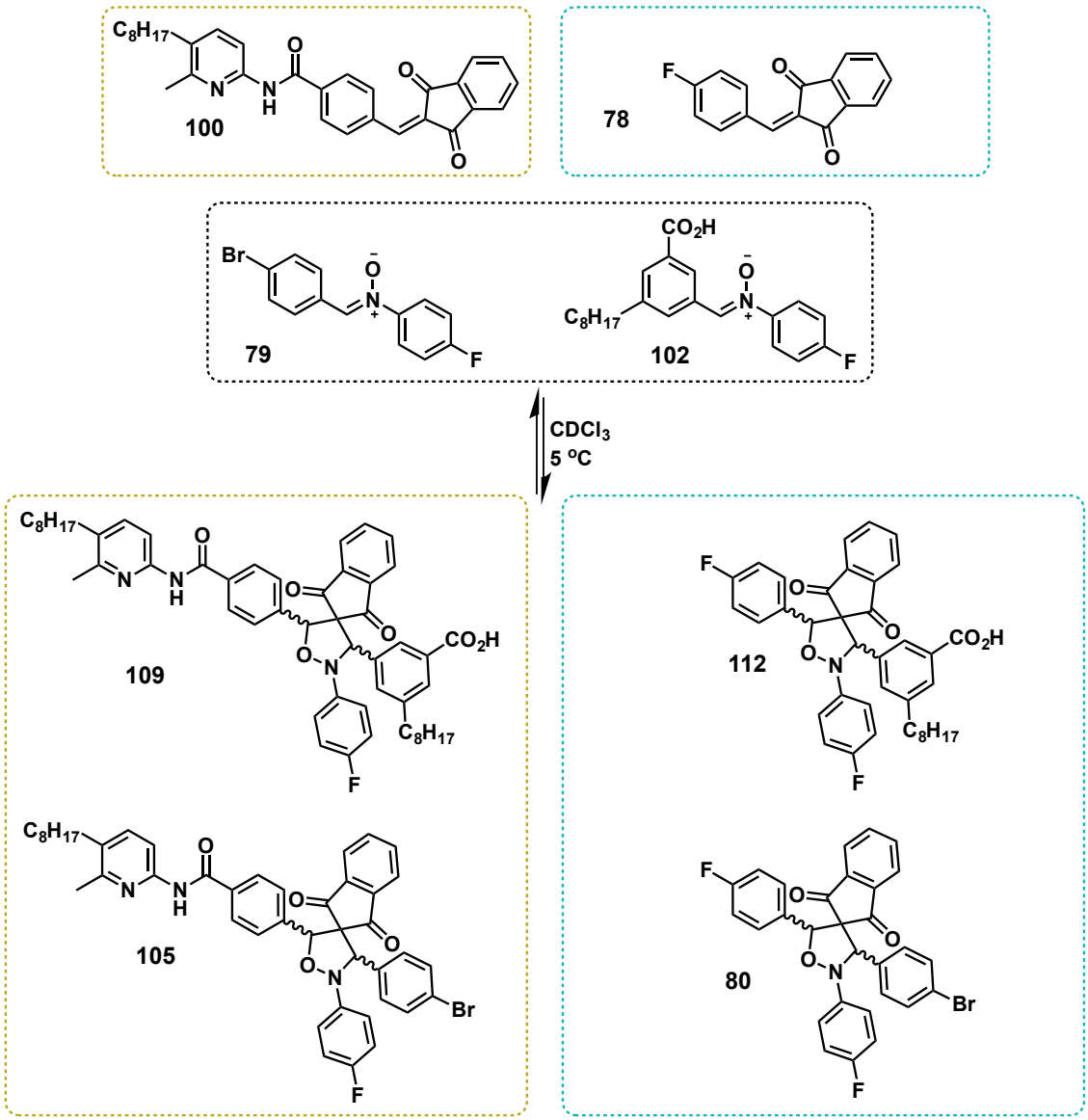


**Scheme 5.1:** A library of compounds can be created by equilibration of indandione **78** and **100** and nitrone **79** and **102**.

Nitrones **79** and **102** and indandiones **78** and **100** were used and any difference in behaviour between the library and the compounds reacting in isolation is investigated. All compounds were mixed at 10 mM in $CDCl_3$ and left for 24

hours at 5 °C. After 24 hours the mixture was analysed with $^{19}F$ NMR spectroscopy (**Figure 5.1**).

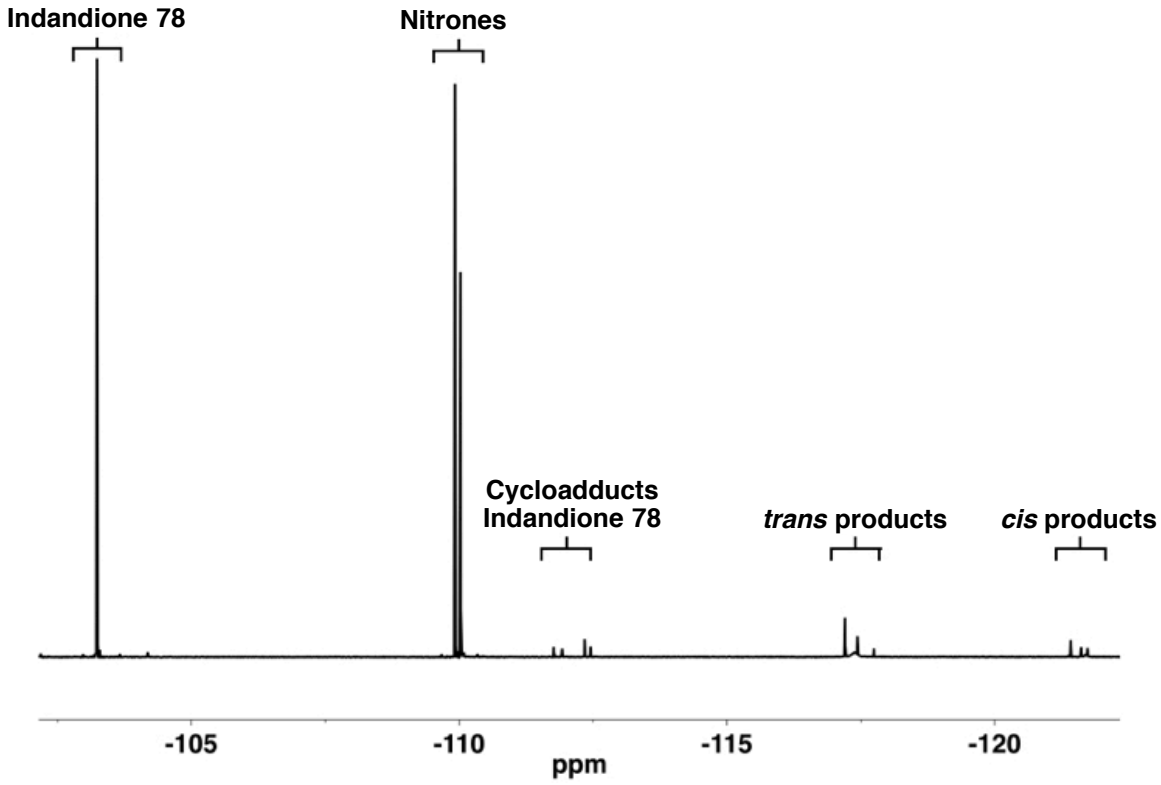


**Figure 5.1:** Partial 376.5 MHz $^{19}F$ NMR spectrum (RT, $CDCl_3$) showing the fluorinated starting materials of the library and the different diastereometric products.

The $^{19}F$ NMR spectrum in **Figure 5.1** shows equilibration of the reaction mixture and the spectrum was deconvoluted in order to obtain the areas under the peaks and the concentration of the library constituents (**Figure 5.2**).

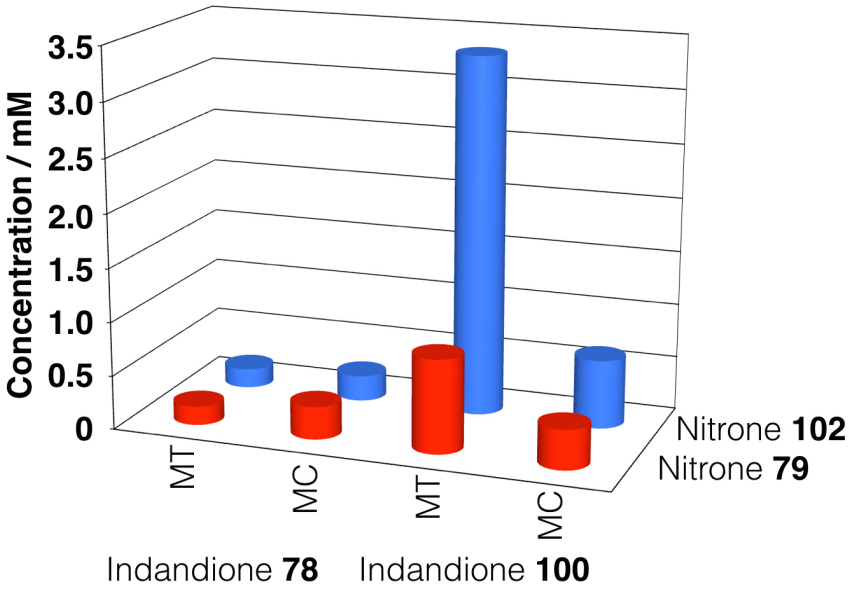


**Figure 5.2:** The concentration of the library constituents after equilibration for 24 hours at 5 °C. The concentrations were obtained by deconvolution of the relevant resonances in the $^{19}$F NMR spectrum.

In **Chapter 4** the investigation to the recognition-mediated cycloaddition between nitrone **102** and indandione **100** was described. When DMSO-$d_6$ was added to the library mixture, reversion of the product ratio was observed. Therefore, in order to investigate the influence of the recognition event in the library, 0.06 mL, 10% of the total volume, of DMSO-$d_6$ was added to the equilibrated library mixture and left for 24 hours at 5 °C (**Figure 5.3**).

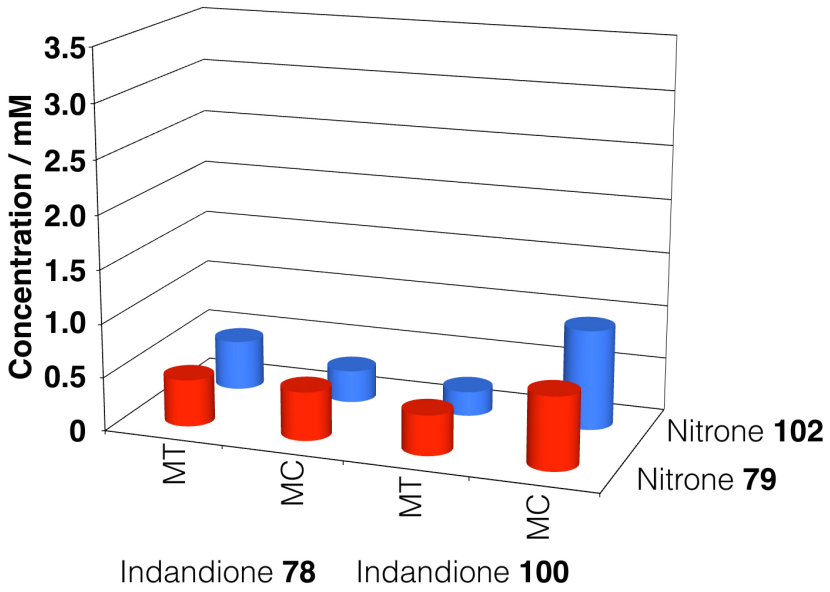


**Figure 5.3:** Upon addition of DMSO-$d_6$ the recognition event is inhibited and the library re-equilibrates.

The addition of DMSO-$d_6$ to the library of cycloadducts breaks up the hydrogen bonds between the recognition sites and hence destabilises the products in which hydrogen bonding is present. This causes the library to re-equilibrate to convert the most stable cycloadduct back to starting materials and into other library constituents. The concentration of MT-**109** decreases from 3.33 mM to 0.23 mM and ends up as the library constituent with the lowest concentration when the hydrogen bonding is inhibited. The selectivity for MT-**109** relative to MC-**109** reverses in the absence of stabilising effects from hydrogen bonding. The ratio between these two cycloadducts in the initial equilibration in the presence of hydrogen bonding stabilisation is 5.2, which decreases to 0.2 after re-equilibration in the absence of stabilisation by hydrogen bonding.

## 5.3 Design and Construction of Dynamic Covalent Libraries

### 5.3.1 Dynamic Covalent Library with Aldehyde 85

The Dynamic Covalent Library (DCL) was designed as a 3 × 3 matrix in which three nucleophiles and three aldehydes that combine to generate a DCL containing nine compounds. Based on previous work[85,96] in the Philp laboratory, the nucleophiles that will be used are two anilines and one hydroxylamine (**Figure 5.4**).

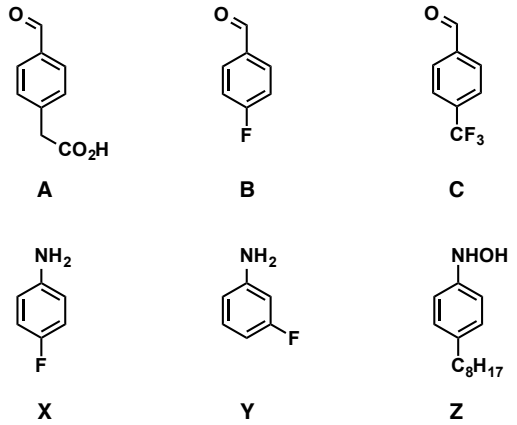


**Figure 5.4:** The compounds used for the construction of the DCL. A few of these compounds have appeared previously in this thesis but have been renumbered for this chapter.

When the compounds from **Figure 5.4** are mixed, it is expected that these form a dynamic mixture of compounds consisting of nine condensation products and six starting materials. Based on previous work, the DCL was created in $CD_2Cl_2$ that was saturated with *p*TSA•$H_2O$ (**Scheme 5.2**).

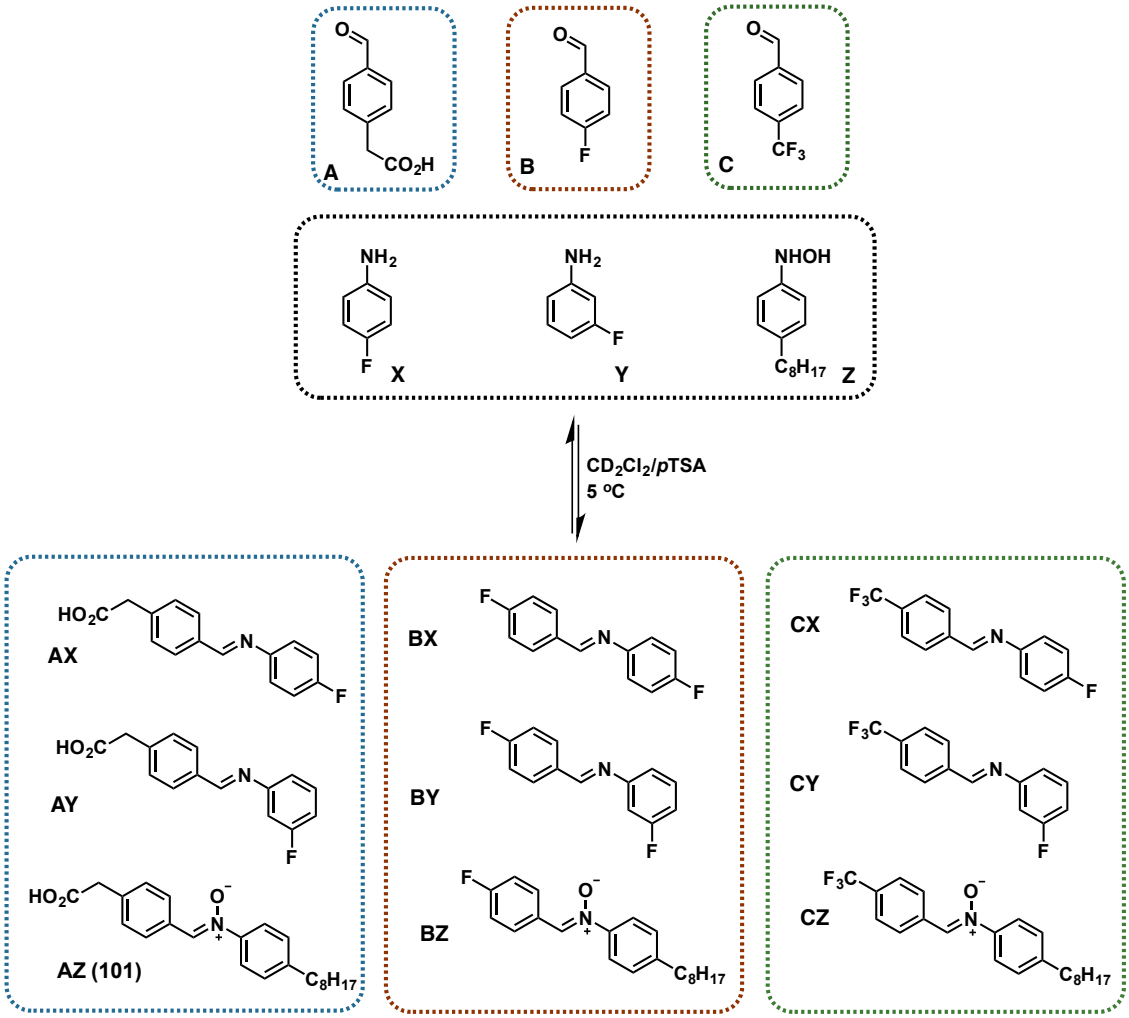


**Scheme 5.2:** Aldehydes **A**, **B** and **C** are mixed with nucleophiles **X**, **Y** and **Z** to form a DCL containing products **AX** – **CZ**. The products are colour coded for clarity. The products containing aldehyde A are shown in the **blue** box, products containing aldehyde B are shown in the **brown** box and products containing aldehyde C are shown in the **green** box.

In order to assign the $^{19}F$ NMR resonances of all the individual constituents of the DCL, a series of experiments is carried out to allow assignment of all individual constituents of the DCL. In these experiments all aldehydes are mixed and one nucleophile is added and conversely, all nucleophiles are mixed and one aldehyde is added to afford six mixtures (**Figure 5.5**).

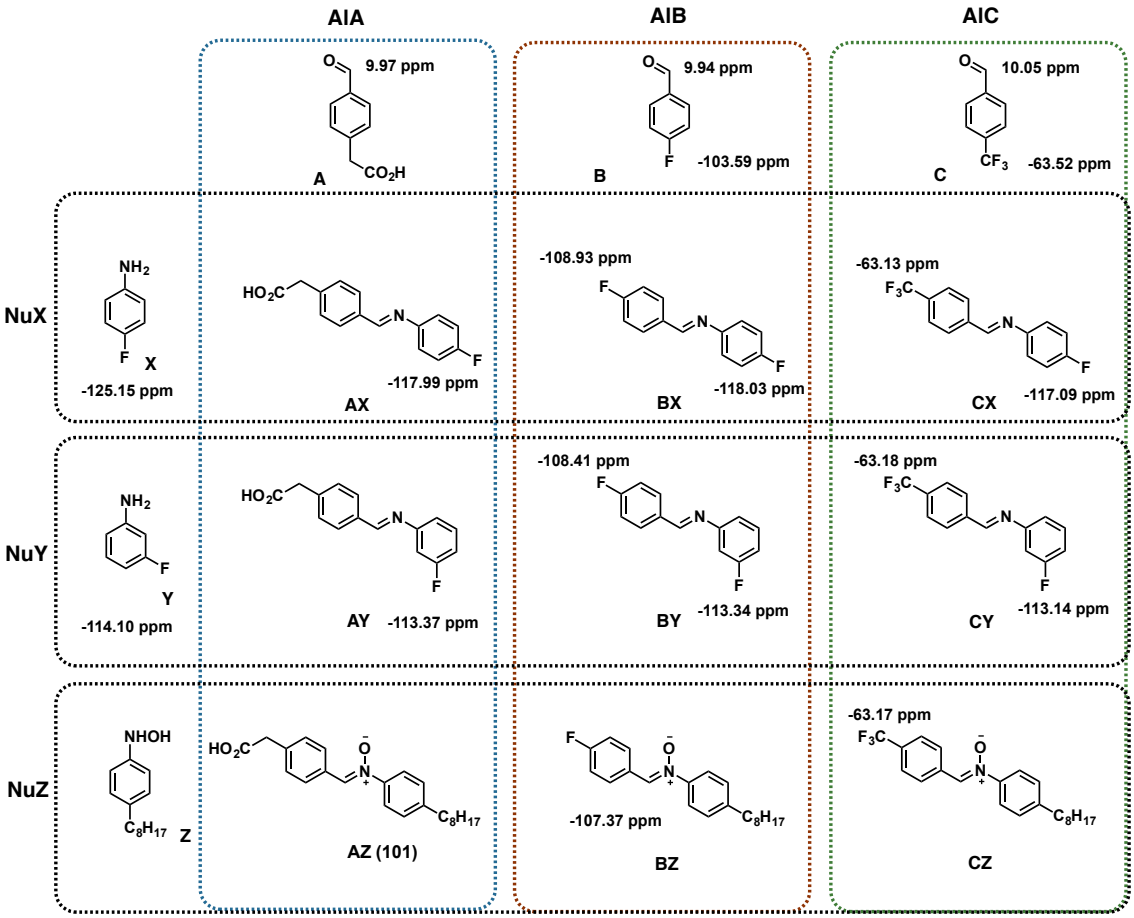


**Figure 5.5:** In order to assign the $^{19}F$ NMR signals of the individual constituents of the DCL, the compounds were mixed as shown to afford six mixtures, each mixture containing three condensation products. All ppm shift values are relative to that of 1-bromo-3-fluoro-4-nitrobenze, which is set to -102.90 ppm.

All samples are mixed in the presence of an internal standard. The internal standard used is 1-bromo-3-fluoro-4-nitrobenzene and all fluorine signals in the $^{19}F$ NMR spectra are referenced to the internal standard signal. The composition of the DCL is monitored by integration of the relevant resonances in the $^{19}F$ NMR spectrum, which is possible for all library constituents except **A** and the corresponding nitrone **AZ** (**101**). However, as the aldehyde proton resonances appear at a distinct region in the $^{1}H$ NMR spectrum, the concentration of **A** can be determined relative to that of the other aldehydes **B** and **C**. The concentration of aldehydes **B** and **C** can be determined relative to the internal standard from the $^{19}F$ NMR spectrum. The concentration of **AZ** can then be determined by determining the concentrations of imines **AX** and **AY** and aldehyde **A** and subtracting that from starting concentration of **A**, which should

afford the concentration of nitrone **AZ** in the DCL. The resonances corresponding to the isoxazolidine protons on the cycloadducts, appear in the $^{1}$H NMR spectral region between 5.00 – 6.00 ppm and therefore do not overlap with other proton resonances.

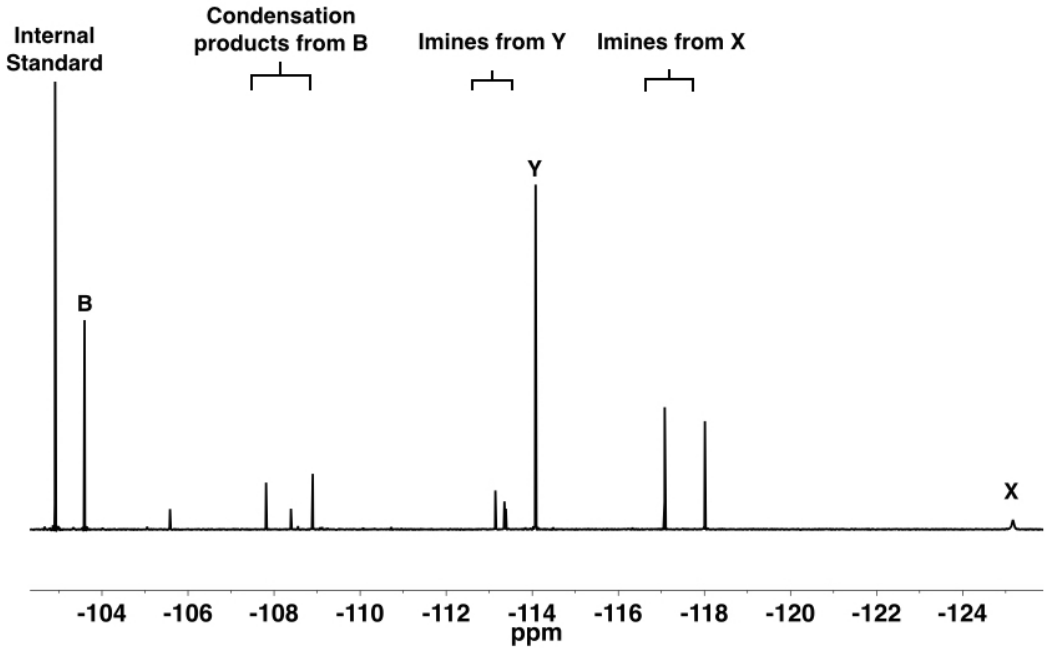


**Figure 5.6:** Partial 376.5 MHz $^{19}$F NMR spectrum (RT, $CD_2Cl_2$) showing the condensation products and starting materials from the DCL. The region showing aldehyde **C** and corresponding condensation products is around -65 ppm and is not shown in this spectrum.

Once aldehydes **A** – **C** and nucleophiles **X** – **Z** are mixed together, the sample is equilibrated at 5 °C for 48 hours after which it is subjected to $^{1}$H and $^{19}$F NMR spectrometric analysis (**Figure 5.7**).

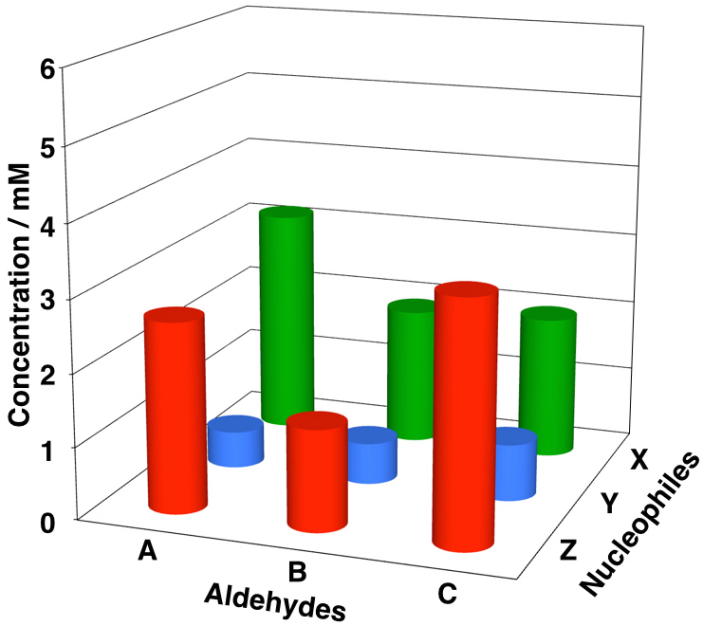


**Figure 5.7:** The concentration of the library constituents after equilibration for 48 hours at 5 °C. The starting concentration of aldehydes **A** – **C** and nucleophiles **X** – **Z** was 10 mM.

Then, either indandione **66** or indandione **77** is added to the library mixture, which initiates the 1,3-dipolar cycloaddition with one of the three nitrones **AZ** – **CZ**. After addition of the dipolarophiles, the DCL is left at 5 °C for another 24 hours after which $^{1}$H and $^{19}$F NMR spectra are recorded.

In order to study the dynamic system coupled to a cycloaddition reaction with an indandione without a recognition-mediated reaction channel, model compound nitrone was added to the equilibrated DCL. When the samples were analysed by $^{1}$H and $^{19}$F NMR spectroscopy, no formation of cycloadducts in the library mixture was observed. In order to obtain the concentration of the cycloadducts between indandione **77** and nitrone **AZ** (**101**), the cycloadduct resonances in the $^{1}$H NMR spectrum must be well visible. However, the resonances corresponding to the isoxazolidine resonances on the products were not visible, probably as a result of the low conversion of nitrone to cycloadduct. The reaction between indandione **77** and nitrone **AZ** (**101**) has been studied in isolation, described in **Chapter 4**, and this investigation has shown that the conversion in this reaction is low compared to the recognition-disabled control.

### 5.3.2 Dynamic Covalent Library with Aldehyde 92

In **Chapter 4** we concluded that the recognition-mediated reaction with nitrone **102** and indandione **100** afforded higher selectivity and conversion compared to the system with nitrone **101**. Therefore, we decided to try to incorporate aldehyde **92** in a DCL in order to investigate whether or not this increased selectivity and conversion is also observed with a dynamic pool or reagents (**Figure 5.8**).

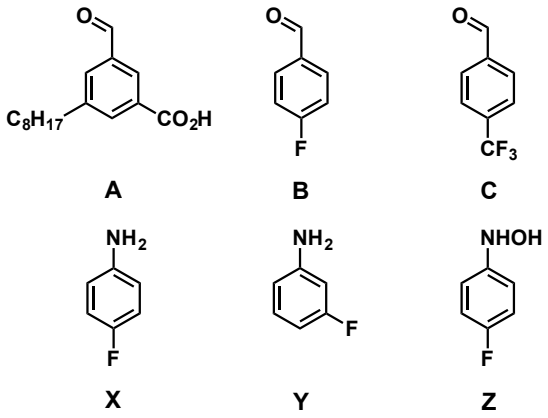


**Figure 5.8:** The aldehydes **A** – **B** and nucleophiles **X** – **Z** are used in the construction of a DCL. Compared to the DCL presented in **Section 5.3.1** another recognition-enabled aldehyde (**A**) is used and the hydroxylamine is equipped with a $^{19}$F-tag.

Because aldehyde **A** is equipped with a solubilising octyl chain, it is not necessary to use a hydroxylamine with a solubilising chain as we did in the library described in **Section 5.3.1**. Therefore, hydroxylamine **Z** is used and this also enables analysis of every library constituent with $^{19}$F NMR spectroscopy as a fluorine atom is incorporated in all library members (**Scheme 5.3**).

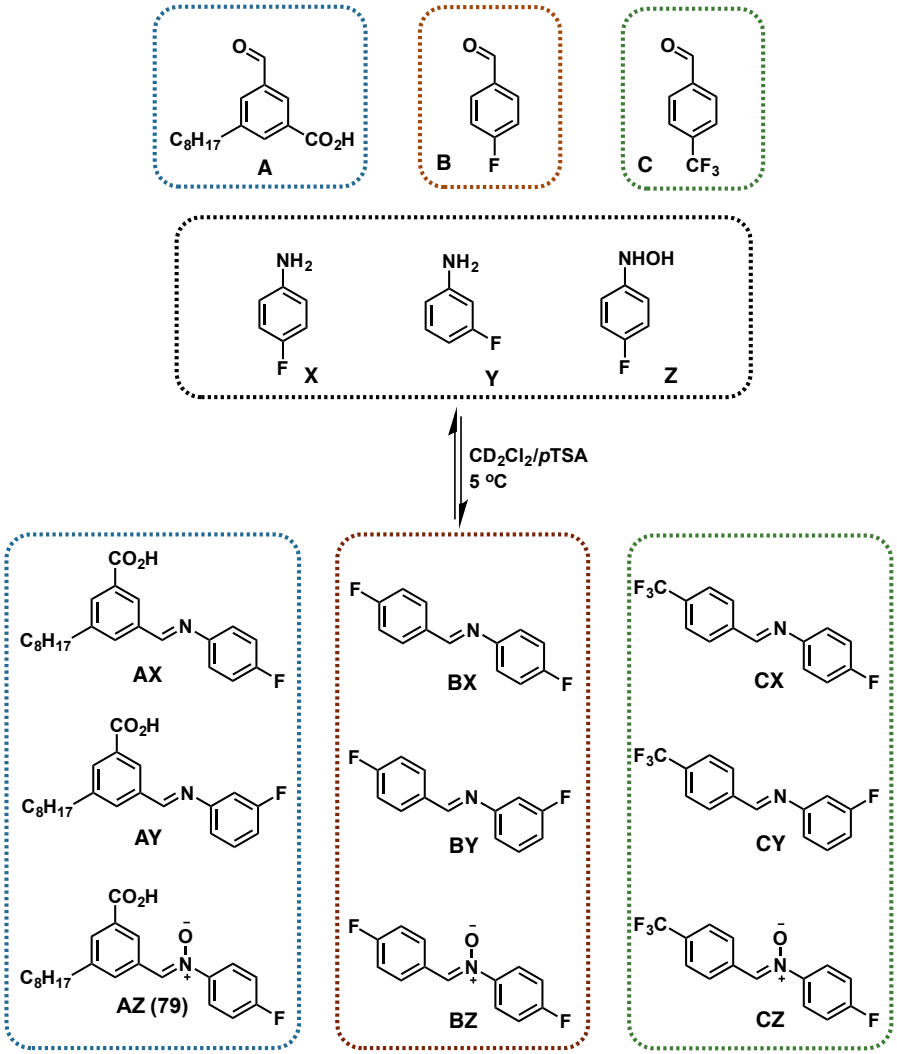


**Scheme 5.3:** A DCL was created by mixing aldehydes **A** – **C** and nucleophiles **X** – **Z**. In contrast with the DCL described in **Section 5.3.1**, all library constituents can be analysed with $^{19}$F NMR spectroscopy.

Similar to the DCL presented in the previous section, the mixture was equilibrated for 48 hours at 5 °C in $CD_2Cl_2$ that was saturated with *p*TSA monohydrate. The samples were analysed with $^{1}$H and $^{19}$F NMR spectroscopy and the resonances were integrated to obtain the concentrations of the library constituents relative to the internal standard 1-bromo-3-fluoro-4-nitrobenzene.

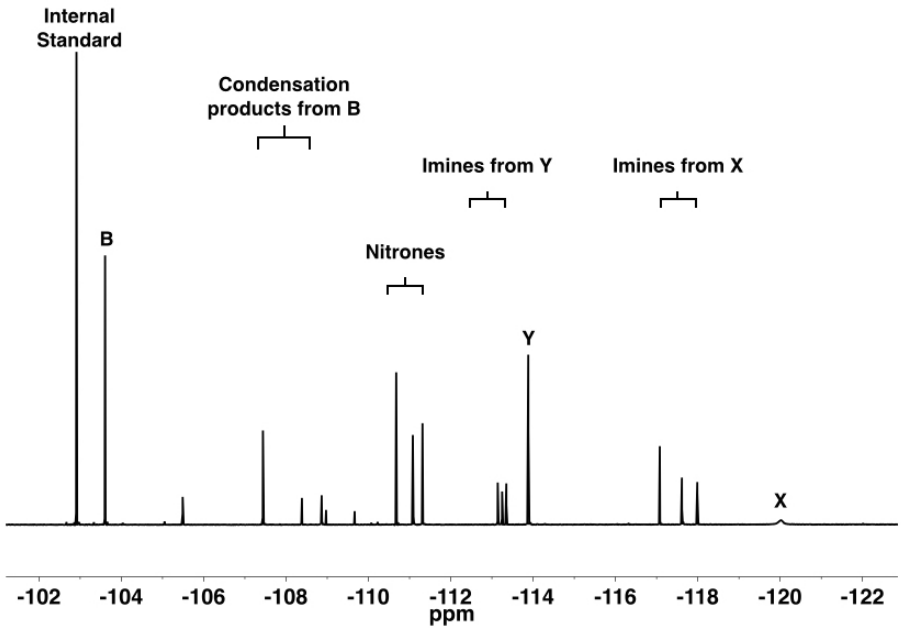


**Figure 5.9:** Partial 376.5 MHz $^{19}F$ NMR spectrum (RT, $CD_2Cl_2$) showing the condensation products and starting materials from the DCL. The region showing aldehyde **C** and corresponding condensation products is around -65 ppm and is not shown in this spectrum.

The resonances corresponding to the library constituents can be deconvoluted and the concentration of each library constituent can be obtained (**Figure 5.10**).

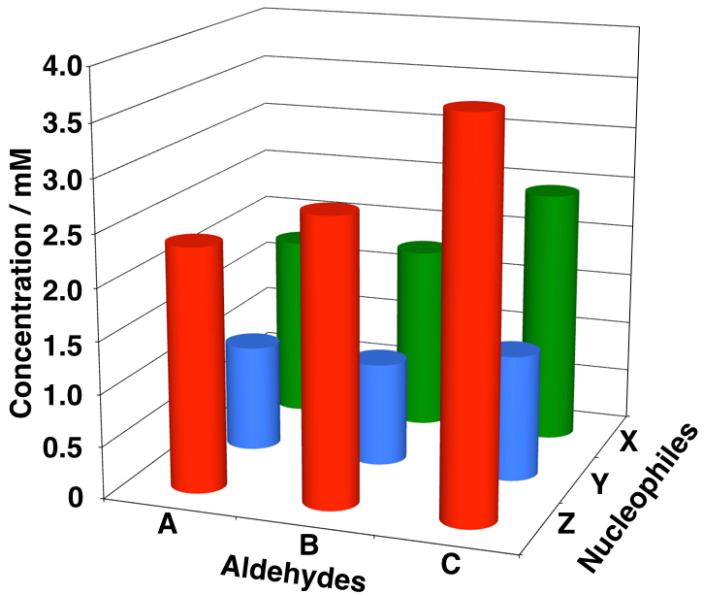


**Figure 5.10:** The concentration of the library constituents after equilibration for 48 hours at 5 °C. The starting concentration of aldehydes **A** – **C** and nucleophiles **X** – **Z** was 10 mM.

After equilibration of the library constituents, indandione **100** was added to the mixture at a final concentration of 10 mM. The sample is left to react at 5 °C for

24 hours and is analysed with $^{1}H$ and $^{19}F$ NMR spectroscopy. The $^{19}F$ NMR spectra do not only show cycloadduct peaks corresponding to the products of the cycloaddition between indandione **100** and nitrones **AZ** – **CZ**. Additionally, formation of indandione **78** was observed in the $^{19}F$ NMR spectrum.

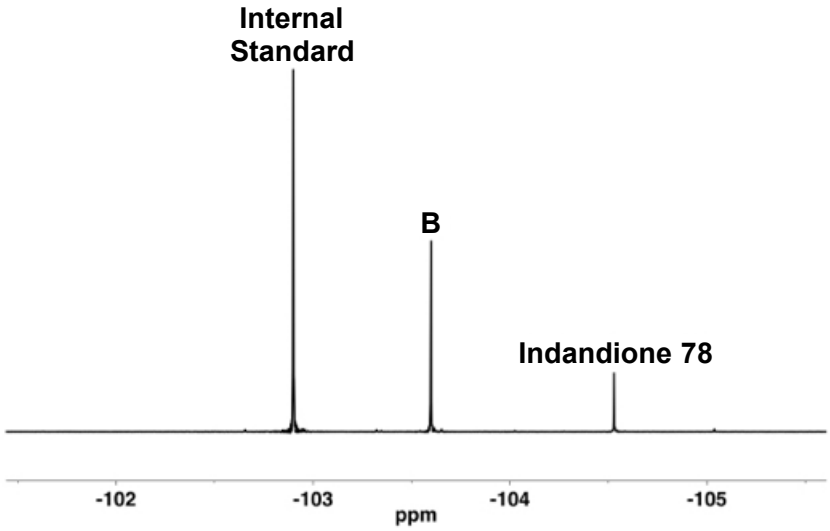


**Figure 5.11:** Partial $^{19}F$ NMR spectrum (376.5 MHz, RT, $CD_2Cl_2$) showing the formation of indandione **78** in the library mixture.

This result indicates that the indandione is not stable under the conditions of the experiment, presumably due to the presence of *p*TSA, and is subject to hydrolysis. As aldehydes **B** and **C** are electrophilic, these can react rapidly with the 1,3-indandione that is forms after the hydrolysis and indandione **78** is formed, and can react with nitrones **AZ** – **CZ** in the library. This hypothesis is confirmed by the observation that nine different cycloadducts are observed in the $^{19}F$ NMR spectrum, presumably caused by the fact that multiple indandiones are present in the library.

## 5.4 Conclusions

The cycloaddition reaction between an indandione and a nitrone is reversible, as experimentally established in **Chapter 3**. The reaction with nitrone **102**, with a benzoic acid recognition site, increases the selectivity of the equilibrium

mixture as well as the conversion. We decided to used this outcome to construct a library of cycloadducts under thermodynamic control with nitrones **79** and **102** and indandiones **78** and **100**. The recognition event leads to excellent selectivity within a dynamic reaction mixture leading to a diastereometric ratio of 5.2 (*trans* / *cis*) of **109**. Addition of DMSO-$d_6$ breaks up the hydrogen bonds and the library re-equilabrates to form all library constituents in roughly the same concentration. To our knowledge, there is one previous example of a reversible cycloaddition reaction that is used in DCC, reported[48] by Lehn and co-workers, based on a Diels-Alder reaction.

Based on previous research in the Philp laboratory, we attempted to construct a DCL with interconverting imines and nitrones and select one nitrone from the DCL by reacting it with indandione **100**. The recognition-mediated reaction pathway was expected to provide more kinetic and thermodynamic stability and therefore we expected to observe selective amplification of one of the cycloadducts. However, we observed formation of different indandiones during the course of the reaction, which disturbed the amplification of one of the cycloadducts.

# 6

# Conclusions and Future Work

## 6.1 Conclusions

The work presented in this thesis focuses on the investigation of the potential of a 2-arylidene 1,3-indandione as a reagent in a self-replicating system. The Philp laboratory has developed several self-replicating systems based on a 1,3-dipolar cycloaddition between a nitrone and a maleimide. A 2-arylidene 1,3-indandione can be used in the 1,3-dipolar cycloaddition with a nitrone instead of the maleimide based dipolarophile. As described in **Chapter 3**, the cycloaddition reaction was studied with model compounds that did not bear a recognition site in order to study the reactivity of the indandione without considering recognition-mediated reaction channels. The cycloaddition reaction was studied both experimentally and computationally and these two methods afforded different results. The computational studies at RM1 and DFT level predict the Michael-*cis* product to be the most stable product both kinetically and thermodynamically, then two products with similar stabilities and one product is predicted to be the least stable. However, in the experimental investigation of the reaction two products are observed in a 1:1 end concentration and one product is formed more slowly than the other. $^{1}$H NMR spectroscopy together with $^{1}$H-$^{1}$H COSY and 1D-NOESY experiments indicated that the two major products have Michael regiochemistry, with Michael-*cis* being the major product after 16 hours. The discrepancy between the results of the computational investigation and the experimental studies is difficult to explain.

In order to assign the stereochemistry and the regiochemistry, it is desirable to analyse the structure using single crystal X-ray crystallography. However, as a result of the reversibility of the reaction, it has not been possible to isolate the products.

2-Functionalised 1,3-indandiones equipped with recognition sites have successfully been synthesised. When these compounds are equipped with a carboxylic acid recognition site, they are not soluble in the desired solvent, $CDCl_3$. Therefore, 1,3-indandione is 2-functionalised with an amidopyridine recognition site. When this compound is also equipped with a solubilising octyl chain it is soluble to 20 mM concentration in $CDCl_3$. Initially, the aim of this work was to construct a self-replicator based on the 2-arylidene-1,3-indandione motif as an alternative for the maleimide-based self-replicating systems previously reported by the Philp laboratory. However, it turned out that the recognition-mediated reaction presumably takes place in the [**A**·**B**] pathway. The existence of a self-replicating autocatalytic cycle is hard to confirm as this requires adding an amount of the pre-formed product to the reaction at $t$ = 0, which should increase the initial rate of formation towards formation of itself.

The reversibility of the cycloaddition reaction has been successfully exploited in the construction of a library of cycloadducts, which we have shown to be responsive to addition of a hydrogen bonding competitive solvent. We have attempted to couple the recognition-mediated 1,3-dipolar cycloaddition with an indandione to a DCL of nitrones and imines, however this attempt was unsuccessful because of the instability of the indandione under the conditions of the experiment.

## 6.2 Future Work

We did not attempt experiments in which the maleimide based systems compete for starting materials because of the reversibility of the indandione-based reaction. The maleimide operates under kinetic control and therefore it

will outcompete the inandione-based system. In order to use the indandione-based dipolarophile in an irreversible 1,3-dipolar cycloaddition another 1,3-dipole, for example azides, could be used. A different 1,3-dipole could make the reaction more favourable and stabilise the cycloadducts so they can be isolated and the relative stereochemistry can be determined. The 2-arylidene-1,3-indandione could also be used as a dienophile in a Diels-Alder reaction, however, presumably the cycloadduct of this reaction would not be stable either as the steric crowding might be significant in the product.

The indandione cycloadducts are not stable as the cycloaddition reaction is reversible. The reversibility of the cycloaddition can be used in Dynamic Covalent Chemistry to create mixtures of interconverting cycloadducts. The cycloaddition between a 2-arylidine-1,3-indandione and a nitrone affords a spiro bicyclic ring system. Thus, from two flat structures, a three dimensional structure is created. In this thesis, a first example is presented of a library under thermodynamic control based on the cycloaddition between indandiones and nitrones and we demonstrated that the library distribution can be influenced by molecular recognition and reversed when the molecular recognition event is broken up. In **Chapter 1**, a few techniques of selecting a library member have been discussed such as phase separation, addition of a template and the introduction of an element of kinetic control. Future research can focus on exploring the reversible 1,3-dipolar cycloaddition in the context of Dynamic Covalent Chemistry.

In terms of obtaining Dynamic Systemic Resolution with indandione-based dipolarophiles, this seems challenging. First of all, the conditions of the dynamic nitrone and imine library should be altered in order to prevent indandione degradation and as the indandione-based 1,3-dipolar cycloaddition is reversible and shows low conversion, obtaining high resolution with this dipolarophile seems difficult. However, a promising result in this respect is the high selectivity that was obtained with indandione **100** and nitrone **102**. Unfortunately, these results could not be reproduced with a dynamic pool of nitrones and imines.

# 7

# Experimental

## 7.1 Experimental Procedures

The chemicals and solvents were purchased from Sigma Aldrich UK, Acros Organics UK, Alfa Aesar UK, Fisher UK, TCI UK Ltd. Fluorochem or Apollo Scientific and were used as delivered unless stated otherwise. Brine refers to a saturated solution of sodium chloride. Thin Layer Chromatography (TLC) was carried out using Macherey-Nagel GmbH & Co. KG DC-Fertigfolien POLYGRAM® SIL G/$UV_{254}$ plates. Spots on the TLC plates were visualised under a UV lamp (254 or 366 nm). Flash column chromatography was performed with Silicycle SillFlash P60. Dry DCM, THF and Toluene were obtained using an MBraun MS SPS-800 solvent purification system, which passes the solvents through a filter column and dispenses the solvents under an Argon atmosphere. Dry MeCN is obtained by distilling purchased MeCN for two hours. Melting points were determined with a Stuart SMP30 melting point apparatus. Electrospray ionisation spectra (ES) were performed on a Micromass LCT spectrometer operating in positive or negative mode from solutions of DCM or methanol. *m/z* values are reported in Daltons and followed by their percentage abundance in parentheses.

## 7.2 NMR Spectroscopy

In order to obtain an NMR spectrum, a compound was dissolved in a deuterated solvent, either $CDCl_3$ or DMSO-$d_6$. The deuterated solvents act as lock and the

residual protonated solvent as reference signal. The obtained NMR spectra were analysed using iNMR software (Version 5.2.0, 2012 Mestrelab Research) or MestReNova software (version 9.0.1-133254). To aid characterisation, 2D experiments like correlation spectroscopy (COSY), Heteronuclear Single Quantum Correlation Spectroscopy (HSQC) and Heteronuclear Multiple-Bond Correlation Spectroscopy (HMBC) were used.

### 7.2.1 $^{1}$H NMR Spectroscopy

The $^{1}$H NMR spectra were recorded on a Bruker Avance (300.1 MHz), Bruker Avance II (400.1 MHz), Bruker Avance (500.1 MHz) or Bruker Avance III (500.1 MHz) spectrometer. The chemical shift ($\delta_H$) is given in parts per million (ppm) and is determined relative to the solvent signal ($CHCl_3$ = 7.26 ppm, DMSO = 2.50 ppm). The number of protons for each resonance is determined as nH based on integral values. The multiplicity is indicated for each signal and the coupling constants (*J*) are calculated using iNMR software or MestReNova software and are reported to the nearest 0.1 Hz. Identical coupling constants are averaged in each spectrum and are reported to the nearest 0.1 Hz.

### 7.2.2 $^{13}$C NMR Spectroscopy

The $^{13}$C NMR spectra were recorded on a Bruker Avance II (100.6 MHz) or a Bruker Avance (125.8 MHz) spectrometer. DEPTQ pulse sequences with proton decoupling were used for spectrum recording. The chemical shift ($\delta_C$) is given in parts per million (ppm) and is determined relative to the solvent signal ($CDCl_3$ = 77.16 ppm, DMSO-$d_6$ = 39.52 ppm). All $^{13}$C NMR spectrum signals reported here are singlets unless stated otherwise in which case their multiplicity is indicated by the symbol d for doublet.

### 7.2.3 $^{19}$F NMR Spectroscopy

The $^{19}$F NMR spectra were recorded on a Bruker Avance II (376.7 MHz) or a Bruker Avance (470.5 MHz) spectrometer using a broadband proton decoupling pulse sequence with the deuterated solvent as the internal lock. The chemical

shift ($\delta_F$) is given in parts per million (ppm) relative to $CCl_3F$ where $\delta_F$ $CCl_3F$ = 0.00 ppm.

## 7.3 Crystallographic Analysis for Compounds 78 and 79

X-ray diffraction studies were performed at 93K using a Rigaku XtaLAB P200 diffractometer using multi-layer mirror monochromated Mo-K$\alpha$ radiation. Intensity data were collected using $\omega$ and $\varphi$ steps accumulating area detector frames spanning a hemisphere of reciprocal space (data were integrated using CrystalClear[102]). All data were corrected for Lorentz, polarisation and long-term intensity fluctuations. Absorption effects were corrected on the basis of multiple equivalent reflections. The structure was solved by direct methods and refined by full-matrix least-squares against $F^2$ (SHELXTL[103]). All hydrogen atoms were assigned riding isotropic displacement parameters and constrained to idealised geometries.

## 7.4 Cycloaddition experiments

The cycloaddition reactions with the model compounds (**Chapter 3**) were performed at 60, 80 and 120 °C. The experiments at 60 °C and 80 °C were performed in 5 mm Norell NMR tubes heated in a water bath that was regulated at the desired temperature. The experiments at 120 °C were performed in a CEM Discover® SP microwave system. For the experiments at 60 °C, a stock solution of the internal standard (4-bromo-3-fluoro-1-nitrobenzene) was prepared in $CDCl_3$ and an amount was transferred to one starting compound to dissolve in in $CDCl_3$. Subsequently, this solution was transferred to the other starting compound to afford a solution of internal standard and all starting compounds at the desired concentration, which was transferred to an NMR tube. For the experiments at 80 and 120 °C, the same method of preparation was used but the solvent used was 1,1,2,2-tetrachloroethane. In order to allow analysis with $^{19}F$ NMR spectroscopy, 10 vol% of $CDCl_3$ was added after the

experiment. The integral of the relevant resonances in the $^{19}F$ NMR spectrum were determined and the conversion was calculated with **Equation 7.1**.

$$Conversion = \frac{\sum Integrals\ of\ Products}{\sum All\ Integrals} \cdot 100\% \qquad \textbf{Equation 7.1}$$

## 7.5 Kinetic Measurements and Deconvolution of NMR Data

### 7.5.1 $^{1}H$ NMR and $^{19}F$ NMR Spectroscopy

500.1 MHz $^{1}H$ NMR spectroscopy and 470.4 MHz $^{19}F$ NMR spectroscopy were used for kinetic analysis described in **Chapter 3** and **4**. Stock solutions of the appropriate compounds were prepared in $CDCl_3$ using a Sartorial BP211D balance (± 0.01 mg). In a typical experiment, an NMR sample was prepared in a 5 mm Norell NMR tube by mixing the stock solutions so that the final volume was 1 mL and each compound is present at the appropriate concentration. The sample was transferred to an NMR spectrometer that was regulated at the desired temperature and 500.1 MHz $^{1}H$ NMR spectra and 470.4 MHz $^{19}F\{^{1}H\}$ NMR spectra were automatically acquired at a desired time interval during a desired time period. Analysis and deconvolution of the collected data was performed using iNMR software (Version 5.2.0, 2012 Mestrelab Research).

From the $^{1}H$ NMR spectra, the progress of the reaction was calculated by monitoring the appearance of the isoxazolidine proton signals on the cycloadducts between 5.00 ppm and 6.00 ppm. From the $^{19}F\{^{1}H\}$ NMR spectra, the progress of the reaction was calculated by monitoring the disappearance of the fluorine signals corresponding to the starting materials and appearance of fluorine signals corresponding to the products.

### 7.5.2 Semi-automatic Deconvolution

The acquired spectra from either $^{1}H$ NMR or $^{19}F$ NMR spectroscopy were analysed using the semi-automatic deconvolution feature in the iNMR software.

Using a suitable script, the iNMR programme opened each spectra individually and a least square optimisation was performed on each selected signal to determine the area of the resonance. The area of the resonances corresponding to the product and to the starting materials, as described in **Section 7.4.1** as well as the signal corresponding to the internal standard were used to calculate the progress of the reaction. Based on the known concentration of the internal standard in the reaction mixture, the concentration for each signal could be calculated. The resulting concentration *vs*. time data was plotted using the ProFit software (Version 6.2.1, Quantum Soft, 2010) or Microsoft Excel for Mac 2011 (Version 14.4.8 (150116)). An example of a semi-automatic deconvolution script can be found in the appendix.

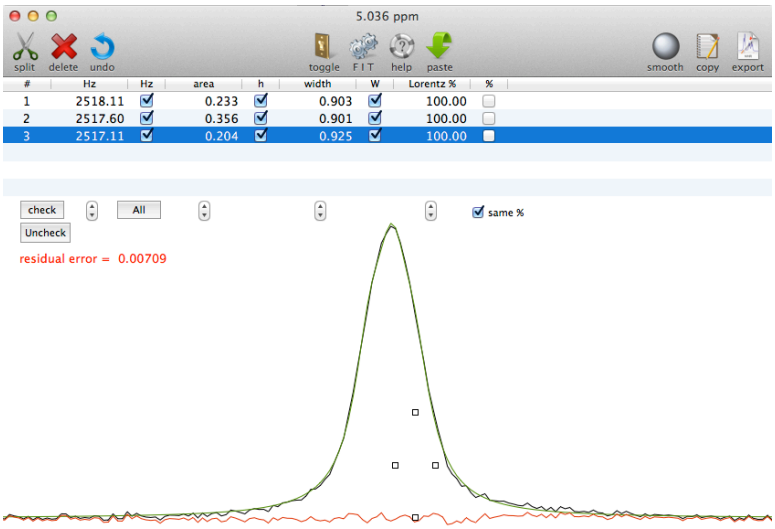


**Figure 7.1:** The deconvolution window in iNMR gives the option to fit a resonance in the $^{1}$H NMR or $^{19}$F NMR spectrum.

## 7.6 Construction and Analysis of Dynamic Covalent Libraries

Initially, $CD_2Cl_2$ was saturated with *p*TSA monohydrate by stirring $CD_2Cl_2$ with a sufficient amount of *p*TSA monohydrate for 30 minutes before filtering the excess *p*TSA monohydrate in order to obtain the solvent that was ready to use in a DCL experiment. A stock solution of 20 mM internal standard 4-bromo-3-fluoro-1-nitrobenzene was prepared using a Sartorial BP211D balance (± 0.01 mg). Subsequently, the internal standard stock solution was used to dissolve an

appropriate amount of the first aldehyde to afford a 20 mM solution of that aldehyde. Then, the aldehyde solution was transferred to an appropriate amount of the second aldehyde to afford a solution of 20 mM of both aldehydes. This process was repeated for the third aldehyde. The process was repeated separately for the nucleophiles in order to afford two solutions; one with all aldehydes at 20 mM and one with all nucleophiles at 20 mM. Subsequently, 0.5 mL of the aldehyde solution and 0.5 mL of the nucleophile solution was transferred to an NMR tube and the NMR tube was sealed with a polyethylene pressure cap to prevent solvent evaporation. The sample was left to react in a thermostatically controlled water bath at 5 $^{o}$C for an appropriate time period.

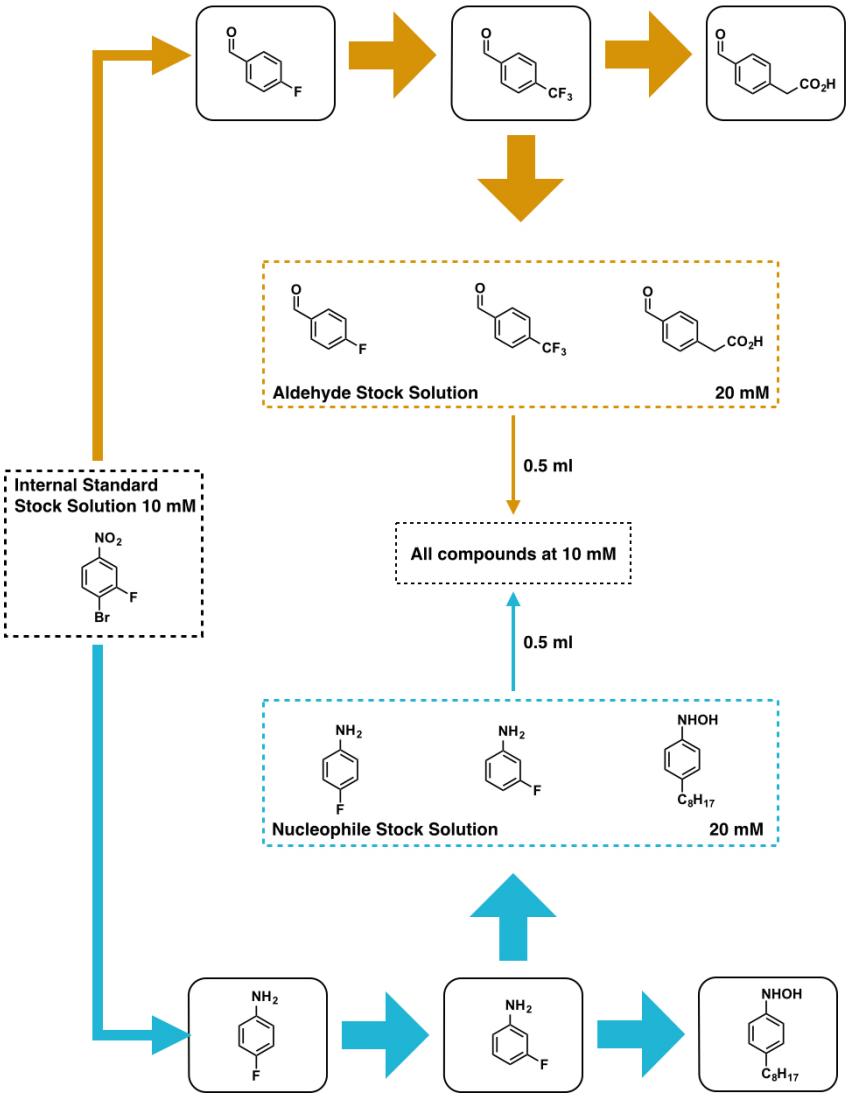


**Figure 7.2:** A DCL is constructed by creating an aldehyde stock solution and a stock solution with all aldehydes. These stock solutions are added together to afford a mixture with all library starting compounds present at 10mM. The internal standard is present at the desired concentration in both stock solutions. Figure adapted for this thesis from reference 96.

The large number of structurally similar compounds makes analysis with $^{1}H$ NMR spectroscopy of DCLs impossible. Therefore $^{19}F$ NMR spectroscopy was used to distinguish the different library constituents and products in the mixture. Concentrations of all compounds were calculated from the relative intensities of each signal compared to the intensity of the internal standard signal.

## 7.7 Kinetic Fitting, Simulation and Extraction of Rate Constants

All kinetic fitting was performed using the SimFit software package (Version 32, Günther von Kiedrowski, 2003). A detailed kinetic model of all possible interactions involved in the studied systems was constructed. This model was converted into a series of rate equations whose solution determine the concentration of reactant and product species as a function of time. The program varies experimentally inaccessible kinetic values until the calculation matches the experimental data.

Kinetic simulations were performed with the Copasi software package[8] (Copasi 4.14 (Build 89)). The extracted kinetic parameters from the SimFit fitting were used as input for construction of the rate law for Copasi. The program uses the rate law to construct a plot, which is pre-defined by the user.

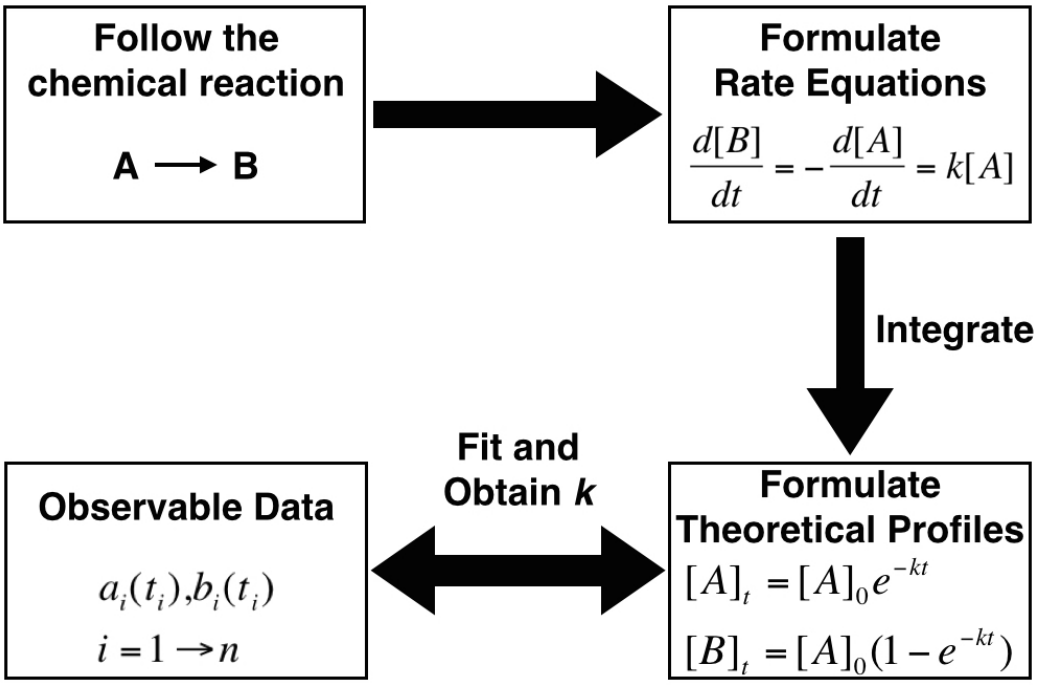


**Figure 7.3:** After the chemical reaction is carried out a kinetic model is constructed and the model is converted to a series of rate equations. Using the SimFit software package, kinetic parameters were extracted.

## 7.8 Computational Methods

All molecular mechanics calculations were performed on a Linux workstation using the OPLS2005 forcefield together with the GB/SA solvation model for chloroform as implemented in Macromodel (Version 10.1, Schrödinger Inc., 2014). Electronic structure calculations were carried out using Gaussian09[104], GAMESS-US[105] or MOPAC2012[106] running on Linux workstation or cluster. The 64-bit Linux version dated 5 December 2014 (Revision 1) of GAMESS or Revision A.02 of Gaussian09 was used in all density functional calculations. The transition state for the reaction was located by generation of an initial guess using a grid scan method using RM1 and then refinement at the RM1 level of theory within MOPAC. This refinement led to the location of a transition state structure possessing single imaginary vibration that corresponded to the reaction coordinate. All semi-empirical electronic structure calculations were carried out using MOPAC2012. Versions in the 15.xxx series were used in all calculations. In all cases, Eigenvector following was used to locate a transition

state structure possessing single imaginary vibration that corresponded to the reaction coordinate, as verified using the THERMO keyword in MOPAC. Relative free energies using density functional methods were performed using Gaussian09 with the keywords `Opt Freq`.

## 7.9 Synthetic Procedures

### 2-(4-Fluorobenzylidene)-1 *H*-indene-1,3(2*H*)-dione[107] - 78

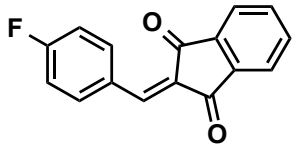


1,3-Indandione (3.48 g, 0.024 mol), 4-fluorobenzaldehyde (2.85 g, 0.023 mol) and triethylamine (0.23 g, 2.24 mmol) were dissolved in ethanol (90 ml) and the mixture was stirred at room temperature for 4 hours. Afterwards the mixture was diluted with dichloromethane (50 ml) and that was washed with 1 M HCl (50 ml), saturated $NaHCO_3$ solution (50 ml) and brine (50 ml) and dried over $MgSO_4$. The $MgSO_4$ was filtered off and the solvent was removed *in vacuo* giving the crude product as a green solid. The product was recrystallised from DCM/hexane to yield the pure product as a green solid (4.84 g, 79%). M.p. 180 - 181 °C. $^1$H NMR (500.1 MHz, $CDCl_3$) δ 8.59 - 8.56 (2H, m, Ar CH), 8.06 - 8.03 (2H, m, Ar CH), 7.89 (1H, s, CH), 7.87 - 7.85 (2H, m, Ar CH), 7.23 (2H, t, *J* = 9.0 Hz, Ar CH). $^{19}$F NMR (376.6 MHz, $CDCl_3$) δ -103.75. $^{13}$C (125.8 MHz, $CDCl_3$) δ 190.3 (CO), 189.3 (CO), 165.7 (d, *J* = 257.9 Hz, CF), 145.6 (CH), 142.5 ($C_{quart}$, Ar C), 140.2 ($C_{quart}$, Ar C), 137.1 (d, *J* = 8.8 Hz, Ar CH), 135.5 (d, *J* = 20.1 Hz, Ar CH), 129.7 (d, *J* = 3.9 Hz, $C_{quart}$, Ar C), 128.7 ($C_{quart}$), 123.5 (Ar CH), 116.3 (d, *J* = 21.4 Hz, Ar CH). ES MS (*m/z*) 527 (100% $[2M+Na]^+$). Slow evaporation of DCM:pentane (1:3) afforded crystals of sufficient quality for single-crystal X-ray diffraction.

**2-(4-(Bromomethyl)phenyl)acetic acid[108] - 84**

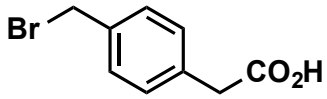


4-Tolylacetic acid (6.78 g, 0.045 mol) was dissolved in chlorobenzene (50 ml) and stirred when bromine (7.46 g, 0.046 mol) was added. The mixture was stirred for 2 hours under irradiation of a 60 W tungsten lamp. Afterwards a white precipitant was filtered off and washed with hexane (100 ml) and dried. The desired product was obtained as a white solid (5.53 g, 54%). M. p.: 169 - 172 °C. $^{1}$H NMR (400.3 MHz, DMSO-$d_6$) δ 7.38 (2H, d, $J$ = 8.3 Hz, Ar CH), 7.24 (2H, d, $J$ = 8.3 Hz, Ar CH), 4.69 (2H, s, methylbromo), 3.57 (2H, s, acetic acid). $^{13}$C NMR (100.7 MHz, DMSO-$d_6$) δ 172.5 (CO), 136.3 ($C_{quart}$, Ar C), 135.3 ($C_{quart}$, Ar C), 129.7 (Ar CH), 129.2 (Ar CH), 40.3 ($CH_2$), 34.4 ($CH_2$). Spectroscopic data is in accordance with that reported previously.[108]

**2-(4-Formylphenyl)acetic acid[82] - 85**

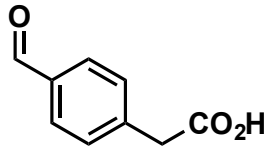


2-(4-(Bromomethyl)phenyl)acetic acid (4.01 g, 0.018 mol) and HMTA (3.78 g, 0.027 mol) were dissolved in EtOH/$H_2O$ (1:1, 30 ml). The reaction mixture was heated to reflux temperature for 4 hours. Then concentrated HCl (2 ml) was added drop wise and the mixture was refluxed for another 30 minutes after which the mixture was cooled to room temperature in a water bath. The mixture was diluted with $H_2O$ (60 ml) and the product extracted with DCM (2 x 100 ml). The DCM was dried over $MgSO_4$ and this was filtered off and the DCM was removed *in vacuo* affording the product as a white solid (1.77, 60%). M. p.: 108 - 118 °C. $^{1}$H NMR (400.1 MHz, DMSO-$d_6$) δ 9.98 (1H, s, aldehyde H), 7.86 (2H, d, $J$ = 8.0 Hz, Ar CH), 7.49 (2H, d, $J$ = 8.0 Hz, Ar CH), 3.71 (2H, s, $CH_2$). $^{13}$C

NMR (125.8 MHz, DMSO-$d_6$) δ 193.2 (CO), 172.5 ($CO_2H$), 142.6 ($C_{quart}$, Ar C), 135.3 ($C_{quart}$, Ar C), 130.8 (Ar CH), 129.9 (Ar CH), 41.2 ($CH_2$). Spectroscopic data is in accordance with that reported previously.[82]

**2-(4-((1,3-Dioxo-1,3-dihydro-2*H*-inden-2-ylidene)methyl)phenyl)acetic acid - 86**

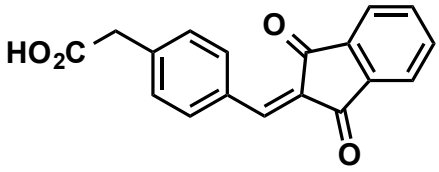


1,3-Indandione (197 mg, 1.34 mmol) and 2-(4-formylphenyl)acetic acid (221 mg, 1.34 mmol) were dissolved in EtOH (25 ml). Pyridine (0.26 mg, 3.35 mmol) was added and the mixture was left stirring at room temperature. After 16 hours the product precipitated from the reaction mixture, it was filtered off and washed with cold EtOH. The product was obtained as a yellow solid (250 mg, 64%). M. p.: 202 - 208 °C. $^1$H NMR (400.1 MHz, DMSO-$d_6$) δ 8.45 (2H, d, Ar CH, $J$ = 8.0 Hz), 7.99 - 7.93 (4H, m, Ar CH), 7.83 (1H, s, CH), 7.46 (2H, d, Ar CH, $J$ = 8.0 Hz), 3.71 (2H, s, $CH_2$). $^{13}$C NMR (100.6 MHz, DMSO-$d_6$) δ 189.9 (CO), 189.1 (CO), 172.5 ($CO_2H$), 145.8 (CH), 142.4 ($C_{quat}$, Ar), 141.4 ($C_{quat}$, Ar), 139.9 ($C_{quat}$, Ar), 136.4 (Ar CH), 136.3 (Ar CH), 134.3 (Ar CH), 131.7 ($C_{quat}$, Ar), 130.4 (Ar CH), 129.3 ($C_{quart}$), 123.6 (Ar CH), 123.5 (Ar CH), 41.2 ($CH_2$). ES MS (*m/z*) 315 (100% $[M+Na]^+$) HRMS (*m/z*) $[M+Na]^+$ calcd. for $C_{18}H_{12}O_4Na$, 315.0633; found, 315.0622.

**4-((1,3-Dioxo-1,3-dihydro-2*H*-inden-2-ylidene)methyl)benzoic acid - 83**

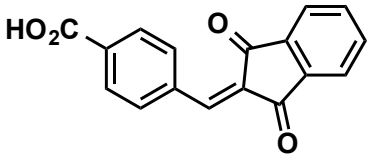

1,3-Indandione (0.98 g, 6.7 mmol), 4-carboxybenzaldehyde (1.00 g, 6.7 mmol) and triethylamine (0.73 g, 7.2 mmol) were dissolved in acetonitrile (25 ml) and the mixture was stirred at room temperature for 3 hours. The mixture was acidified with 1 M HCl to pH 3 and extracted with DCM. The DCM was washed with saturated $NaHCO_3$ (50 ml) and brine (50 ml). The DCM is dried over $MgSO_4$, which is filtered off, and the DCM is removed *in vacuo* and a yellow solid is obtained. This is washed with $H_2O$ and chloroform and dried under vacuum (0.65 g, 33%). M.p. 275 - 277 °C. $^1$H NMR (400.1 MHz, DMSO-$d_6$) δ 8.54 - 8.51 (2H, m, Ar CH), 8.08 - 8.05 (2H, m, Ar CH), 8.04 - 8.01 (2H, m, Ar CH), 7.99 - 7.97 (2H, m, Ar CH), 7.90 (1H, s, CH). $^{13}$C NMR (100.6 MHz, DMSO-$d_6$) δ 189.5 (CO), 188.8 (CO), 167.1 ($CO_2$H), 143.9 (CH), 142.5 ($C_{quart}$, Ar C), 140.1 ($C_{quart}$, Ar C), 136.9 ($C_{quart}$, C), 136.6 (Ar CH), 134.2 ($C_{quart}$, Ar C), 133.9 (Ar CH), 131.7 ($C_{quart}$, Ar C), 129.7 (Ar CH), 123.7 (Ar CH). ES MS (*m/z*) 277 (100% $[M-H]^-$). HRMS (*m/z*) $[M-H]^+$ calcd. for $C_{17}H_9O_4$, 277.0495; found, 277.0507.

**4-Formylbenzoyl chloride - 94**

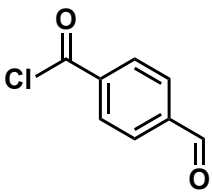

4-Formylbenzoic acid (2.00 g, 0.013 mol) was dissolved in anhydrous toluene (50 ml) and thionyl chloride (33.31 g, 0.28 mol) was added drop wise to the stirring solution under $N_2$ atmosphere. The mixture was heated to 160 °C and was left to react for 5 hours. Then the mixture was cooled down to room

temperature and left to stir over night. Afterwards the solvent was removed *in vacuo*. The residue was then dried under vacuum for 1 hour to remove thionyl chloride. The desired product was obtained as a white solid (2.21 g, 91%), which was used without further purification. M. p.: 41 - 44 °C. $^{1}$H NMR (400.1 MHz, $CDCl_3$) δ 10.14 (1H, s, aldehyde H), 8.29 - 8.26 (2H, m, Ar H), 8.04 - 8.01 (2H, m, Ar H). $^{13}$C NMR (100.7 MHz, $CDCl_3$) δ 191.1 (COCl), 167.9 (CO), 140.6 ($C_{quart}$, Ar C), 137.7 ($C_{quart}$, Ar C), 131.9 (Ar CH), 129.9 (Ar CH). Spectroscopic data is in accordance with that reported previously.[96]

**_N_-(4,6-Dimethylpyridin-2-yl)-4-formylbenzamide[96] - 95**

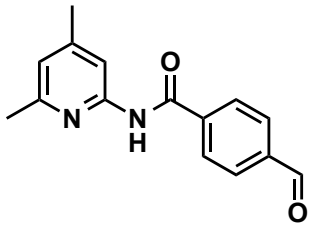


4,6-Dimethylpyridin-2-amine (2.08 g, 0.017 mol) and triethylamine (2.56 g, 0.025 mol) were dissolved in anhydrous DCM (20 ml) and cooled to 0 °C. 4-formylbenzoyl chloride was dissolve in anhydrous DCM (30 ml) and this was added drop wise to the stirring cooled 4,6-dimethylpyridin-2-amine solution. After addition of the acyl chloride the mixture was allowed to warm up to room temperature and was left to react over night. Afterwards the DCM was washed with 1 M HCl (3 x 50 ml) and the combined aqueous phase was extracted with DCM (3 x 50 ml). The combined organic phase was washed with saturated $NaHCO_3$ solution (100 ml) and brine (2 x 100 ml). The DCM was dried over $MgSO_4$, which is filtered off and the solvent is removed *in vacuo* yielding a white solid. The crude product was purified with silica gel flash chromatography (eluting with DCM/EtOAc (3:2)) yielding the pure product as a white solid (2.02 g, 61%). M. p.: 125 - 130 °C. $^{1}$H NMR (400.1 MHz, $CDCl_3$) δ 10.09 (1H, s, aldehyde), 8.78 - 8.75 (1H, broad, NH), 8.07 - 8.01 (3H, m, Ar CH), 7.98 (2H, d, Ar CH, $J$ = 8.4 Hz), 6.78 (1H, s, Ar CH), 2.37 (3H, s, $CH_3$), 2.36 (3H, s, $CH_3$). $^{13}$C (125.8 MHz, $CDCl_3$) δ 191.4 (CO), 164.5 (amide CO), 156.6 ($C_{quart}$, Ar C),

150.6 ($C_{quart}$, Ar C), 150.4 ($C_{quart}$, Ar C), 139.6 ($C_{quart}$, Ar C), 138.6 ($C_{quart}$, Ar C), 129.9 (Ar CH), 127.9 (Ar CH), 121.1 (Ar CH), 111.8 (Ar CH), 23.7 ($CH_3$), 21.3 ($CH_3$). ES MS (*m/z*) 287 (100% $[M+H+CH_3OH]^+$). Spectroscopic data is in accordance with that reported previously.[96]

**_N_-(4,6-dimethylpyridin-2-yl)-4-((1,3-dioxo-1,3-dihydro-2_H_-inden-2-ylidene)methyl)benzamide - 96**

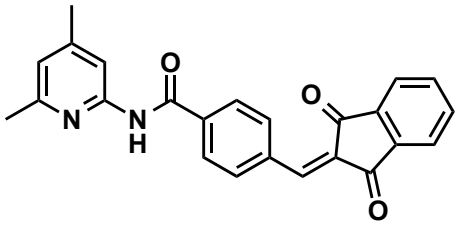


*N*-(4,6-Dimethylpyridin-2-yl)-4-formylbenzamide (200 mg, 0.79 mmol) and 1,3-indandione (115 mg, 0.79 mmol) were dissolved in ethanol (20 ml) and pyridine (98 mg, 1.24 mmol) was added. The mixture was stirred for 16 hours at room temperature. A yellow precipitate was formed and filtered off, washed with cold ethanol and collected as the pure product (130 mg, 43%). M.p. 230 - 233 °C. $^1$H NMR (500.1 MHz, $CDCl_3$) δ 8.67 (1H, broad, NH), 8.58 (2H, d, *J* = 9.0 Hz, Ar CH), 8.10 - 8.06 (5 H, m, Ar CH), 7.95 (1H, s, CH), 7.90 - 7.87 (2H, m, Ar CH), 6.83 (1H, s, Ar CH), 2.47 (3H, s, $CH_3$), 2.40 (3H, s, $CH_3$). $^{13}$C NMR (125.8 MHz, $CDCl_3$) δ 195.5 (CO), 189.8 (CO), 183.0 (amide CO), 164.5 ($C_{quart}$, Ar C), 161.5 ($C_{quart}$, Ar C), 144.7 (CH), 142.6 ($C_{quart}$), 140.2 ($C_{quart}$, Ar C), 137.6 ($C_{quart}$, Ar C), 136.1 ($C_{quart}$, C), 135.7 (Ar CH), 135.6 (Ar CH), 134.1 (Ar CH), 130.8 ($C_{quart}$, Ar C), 127.5 (Ar CH), 123.6 (Ar CH), 120.9 (Ar CH), 111.8 (Ar CH), 23.8 ($CH_3$), 21.4 ($CH_3$). ES MS (pos. *m/z*) 383 (100% $[M+H]^+$). HRMS (*m/z*) $[M+H]^+$ calcd. for $C_{24}H_{19}O_2N_2$, 383.1390; found, 383.1380.

**_N_-(4-Fluorophenyl)hydroxylamine[85] - 65**

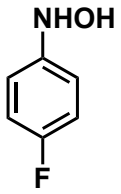


4-Fluoronitrobenzene (1.04 g, 7.37 mmol) was dissolved in anhydrous THF (50 ml) with Rh/C (200 mg) under Ar atmosphere. Hydrazine (0.61 g, 0.019 mol) was added drop wise to the stirring solution. The mixture was allowed to stir for 1.5 hours before $MgSO_4$ was added and the Rh/C and $MgSO_4$ were filtered off. The THF was concentrated *in vacuo* and the crude product was dried on vacuum for 1 hour. Afterwards the product was recrystallised from EtOAc/hexane, which afforded the product as white crystals (0.35 g, 37%). M. p.: 91 - 93 °C. $^1$H NMR (400.1 MHz, $CDCl_3$) δ 6.99 - 6.98 (2H, m, Ar CH), 7.97-6.96 (2H, m Ar H), 6.70 (1H, s, OH), 5.84 - 5.68 (1H, broad, NH). $^{19}$F NMR (376.6 MHz, $CDCl_3$) δ -122.34. $^{13}$C NMR (100.7 MHz, $CDCl_3$) δ 158.8 (d, $J$ = 239.7, CF), 145.7 ($C_{quart}$, Ar C), 116.5 (d, $J$ = 9.1 Hz, Ar CH), 115.7 (d, $J$ = 22.2 Hz, Ar CH). Spectroscopic data is in accordance with that reported previously.[96]

**1-(4-Bromophenyl)-_N_-(4-fluorophenyl)methanimine oxide[52] - 79**

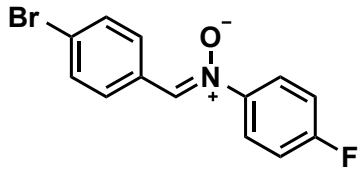


*N*-(4-Fluorophenyl)hydroxylamine (100.6 mg, 0.79 mmol) and 4-bromobenzaldehyde (145.5 mg, 0.79 mmol) were dissolved in EtOH (20 ml). Mixture was cooled to -20 °C over night and the product is filtered off. The product is obtained as white crystals (118.5 mg, 51%). M. p. 137 - 139 °C. $^1$H NMR (400.3 MHz, $CDCl_3$) δ 8.28 - 8.24 (2H, m, Ar CH), 7.85 (1H, s, CH), 7.80 - 7.75 (2H, m, Ar CH), 7.61 (2H, d, $J$ = 8.8 Hz, Ar CH), 7.20 - 7.14 (2H, m, Ar

CH). $^{19}$F NMR (376.6 MHz, $CDCl_3$) δ -110.45. $^{13}$C NMR (100.7 MHz, $CDCl_3$) δ 161.9 (d, *J* = 43.3 Hz, CF), 147.1 ($C_{quart}$, Ar C), 133.5 (d, *J* = 3.0 Hz, $C_{quart}$, Ar C), 132.1 (CH), 130.4 (Ar CH), 129.5 (Ar CH), 125.1 ($C_{quart}$, Ar C), 123.8 (d, *J* = 9.1 Hz, Ar CH), 116.3 (d, *J* = 23.2 Hz, Ar CH). ES MS (*m/z*) 316 (100% $[M+Na]^+$). HRMS (*m/z*) $[M+Na]^+$ calcd. for $C_{13}H_9BrFNONa$, 315.9744; found, 315.9731. The crystals that were obtained were of sufficient quality for single-crystal X-ray diffraction.

**(*Z*)-1-(4-((4,6-Dimethylpyridin-2-yl)carbamoyl)phenyl)-*N*-(4-fluorophenyl)methanimine oxide[85] - 110**

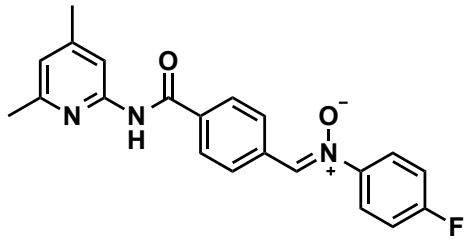


*N*-(4,6-Dimethylpyridin-2-yl)-4-formylbenzamide (50.8 mg, 0.2 mmol) and *N*-(4-fluorophenyl)hydroxylamine (25.4 mg, 0.2 mmol) were dissolved in EtOH (3.5 ml) and cooled to -20 °C for 16 hours. The resulting precipitant was filtered off and washed with cold EtOH and isolated as the desired product (42.2 mg, 58%. M. p.: 212 - 213 °C. $^1$H NMR (400.3 MHz, $CDCl_3$) δ 8.53 - 8.47 (3H, broad m, NH, Ar CH), 8.05 - 8.00 (3H, m, Ar CH), 7.97 (1H, s, CH), 7.82 - 7.78 (2H, m, Ar CH), 7.22 - 7.16 (2H, m, Ar CH), 6.79 (1H, s, Ar CH), 2.44 (3H, s, $CH_3$), 2.37 (3H, s, $CH_3$). $^{19}$F NMR (376.6 MHz, $CDCl_3$) δ -110.11. $^{13}$C NMR (100.7 MHz, $CDCl_3$) δ 170.8 (CO), 163.3 (d, *J* = 251.8 Hz, CF), 156.7 ($C_{quart}$, Ar C), 150.8 ($C_{quart}$, Ar C), 150.4 ($C_{quart}$, Ar C), 145.3 (d, *J* = 2.0 Hz, $C_{quart}$, Ar C), 136.0 (CH), 133.8 (Ar CH), 133.4 (Ar CH), 129.2 (Ar CH), 127.7 (Ar CH), 123.9 (d, *J* = 8.1 Hz, Ar CH), 121.0 (Ar CH), 116.3 (d, *J* = 23.2 Hz, Ar CH), 111.8 (Ar CH), 24.0 ($CH_3$), 21.5 ($CH_3$). ES MS (*m/z*) 364 (100% $[M+H]^+$). HRMS (*m/z*) $[M+H]^+$ calcd. for $C_{21}H_{19}O_2N_3F$, 364.1461; found, 364.1446. Spectroscopic data in accordance with that reported previously.[96]

**(*Z*)-*N*,1-bis(4-fluorphenyl)methanimine oxide[86] - 81**

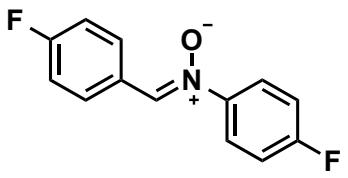

*N*-(4-fluorophenyl)hydroxylamine (100.6 mg, 0.79 mmol) and 4-fluorobenzaldehyde (98.0 mg, 0.79 mmol) were dissolved in EtOH (20 ml). Mixture was put in the freezer over night and the product is filtered off. The product is obtained as white crystals (114.23 mg, 62%). M. p.: 161 - 162 °C. $^{1}$H NMR (400.1 MHz, $CDCl_3$) δ 8.45 - 8.40 (2H, m, Ar H), 7.86 (1H, s, CH), 7.79 - 7.74 (2H, m, Ar CH), 7.18 - 7.13 (4H, m, Ar CH). $^{19}$F NMR (376.6 MHz, $CDCl_3$) δ -106.87 (1F), -110.75 (1F). $^{13}$C (100.7 MHz, $CDCl_3$) δ 163.8 (d, *J* = 254.8 Hz, CF), 163.2 (d, *J* = 251.8 Hz, CF), 145.2 (d, *J* = 4.0 Hz, $C_{quart}$, Ar C), 133.4 (CH), 131.4 (d, *J* = 8.0 Hz, Ar CH), 127.1 (d, *J* = 3.1 Hz, $C_{quart}$, Ar C), 123.8 (d, *J* = 9.1 Hz, Ar CH), 116.2 (d, *J* = 22.2 Hz, Ar CH), 116.0 (d, *J* = 21.2 Hz, Ar CH). Spectroscopic data in accordance with that reported previously.[86]

**Octylboronic acid[109]**

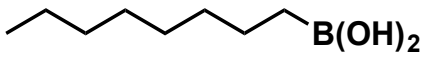

1-Bromooctane (10.2 g, 0.05 mol), Mg turnings (1.41 g, 0.06 mol) and iodine (0.68 g, 5.36 mmol) were mixed in anhydrous THF (100 ml) and heated to reflux under an argon atmosphere. After 16 hours, the reaction mixture was cooled down to room temperature and subsequently to -78 °C with dry ice and acetone. At this temperature, $B(OMe)_3$ (8.20 g, 0.08 mol) was added and the mixture was stirred for 10 minutes after which the reaction mixture was warmed up to room temperature over 1 hour. The reaction mixture was neutralised with 1M HCl (20 ml), transferred into a separating funnel and the organic layer was separated. The THF was removed *in vacuo* and the resulting solid dissolved in diethyl ether (50 ml). The diethyl ether was washed with brine (1x, 50 ml), dried with $MgSO_4$,

filtered and removed *in vacuo*. The resulting solid was recrystallised in hexane affording the product as a white solid (5.95 g, 75%). M. p.: 86 - 90 °C. $^{1}$H NMR (400.3 MHz, $CDCl_3$) δ 1.41 - 1.24 (12H, broad multiplet, $(CH_2)_6$), 0.88 (2H, t, $J$ = 6.9 Hz, $CH_2$), 0.81 (3H, t, $J$ = 7.8 Hz, $CH_3$). $^{13}$C NMR (100.7 MHz, $CDCl_3$) δ 31.4 ($CH_2$), 30.9 ($CH_2$), 28.4 ($CH_2$), 28.2 ($CH_2$)*, 23.3 ($CH_2$), 21.7 ($CH_2$), 13.1 ($CH_3$). Spectroscopic data is in accordance with that reported previously.[109]

* signals overlap

**Tetrakis(triphenylphospine)palladium(0) – $Pd(PPh_3)_4$[110]**

$PdCl_2$ (1.10 g, 6.20 mmol) and triphenylphosphine (8.08 g, 30.8 mmol) were dissolved in anhydrous DMSO under argon atmosphere. The mixture was heated to 170 $^{o}$C, which caused the solution to turn subsequently green, yellow, orange and red. Once the mixture reached 170 $^{o}$C, it was left stirring for 20 minutes at this temperature before the heating was turned off. Hydrazine monohydrate (0.79 g, 24.8 mmol) was added and the heating source was removed from the reaction mixture. The reaction mixture was left stirring to cool down to room temperature. The mixture was filtered which afforded a light green solid, which was dried under $N_2$ (6.85 g, 96%).

**3-(Bromomethyl)benzoic acid[105] - 87**

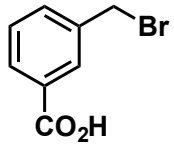


3-Tolylbenzoic acid (10.0 g, 0.07 mol) was dissolved in chlorobenzene (80 ml) and stirred when bromine (10.60 g, 0.066 mol) was added. The mixture was stirred for 2 hours under irradiation of a 60 W tungsten lamp. Afterwards, a white precipitant was filtered off and washed with hexane (100 ml) and dried. The desired product was obtained as a white solid (6.64 g, 44%). M. p.: 135 °C. $^{1}$H NMR (500.1 MHz, DMSO-$d_6$) δ 8.04 - 8.03 (1H, m, Ar CH), 7.90 - 7.87 (1H, m, Ar CH), 7.71 - 7.69 (1H, m, Ar CH), 7.51 (1H, d, $J$ = 6.0 Hz, Ar CH), 4.80

(2H, s, $CH_2$). $^{13}C$ NMR (100.7 MHz, DMSO-$d_6$) δ 166.9 ($CO_2H$), 133.7 (Ar CH), 131.2 ($C_{quart}$, Ar C), 130.9 ($C_{quart}$, Ar C), 130.1 (Ar CH), 129.4 (Ar CH), 129.1 (Ar CH), 33.7 ($CH_2$).

**3-Formylbenzoic acid[82] - 88**

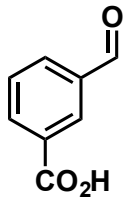


3-(Bromomethyl)benzoic acid (3.5 g, 0.016 mol) and HMTA (3.42 g, 0.024 mol) were dissolved in EtOH/$H_2O$ (1:1, 30 ml). The reaction mixture was heated to reflux temperature for 4 hours. Then concentrated HCl (1 ml) was added drop wise and the mixture was refluxed for another 30 minutes after which the mixture was cooled to room temperature in a water bath. The mixture was diluted with $H_2O$ (60 ml) and the product extracted with DCM (2 x 100 ml). The DCM was dried over $MgSO_4$ and this was filtered off and the DCM was removed *in vacuo* affording the product as a white solid (1.92 g, 80%). M. p.: 168 - 171 °C. $^1H$ NMR (400.1 MHz, DMSO-$d_6$) δ 10.09 (1H, s, aldehyde H), 8.44 (1H, td, *J* = 1.6, 0.4 Hz, Ar CH), 8.24 (1H, dt, *J* = 7.9, 1.6 Hz, Ar CH), 8.15 (1H, dt, *J* = 7.9, 1.6 Hz, Ar CH), 7.74 (1H, t, *J* = 7.6 Hz, Ar CH). $^{13}C$ NMR (100.7 MHz, DMSO-$d_6$) δ 192.9 (CO), 166.5 ($CO_2H$), 136.4 ($C_{quart}$, Ar C), 134.8 (Ar CH), 133.1 (Ar CH), 131.8 ($C_{quart}$, Ar C), 130.4 (Ar CH), 129.7 (Ar CH). Spectroscopic data is in accordance with that recorded with the commercially available compound.

**3-Bromo-5-formylbenzoic acid[111] - 89**

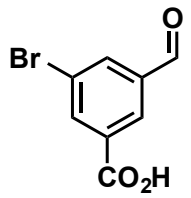


3-Formylbenzoic acid (1.00 g, 6.66 mmol) and NBS (1.30 g, 7.30 mmol) were dissolved in concentrated $H_2SO_4$ (15 ml) and the mixture was stirred over night at room temperature. Afterwards the mixture was poured on ice, which was cooled on an ice water bath. The white solid was filtered and recrystallised in water affording a white solid (0.88 g, 58%). M. p.: 165 - 166 °C. $^1$H NMR (500.1 MHz, DMSO-$d_6$) δ 10.04 (1H, s, aldehyde H), 8.40 (1H, t, $J$ = 1.5 Hz, Ar CH), 8.30 (2H, m, Ar CH). $^{13}$C NMR (100.7 MHz, DMSO-$d_6$) δ 191.6 (CO), 165.2 ($CO_2H$), 138.2 ($C_{quart}$, Ar C), 136.8 (Ar CH), 135.7 (Ar CH), 133.9 ($C_{quart}$, Ar C), 128.8 (Ar CH), 122.6 ($C_{quart}$, Ar C). Spectroscopic data is in accordance with that reported previously.[111]

***tert*-Butyl 3-bromo-5-formylbenzoate[112] - 90**

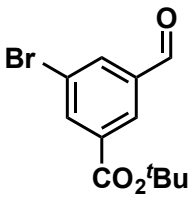


3-Bromo-5-formylbenzoic acid (2.42 g, 0.01 mol) was dissolved in *N,N*-dimethylacetamide (60 ml) and heated to reflux under Ar atomosphere. Then *N,N*-di-*tert*-butoxyformamide (8.59 g, 0.042 mol) was added to the refluxing solution. The mixture is allowed to stir for 3.5 hours before it is cooled down to room temperature. The reaction mixture is washed with $H_2O$ (50 ml), saturated $NaHCO_3$ solution (50 ml) and brine (50 ml), dried over $MgSO_4$, filtered and the solvent was removed *in vacuo*. The product was recovered as a brown oil (2.07 g, 77 %). $^1$H NMR (300.1 MHz, $CDCl_3$) δ 10.01 (1H, s, aldehyde), 8.38 (1H, t, $J$

= 1.5 Hz, Ar CH), 8.35 - 8.33 (1H, m, Ar CH), 8.17 - 8.15 (1H, m, Ar CH), 1.61 (s, 9H, *tert*-butyl). $^{13}$C NMR (100.6 MHz, $CDCl_3$) δ 190.1 (CO), 167.0 (CO), 138.4 (Ar CH), 138.0 ($C_{quart}$, Ar C), 135.6 (Ar CH), 130.5 (Ar CH), 129.8 ($C_{quart}$, Ar C), 123.6 ($C_{quart}$, Ar C), 82.8 ($C_{quart}$, C), 28.2 (*tert*-butyl $CH_3$). Spectroscopic data is in accordance with that reported previously.[108]

**_tert_-Butyl 3-formyl-5-octylbenzoate[108] - 91**

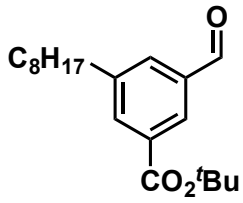


*tert*-Butyl 3-bromo-5-formylbenoate (1.10 g, 3.86 mmol), octylboronic acid (0.67 g, 4.24 mmol), $K_2CO_3$ (1.60 g, 11.58 mmol) were dissolved in Toluene/$H_2O$ (3:1, 24 ml) and the mixture was degassed with Ar for 20 minutes. Tetrakis(triphenylphospine)palladium(0) (220 mg, 0.19 mmol) was added and the mixture was heated to 95 °C, and stirred for 96 hours under Ar atmosphere. The solvent mixture was removed *in vacuo* and the remaining solid was redissolved in DCM (30 ml) and washed with $H_2O$ (30 ml) and brine (30 ml), dried over $MgSO_4$, filtered and concentrated *in vacuo*. The product was purified using silica flash column chromatography (eluting with DCM) to obtain the product as a brown oil (810 mg, 66%). $^1$H NMR (400.3 MHz, $CDCl_3$) δ 10.04 (1H, s, aldehyde H), 8.27 (1H, t, *J* = 1.5 Hz, Ar CH), 8.07 (1H, t, *J* = 1.5 Hz, Ar CH), 7.86 (1H, t, *J* = 1.5 Hz, Ar CH), 2.74 - 2.70 (2H, t, *J* = 7.8 Hz, $CH_2$), 1.69 - 1.60 (2H, m, $CH_2$), 1.35 - 1.24 (10H, m, $(CH_2)_5$), 0.88 (3H, t, *J* = 7.0 Hz, $CH_3$). $^{13}$C NMR (125.8 MHz, $CDCl_3$) δ 192.1 (CO), 165.0 ($CO_2{}^tBu$), 144.4 ($C_{quart}$, Ar C), 136.6 ($C_{quart}$, Ar C), 135.4 (Ar CH), 133.1 (Ar CH), 132.5 (Ar CH), 129.1 ($C_{quart}$, Ar C), 81.9 ($C_{quart}$, $^t$Bu C), 35.6 ($CH_2$), 32.0 ($CH_2$), 31.3 ($CH_2$), 29.5 ($CH_2$), 29.3 ($CH_2$)*, 28.3 ($CH_3$, $^t$Bu $CH_3$), 22.8 ($CH_2$), 14.2 ($CH_3$).

* Signals overlap

**3-Formyl-5-octylbenzoic acid[86] - 92**

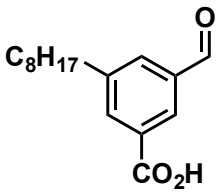


*tert*-Butyl 3-formyl-5-octylbenzoate (800 mg, 2.5 mmol) was dissolved in DCM (10 ml) and trifluoroacetic acid (4.6 g, 40 mmol) was added. The mixture was stirred for 3 hours at room temperature. Afterwards, the reaction mixture was washed three times with brine (10 ml), dried over $MgSO_4$ and the solvent was removed *in vacuo*. The product was obtained as a white solid (621 mg, 95%). M. p.: 84 - 90 °C. $^1$H NMR (400.1 MHz, $CDCl_3$) δ 10.08 (1H, s, aldehyde H), 8.43 (1H, t, *J* = 1.6 Hz, Ar CH), 8.20 (1H, t, *J* = 1.6 Hz, Ar CH), 7.96 (1H, t, *J* = 1.6 Hz, Ar CH), 2.76 (2H, t, *J* = 8.0 Hz, $CH_2$), 1.72 - 1.62 (2H, broad, $CH_2$), 1.39 - 1.20 (10H, broad, $(CH_2)_5$), 0.87 (3H, t, *J* = 7.0 Hz, $CH_3$). $^{13}$C NMR (100.7 MHz, $CDCL_3$) δ 191.7 (CO), 171.4 ($CO_2H$), 145.0 ($C_{quart}$, Ar C), 136.9 ($C_{quart}$, Ar C), 136.0 (Ar CH), 133.7 (Ar CH), 130.4 (Ar CH), 130.0 ($C_{quart}$, Ar C), 35.6 ($CH_2$), 32.0 ($CH_2$), 31.3 ($CH_2$), 29.5 ($CH_2$), 29.3 ($CH_2$)*, 22.8 ($CH_2$), 14.2 ($CH_3$). ES MS (*m/z*) 261 (100% $[M-H]^-$). HRMS (*m/z*) $[M-H]^-$ calcd. for $C_{16}H_{22}O_3$, 262.1569; found, 261.1496.

* Signals overlap

**(*Z*)-1-(3-Carboxy-5-octylphenyl)-*N*-(4-fluorophenyl)methanimine oxide[53] - 102**

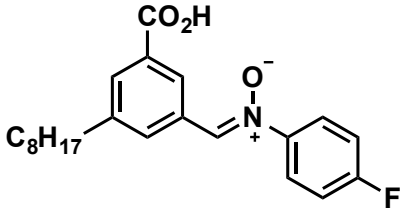


3-Formyl-5-octylbenzoic acid (52.2 mg, 0.20 mmol) and *N*-(4-fluorophenyl)hydroxylamine ( 25.3 mg, 0.20 mmol) were dissolved in $CHCl_3$ and

kept at -10 °C for 24 hours. The solution was concentrated and the product was obtained as a white solid (46.5 mg, 63%). M. p.: 98 - 103 °C . $^{1}$H NMR (400.3 MHz, $CDCl_3$) δ 8.85 (1H, m, Ar CH), 8.55 (1H, m, Ar CH), 8.01 (1H, m, Ar CH), 7.97 (1H, s, CH), 7.83 - 7.80 (2H, m, Ar CH), 7.20 - 7.16 (2H, m, Ar CH), 2.74 (2H, t, *J* = 7.8 Hz, $CH_2$), 1.71 - 1.64 (2H, m, $CH_2$), 1.36 - 1.25 (10H, broad, $(CH_2)_5$), 0.87 (3H, t, *J* = 7.0 Hz, $CH_3$). $^{19}$F NMR (376.6 MHz, $CDCl_3$) δ -110.39. $^{13}$C NMR (100.7 MHz, $CDCl_3$) δ 170.9 ($CO_2H$), 163.8 (d, *J* = 251.8 Hz, $C_{quart,}$ Ar CF), 145.1 (d, *J* = 3.1 Hz, $C_{quart}$, Ar C), 144.5 ($C_{quart}$, Ar C), 134.6 (CH), 133.4 ($C_{quart}$, Ar C), 132.7 ($C_{quart}$, Ar C), 130.8 (Ar CH), 130.1 (Ar CH), 129.2 (Ar CH), 123.9 (d, *J* = 9.1 Hz, Ar CH), 116.3 (d, *J* = 23.2, Ar CH), 36.0 ($CH_2$), 32.0 ($(CH_2)_5$), 31.5 ($(CH_2)_5$), 29.6 ($(CH_2)_5$), 29.4 ($(CH_2)_5$)*, 22.4 ($(CH_2)_5$), 14.2 ($CH_3$). ES MS (*m/z*) 372 (100% $[M+H]^+$). HRMS (*m/z*) $[M+H]^+$ calcd. for $C_{22}H_{27}O_3NF$, 372.1969; found, 372.1963.

* Signals overlap

**3-((1,3-Dioxo-1,3-dihydro-2*H*-inden-2-ylidene)methyl)-5-octylbenzoic acid - 93**

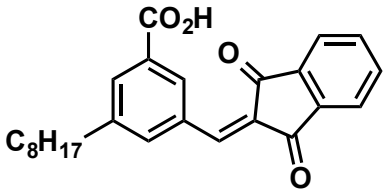


3-Formyl-5-octylbenzoic acid (110 mg, 0.42 mmol) and 1,3-indandione (61.3 mg, 0.42 mmol) were dissolved in EtOH and pyridine (83.06 mg, 1.05 mmol) was added. The mixture was left to stir for 16 hours when a yellow precipitate was observed. The precipitate was filtered off and washed with cold EtOH. The product was obtained as a yellow solid (65 mg, 40%). M. p.: 203 - 205 °C. $^{1}$H NMR (400.3 MHz, DMSO-$d_6$) δ 8.95 - 8.94 (1H, m, Ar CH), 8.48 - 8.47 (1H, m, Ar CH), 8.03 - 7.95 (5H, m, Ar CH), 7.88 (1H, s, CH), 2.72 (2H, t, *J* = 7.8 Hz, $CH_2$), 1.68 - 1.61 (2H, m, $CH_2$), 1.31 - 1.22 (10H, broad, $(CH_2)_5$), 0.84 (3H, t, *J* = 7.1 Hz, $CH_3$). $^{13}$C NMR (100.7 MHz, DMSO-$d_6$) δ 189.2 (CO), 188.4 (CO), 166.9 ($CO_2H$), 144.5 ($C_{quart}$, Ar C) 143.3 (CH), 142.0 ($C_{quart}$, Ar C), 139.5 ($C_{quart}$, Ar C),

137.7 ($C_{quart}$, Ar C), 136.1 (Ar CH), 135.9 (Ar CH), 133.2 (Ar CH), 133.0 (Ar CH), 131.8 ($C_{quart}$, Ar C), 131.3 ($C_{quart}$, Ar C), 130.0 ($C_{quart}$, Ar C), 123.2 (Ar CH), 123.1 ($C_{quart}$), 34.6 ($CH_2$), 31.3 (($CH_2$)$_5$), 30.6 (($CH_2$)$_5$), 28.8 (($CH_2$)$_5$), 28.6 (($CH_2$)$_5$), 28.5 (($CH_2$)$_5$), 22.1 (($CH_2$)$_5$), 13.9 ($CH_3$). ES MS (*m/z*) 413 (100% $[M+Na]^+$). HRMS (*m/z*) $[M+Na]^+$ calcd. for $C_{25}H_{26}O_4Na$, 413.1729; found, 413.1722.

**5-Bromo-6-methylpyridin-2-amine[86] - 97**

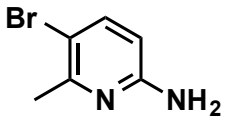


6-Methylpyridin-2-amine (6.1 g, 0.056 mol) and NBS (10 g, 0.056 mol) were dissolved in acetonitrile (75 ml) and stirred for 16 hours at room temperature. The solution was concentrated *in vacuo* and the remaining solution was left on ice, which cause the product to crystalize out of the solution. The product was collected as a light brown solid in sufficient quality for further conversion. M. p.: 70 - 74 °C. $^1$H NMR (500.1 MHz, $CDCl_3$) δ 7.46 (1H, d, *J* = 8.6 MHz, Ar CH), 6.22 (1H, d, *J* = 8.6 MHz, Ar CH), 4.65 (2H, broad, $NH_2$), 2.49 (3H, s, $CH_3$). $^{13}$C NMR (100.6 MHz, $CDCl_3$) δ 157.0 ($C_{quart}$, Ar C), 155.2 ($C_{quart}$, Ar C), 141.5 (Ar CH), 108.7 ($C_{quart}$, Ar C), 107.8 (Ar CH), 29.7 ($CH_3$).

**4-Formyl-*N*-(5-bromo-6-methylpyridin-2-yl)benzamide[108] - 98**

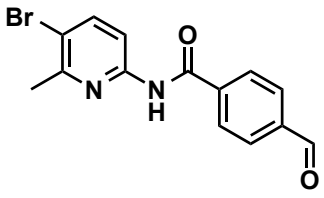


5-Bromo-6-methylpyridin-2-amine (2.30 g, 9.83 mmol) and triethylamine (1.14 g, 11.3 mmol) were dissolved in anhydrous DCM (30 ml) under Ar and cooled to 0 $^o$C. 4-formylbenzoyl chloride (1.20 g, 7.56 mmol) was dissolved in anhydrous DCM (20 ml) under Ar. The solution with 4-formylbenzoyl chloride was added

dropwise to the solution with the amine, on ice under argon atmosphere. The mixture was allowed to stir for 96 hours. Then, the reaction mixture was washed three times with 1 M HCl (50 ml) and the aqueous phases were combined and washed three times with DCM (50 ml). The combined organic phases were washed with brine (50 ml), dried over $MgSO_4$, filtered and the solvent was removed *in vacuo*. The product was purified with silica flash column chromatography (eluting with DCM/EtOAc (5:1)) to afford the pure product as a white solid (1.79 g, 50%). M. p.: 153 - 155 °C. $^1$H NMR (400.1 MHz, $CDCl_3$) δ 10.11 (1H, s, aldehyde H), 8.58 (1H, broad, NH), 8.12 - 8.06 (3H, m, Ar CH), 8.02 - 8.00 (2H, m, Ar CH), 7.85 (1H, d, *J* = 9.0 Hz, Ar CH), 2.57 (3H, s, $CH_3$). $^{13}$C NMR (100.7 MHz, $CDCl_3$) δ 191.4 (CO), 164.5 (amide CO), 156.0 ($C_{quart}$, Ar C), 149.4 ($C_{quart}$, Ar C), 142.2 (Ar CH), 139.2 ($C_{quart}$, Ar C), 138.9 ($C_{quart}$, Ar C), 130.2 (Ar CH), 128.0 (Ar CH), 116.0 ($C_{quart}$, Ar C), 113.0 (Ar CH), 24.6 ($CH_3$). ES MS (*m/z*) 317 (100% $[M-H]^-$). HRMS (*m/z*) $[M-H]^-$ calcd. for $C_{14}H_{10}O_2N_2Br$, 316.9931; found, 316.9930.

**4-Formyl-*N*-(6-methyl-5-octylpyridin-2-yl)benzamide[109] - 99**

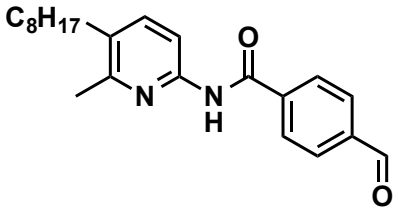


4-Formyl-*N*-(5-iodo-6-methylpyridin-2-yl)benzamide (250 mg, 0.68 mmol, octylboronic acid (162 mg, 1.02 mmol), $K_2CO_3$ (282 mg, 2.04 mmol) were dissolved in Toluene/$H_2O$) (3:1, 16 ml) and the mixture was degassed for 20 minutes with Argon. Tetrakis(triphenylphospine)palladium(0) (60 mg, 0.05 mmol) was added and the mixture was heated to 95 $^o$C, and stirred for 96 hours under Ar atmosphere. The solvent mixture was removed *in vacuo* and the remaining solid was redissolved in DCM (30 ml) and washed with $H_2O$ (30 ml) and brine (30 ml), dried over $MgSO_4$, filtered and concentrated *in vacuo*. The product was purified using silica flash column chromatography (eluting with

DCM/EtOAc (10:1)) to obtain the product as a white solid (220 mg, 88%). M. p.: 74 - 80 °C. $^{1}$H NMR (400.1 MHz, $CDCl_3$) δ 10.10 (1H, s, aldehyde H), 8.53 - 8.51 (1H, broad, NH), 8.10 - 8.06 (3H, m, Ar CH), 8.01 - 7.98 (2H, m, Ar CH), 7.49 (1H, d, *J* = 8.0 Hz, Ar CH), 2.58 (2H, t, *J* = 8.0 Hz, $CH_2$), 2.44 (3H, s, $CH_3$), 1.60 - 1.52 (2H, m, $CH_2$), 1.39 - 1.22 (10H, broad, $(CH_2)_5$), 0.87 (3H, t, *J* = 7.2 Hz, $CH_3$). $^{13}$C NMR (100.7 MHz, $CDCl_3$) δ 191.5 (CO), 164.5 (amide CO), 154.9 ($C_{quart}$, Ar C), 148.3 ($C_{quart}$, Ar C), 139.7 ($C_{quart}$, Ar C), 139.1 (Ar CH), 138.6 ($C_{quart}$, Ar C), 132.9 ($C_{quart}$, Ar C), 130.1 (Ar CH), 128.0 (Ar CH), 111.7 (Ar CH), 32.2 ($CH_2$), 32.0 ($(CH_2)_5$), 30.1 ($CH_2$), 29.6* ($(CH_2)_5$), 29.4 ($(CH_2)_5$), 22.8 ($(CH_2)_5$), 21.8 ($CH_3$), 14.2 ($CH_3$).

* signals overlap

**4-((1,3-Dioxo-1,3-dihydro-2*H*-inden-2-ylidene)methyl)-*N*-(6-methyl-5-octylpyridin-2-yl)benzamide - 100**

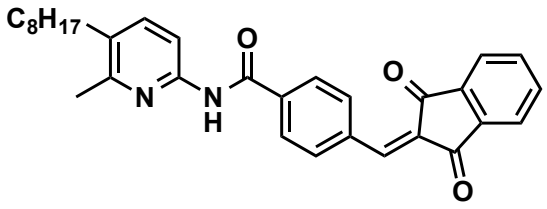


4-Formyl-*N*-(6-methyl-5-octylpyridin-2-yl)benzamide (120 mg, 0.25 mmol) and 1,3-indandione (36 mg, 0.25 mmol) were dissolved in ethanol (20 ml) and pyridine (31.6 mg, 0.4 mmol) was added. The mixture was stirred and after 16 hours a precipitate was observed and filtered. The solid was washed with cold ethanol and the product was collected as a yellow solid (120 mg, 53%). M. p.: 225 - 226 °C. $^{1}$H NMR (500.1 MHz, $CDCl_3$) δ 8.56 - 8.54 (2H, d, *J* = 8.5 Hz, Ar CH), 8.51 - 8.49 (1H, broad, NH), 8.13 (1H, d, *J* = 8.0 Hz, Ar CH), 8.07 - 8.03 (4H, m, Ar CH), 7.93 (1H, s, CH), 7.87 - 7.85 (2H, m, Ar CH), 7.50 (1H, d, *J* = 8.5 Hz, Ar CH), 2.59 (2H, t, *J* = 7.50 Hz, $CH_2$), 2.46 (3H, s, $CH_3$), 1.59 - 1.54 (2H, m, $CH_2$), 1.40 - 1.24 (10H, broad, $(CH_2)_5$), 0.89 (3H, t, *J* = 7.0 Hz, $CH_3$). $^{13}$C NMR (100.7 MHz, $CDCl_3$) δ 189.9 (CO), 188.9 (CO), 164.6 (amide CO), 155.0 ($C_{quart}$), 148.4 ($C_{quart}$, Ar C), 144.9 (CH), 139.1 (Ar CH), 137.9 ($C_{quart}$, Ar C), 136.2 ($C_{quart}$, Ar C), 135.9 ($C_{quart}$, Ar C), 135.7 (Ar CH), 134.3 (Ar CH), 132.8

($C_{quart}$, Ar C), 130.9 ($C_{quart}$, Ar C), 127.6 ($C_{quart}$, Ar C), 123.7 (Ar CH), 127.6 (Ar CH), 111.6 (Ar CH), 32.3 ($CH_2$), 32.0 (($CH_2$)$_5$), 30.2 ($CH_2$), 29.6* (($CH_2$)$_5$), 29.4 (($CH_2$)$_5$), 22.8 (($CH_2$)$_5$), 21.8 ($CH_3$), 14.3 ($CH_3$). ES MS (*m/z*) 481 (100% $[M+H]^+$). HRMS (*m/z*) $[M+H]^+$ calcd. for $C_{31}H_{33}O_3N_2$, 481.2491; found, 481.2474.
* signals overlap

**1-Nitro-4-octylbenzene[109] - 106**

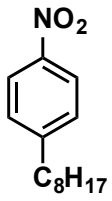


1-Bromo-4-nitrobenze (182 mg, 0.90 mmol), octylboronic acid (214 mg, 1.35 mmol) and $K_2CO_3$ (373 mg, 2.70 mmol) are dissolved in toluene/$H_2O$ (9:3 ml) and the mixture is degassed with argon for 15 minutes. Then, $Pd(PPh_3)_4$ (73 mg, 0.063 mmol) was added and the reaction mixture was heated up to 95 °C and stirred for 48 hours at this temperature under an argon atmosphere. Subsequently, the mixture was cooled down and the solvents were removed under vacuum. The remaining oil was dissolved in DCM (20 ml) and washed with $H_2O$ (20 ml) and brine (20 ml). The DCM solution was then dried over $MgSO_4$, filtered and the solvent was removed *in vacuo*, affording a brown oil. The crude product was purified using silica gel flash chromatography (eluting with DCM/hexane (1:2)), which afforded the pure product as a green oil (72 mg, 34%). $^1$H NMR (400.3 MHz, $CDCl_3$) δ 8.14 - 8.12 (2H, m, Ar CH), 7.33 - 7.30 (2H, m, Ar CH), 7.60 (2H, t, *J* = 7.6 Hz, $CH_2$), 1.67 - 1.60 (2H, m, $CH_2$), 1.34 - 1.22 (10H, m, ($CH_2$)$_5$), 0.88 (3H, t, *J* = 7.0 Hz, $CH_3$). $^{13}$C NMR (100.7 MHz, $CDCl_3$) δ 151.0 ($C_{quart}$, Ar C), 146.3 ($C_{quart}$, Ar C), 129.2 (Ar C), 123.7 (Ar C), 36.0 ($CH_2$), 32.0 ($CH_2$), 31.1 (($CH_2$)$_5$), 29.5 (($CH_2$)$_5$), 29.3* (($CH_2$)$_5$), 22.8 (($CH_2$)$_5$), 14.2 ($CH_3$).
* signals overlap

**_N_-(4-Octylphenyl)hydroxylamine[108] - 107**

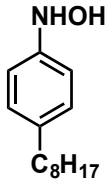


1-Nitro-4-octylbenzene (98 mg, 0.42 mmol) was dissolved in anhydrous THF (10 ml) and Rh/C 10% (45 mg) was added. Hydrazine monohydrate (0.12 ml, 3.78 mmol) was added dropwise and the reaction was left to stir at room temperature under argon atmosphere. The reaction was followed by TLC (DCM/EtOAc (3:2)) and was quenched after 20 minutes by addition of $MgSO_4$. The reaction mixture was filtered through celite in order to remove the catalyst and the solvent was removed *in vacuo*, which afforded the product as a white solid (56 mg, 64%). M. p.: 73 - 77 °C. $^1$H NMR (400.3 MHz, $CDCl_3$) δ 7.10 (2H, d, *J* = 8.6 Hz, Ar CH), 6.93 (2H, d, *J* = 8.6 Hz, Ar CH), 6.71 (1H, broad, OH), 5.14 (1H, broad, NH), 2.55 (2H, t, *J* = 7.6 Hz, $CH_2$), 1.59 - 1.54 (2H, m, $CH_2$), 1.34 - 1.23 (10H, broad, $(CH_2)_5$), 0.88 (3H, t, *J* = 6.8 Hz, $CH_3$). $^{13}$C NMR (100.7 MHz, $CDCl_3$) δ 161.6 ($C_{quart}$, Ar C), 152.2 ($C_{quart}$, Ar C), 129.0 (Ar CH), 115.0 (Ar CH), 35.4 ($CH_2$), 32.0 ($CH_2$), 31.8 ($(CH_2)_5$), 29.6* ($(CH_2)_5$), 29.4 ($(CH_2)_5$), 22.8 ($(CH_2)_5$), 14.3 ($CH_3$). ES MS (*m/z*) 206 (100% $[M\text{-}OH+2H]^+$), 222 (5% $[M+H]^+$). HRMS (*m/z*) $[M+H]^+$ calcd. for $C_{14}H_{24}ON$, 222.1852; found, 222.1847.

* signals overlap

**(*Z*)-1-(4-(Carboxymethyl)phenyl)-*N*-(4-octylphenyl)methanimine oxide[96] - 101**

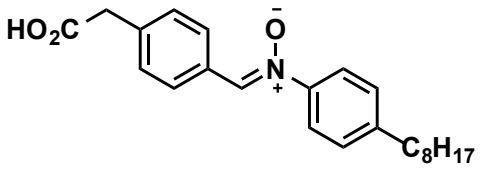


2-(4-Formylphenyl)acetic acid (8.2 mg, 0.05 mmol) and *N*-(4-octylphenyl)hydroxylamine (12 mg, 0.05 mg) were mixed in $CDCl_3$ (2 ml) and stored at -20 °C for 48 hours. The solvent was partially evaporated and the solid was filtered off and the remaining solvent was evaporated affording the product

as a white solid (13.4 mg, 73%). M. p.: 137 - 141 °C. $^{1}$H NMR (400.3 MHz, $CDCl_3$) δ 8.26 (2H, d, *J* = 8.3 Hz, Ar CH), 7.92 (1H, s, CH), 7.67 (2H, d, *J* = 8.5 Hz, Ar CH), 7.34 (2H, d, *J* = 8.3 Hz, Ar CH), 7.26* (Ar CH), 3.64 (2H, s, $CH_2$), 2.66 (2H, t, *J* = 8.0 Hz, $CH_2$), 1.66 - 1.59 (2H, m, $CH_2$), 1.34 - 1.24 (10H, m, $(CH_2)_5$), 0.90 - 0.87 (3H, m, $CH_3$). $^{13}$C NMR (100.7 MHz, $CDCl_3$) δ 174.1 ($CO_2H$), 154.9 ($C_{quart}$, Ar C), 146.6 ($C_{quart}$, Ar C), 145.6 ($C_{quart}$, Ar C), 137.5 ($C_{quart}$, Ar C), 136.0 (CH), 129.8 (Ar CH), 129.7 (Ar CH), 129.2 (Ar CH), 121.8 (Ar CH), 41.5 ($CH_2$), 35.7 ($CH_2$), 32.0 ($CH_2$), 31.4 ($(CH_2)_5$), 29.6 ($(CH_2)_5$), 29.4 ($(CH_2)_5$), 29.4 ($(CH_2)_5$), 22.8 ($(CH_2)_5$), 14.3 ($CH_3$). ES MS (*m/z*) 368 (100% $[M+H]^+$). HRMS (*m/z*) $[M+H]^+$ calcd. for $C_{23}H_{30}O_3N$, 368.2220; found, 368.2210.

* overlaps with $CHCl_3$ residual solvent signal

# 8

# References


1 J. Ladyman, J. Lambert, K. Wiesner, *Euro. Jnl. Phil. Sci.*, 2013, **3**, 33-67.

2 S. H. Strogatz, *Nature*, 2001, **410**, 268-276.

3 D. Rind, *Science*, 1999, **284**, 105-107.

4 Themed Issue on complexity, *Science*, 1999, **284**, 1-212.

5 W. B. Arthur, *Science*, 1999, **284**, 107-109.

6 R. Foote, *Science*, 2007, **318**, 410-412.

7 M. E. J. Newman, *SIAM Rev.*, 2003, **45**, 167-256.

8 S. Hoops, S. Sahle, R. Gauges, C. Lee, J. Pahle, N. Simus, M. Singhal, L. Xu, P. Mendes, U. Kummer, *Bioinformatics*, 2006, **22**, 3067-3074.

9 G. Ashkenasy, R. Jagasia, M. Yadav, M. R. Ghadiri, *Proc. Natl. Acad. Sci. U.S.A.*, 2004, **101**, 10872-10877.

10 (a) A. J. Lotka, *Proc. Natl. Acad. Sci. U.S.A.*, 1920, **6**, 410-415. (b) A. J. Lotka, *J. Am. Chem. Soc.*, 1920, **42**, 1595-1599. (c) V. Volterra, *Nature*, 1926, **118**, 558-560.

11 I. R. Epstein, J. A. Pojman, *An Introduction to Nonlinear Chemical Dynamics*, Oxford University Press, New York, Oxford, 1998.

12 T. Fujii, Y. Rondelez, *ACS Nano*, 2013, **7**, 27-34.

13 J. K. Parrish, L. Edelstein-Keshet, *Science*, 1999, **284**, 99-101.

14 C. Darwin, *On the Origin of Species*, John Murray, London, 1859.

15 A. K. Lal, *Astrophys. Space Sci.*, 2008, **317**, 267-278.

16 L. Boiteau, R. Pascal, *Orig. Life Evol. Biosph.*, 2011, **41**, 23-33.

17 A. Pross, *J. Syst. Chem.*, 2011, **2**, 1-14.

18 A. Pross, *Origins Life Evol. B.*, 2004, **34**, 307-321.

19 G. F. Joyce, *Nature*, 2002, **418**, 214-221.

20 D. M. J. Lilley, F. Eckstein, *Ribozymes and RNA Catalysis*, RSC Publishing, Cambridge, 2008.

21 M. W. Powner, B. Gerland, J. D. Sutherland, *Nature*, 2009, **459**, 239-242.

22 (a) P. Thaddeus, *Phil. Trans. R. Soc. B*, 2006, **361**, 1681-1687. (b) R. A. Sanchez, J. P. Ferris, L. E. Orgel, *Science*, 1966, **154**, 784-785. (c) M. A. Pasek, D. S. Lauretta, *Astrobiology*, 2005, **5**, 515-535. (d) D. E. Bryant, T. P. Kee, *Chem. Commun.*, 2006, 2344-2346.

23 D. J. Ritson, J. D. Sutherland, *Angew. Chem. Int. Ed.*, 2013, **52**, 5845-5847.

24 L. E. Orgel, *Nature*, 1992, **358**, 203-209.

25 J. Huck, D. Philp, *Supramolecular Chemistry: From Molecules to Nanomaterials*, J. W. Steed, P. A. Gale, John Wiley & Sons, Ltd. New York, 2012.

26 A. Vidonne, D. Philp, *Eur. J. Org. Chem.*, 2009, 593-610.

27 E. Wintner, J. Rebek, Jr., *Act Chem. Scand.*, 1996, **50**, 469-485.

28 N. Paul, G. F. Joyce, *Curr. Opin. Chem. Biol.*, 2004, **8**, 634-639.

29 A. Robertson, A. J. Sinclair, D. Philp, *Chem. Soc. Rev.*, 2000, **29**, 141-152.

30 D. N. Reinhoudt, D. M. Rudkevich, F. de Jong, *J. Am. Chem. Soc.*, 1996, **118**, 6880-6889.

31 R. Plasson, A. Brandenburg, L. Jullien, H. Bersini, *J. Phys. Chem.*, 2011, **115**, 8073-8085.

32 E. Kassianidis, R. J. Pearson, E. A. Wood, D. Philp, *Faraday Discuss.*, 2010, **145**, 235-254.

33 R. Bennes, D. Philp, N. Spencer, B. M. Kariuki, K. D. M. Harris, *Org. Lett.*, 1999, **7**, 1087-1090.

34 M. I . Page, W. P. Jencks, *Proc. Natl. Acad. Sci. U.S.A.*, 1971, **68**, 1678-1683.

35 G. von Kiedrowski, *Bioorganic Chem. Front.*, 1993, **3**, 113-146.

36 G. von Kiedrowski, *Angew. Chem. Int. Ed.*, 1986, **25**, 932-935.

37 T. Tjivikua, P Ballester, J. Rebek, Jr., *J. Am. Chem. Soc.*, 1990, **112**, 1249-1250.

38 J. Rebek, Jr., *Angew. Chem. Int. Ed. Engl.*, 1990, **29**, 245-255.

39 F. M. Menger, A. V. Eliseev, N. A. Khanjin, *J. Am. Chem. Soc.*, 1994, **116**, 3613-3614.

40 (a) C. G. Swain, J. F. Brown, Jr., *J. Am. Chem. Soc.*,1952, **74**, 2538-2543. (b) P. R. Rony, *J. Am. Chem. Soc.*, 1969, **91**, 6090-6096. (c) G. D. Titskii, L. M. Litvinenko, *Zh. Obsch. Khim*, 1970, **40**, 2680. (d) C.-W. Su, J. W. Watson, *J. Am. Chem. Soc.*, 1974, **96**, 1854-1857.

41 M. M. Conn, E. A. Wintner, J. Rebek, Jr., *J. Am. Chem. Soc.*, 1994, **116**, 8823-8824.

42 F. M. Menger, A. V. Eliseev, N. A. Khanjin, M. J. Sherrod, *J. Org. Chem.*, 1995, **60**, 2870-2878.

43 E. A. Wintner, B. Tsao, J. Rebek, Jr., *J. Org. Chem.*, 1995, **60**, 7997-8001.

44 V. Rotello, J.-I. Hong, J. Rebek Jr., *J. Am. Chem. Soc.*, 1991, **113**, 9422-9423.

45 A. Terfort, G. von Kiedrowski, *Angew. Chem. Int. Ed.*, 1992, **31**, 654-656.

46 B. Wang, I. O. Sutherland, *Chem. Commun.*, 1997, 1495-1496.

47 M. Kindermann, I. Stahl, M. Reimold, W. M. Pankau, G. von Kiedrowski, *Angew. Chem. Int. Ed.*, 2005, **44**, 6750-6755.

48 P. J. Boul, P. Reutenauer, J.-M. Lehn, *Org. Lett.*, 2005, **7**, 15-18.

49 (a) R. J. Pearson, E. Kassianidis, D. Philp, *Tetrahedron Lett.*, 2004, **45**, 4777-4780. (b) R. J. Pearson, E. Kassianidis, A. M. Z. Slawin, D. Philp, *Org. Biomol. Chem.*, 2004, **2**, 3434-3441. (c) R. J. Pearson, E.

Kassianidis, A. M. Z. Slawin, D. Philp, *Chem. Eur. J.*, 2006, **12**, 6829-6840.

50 (a) E. Kassianidis, R. J. Pearson, D. Philp, *Org. Lett.*, 2005, **7**, 3833-3836. (b) E. Kassianidis, R. J. Pearson, D. Philp, *Chem. Eur. J.*, 2006, **12**, 8798-8812.

51 J. M. Quayle, A. M. Z. Slawin, D. Philp, *Tetrahedron Lett.*, 2002, **43**, 7229-7233.

52 V. C. Allen, D. Philp, N. Spencer, *Org. Lett.*, 2001, **3**, 777-780.

53 E. Kassianidis, D. Philp, *Angew. Chem. Int. Ed.*, 2006, **45**, 6344-6348.

54 J. M. Berg, J. L. Tymoczko, L. Stryer, *Biochemistry*, W. H. Freeman, New York, 6th edition, 2006.

55 (a) T. R. Kelly, C. Zhao, G. J. Bridger, *J. Am. Chem. Soc.*, 1989, **111**, 3744-3745. (b) T. R. Kelly, G. J. Bridger, C. Zhao, *J. Am. Chem. Soc.*, 1990, **112**, 8024-8034.

56 (a) R. J. Pieters, I. Huc, J. Rebek Jr., *Angew. Chem. Int. Ed. Engl.*, 1994, **33**, 1579-1581. (b) R. J. Pieters, I. Huc, J. Rebek Jr., *Tetrahedron*, 1995, **51**, 485-498.

57 E. Kassianidis, D. Philp, *Chem. Commun.*, 2006, 4072-4074.

58 H. Kitano, *Science*, 2002, **295**, 1662-1664.

59 M. G. Katze, *Systems Biology*, Springer, Berlin, Heidelberg, 2013.

60 (a) N. Wagner, G. Ashkenasy, *Chem. Eur. J.*, 2009, **15**, 1765-1775. (b) J. Stankiewicz, L. H. Eckardt, *Angew. Chem. Int. Ed.*, 2006, **45**, 342-344. (c) R. F. Ludlow, S. Otto, *Chem. Soc. Rev.*, 2008, **37**, 101-108. (d) G. von Kiedrowski, S. Otto, P. Herdewijn, *J. Syst. Chem.*, 2010, **1**, 1-6. (e) R. A. R. Hunt, S. Otto, *Chem. Commun.*, 2011, **47**, 847-858.

61 (a) J. M. Lehn, *Chem. Eur. J.*, 1999, **5**, 2455-2463. (b) J.-M. Lehn, A. V. Eliseev, *Science*, 2001, **291**, 2331-2332. (c) S. J. Rowan, S. J. Cantrill, G. R. L. Cousins, J. K. M. Sanders, J. F. Stoddart, *Angew. Chem. Int. Ed.*, 2002, **41**, 898-952. (d) J.-M. Lehn, *Chem. Soc. Rev.*, 2007, **36**, 151-160. (e) J. N. H. Reek, S. Otto, *Dynamic Combinatorial Chemistry*, Wiley-VHC Verlag GmbH & Co. KGaA, Weinheim, 2010. (f) J. Li, P. Nowak, S. Otto, *J. Am. Chem. Soc.*, 2013, **135**, 9222-9239.

62 G. Biosa, S. Bastianoni, M. Rustici, *Chem. Eur. J.*, 2006, **12**, 3430-3437.

63 (a) R. Chakrabarty, P. S. Mukherjee, P. J. Stang, *Chem. Rev.*, 2011, **111**, 6810-6918. (b) D. Philp, J. F. Stoddart, *Angew. Chem. Int. Ed. Engl.*, 1996, **35**, 1154-1196. (c) J.-M. Lehn, *Science*, 2002, **295**, 2400-2403. (d) J.-M. Lehn, *Proc. Natl. Acad. Sci. U.S.A.*, 2002, **99**, 4763-4768.

64 N. K. Terret, *Combinatorial Chemistry*, Oxford University Press, Oxford, 1998.

65 J.-M. Lehn, *Supramolecular Chemistry*, VCH, Weinheim, 1995.

66 E. V. Anslyn, D. A. Dougherty, *Modern Physical Organic Chemistry*, University Science Books, USA, 2006.

67 (a) B. Hasenknopf, J.-M. Lehn, B. O. Kneisel, G. Baum, D. Fenske, *Angew. Chem. Int. Ed. Engl.*, 1996, **35**, 1838-1840. (b) B. Hasenknopf, J.-M. Lehn, N. Boumediene, A. Dupont-Gervais, A. Van Dorsselaer, B. Kneisel, D. Fenske, *J. Am. Chem. Soc.*, 1997, **119**, 10956-10962.

68 I. Huc, J. M. Lehn, *Proc. Natl. Acad. Sci. U.S.A.*, 1997, **94**, 2106-2110.

69 B. de Bruin, P. Hauwert, J. N. H. Reek, *Angew. Chem. Int. Ed.*, 2006, **45**, 2660-2663.

70 K. Severin, *Chem. Eur. J.*, 2004, **10**, 2565-2580.

71 P. T. Corbett, S. Otto, J. K. M. Sanders, *Chem. Eur. J.*, 2004, **10**, 3139-3143.

72 P. T. Corbett, J. K. M. Sanders, S. Otto, *J. Am. Chem. Soc.*, 2005, **127**, 9390-9392.

73 B. Brisig, J. K. M. Sanders, S. Otto, *Angew. Chem. Int. Ed.*, 2003, **42**, 1270-1273.

74 J. M. A. Carnall, C. A. Waudby, A. M. Belenguer, M.C. A. Stuart, J. J. P. Peyralans, S. Otto, *Science*, 2010, **327**, 1502-1506.

75 W. L. Noorduin, T. Izumi, A. Millemaggi, M. Leeman, H. Meekes, W. J. P. van Enckevort, R. M. Kellogg, B. Kaptein, E. Vlieg, D. G. Blackmond, *J. Am. Chem. Soc.*, 2008, **130**, 1158-1159.

76 V. del Amo, D. Philp, *Chem. Eur. J.*, 2010, **16**, 13304-13318.

77 M. Sakulsombat, Y. Zhang, O. Ramström, *Top. Curr. Chem.*, 2012, **322**, 55-86.

78 P. Vongvilai, M. Angelin, R. Larsson, O. Ramström, *Angew. Chem. Int. Ed.*, 2007, **46**, 948-950.

79 Lei Hu, O. Ramström, *Chem. Commun.*, 2014, **50**, 3792-3794.

80 E. Moulin, N. Guiseppone, *Top. Curr. Chem.*, 2012, **322**, 87-106.

81 S. Xu, N. Giuseppone, *J. Am. Chem. Soc.*, 2008, **130**, 1826-1827.

82 V. del Amo, A. M. Z. Slawin, D. Philp, *Org. Lett.*, 2008, **10**, 4589-4592.

83 (a) P. T. Glink, A. I. Oliva, J. F. Stoddart, A. J. P. White, D. J. Williams, *Angew. Chem. Int. Ed.*, 2001, **40**, 1870-1875. (b) S. J. Cantrill, S. J. Rowan, J. F. Stoddart, *Org. Lett.*, 1999, **1**, 1363-1366. (c) C. S. Hartley, E. L. Elliot, J. S. Moore, *J. Am. Chem. Soc.*, 2007, **129**, 4512-4513.

84 S. M. Turega, C. Lorenz, J. W. Sadownik, D. Philp, *Chem. Commun.*, 2008, 4076-4078.

85 J. W. Sadownik, D. Philp, *Angew. Chem. Int. Ed.*, 2008, **47**, 9965-9970.

86 C. C. Robertson, PhD Thesis, University of St Andrews, 2011.

87 (a) F. Garciatellado, J. Albert, A. D. Hamilton, *J. Chem. Soc. Chem. Commun.*, 1991, 1761-1763. (b) F. Garciatellado, S. Goswami, S. K. Chang, S. J. Geib, A. D Hamilton, *J. Am. Chem. Soc.*, 1990, **112**, 7393-7394. (c) M. S. Goodman, J. Weiss, A. D. Hamilton, *Tetrahedron Lett.*, 1994, **35**, 8943-8946.

88 I. Flemming, *Pericyclic Reactions*, Oxford University Press, Oxford, 1999.

89 N. Luo, X. Sun, W. Wei, X. Zhang, M. Yan, *Tetrahedron: Asymmetry*, 2013, **24**, 402-408.

90 D. Pizzirani, M. Roberti, S. Grimaudo, A. D. Cristina, R. M. Pipitone, M. Tolomeo, M. Recanatini, *J. Med. Chem.*, 2009, **52**, 6936-6940.

91 J. Clayden, N. Greeves, S. Warren, P. Wothers, *Organic Chemistry*, Oxford University Press, Oxford, 2001.

92 (a) Z. N. Siddiqui, T. Khan, *Tetrahedron Lett.*, 2013, **54**, 3759-3764. (b) S. V. Ryabukhin, A. S. Plason, D. M. Volochnyuk, S. E. Pipko, A. N. Shivanyuk, A. A. Tolmachev, *J. Comb. Chem.*, 2007, **9**, 1073-1078.

93 L. F. Tietze, *Chem. Rev.*, 1996, **96**, 115-136.

94 (a) K. C. Majumdar, A. Taher, R. K. Nandi, *Tetrahedron*, 2012, **68**, 5693-5718. (b) L. F. Tietze, P. Saling, *Synlett.*, 1992, 281-282.

95 A. Vidonne, D. Philp, *Tetrahedron*, 2008, **64**, 8464-8475.

96 H. Mackenzie, MPhil Thesis, University of St Andrews, 2012.

97 G. B. Rocha, R. O. Freire, A. M. Simas, J. J. P. Stewart, *J. Comput. Chem.*, 2006, **27**, 1101-1111.

98 Examples include: (a) J. K. Gallos, C. I. Stathakis, S. S. Kotoulas, A. E. Koumbis, *J. Org. Chem.*, 2005, **70**, 6884-6890. (b) S. E. Denmark, J. I. Montgomery, L. A. Kramps, *J. Am. Chem. Soc.*, 2006, **128**, 11620-11630. (c) K. Aouadi, E. Jeanneau, M. Msaddek, J-P. Praly, *Tetrahedron Lett.*, 2012, **53**, 2817-2821.

99 M. Karplus, *J. Am. Chem. Soc.*, 1963, **85**, 2870-2871.

100 M. Hesse, H. Meier, B. Zeeh, *Spectroscopic Methods in Organic Chemistry*, Thieme, Stuttgart, 2008.

101 M. Miyoura, A. Suzuki, *Chem. Rev.*, 1995, **95**, 2457-2483.

102 CrystalClear Version 2.0. 2009, Rigaku Corporation, Akishima, Tokyo, Japan.

103 G. M. Sheldrick, *Acta Cryst.*, 2008, **A64**, 112–122.

104 Gaussian 09, Revision A.02, M. J. Frisch, G. W. Trucks, H. B. Schlegel, G. E. Scuseria, M. A. Robb, J. R. Cheeseman, G. Scalmani, V. Barone, B. Mennucci, G. A. Petersson, H. Nakatsuji, M. Caricato, X. Li, H. P. Hratchian, A. F. Izmaylov, J. Bloino, G. Zheng, J. L. Sonnenberg, M. Hada, M. Ehara, K. Toyota, R. Fukuda, J. Hasegawa, M. Ishida, T. Nakajima, Y. Honda, O. Kitao, H. Nakai, T. Vreven, J. A. Montgomery, Jr., J. E. Peralta, F. Ogliaro, M. Bearpark, J. J. Heyd, E. Brothers, K. N. Kudin, V. N. Staroverov, R. Kobayashi, J. Normand, K. Raghavachari, A. Rendell, J. C. Burant, S. S. Iyengar, J. Tomasi, M. Cossi, N. Rega, J. M. Millam, M. Klene, J. E. Knox, J. B. Cross, V. Bakken, C. Adamo, J. Jaramillo, R. Gomperts, R. E. Stratmann, O. Yazyev, A. J. Austin, R. Cammi, C. Pomelli, J. W. Ochterski, R. L. Martin, K. Morokuma, V. G. Zakrzewski, G. A. Voth, P. Salvador, J. J. Dannenberg, S. Dapprich, A. D. Daniels, Ö. Farkas, J. B. Foresman, J. V. Ortiz, J. Cioslowski, and D. J. Fox, Gaussian, Inc., Wallingford CT, 2009.

105 (a) M. W. Schmidt, K. K. Baldridge, J. A. Boatz, S. T. Elbert, M. S. Gordon, J. H. Jensen, S. Koseki, N. Matsunaga, K. A. Nguyen, S. Su, T. L. Windus, M. Dupuis, J. A. Montgomery, *J. Comput. Chem.*, 1993, **14**,

1347-1363. (b) M. S. Gordon, M. W. Schmidt, C. E. Dijkstra, G. Frenking, K. S. Kim, G. E. Scuseria, *Theory and Applications of Computational Chemistry: The First Forty Years*, Elsevier, Amsterdam, 2005, 1167.

106 J. J. P. Stewart, MOPAC2012, Stewart Computational Chemistry, Colorado Springs, CO, USA. http://openmopac.net.

107 R. Karthik, S. R. Jasmin, S. Sasikumar, S. B. Kalvan, A. J. M. Christina, A. Jagan, S. K. Sundara, *Pharmacologyonline*, 2008, **2**, 176-191.

108 J. Hück, PhD Thesis, Univeristy of St Andrews, 2011.

109 C. Ren, S. Xu, J. Xu, H. Chen, H. Zeng, *Org. Lett.*, 2011, **13**, 3840-3843.

110 R. F. Heck, *Palladium Reagents in Organic Synthesis*, Academic Press Ltd, 1985.

111 D. Zhao, J. S. Moore, *J. Org. Chem.*, 2002, **67**, 3548-3554.

112 S. D. Straight, J. Andréasson, G. Kodis, A. L. Moore, T. A. Moore, D. Gust, *J. Am. Chem. Soc.*, 2005, **127**, 2717-2724.

# 9

# Appendices

## Appendix 1: Typical Semi-Automatic Deconvolution Script for iNMR

```
-- Dinit.lua   semi-automatic deconvolution of a kinetic
     experiment

-- DEFINITIONS

HOME = HOME or "/Users/david/Desktop/Kinetics/DBKin2_19F"
           -- define here your home directory
                          -- never forget the initial slash
     !
filename = "dbKin2_19F.txt"   --here we save the table of
     integrals

NumSpectra = 75     -- number of points for the kinetic
     study
NumRegions = 4 -- regions to deconvolute

P = 1          -- first spectrum to process
R = 1          -- first region to process
          -- you can start from higher values, if you wish

F = {}         -- central frequencies
par = {}  -- parameter for the deconvolution
-- they must be obtained from a preliminary deconvolution
     performed on the first spectrum
dx = 0.5  -- (constant) region to zoom in, in ppm units,
     based upon experience and observation

local i = 1    -- progressive index, simplifies the editing
     of this script
-- for example, you can reorder the definitions below and
     they will still work


-- proton 1
F[i] = -101.75
par[i] = [[
Parameters for 1 peak
  frequency (Hz)     intensity      width (Hz)   Lorentzian
     %

      -47860.78        47.075         10.0       100.0000
]]
i = i + 1


-- proton 2
```

```
F[i] = -109.89
par[i] = [[
Parameters for 1 peak
  frequency (Hz)     intensity      width (Hz)   Lorentzian
     %

      -51685.37        41.770         10.0       100.0000
]]
i = i + 1


-- proton 3
F[i] = -117.1
par[i] = [[
Parameters for 1 peak
  frequency (Hz)     intensity      width (Hz)   Lorentzian
     %

      -55077.07        4.544          10.0       100.0000
]]
i = i + 1


-- proton 4
F[i] = -121.40
par[i] = [[
Parameters for 1 peak
  frequency (Hz)     intensity      width (Hz)   Lorentzian
     %

      -57098.76        4.253          10.0       100.0000
]]
i = i + 1


-- end of definitions ------------------------------------
     ---

-- ************->    HERE WE GO:    <-***************

io.output(HOME..filename)          -- create/open the file
     were the results will be stored
io.write("point")   -- header
for i = 1,NumRegions do
     io.write("\tppm\tarea")
end
io.write("\n")

spectral = getf("x")                    -- read some
     experimental parameters
```

```
conversion = 1.0 / spectral.MHz         -- useful to
     convert from Hz to ppm
spectral = getf("y")
step = spectral.width / spectral.size
Y = spectral.start + step * (spectral.size -0.1 -P+1)  --
     position of the first row on its dummy ppm scale

io.write( string.format("\n\t%02d\t", P ) )  -- report the
     experiment no.
mark('h', Y )       -- choose a row
extract()           -- extract the coresponding 1D spectrum
delint()            -- we need to normalize the intensities
region( -130.0, -90.0 )  -- region containing protons no. 1
     and 9
press 'i'           -- first integral, automatically set to
     1
intreg( 1, 300 )    -- we set it to 300 to have manageable
     numbers (>1 and <300)

region( F[R] + dx, F[R] - dx )
press "z"
adj()
print("select the signal, then run fnext")
selection = true
```